

Novel functions of Rif1 at telomeres and double strand breaks in *S. cerevisiae*

A Thesis Submitted to Newcastle University
for the Degree Doctor of Philosophy

Yuan Xue

School of Clinical Medical Sciences - Institute for Ageing and Health

June 2011



For my parents

张义德 & 薛华珍

ACKNOWLEDGEMENT

In writing this thesis, and during the seemingly never-ending four years of my PhD, I have received much help from a great variety of people. First of all, I would like to thank my parents for their unconditioned love and support throughout the years. I feel very much in debt to them and hope that I would be able to pay back their love someday. I hope that by completing this PhD I may have fulfilled some of their wishes.

I would like to thank my supervisor Dr Laura Maringele for giving me this opportunity to work on an interesting project and for providing me with a full scholarship. I was given the chance to participate in an international conference on telomere biology, which has been a very valuable experience. More importantly, under her influence (both positive and negative) I have developed in to a better researcher and a stronger person. Training in her lab has taught me to be self-reliant and self-motivated. I have learned to pursue my own direction of research and stand my ground when needed. My presentation and communication skills have significantly improved and I have also learned to initiate scientific collaborations worldwide. On top of this, I was challenged to perform under time pressure and emotional stress. Yet all these experience have strengthened my character and prepared me for greater challenges in the future.

During my PhD I have benefited immensely from numerous mentors of mine. Professor Ioakim Spyridopoulos has been constantly encouraging and enthusiastic about my work. Not only has he assisted me with the statistical analysis for this thesis, he has given me a lot of guidance in my career and life in general. I am grateful to Professor David Lydall and Dr Gabriele Saretzki for assessing my yearly reports; without them I would not have progressed to the same level that I have done. I feel deeply in debt to Paul Herron, my mentor in the Hokutou Ryu Iiu Jitsu club, who has influenced me to think out of the box, and has been fully supportive during the difficult times. I would also like to express my gratitude to my Jitsu club, especially to my sensei Jamie Driscoll for giving me such good training. It was Jitsu training that has purified my mind and engaged me in deliberate practice, which is essential for the success of any project, including my PhD.

I would like to thank my dear friends and colleagues at the Crucible Lab: Stephano for his perfect pasta and tiramisu, and his distinct sense of humor; Sanne for being such a cheerful and supportive friend; Rafal for providing endless laughter and funny stories in and outside of the lab; Chatchawan for being understanding and helpful. Special thanks to my friend Sun Yung for assisting me on the formatting of this thesis, as well as his good advice for my viva.

Two special people deserve my deepest and most heartfelt gratitude-Iglike Ivanova and Michael Rushton. They are my best friends and have supported me in every situation; without them finishing this thesis in time would not have been possible. I am very grateful that they have put in tremendous time and effort in this thesis. I have been extremely lucky to have them beside me during my PhD. Iglike and Michael influenced me in very different, yet positive ways. Iglike has inspired me to be organized and to deliver the highest standard of work. I have always benefited from her creative ideas and her common sense. On the other hand, Michael's relaxed yet focused attitude has been an inspiration for me. From him I learned to identify the most important problem and to focus all my energy to solve that problem, in doing so I become focused and relaxed. Both of my friends have influenced me to work steadily and consistently towards my goal. Most importantly, they have always been there for me during the hardship and being extremely patient, helpful, understanding and forgiving.

In the end, I am very thankful that I was given all these opportunities in life along with all these great people to assist me when the time requires. Good luck to any of you who is reading this thesis and who is on the pursuit of a PhD. May the force be with you!

ABSTRACT

Telomeres cap the end of linear chromosomes and are vital for the genomic stability of eukaryotic cells. The function of telomeres depends on the interaction between the telomeric DNA and specialised telomere-bound proteins. In this study, I show that the budding yeast Rif1 (Rap1-interacting factor) exhibits unique telomere capping properties, which are distinct from its known functions. Deletion of *RIF1* enhances the capping defect of the *cdc13-1* mutant, whereas overexpression of *RIF1* rescues the thermosensitivity of *cdc13-1* cells, and lowers the single-stranded DNA levels at damaged subtelomeres. Interestingly, Rif1 is recruited to internal damaged loci upon telomere uncapping, where it inhibits the binding of checkpoint proteins to these regions. The recruitment of Rif1 appears to be Rap1-independent as demonstrated by a mutant strain in which the Rif1-Rap1 interacting sequence was removed. In addition, Rif1 was also found essential for survival of yeast cells lacking telomeres through a checkpoint adaptation process. Furthermore, an unexpected telomere-independent role of Rif1 was discovered at an induced double strand break. Rif1 is recruited to the break site when overexpressed, where it promotes DNA repair via the non-homologous end joining pathway.

My results suggest that the budding yeast Rif1 is involved in end protection of telomeres and checkpoint adaptation. Budding yeast Rif1 may interact with the Cdc13, Stn1, and Ten1 (CST) complex and together cap the chromosome ends; scRif1 and CST may represent the functional equivalent of the vertebrate shelterin complex in the budding yeast telomeres. My study highlights the conserved function of Rif1, and implies that Rif1 may have a significant role in genomic stability and carcinogenesis in humans.

PUBLICATIONS

Data from this thesis contributed to the following paper:

Yuan Xue, Michael D. Rushton, Laura Maringele. 'A novel checkpoint inhibitory pathway regulated by Rif1' PLOS Genetics, in press.

ABBREVIATIONS

ATM	Ataxia telangiectasia mutated
ATR	Ataxia telangiectasia-mutated and Rad3-related
CDC13	Cell division cycle 13
CDC5	Cell division cycle 5
CDK1	Cyclin-dependent kinase 1
ChIP	Chromatin immunoprecipitation
CHK1	Checkpoint Kinase 1
CIN	Chromosomal instability
CKB1	Casein kinase beta subunit 1
CKB2	Casein kinase beta subunit 2
CST	Cdc13, Stn1, Ten1 complex
DDC1	DNA damage checkpoint 1
DDC2	DNA damage checkpoint 2
DDR	DNA damage response
DNA2	DNA synthesis defective 2
DNA-PK	DNA-dependent protein kinase
DNL4	DNA Ligase 4
DSB	Double strand break
dsDNA	Double-stranded DNA
DUN1	DNA-damage uninducible 1
EST1	Ever short telomeres 1
EST2	Ever short telomeres 2
EST3	Ever short telomeres 3
EST4	Ever short telomeres 4, alias CDC13

EXO1	Exonuclease 1
FEAR	Cdc fourteen early anaphase release
H3	Histone 3
H4	Histone 4
HEAT repeats	Huntingtin, elongation factor 3 (EF3), protein phosphatase 2A (PP2A), and the yeast PI3-kinase TOR1
HML	Hidden MAT Left
HMR	Hidden MAT right
HR	Homologous recombination
IR	Ionising radiation
LIF1	Ligase interacting factor 1
MEC1	Mitosis entry checkpoint1
MEC3	Mitosis entry checkpoint3
MEN	Mitotic exit network
MMS	methyl methanesulfonate
MRE11	Meiotic recombination 11
MRX	Mre11-Rad50-Xrs2 complex
NHEJ	Non homologous end joining
OB fold	Oligonucleotide/oligosaccharide binding fold
ORC	Origin of replication complex
PCNA	Proliferating cell nuclear antigen
PDS1	Precocious dissociation of sisters 1
PIKKs	Phosphatidylinositol 3-kinases
POL12	Polymerase 12
POT1	Protection of telomeres 1
PTC2	Phosphatase type two C 2
PTC3	Phosphatase type two C 3
RAD17	Radiation sensitive 17

RAD24	Radiation sensitive 24
RAD50	Radiation sensitive 50
RAD51	Radiation sensitive 51
RAD52	Radiation sensitive 52
RAD53	Radiation sensitive 53
RAD54	Radiation sensitive 54
RAD55	Radiation sensitive 55
RAD57	Radiation sensitive 57
RAD9	Radiation sensitive 9
RAP1	Repressor and activator protein 1
RFC	Replication Factor C
RIF1	RAP1-interacting factor 1
RIF2	RAP1-interacting factor 2
RPA	Replication factor A
SAE2	Sporulation in the absence of spo eleven 2
SGS1	Slow growth suppressor 1
SIR2	Silent information regulator 2
SIR3	Silent information regulator 3
SIR4	Silent information regulator 4
SRS2	Suppressor of rad six 2
ssDNA	Single-stranded DNA
STN1	Suppressor of cdc thirteen 1
TEL1	Telomere maintenance 1
TEN1	Telomeric pathways with stn1
TERT	Telomerase reverse transcriptase
TIN2	TRF1 interacting protein 2
TLC1	Telomerase component 1

TPP1	Tripeptidyl peptidase 1
TR	Telomerase RNA
TRF1	Telomeric repeat binding factor 1
TRF2	Telomeric repeat binding factor 2
TRF3	Telomeric repeat binding factor 3
WT	Wild type
YKU70	Yeast KU 70
YKU80	Yeast KU 80

DECLARATION

I, Yuan Xue, confirm that no part of the material offered has perviously been submitted by me for a degree in this or any other University. Material generated through joint work has been acknowledged and the appropriate publications cited. In all other cases, material from the work of others has been acknowledged, and quotations and paraphrases suitably indicated.

Signature:

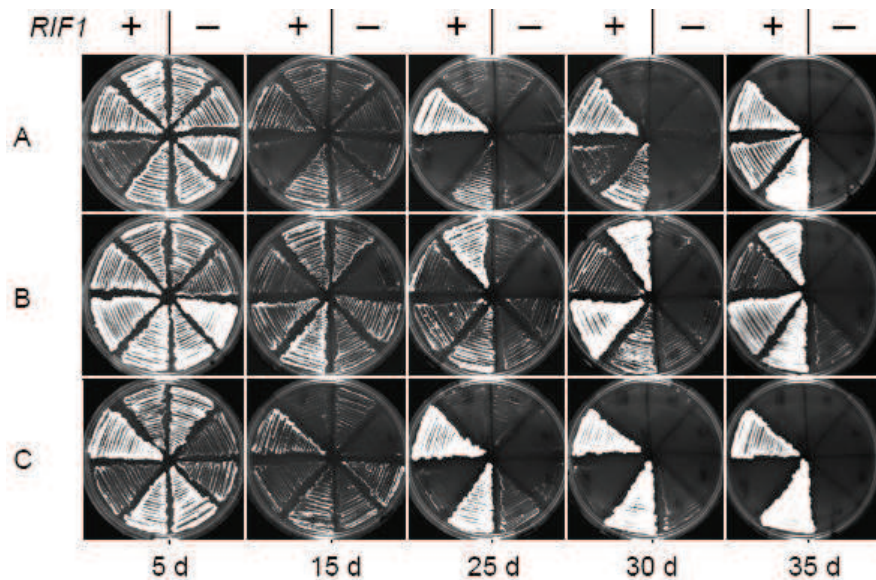
Date: 30 June 2011

Table 2.1.1 Yeast strains used in this study

Strain	Genotype	Source
LMY202	<i>MATa ade2-1 trp1-1 can1-100 leu2-3,112 his3-11,15 ura3 GAL+ psi+ ssd1-d2 RAD5 (Wild type)</i>	Rodney Rothstein
LMY1	<i>Diploid TLC1/tlc1::HIS3 RAD52/rad52::TRP1 EXO1/exo1::LEU2 RIF1/rif1::kanMX6</i>	This study
LMY3	<i>Diploid TLC1/tlc1::HIS3 RAD52/rad52::TRP1 EXO1/exo1::LEU2</i>	This study
LMY5	<i>Diploid TLC1/tlc1::HIS3 RAD52/rad52::TRP1 EXO1/exo1::LEU2 RIF1/rif1::ura3</i>	This study
LMY6	<i>Diploid TLC1/tlc1::HIS3 RAD52/rad52::TRP1 EXO1/exo1::LEU2 RIF1/rif1::ura3 RAD9/rad9::kanMX6</i>	This study
LMY8	<i>Diploid TLC1/tlc1::HIS3 RAD52/rad52::TRP1 EXO1/exo1::LEU2 RIF1/rif1::ura3 LIG4/lig4::kanMX6</i>	This study
LMY9	<i>Diploid TLC1/tlc1::HIS3 RAD52/rad52::TRP1 EXO1/exo1::LEU2 RIF1/RIF1-13myc::kanMX6</i>	This study
LMY12	<i>Diploid TLC1/tlc1::HIS3 RAD52/rad52::TRP1 EXO1/exo1::LEU2 RIF1CHK1/rif1chk1::kanMX6</i>	This study
LMY14	<i>Diploid TLC1/tlc1::HIS3 RAD52/rad52::TRP1 EXO1/exo1::LEU2 RIF2/rif2::kanMX6</i>	This study
LMY16	<i>Diploid TLC1/tlc1::HIS3 RAD52/rad52::TRP1 EXO1/exo1::LEU2 RIF1/rif1::ura3 CHK1/chk1::kanMX6</i>	This study
LMY20	<i>Diploid TLC1/tlc1::HIS3 RAD52/rad52::TRP1 EXO1/exo1::LEU2 MRC1/mrc1::kanMX6</i>	This study
LMY22	<i>Diploid TLC1/tlc1::HIS3 RAD52/rad52::TRP1 EXO1/exo1::LEU2 CKB2/ckb2::kanMX6</i>	This study
LMY207	<i>MATalpha yku70::HIS3</i>	David Lydall
LMY368	<i>MATalpha yku70::HIS3 rif1::URA3</i>	David Lydall
LMY310	<i>MATa rif2::kanMX6</i>	This study
LMY255	<i>MATalpha rif1::kanMX6 yku70::HIS3</i>	This study
LMY307	<i>MATa rif1::kanMX6</i>	This study
LMY472	<i>MATalpha yku70::HIS3 rif2::kanMX6</i>	This study
LMY538	<i>Diploid YKU70/yku70::HIS3 RIF1/rif1::URA3 RIF2/rif2::kanMX6</i>	This study
LMY593	<i>MATa rif1::URA3 rif2::kanMX6</i>	This study
R25	<i>MATa yku70::HIS3 rif1::URA3 rif2::LEU2</i>	Laura Maringele
R26	<i>MATa yku70::HIS3 rif1::URA3 rif2::LEU2</i>	Laura Maringele
R37	<i>MATa yku70::HIS3 rif1::URA3 rif2::LEU2 rad52::TRP1</i>	Laura Maringele
R38	<i>MATa yku70::HIS3 rif1::URA3 rif2::LEU2 rad52::TRP1</i>	Laura Maringele
LMY78	<i>MATalpha cdc13-1 RIF1::13MYC::kanMX6</i>	This study
LMY712	<i>MATa cdc13-1 RIF1::13MYC::kanMX6 yku70::natMX6</i>	This study
LMY420	<i>MATalpha cdc13-1 rif1::URA3</i>	David Lydall
LMY204	<i>MATa cdc13-1</i>	David Lydall
LMY514	<i>MATalpha cdc13-1 rif2::kanMX6</i>	This study
LMY415	<i>MATa cdc13-1 ADE2+ bar1::LEU2 DDC2::YFP</i>	Laura Maringele
LMY416	<i>MATa cdc13-1 ADE2+ bar1::LEU2 DDC2::YFP rif1::URA3</i>	Laura Maringele
LMY336	<i>MATa cdc13-1 rad9::HIS3</i>	David Lydall
LMY378	<i>MATalpha cdc13-1 rad9::LEU2 rif1::URA3</i>	This study
LMY335	<i>MATa cdc13-1 rad24::TRP1</i>	David Lydall
LMY376	<i>MATalpha cdc13-1 rad24::TRP1 rif1::URA3</i>	This study
LMY374	<i>MATa cdc13-1 mec1::TRP1 sml1::HIS3 rif1::URA3</i>	This study
LMY380	<i>MATa cdc13-1 exo1::LEU2 rif1::URA3</i>	This study
LMY366	<i>MATalpha cdc13-1 bub2::URA3</i>	David Lydall
LMY589	<i>MATa cdc13-1 bub2::URA3 Rif1::kanMX6</i>	This study
LMY590	<i>MATalpha cdc13-1 int bub2::URA3 Rif1::kanMX6</i>	This study
LMY591	<i>MATa cdc13-1 mad2::URA3 Rif1::kanMX6</i>	This study
LMY592	<i>MATalpha cdc13-1 mad2::URA3 Rif1::kanMX6</i>	This study
LMY465	<i>MATa cdc13-1 GAL::kanMX6::RIF1 (URA3 on plasmid)</i>	This study
LMY185	<i>MATalpha cdc13-1 rad17::LEU2 (URA3 on plasmid)</i>	David Lydall
LMY520	<i>MATa cdc13-1 mec3::kanMX6</i>	This study
LMY463	<i>cdc13-1 GAL-GFP-RIF1::kanMX6</i>	This study
LMY348	<i>MATa cdc13-1 rif1::kanMX6</i>	This study
LMY509	<i>MATa cdc13-1 RIF1cΔ-13MYC::kanMX6</i>	This study
LMY510	<i>MATa cdc13-1 RIF1cΔ-13MYC::kanMX6</i>	This study
LMY680	<i>MATa cdc13-1 RIF2-13MYC::kanMX6</i>	This study
LMY675	<i>MATa cdc13-1 SIR2-13MYC::kanMX6</i>	This study
LMY677	<i>MATa cdc13-1 SIR4-13MYC::kanMX6</i>	This study
LMY738	<i>MATa cdc13-1 GAL1::kanMX6::RIF1cΔ-13MYC::natMX6</i>	This study
LMY739	<i>MATa cdc13-1 GAL1::kanMX6::RIF1cΔ-13MYC::natMX6</i>	This study
LMY581	<i>MATa hmrΔ::ADE1 hmlΔ::ADE1 ade3::GAL-HO ade1-100 leu2-3,112 lys5 trp1::hisG ura3-52 (Alias JKM139)</i>	James Haber
LMY711	<i>MATa DDC2-3HA::natMX6 rif1::knMX6 (JKM139 derivative)</i>	This study
LMY565	<i>MATa hml::ADE1 hmr::ADE1 ade3::GAL10::HO RIF1-13MYC::kanMX6 (JKM139 derivative)</i>	This study
LMY582	<i>MATa hml::ADE1 hmr::ADE1 ade3::GAL10::HO rif1::kanMX6 (JKM139 derivative)</i>	This study
LMY635	<i>MATa hml::ADE1 hmr::ADE1 ade3::GAL10::HO GAL-RIF1::kanMX6 (JKM139 derivative)</i>	This study
LMY637	<i>MATa hml::ADE1 hmr::ADE1 ade3::GAL10::HO GAL-RIF1::kanMX6 (JKM139 derivative)</i>	This study
LMY735	<i>MATa ADH1-3HA-RIF1::natMX6 (JKM139 derivative)</i>	This study
LMY736	<i>MATa ADH1-3HA-RIF1::natMX6 (JKM139 derivative)</i>	This study

SUPPLEMENTARY FIGURES

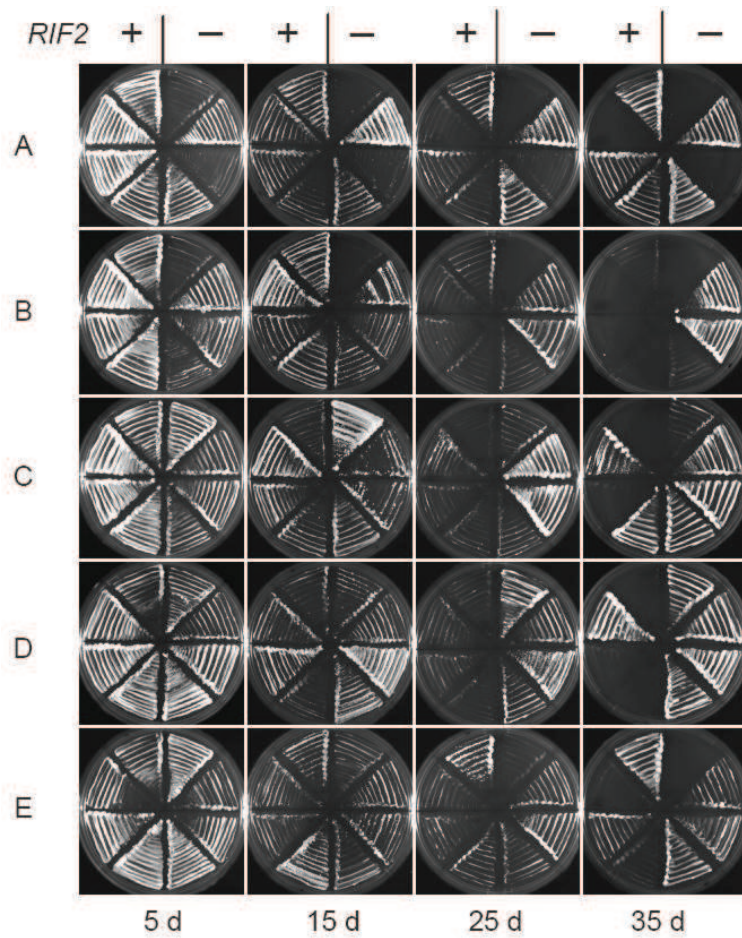
tlc1Δrad52Δexo1Δ



Supplementary Figure1. Effect of RIF1 on escaping senescence.

Lanes A-C show independent *tlc1Δrad52Δexo1Δ* strains on YEPD plates. Strains on the right half of each plate are also *rif1Δ*. All strains was passaged every 5 days since germination, and photographed at day 5, 15, 25 and 35 (from left to right).

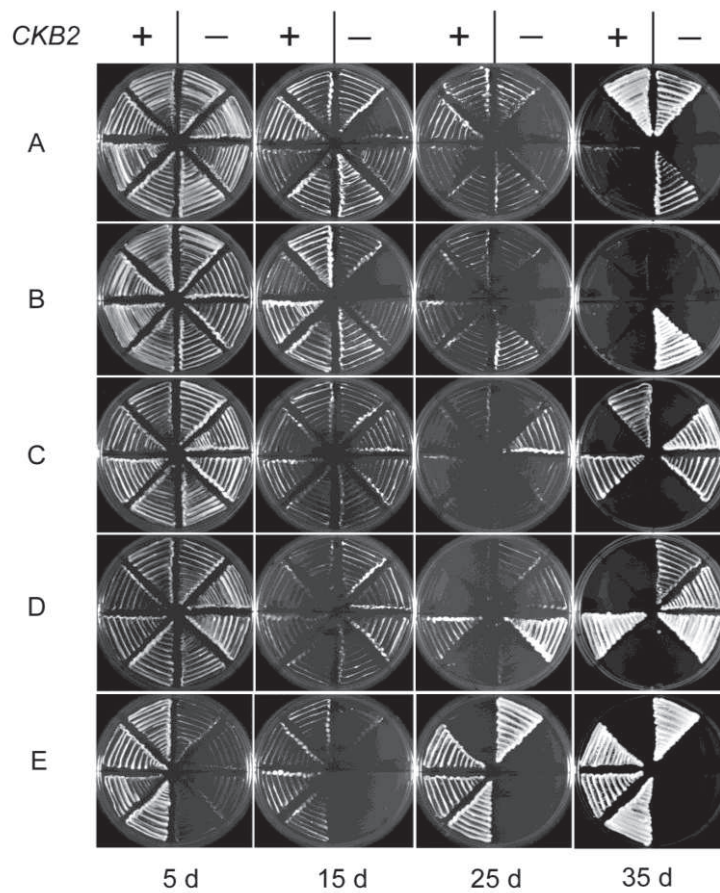
tlc1Δrad52Δexo1Δ



Supplementary Figure2. Effect of *RIF2* on escaping senescence.

Lanes A-E show independent *tlc1Δrad52Δexo1Δ* strains on YEPD plates. Strains on the right half of each plate are also *rif2Δ*. All strains was passaged every 5 days since germination, and photographed at day 5, 15, 25 and 35 (from left to right).

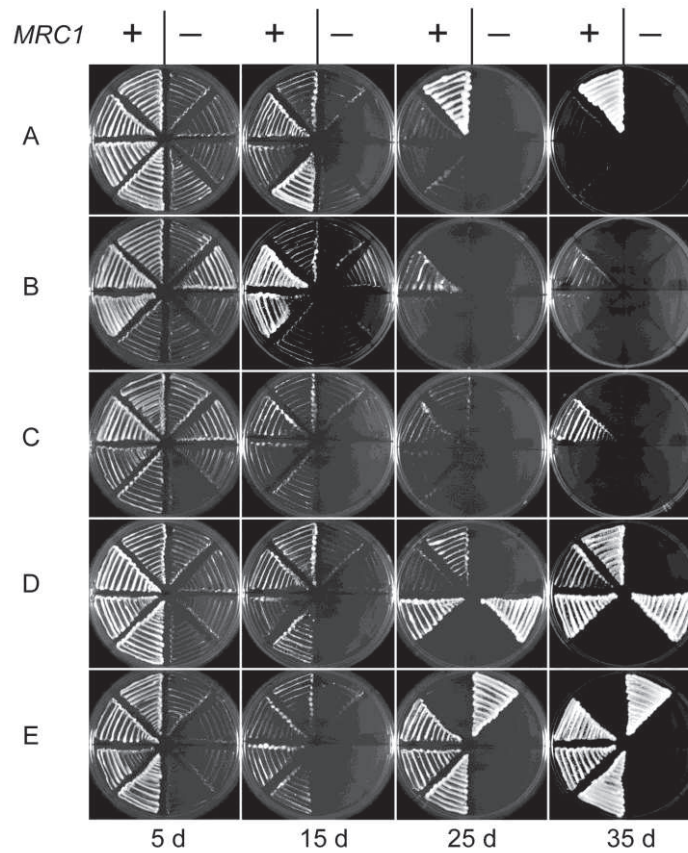
tlc1Δrad52Δexo1Δ



Supplementary Figure3. Effect of *CKB2* on escaping senescence.

Lanes A-E show independent *tlc1Δrad52Δexo1Δ* strains on YEPD plates. Strains on the right half of each plate are also *ckb2Δ*. All strains was passaged every 5 days since germination, and photographed at day 5, 15, 25 and 35 (from left to right).

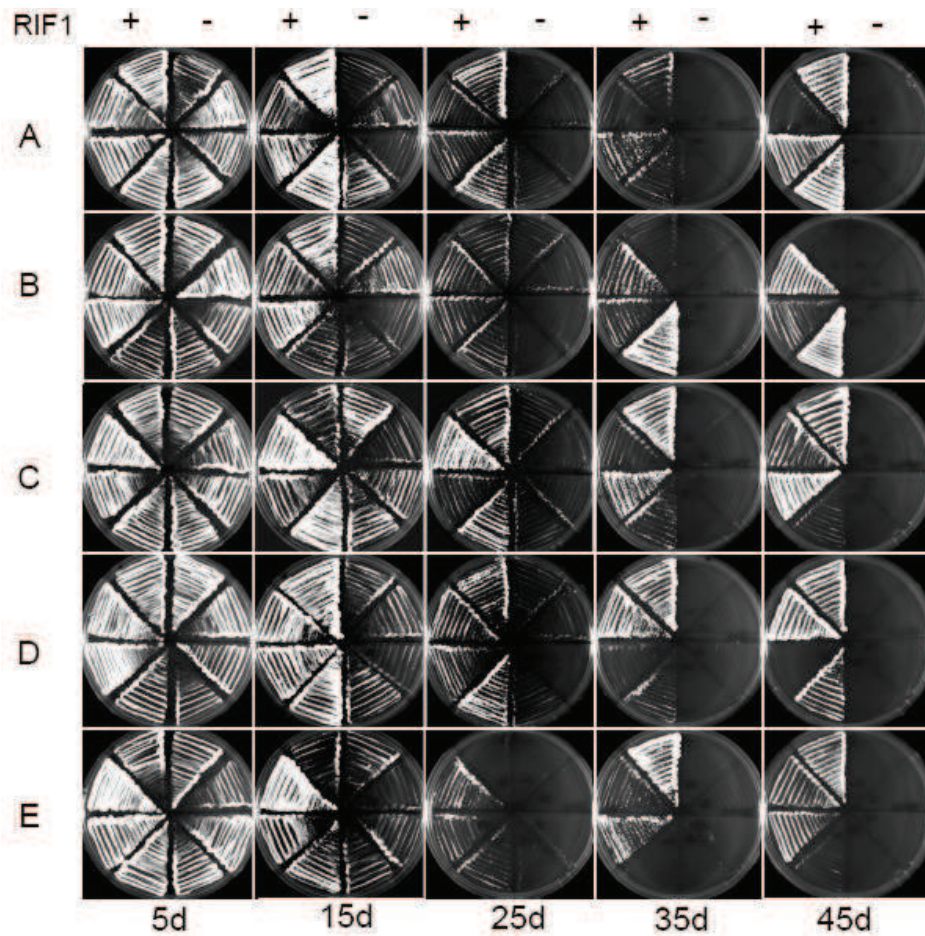
tlc1Δrad52Δexo1Δ



Supplementary Figure4. Effect of *MRC1* on escaping senescence.

Lanes A-E show independent *tlc1Δrad52Δexo1Δ* strains on YEPD plates. Strains on the right half of each plate are also *mrc1Δ*. All strains was passaged every 5 days since germination, and photographed at day 5, 15, 25 and 35 (from left to right).

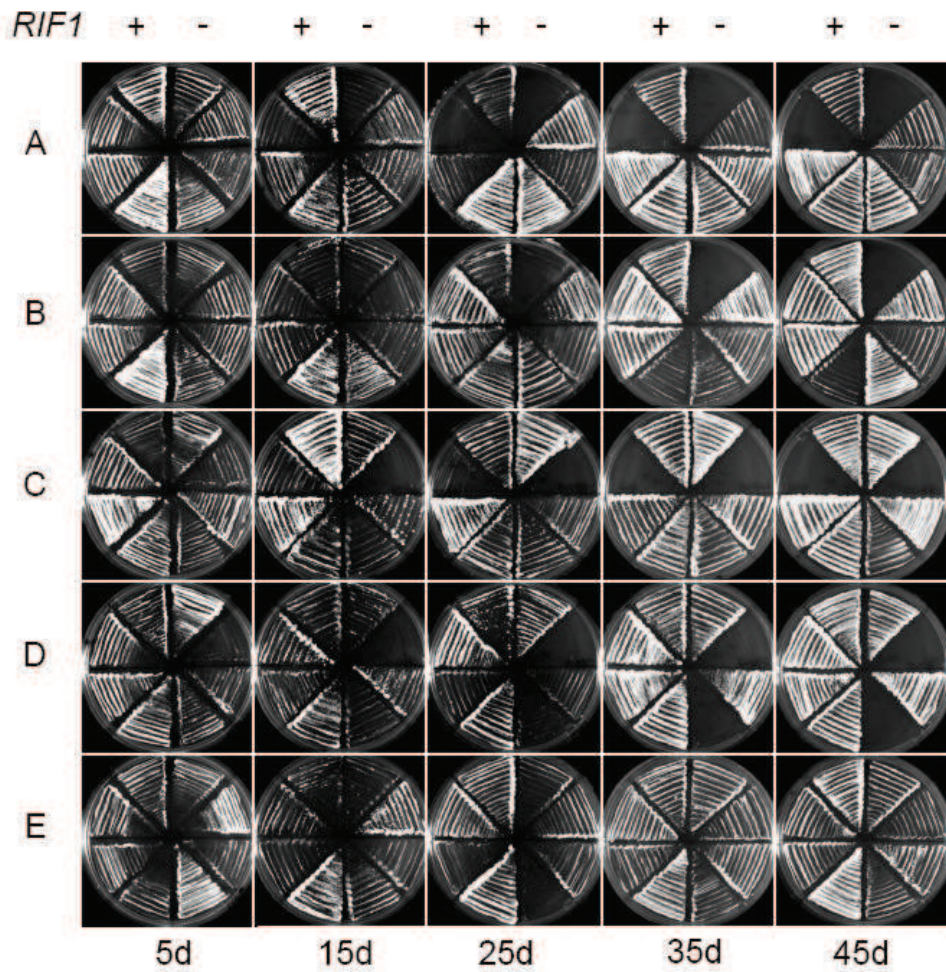
tlc1Δrad52Δexo1Δlig4Δ



Supplementary Figure 5. Effect of *LIG4* on escaping senescence.

Lanes A-E show independent *tlc1Δrad52Δexo1Δlig4Δ* strains on YEPD plates. Strains on the right half of each plate are also *rif1Δ*. All strains were passaged every 5 days since germination, and photographed at day 5, 15, 25, 35 and 45 (from left to right).

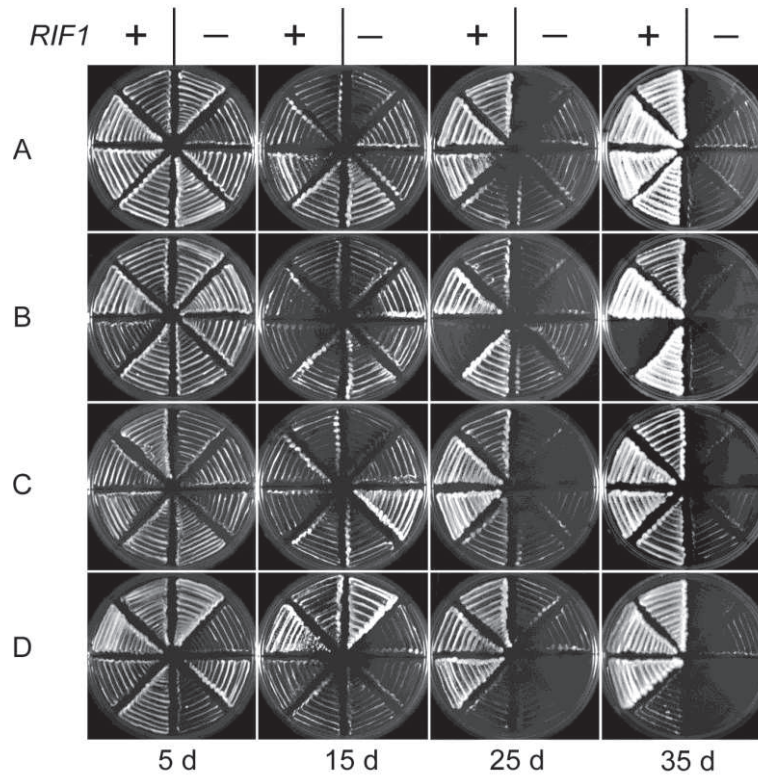
tlc1Δrad52Δexo1Δrad9Δ



Supplementary Figure 6. Effect of *RAD9* on escaping senescence.

Lanes A-E show independent *tlc1Δrad52Δexo1Δrad9Δ* strains on YEPD plates. Strains on the right half of each plate are also *rif1Δ*. All strains was passaged every 5 days since germination, and photographed at day 5, 15, 25, 35 and 45 (from left to right).

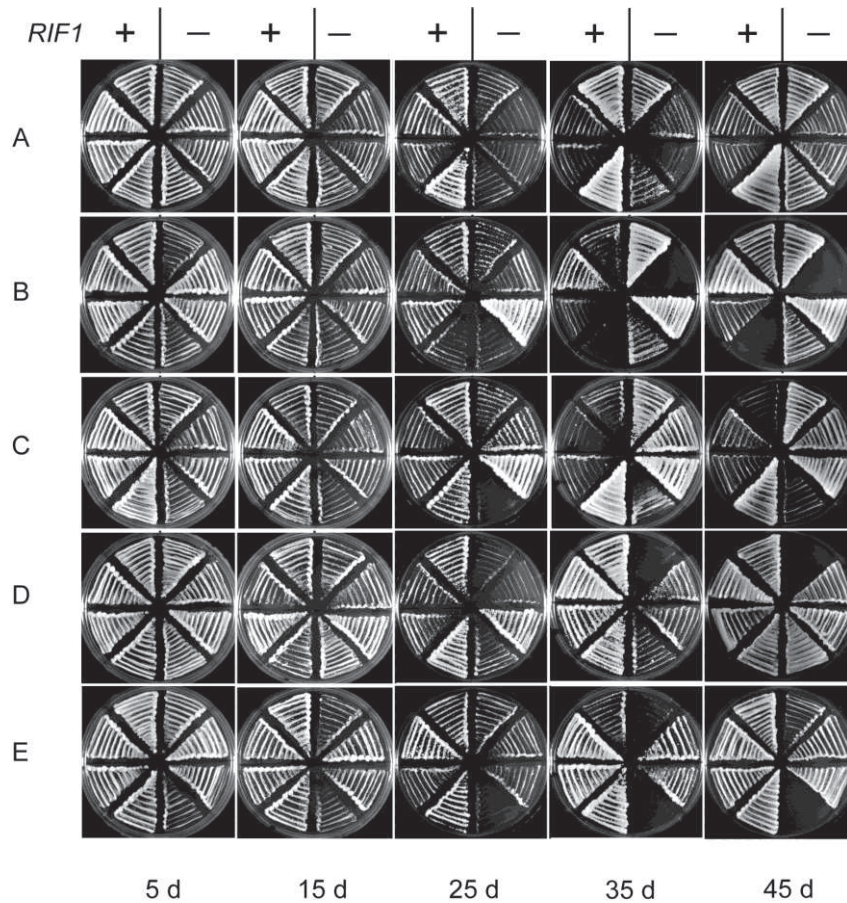
tlc1Δrad52Δexo1Δchk1Δ



Supplementary Figure 7. Effect of *CHK1* on escaping senescence.

Lanes A-D show independent *tlc1Δrad52Δexo1Δchk1Δ* strains on YEPD plates. Strains on the right half of each plate are also *rif1Δ*. All strains were passaged every 5 days since germination, and photographed at day 5, 15, 25 and 35 (from left to right).

tlc1Δrad52Δexo1Δrad24Δ



Supplementary Figure 8. Effect of *RAD24* on escaping senescence.

Lanes A-E show independent *tlc1Δrad52Δexo1Δrad24Δ* strains on YEPD plates. Strains on the right half of each plate are also *rif1Δ*. All strains were passaged every 5 days since germination, and photographed at day 5, 15, 25, 35 and 45 (from left to right).

TABLE OF CONTENTS

Chapter I: Introduction	7
1.1 Telomere architecture and function	7
1.2 Telomere binding proteins	9
The shelterin complex.....	9
The CST complex	11
Ku70/80.....	13
The SIR complex.....	15
Rap1	16
Rif1	18
Rif2	20
1.3 Telomere replication and telomerase	21
1.3.1 Telomere replication.....	21
1.3.2 Telomerase	25
1.4 Telomeres and genomic instability	26
1.5 The G2/M DNA damage checkpoint response in budding yeast.....	29
1.6 Telomere uncapping model systems	32
1.6.1 The <i>cdc13-1</i> model system	32
1.6.2 The <i>yku70Δ</i> model system	35
1.7 Checkpoint adaptation.....	36

1.8 Non-Homologous End Joining and Homologous Recombination.....	40
1.9 Cellular senescence and crisis.....	43
1.10 Type I and Type II survivors.....	44
1.11 PAL survivors.....	45
1.12 Aim.....	49
Chapter II: Materials & Methods.....	50
2.1. Yeast strains.....	50
2.2 Recipes for yeast media.....	50
2.3 Cryogenic storage and growing of yeast strains.....	53
2.4 Mating and sporulation.....	53
2.5 Passage of telomerase negative strains on YEPD plates.....	54
2.6 Spot test.....	54
2.7 Scoring of G2/M arrested cells.....	55
2.8 Gene disruption using Longtine plasmids.....	56
2.8.1 One-step gene deletion and tagging.....	56
2.8.2 High efficiency Lithium Acetate (LiAc) yeast transformation.....	57
2.8.3 Hot-Start PCR test for gene deletion.....	58
2.8.4 Marker swapping.....	59
2.8.5 <i>RIF1</i> overexpression and C-terminal deletion.....	60
2.9 QAOS assay.....	62
2.9.1 The principle of QAOS.....	62
2.9.2 ssDNA preparation.....	64

2.9.4 Buffers.....	65
2.9.5 Equilibration of total genomic DNA.....	66
2.9.6 Prepare ssDNA standards	67
2.9.7 ssDNA measurement using Taqman probes.....	67
2.9.8 Development of a SYBR Green based QAOS assay	68
2.10 Western Blot	69
2.10.1 TCA protein extraction	69
2.10.2 SDS-PAGE, blotting and detection	70
2.10.3 Buffers.....	71
2.11 Southern Blotting.....	72
2.11.1 Yale Quick DNA extraction from yeast.....	72
2.11.2 Digoxigenin (DIG) labelling of nucleic acid probe	73
2.11.3 Procedure and buffers	73
2.12 Chromatin immunoprecipitation	76
2.12.1 Procedures	76
2.12.2 qPCR measurement of ChIP samples using Taqman probes	78
2.12.2 SYBR green qPCR measurement of ChIP samples	78
2.12.3 qPCR primers for the inducible DSB system	79
2.13 Gene expression and RT-PCR.....	80
2.13.1 RNA extraction	80
2.13.2 Reverse transcription.....	81
2.13.3 qPCR.....	81

2.14 Statistics	82
2.15 Antibody used in the study	82
Chapter III: The role of Rif1 in PAL survivors.....	83
3.1 Rif1 is essential for the survival of <i>tlc1Δ rad52Δ exo1Δ</i> cells.	83
3.2 Effect of Rif2, Ckb2, Lig4 and checkpoint proteins on escaping senescence	85
3.3 Deletion of RAD9 and RAD24 bypass the requirement of <i>RIF1</i> in generating PAL survivors.....	88
3.4 Discussion.....	90
3.4.1 The role of Rif1 in adaptation	90
3.4.2 Rif1 is not essential for long-term maintenance of PAL survivors	92
Chapter IV: The role of Rif1 in <i>cdc13-1</i> mutants.....	94
4.1 Deletion of Rif1 lowers the maximum permissive temperature of <i>cdc13-1</i> cells	94
4.2 The DNA damage checkpoint pathway arrests <i>cdc13-1 rif1Δ</i> cells at 25°C.....	99
4.3 ssDNA accumulation in <i>cdc13-1</i> and <i>cdc13-1 rif1Δ</i> cells	103
4.4 Overexpression of <i>RIF1</i> rescues <i>cdc13-1</i> mutants at non-permissive temperatures..	105
4.5 Overexpression of <i>RIF1</i> overrides G2/M checkpoint in <i>cdc13-1</i> cells	109
4.6 Rif1 is recruited to telomere damage	112
4.7 Effect of Rif1 on the recruitment of checkpoint proteins and helicase to DNA damage	118
4.8 C-terminal deleted Rif1 is recruited to telomere damage in <i>cdc13-1</i> cells.....	120
4.9 Overexpression of C-terminal deleted Rif1 rescues <i>cdc13-1</i> at 32°C.....	122

4.10 scRif1 contains potential N-terminal HEAT-repeats but lacks the C-terminal DNA binding domain	124
4.11 Discussion.....	128
4.11.1 Checkpoint inhibitory role of Rif1.....	129
4.11.2 Nuclease inhibitory role of Rif1	129
4.11.3 Rap1 independent role of Rif1.....	130
4.11.4 The role of Rif1 in repair and adaptation	132
Chapter V: The role of Rif1 in <i>yku70Δ</i> system	137
5.1 The effect of <i>RIF1</i> and <i>RIF2</i> deletion in <i>yku70Δ</i> cells.....	137
5.2 The relationship between temperature sensitivity and telomere length	139
5.3 <i>RAD51</i> and <i>RAD52</i> are essential for the survival of <i>yku70Δ rif1Δ</i> and <i>yku70Δ rif1Δ rif2Δ</i> cells at high temperatures	144
5.4 Recruitment of Rif1 protein in <i>yku70Δ</i> cells	146
5.5 Recruitment of Rif1 in <i>cdc13-1 yku70Δ</i> cells	148
5.6 Discussion.....	150
Chapter VI: The role of Rif1 at double strand breaks	154
6.1 The HO-inducible DSB system.....	154
6.2 Recruitment of Rif1 to a single DSB	157
6.3 Recruitment of Rap1 to a DSB	161
6.4 Strand resection is independent of Rif1 and Rif2	163
6.5 Checkpoint activation at DSB is independent of Rif1	165
6.6 Overexpression of <i>RIF1</i> promotes checkpoint adaptation to a single DSB	168

6.7 Overexpression of Rif1 facilitates NHEJ repair of a DSB	170
6.8 Discussion.....	172
6.8.1 Recruitment of Rif1 to a DSB	172
6.8.2 Functions of Rif1 at a DSB.....	172
Chapter VII: Phosphorylation of Rif1	175
7.1 Introduction	175
7.2 Rif1 modification during senescence.....	176
7.3 Rif1 is phosphorylated upon telomere uncapping	176
7.4 Phosphorylation of Rif1 upon telomere uncapping depends on cell cycle arrest	180
7.5 C-terminal deleted Rif1 is phosphorylated upon telomere uncapping	182
7.6 C-terminal deleted Rif1 is phosphorylated upon global DNA damage.....	182
7.7 Rif1 contains putative phosphorylation sites of Cdk1 and ATM/ATR	186
7.8 Discussion.....	189
Chapter VIII: Final discussion	192
8.1 Rif1 in budding yeast and humans.....	192
8.2 Checkpoint adaptation and the initiation of CIN	193
8.4 Adaptation and cancer.....	198
References	200

Chapter I: Introduction

1.1 Telomere architecture and function

In almost all eukaryotic cells, the ends of linear chromosomes are protected by a specialised structure called the telomeres (Ferreira et al, 2004). To date two main functions of the telomeres have been identified, these are: 1) to maintain the ends of linear chromosomes during replication, and 2) acting as a cap 'hiding' the end of the chromosomes from the DNA damage responses.

Structurally, telomeres are a complex formed by a specific network of interactions between DNA, RNA and proteins (Giraud-Panis et al, 2010). Telomeric DNA is conserved in a diversity of species and is usually composed of short tandem repeats, with one DNA strand very rich in guanine bases (referred to as the G strand). In contrast to the conservation in telomeric sequences, the length of the telomere varies dramatically. For example, telomere repeats in ciliates are only tens of bases in length, while rodents and plants have extremely long telomeres of 50kb and more. This variation in telomere length also exists between different types of cells in the same species, and even from one telomere to another in the same cell. The length of the telomeres in many organisms including budding yeast is maintained by an enzyme called telomerase, which adds telomeric repeats to the end of short telomeres (For details see section 1.3).

Another conserved feature of telomeres is a single-strand overhang. In most cases, this single-stranded overhang occurs on the G strand hence is known as the G tail or 3' overhang. However, a 5' overhang has also been observed in *C.elegans* and transiently during S phase in human cells (Cimino-Reale et al, 2003; Raices et al, 2008).

Budding yeast telomeres are composed of ~350 CA/TG repeats that can be described with the general consensus of $C_{1-3}A/TG_{1-3}$. G tails as long as 30 single-stranded nucleotides are present during S phase but are not detectable in other stages of the cell cycle. The formation of the G tail is telomerase independent (Wellinger et al, 1996). Other repeats, called subtelomeric repeats, are also found in proximity to the telomere. All yeast telomeres contain a ~475bp X' element and some have an additional Y' element that can be repeated up to four times per chromosome end (Louis & Vershinin, 2005).

In human, mouse and plant cells, purified telomeres were observed to form lasso-like structures under the electronic microscope, which are known as the t-loops (Palm & de Lange, 2008). The formation of the t-loop is thought to be carried out by the invasion of the 3' overhang in to the double-stranded telomeric DNA and the subsequent base pairing with the C strand. The size of the t-loop varies from 1-25kb in human cells. However, it is not known if the t-loop represents the predominate form of the protected chromosome ends *in vivo*.

Another 3D structure that telomeres from different organisms can adopt is called the G-quadruplex (Lipps & Rhodes, 2009). In a quadruplex, four guanines are held together in planar arrangement through Hoogsteen hydrogen bonds. Several G-quartets planes stack on top of each other to create a helical quadruplex. Amazingly, once formed, the G-quadruplex structure is more stable than linear dsDNA. The formation of G-quadruplex requires K^+ or Na^+ , which is abundant in physiological buffer conditions. For many years, G-quadruplex was merely considered an interesting *in vitro* observation, and was hypothesised to exist in G rich sequences such as telomeres. However only until recently it was discovered that G-quadruplex also exists *in vivo* and can regulate many important cellular events.

For a long time, telomeres were considered to be transcriptionally silent. However, recently evidence uncovered that telomeres are in fact transcribed in to many non-coding RNAs called TERRA (TElomeric Repeat containing RNA, reviewed by Feuerhahn et al, 2010). These RNA can be detected by Northern blot as well as can be directly visualised by RNA-FISH on human and mice telomeres *in vivo* (Azzalin et al, 2007). It has been suggested that TERRA acts as a natural ligand that binds and inhibits telomerase activity (Luke et al, 2008).

1.2 Telomere binding proteins

Initially the properties of the telomere were thought to be a result of its unique repetitive DNA sequence. However, it soon became apparent that the telomere is bound by an abundant and versatile array of proteins. These proteins perform crucial functions at telomeres, such as facilitating chromosome end replication as well as capping the telomeres.

The shelterin complex

In humans, more than 200 proteins are found to be associated with telomeres (de Lange, 2005). While most of the association is transient, a protein complex called shelterin was found to be present at the telomere throughout the cell cycle and is crucial for telomere protection. The human shelterin complex consists of six characterised components: TRF1, TRF2, POT1, TIN2, RAP1, TPP1 and the newly discovered TRF3 (de Lange, 2005; Persengiev et al, 2003). The homodimers TRF1 and TRF2 bind directly to the double-stranded TTAGGG sequence via their Myb/SANT domains, while Pot1 binds the 3' ss overhang with OB fold

motifs. The dsDNA and ssDNA part of the telomere are bridged together by TIN2, which tethers TRF1, TRF2 and POT1 to the telomere via an interaction with TPP1.

There is mounting evidence suggesting that shelterin is involved in telomere capping. For example, dysfunction of TRF2 leads to chromosome end fusion and sudden telomere truncations (Smogorzewska et al, 2002; Wang et al, 2004). Also inhibition of TRF2, TIN2, and POT1 activates the ATM kinase and leads to cell cycle arrest during the G1/S phase of the cell cycle (Karlseder et al, 1999). In addition, shelterin also inhibits telomerase action, as POT1 inhibition in human cells causes telomere elongation (Hockemeyer et al, 2005).

How does shelterin protect telomeres? It has been suggested that shelterin proteins help to fold telomeres into a higher order structure (such as the T-loop), which is a 'closed' conformation which inhibits telomerase access and is undetectable by the DNA damage surveillance machinery (de Lange, 2005). In contrast, disruption of the shelterin complex results in an 'open' and linear conformation, which allows telomerase to act on short telomeres, but also renders the telomere visible to the DNA damage surveillance machinery.

Many components of the shelterin complex have also been found in other organisms. For example, TRF1, TRF2, Rap1 and POT1 homologs have been identified in fission yeast. Furthermore, the structure and function of the shelterin complex in *S.pombe* is very similar to that of mammalian cells. POT1-like proteins are present in nearly all eukaryotes but these orthologs seem to have distinct roles in different organisms (Baumann & Price, 2010). In contrast to fission yeast, budding yeast appear to have a quite different telomere protein components, with Rap1 the only conserved protein of the shelterin complex present in *S.cerevisiae*.

The CST complex

While human cells depend on the shelterin complex to protect their telomeres, budding yeast mainly rely on the CST complex for the same function. In budding yeast, the CST complex consists of Cdc13, Stn1 and Ten1 arranged in a trimeric structure which binds directly to the G tail *in vivo* (Grandin et al, 2001; Grandin et al, 1997). Recently experiments have shown the structure of the CST complex to be remarkably similar to that of the major DNA replication factor Rpa (Gao et al, 2007). Like each Rpa subunit; Cdc13, Stn1 and Ten1 all have OB folds, which are frequently found in ssDNA binding proteins, with the β barrels in the OB fold recognising ssDNA (Theobald & Wuttke, 2004). These results suggest that these complexes may have evolved from a common ancestor. However, unlike Rpa which binds all ssDNA independent of its sequence, Cdc13 of the CST complex binds preferably to telomeric repeat ssDNA.

At telomeres, the CST complex carries out at least two essential functions: telomere capping and telomerase recruitment. The telomere capping ability of CST was first discovered using a temperature sensitive mutant of *cdc13-1* (Garvik et al, 1995). Under non-permissive temperatures, *cdc13-1* accumulates extensive ssDNA at subtelomeric regions which efficiently activates the DNA damage response. Similarly, temperature sensitive *stn1* and *ten1* mutants also display very similar phenotypes to that of *cdc13-1* cells (Grandin et al, 1997). Furthermore, later studies found that the capping function of Cdc13 seems to be dependent on its interacting partners Stn1 and Ten1, and overexpression of *STN1* can provide a capping function in the absence of Cdc13 (Petreaca et al, 2007). These data suggest that Cdc13, Stn1 and Ten1 redundantly protect the telomere.

Interestingly, the telomerase recruitment function of the CST complex can be genetically separated from its capping function (Nugent et al, 1996). An alternative *CDC13* mutant -

cdc13-2^{est2} shows progressive telomere shortening and senescence similar to telomerase negative cells, but has no defects in telomere capping. It was later found that Cdc13 can physically interact with the telomerase component Est1, providing a direct link of the CST complex in the recruitment of telomerase in late S phase of the cell cycle to elongate telomeres (Bianchi et al, 2004; Pennock et al, 2001; Taggart et al, 2002). Cell cycle regulated phosphorylation of Cdc13 by Mec1, Tel1 and Cdk1 was required for telomerase recruitment (Li et al 2009, Tseng et al 2006, 2009, Zhang & Durocher 2010). A recent structural study of Cdc13 revealed that Cdc13 may in fact form a dimer *in vivo*, via its long alpha helix in the N terminal regions, and that dimerisation of Cdc13 is possibly required for the recruitment of telomerase (which also functions as a dimer) (Mitchell et al, 2010).

In addition to telomere capping and telomerase regulation, a new role of the CST complex in telomere replication has recently emerged. It appears that Cdc13 functionally and physically interacts with the catalytic subunit of DNA polymerase α /primase. This interaction might be required to stimulate the activity of polymerase α to fill in the terminal C strand gap that remains after telomerase action (Qi & Zakian, 2000). Furthermore, Stn1 also interacts with Plo12, the regulatory subunit of polymerase α (Grossi et al, 2004).

The CST complex was initially believed to be a unique complex in budding yeast, however, homologs of Stn1 and Ten1 were recently discovered in fission yeast, plant and humans, suggesting that CST is more evolutionarily conserved than originally thought (Martin et al, 2007; Miyake et al, 2009). In humans, a protein called Ctc1 forms a complex with Stn1 and Ten1. Human Ctc1 forms a trimer with Stn1/Ten1; however this complex does not appear to bind the G overhang at telomeres. The human CST seems to have a different role to that observed in budding yeast, because CST was found to associate with only a fraction of telomeres, and its binding to ssDNA is sequence unspecific (Miyake et al, 2009). Curiously, the Ctc1 and Stn1 dysfunction in human cells and plants did not cause the same effect as

observed in budding yeast (Miyake et al, 2009; Surovtseva et al, 2009) . This suggests that plants use alternative telomeric components to provide sufficient end protection. Instead, the human CST complex might be involved in telomere replication (Giraud-Panis et al, 2010).

Since some organisms have both shelterin and CST complexes (*S.pombe*, human and plant), an interesting question still remains as to how these two complexes co-evolved and whether there is any interaction between them. It is known that hCtc binds to telomeres independently of Pot1, but human Stn1 was co-purified with the shelterin component Tpp1, suggesting a physical interaction exists between them (Miyake et al, 2009; Wan et al, 2009).

Ku70/80

The Ku heterodimer complex consists of a 70kDa and an 80kDa subunit, referred to as Ku70 and Ku80, respectively (Fisher & Zakian, 2005). The budding yeast Ku (yku) shares many structural and functional similarities with other organisms. However, yku80 does not contain the C-terminal domain that interacts with DNA-PKcs, whilst this domain is present in vertebrates. Ku was first identified to play an important role in DSB repair; specifically in the non-homologous end-joining pathway (details follow in section 1.8). Mammalian Ku is also involved in the V(D)J recombination, since mice lacking Ku have severe combined immunodeficiency. Consistent with its function in DSB repair, Ku can bind a dsDNA end without the need of any specific sequence (Tuteja & Tuteja, 2000; Walker et al, 2001) . Once bound, Ku70 and Ku80 form an asymmetric ring like structure which can move freely along the duplex DNA (Walker et al, 2001).

Apart from its role at DSBs, Ku also has a conserved role at telomeres. In budding yeast, Ku has been found to directly bind to telomeres and spread several kilobases into the subtelomeric region (Gravel et al, 1998). There is an intriguing interplay between Ku binding at the telomere and Ku binding at a DSB, as the induction of an internal DSB results in relocalisation of Ku to the DSB (Martin et al, 1999). This observation has led to the hypothesis that telomeres may act as a reservoir for factors that are involved in damage repair and that upon the presence of a DSB these factors relocalise to the site of the damage (Martin et al, 1999). The role of Ku at telomeres is quite different to the role of Ku at a DSB. At telomeres, Ku has four primary functions including 1) Regulation of telomere length, 2) protection of telomeres from degradation, 3) protection of telomeres from fusions, and 4) telomere silencing.

The role of Ku in telomere length regulation was first identified when deletion of either *yKu70* or *yKu80* resulted in a dramatic shortening of the telomere (Boulton & Jackson, 1996). It has therefore been suggested that Ku promotes telomere lengthening, and this hypothesis is further strengthened by the discovery that Ku can directly bind to the stem loop region of the *TLC1* component of telomerase. Consequently, it is believed that Ku positively regulates telomere length via a direct interaction with telomerase (Fisher & Zakian, 2005).

In addition, it has also been identified that Ku protects telomeres from degradation and recombination. A role in protecting telomeres from degradation is apparent from the length of the G tails at telomeres. In wild type cells, telomeres acquire long G tails only in the late S phase of the cell cycle, corresponding to the time when they are elongated. However, in *yKu70Δ* or *yKu80Δ* cells, long G tails are present throughout the entire cell cycle (Gravel et al, 1998). This is most likely due to degradation of the C strand at the telomere, as deletion

of the 5' to 3' exonuclease Exo1 suppressed the long G tail phenotype of *yKu80Δ* cells (Bertuch & Lundblad, 2004). The persistent long G tail phenotype of *yKu70Δ* cells does not initially activate the DDR. However, it has been shown that at 37°C the telomere abnormality of *yKu70Δ* is exacerbated and Exo1 degradation of the C strand progresses into the subtelomeres of the chromosomes (Maringele & Lydall, 2002). The extensive ssDNA generated activates a Rad9 dependent checkpoint response, resulting in cell cycle arrest (details follow in section 1.6.2).

A third role of Ku at telomeres is in telomeric silencing (Boulton & Jackson, 1998). The current hypothesis is that Ku is involved in the recruitment of Sir3 and Sir4 to the telomere (Martin et al, 1999). Sir3 and Sir4 along with Sir2 are responsible for initiating and maintaining chromatin silencing at telomeres through histone deacetylation.

The SIR complex

In *S.cerevisiae*, the Sir complex consists of Sir2, Sir3 and Sir4 and was originally identified for its role in silencing at the mating type loci *HMLα* and *HMRα* (Braunstein & Sobel, 1996). Sir2 provides the catalytic component of the Sir complex, and is a NAD⁺ dependent deacetylase required for the deacetylation of K9 and K14 of Histone 3 (H3) and K16 of Histone 4 (H4) (Landry et al, 2000). Deacetylation of the histone tails of H3 and H4 acts as a signal for the recruitment of Sir3 and Sir4 to form the Sir complex along with Sir2. The deacetylation of the histone tails of H3 and H4 leads to the formation of a condensed and compacted chromatin structure which resembles heterochromatin in higher eukaryotes, and is referred to as chromatin silencing in budding yeast (Gartenberg, 2000). Hence, the primary function of the Sir complex is to repress transcription at specific loci by inducing chromatin silencing through histone tail deacetylation. Sir2, as the catalytic component of the Sir complex, is responsible for the initiation of chromatin condensation through histone deacetylation;

whereas it is believed that Sir3 and Sir4 function to maintain the condensed chromatin structure as well as spreading silencing to neighbouring regions. Chromatin silencing induced by the Sir complex is targeted to three regions of the *S.cerevisiae* genome – the telomeres, the mating type loci and the rDNA repeats. This high level of regulation in the recruitment of the Sir complex is brought about by three transcription factors (Rap1, ORC and Abf1) which recruit the Sir complex to its target loci.

An additional role of Sir proteins in promoting chromatin silencing at DSBs has also been discovered, where Sir2, Sir3 and Sir4 have all been shown to relocate to a DSB (Martin et al, 1999; Mills et al, 1999). How the Sir complex is recruited to a DSB break is not clear, as Rap1, ORC and Abf1 are not known to relocate to a DSB. However, there is evidence that Sir3 and Sir4 may interact with Ku at a DSB (Martin et al, 1999). Although the exact role of the Sir complex at DSBs is not fully understood, it has been suggested that the chromatin silencing induced by the Sir complex may be important in promoting NHEJ repair (Tsukamoto et al, 1997).

Rap1

In *S.cerevisiae*, Rap1 (repressor and activator protein 1) is a DNA binding protein which interacts with a host of other proteins. Its most characterised function is at telomeres where it directly binds the double-stranded telomeric repeats. scRap1's function at telomeres is in the negative regulation of telomere length through its interaction with the telomere binding proteins Rif1 and Rif2 (Levy & Blackburn, 2004). Rap1 is thought to regulate telomere length through a negative feedback loop, where increased binding of Rap1 (and therefore Rif1 and Rif2) leads to a reduced recruitment of telomerase. (Levy & Blackburn, 2004). scRap1 is also involved in telomeric silencing at the telomeres, through its interactions with Sir3 and Sir4, which are required for the establishment of telomeric silencing.

scRap1 also has a profound role in the regulation of transcription, as both an activator and repressor of transcription. scRap1's effect on transcription is widespread and is believed to bind ~5% of all promoters in the *S.cerevisiae* genome (Pina et al, 2003). Rap1 is able to bind many promoters by having a very flexible DNA binding motif (Idrissi & Pina, 1999; Vignais et al, 1987).

Central to scRap1's function is its structure. scRap1 is able to bind directly to DNA through a DNA binding domain which contains two Myb-type helix-turn-helix domains (Chong et al, 1995). Once recruited to DNA scRap1 carries out its functions through a range of specific protein-protein interactions, these interactions are carried out through the C-terminal domain of scRap1. Specifically the Sil domain (amino acids 635-827) within the C-terminal domain is required for its interaction with a host of proteins including; Rif1, Rif2, Sir2 and the SWI/SNF complex (Idrissi et al, 2001). Furthermore, deletion of the Sil domain leads to aberrant telomeric silencing and loss of regulation of telomere length (Graham et al, 1999; Wotton & Shore, 1997).

The human orthologue (hRap1) of scRap1 has been identified, and like its budding yeast counterpart is located at telomeres where it is believed to negatively regulate telomere length (Li et al, 2000). However, hRap1 only contains one myb -type helix-turn-helix motif rather than two, and so is unable to bind DNA directly itself. Instead, hRap1 is recruited to telomeres by the shelterin protein Trf2. Like scRap1, hRap1 protein-protein interactions are mediated through its C-terminal domain (Li et al, 2000).

Rif1

The budding yeast Rif1 (scRif1) was first discovered as a Rap1-interaction partner in a yeast two-hybrid assay (Hardy et al, 1992). *RIF1* encodes a large protein of 1916 amino acids with a predicted molecular mass of 219 kDa (NP-009834, NCBI database). scRif1 was found by ChIP to be associated with yeast telomeres throughout the cell cycle, therefore it is thought to be a component of the yeast telomere (Smith et al, 2003b). scRif1 appears to be tethered to telomere repeats by its interaction with the Rap1 C terminus, and immunofluorescence on chromatin spreads confirmed that Rif1 and Rap1 form discrete foci at early S phase (Mishra & Shore, 1999; Smith et al, 2003b).

The most well known function of scRif1 is that it negatively regulates telomere length. In the absence of scRif1, yeast telomeres become elongated to almost human-like length (Hardy et al, 1992; Teixeira et al, 2004). The Rif1 interacting partner Rif2 also has a similar but milder effect. Together Rif1 and Rif2 were shown to synergistically inhibit telomere length (Wotton & Shore, 1997). Because this lengthening is telomerase dependent, the Rif proteins are negative regulators of telomerase. However, the molecular mechanism of how Rif1 inhibits telomerase action is still unknown. A counting mechanism has been proposed by Marcand et al (Marcand et al, 1997), in which they suggest that the number of Rif proteins bound to telomeres is proportionate to telomere length. Therefore longer telomeres have a stronger inhibitory effect on telomerase recruitment. When the telomere shortens, the number of Rif proteins bound to telomeres also reduces, which in turn reduces telomerase inhibition.

Apart from its role on telomere length regulation, a role for Rif1 in silencing at the telomere and mating type loci has also been discovered (Hardy et al, 1992). To date, most of the known functions of Rif1 depend on its interaction with the C-terminus of Rap1. However, new data suggest a genetic interaction between Rif1 and the polymerase α -primase

complex, as deletion of Rif1 greatly enhances the temperature sensitive phenotype of the polymerase α -primase mutants (*pol1-1*, *cdc17-1*, *pri-2*)

Compared to the budding yeast Rif1, fission yeast Rif1 appears to have many conserved functions (Kano & Ishikawa, 2001). In fission yeast, Rif1 is recruited to telomeres via its interaction with the telomere binding protein Taz1. ChIP analyses showed that Rif1 is associated with telomeric DNA. However, it is likely that not all Rif1 is telomere bound. Similar to budding yeast, spRif negatively regulates telomere length but its effect is only mild. In addition, spRif1 has no effect on silencing, however spRif1 deleted cells display a meiosis defect (Kano & Ishikawa, 2001). In fission yeast, telomeres gather at the nuclear envelope during early meiosis, forming a 'bouquet' structure (Tomita & Cooper, 2007). The telomere 'bouquet' persists while the microtubules pull the nucleus back and forth in the cytoplasm; this creates an elongated nuclear shape known as the 'horsetail'. During the 'horsetail' stage, homologous sequences pair up and meiotic recombination occurs. Afterwards the diploid yeast cell goes through two rounds of nuclear division and generates four haploid spores. Fission yeast cells lacking *RIF1* behave normal in telomere clustering in early meiosis; however they display aberrant spore formation and reduced spore viability (Kano & Ishikawa, 2001).

Compared to yeast Rif1, human Rif1 seems to have changed rapidly during evolution. The primary amino acid sequences between *S.pombe*, *S.cerevisiae* and human Rif1 share low sequence homology. Recent bioinformatic studies suggest that the N terminus of Rif1 is conserved in many eukaryotes, however vertebrate Rif1 has a newly acquired C-terminal DNA binding domain (Xu et al, 2010).

In contrast to yeast, human Rif1 is not involved in telomere length regulation, and is not associated with normal telomeres. Instead, it preferentially binds dysfunctional telomeres (Silverman et al, 2004; Xu & Blackburn, 2004). These telomeres are recognized as sites of

DNA damage, causing the accumulation of factors including Nbs1, 53BP1, ATM, Rad17, and γ -H2AX at chromosome ends (known as the telomere dysfunction-induced foci or TIFs). Rif1 was found to co-localise with TIF signal. Additionally, Rif1 is also found to localize at DNA damage sites induced by MMS and IR (Silverman et al, 2004; Xu & Blackburn, 2004).

Apart from its role in the DNA damage response, recent data suggests that hRif1 may also be playing a role in DNA replication (Xu et al, 2010). Rif1 was identified as a novel component of the Bloom syndrome helicase (BLM, homolog of the budding yeast Sgs1), and interacts with BLM via its C-terminal domain. Upon replication stress, both Rif1 and BLM are recruited to stalled replication forks in a similar kinetics, and it was suggested that Rif1 is involved in promoting recovery of stalled replication forks. However, only half of Rif1 in the cell is associated with BLM, hinting that Rif1 may have other functions independent of BLM.

A number of studies suggest that hRif1 may have a role in carcinogenesis. A recent study found that human *RIF1* is fused with another gene called *PKD1L1* in breast cancers as a result of chromosome translocations (Howarth et al, 2008). A mutation screen also showed that a breast cancer cell line had two non-conservative point mutations in *RIF1* (Sjoblom et al, 2006). Furthermore, *RIF1* is highly expressed in human breast tumours (Wang et al, 2009). Together these data suggests that modification of Rif1 may increase the risk of breast cancer.

Rif2

Rif2 was originally identified in a yeast two-hybrid screen of the *S.cerevisiae* genomic DNA library using the Rap1 C-terminus as bait (Wotton & Shore, 1997). *RIF2* encodes a 395 aa protein with a predicted molecular mass of 46 kDa. Interestingly, Rif2 is not related to

scRif1, and no Rif2 homologs have been identified in higher eukaryotes to date. However, Rif2 is believed to have evolved from a common ancestor with the Origin of Replication Complex 4 (ORC4) (Marcand et al, 2008). The yeast two-hybrid assay revealed that Rif2 interacts with the same region of the Rap1 C-terminus as Rif1, however Rif2 also interacts with Rif1 and this interaction is independent of Rap1 (Wotton & Shore, 1997). Rif2 has a role in telomere silencing at *HMR*, however this effect is dependent on Rif1. Furthermore, Rif2 is believed to inhibit NHEJ at telomeres (Marcand et al, 2008).

1.3 Telomere replication and telomerase

1.3.1 Telomere replication

Our current understanding of how telomeres are replicated in higher eukaryotes is still very limited; however some key mechanisms have begun to be elucidated in budding yeast. Essentially, it is thought that the majority of the telomeric DNA is replicated by the conventional semi-conservative DNA replication machinery (Chakhparonian & Wellinger, 2003). As shown in Fig 3.1.1, origin firing occurs internal to the telomeric repeats, which are recognised by the polymerase α - primase complex to initiate replication in association with other polymerases. The G strand and the C strand are replicated by leading and lagging strand synthesis, respectively. While the leading strand is characterised by continuous DNA synthesis, the lagging strand contains short Okazaki fragments that are later extended and substituted by DNA polymerases, followed by ligation of the DNA fragments. However, this

mechanism is not sufficient to maintain telomeres, because removal of the outmost RNA primer on the lagging strand would cause the daughter strand to be shorter than the parental strand. Losing DNA with every cell division, the daughter strand would gradually shorten until telomeres become too short to carry out essential functions. This problem is known as the 'end replication problem', and is commonly encountered in human somatic cells. In many organisms including budding yeast, the end replication problem is solved by telomerase. Interestingly, the leading strand and lagging strand have distinct fates (Bailey et al, 2010). Recent studies in budding yeast found that these two strands are indeed processed differently (Faure et al, 2010). Following telomere replication, the leading strand contains a blunt end and therefore may be sensed as a DSB. This triggers a mild checkpoint response which activates Tel1 and Mec1. These kinases, with the assistance of the major cyclin-dependent kinase Cdk1, recruit the MRX nuclease to the telomere end. MRX resects the C strand revealing the single-stranded 3' overhang, which can be readily bound by the Cdc13-Ten1-Stn1 complex. In contrast, the lagging strand naturally contains a G tail hence does not need further processing, and indeed MRX was not found to be associated with the lagging strand (Faure et al, 2010). Cdc13 in turn recruits telomerase to elongate the G strand, and polymerase α to co-operate in synthesis of the C strand. This replication co-operation is crucial to avoid over-extension of the G tail (Parenteau & Wellinger, 1999) Interestingly telomerase is not recruited to telomeres during every cell cycle. Instead, Est1 and Est2 are associated only with short telomeres during late S phase. Cdc13 does not appear to regulate tethering to short telomeres because Cdc13 was associated independently of telomere length (Bianchi & Shore, 2007). However Tel1 was detected throughout the cell cycle preferentially onto short telomeres. It appears that short telomeres could be a signal for Tel1 or Mec1 recruitment and that they may alter the ability of Cdc13 to recruit telomerase. This could be achieved through Tel1/Mec1 dependent Cdc13 phosphorylation, however the evidence for this is contradictory (Gao et al, 2010; Tseng et al, 2006). In mammalian cells telomerase is active during embryogenesis and in stem cells.

The expression of the enzyme is later down-regulated in adult tissues and this leads to gradual telomere shortening, senescence or apoptosis (Geserick & Blasco, 2006). It is clear that the main function of telomerase in both yeast and mammalian cells is to renew short telomeres. However in mammalian cells telomerase has also telomere-independent functions. These include DNA repair, apoptosis resistance, chromatin structure alteration and gene expression regulation (Choi et al, 2008; Park et al, 2009; Smith et al, 2003b). Such functions have not yet been identified in yeast.

Fig 1.3.1 Telomere replication in *S. cerevisiae*.

1.3.2 Telomerase

The essential components of telomerase, identified in most eukaryotes are the catalytic subunit - telomerase reverse transcriptase (TERT) and the RNA component - telomerase RNA (TR). During DNA replication TERT utilises TR as a template to synthesize new telomere repeats and aids their addition to the chromosome end. Functional telomerase in yeast and mammalian cells forms a dimer and requires additional factors for correct assembly and recruitment to telomeres (Arai et al, 2002; Prescott & Blackburn, 1997). Similarly to other reverse transcriptases, telomerase adds one deoxynucleotide at a time to the 3' overhang. In addition telomerase also possesses a cleaving activity that can process non-telomeric DNA to generate a suitable primer for telomerase (Oulton & Harrington, 2004; Wang & Blackburn, 1997). TERT and other telomerase associated proteins were first identified in screens for gene deletions or mutations that lead to loss of telomeric sequence and decline in cell viability (Lendvay et al, 1996; Lundblad & Szostak, 1989) . These screens uncovered the genes in the ever short telomere epistasis group, named after their short telomere phenotype: *EST1*, *EST2* (TERT), *EST3* and *EST4* (*CDC13*). Interestingly deletion of any of these genes, and mutation from the essential gene *CDC13* leads to the same phenotype: progressive loss of telomeres and senescence. *TLC1* (telomerase component 1) is the yeast telomerase RNA and was later discovered in a screen for genes that cause telomeric silencing when expressed in high levels (Singer & Gottschling, 1994) . After continuous propagation of *tlc1Δ*, *est1Δ*, *est2Δ* or *est3Δ* mutants, rare survivors appear due to activation of telomerase-independent mechanisms for telomere maintenance. Therefore, all genes in this group are indispensable for the *in vivo* function of telomerase, although they have different roles. While *EST2* and *TLC1* encode TERT and TR respectively and are required for the enzymatic activity of telomerase; Est1 and Est4 mostly regulate the recruitment of the enzyme. Est1 interacts with both components of telomerase Est2 and *TLC1* and mediates their association to telomeres via the 3' overhang binding protein Cdc13. These interactions

are essential for telomerase function, as deletion of *EST1* leads to progressive telomere loss, similar to a telomerase null mutant. Two homologs of *EST1* have been found in mammalian cells – hEst1A and hEst1B. *EST3* is a GTPase, that forms dimers through Mg^{2+} co-ordination and is believed to interact with Est2, however the exact role of this protein in the telomerase holoenzyme remains elusive (Shubernetskaya et al, 2011).

1.4 Telomeres and genomic instability

Genomic instability is a feature of almost all human cancers (Negrini et al, 2010), however according to a recent review some patients of acute myeloid leukemia contained normal karyotype (Mrózek et al, 2004). The most common form of genomic instability is called chromosomal instability (CIN), which refers to the increased frequency of changes in chromosome numbers (aneuploidy) or structures (e.g. deletions, insertion, translocations) in cancer cells. Genomic instability is present in all stages of cancer, from pre-cancerous lesions to advanced cancers (Bartkova et al, 2005; Gorgoulis et al, 2005; Lengauer et al, 1997), and tumour cells continue to acquire genomic instability over time (Nowell, 1976).

The first evidence that telomeres are important for maintaining chromosome stability came in the cytogenetic analysis of maize chromosomes by McClintock (McClintock, 1941). In the absence of telomeres, chromosome ends in maize becomes adhesive and tend to fuse to each other, causing cycles of breakage-fusion-bridge patterns. Since then, several hypotheses have been proposed to explain how telomere defects can induce genomic instability in human cancers. One hypothesis (Maser & DePinho, 2002) proposes that during ageing, continuous cell division in the absence of telomerase could lead to telomere

shortening and trigger replicative senescence (Hayflick limit). If somatic mutations occur to inactivate the retinoblastoma/p53 checkpoints, cells could then bypass senescence. Once beyond the Hayflick limit, telomeres continue to degrade until they become extremely short, triggering the fusion-bridge-breakage cycles (Fig 1.4A). This process has the potential to generate the diverse chromosome abnormalities that is associated with carcinogenesis. In addition, it is known that cancer incidence increases exponentially near the end of human life (McMurray & Gottschling, 2003), and this hypothesis could explain the strong correlation between cancer and ageing.

A second hypothesis proposes that the increased amount of spontaneous DSB induction at the telomere/ subtelomeric regions could drive genomic instability (Fig 1.4 B)(Murnane, 2010). According to this hypothesis, pre-cancerous cells experience increased replication stress due to continuous cell division, which leads to stalled replication forks at regions that are difficult to replicate (Tsantoulis et al, 2008). These regions are known as fragile sites and telomeres and subtelomeric regions are shown to be fragile sites in mammalian cells (Sfeir et al, 2009). If the replication fork is not stabilised, it could collapse and be processed into a DSB. At normal telomeres, classical HR and NHEJ repair mechanisms are mainly inhibited, thus cells would resort to repair the broken chromosome by illegitimate repair pathways, such as alternative NHEJ (A-NHEJ). This eventually leads to breakage/fusion/bridge cycles and gross chromosome rearrangement.

The third possibility is that telomere uncapping could contribute to genomic instability. E.g. inactivation of the human shelterin complex component Trf2 results in chromosome end fusions, anaphase bridges that are typically observed in human cancers (van Steensel et al, 1998). The fused chromosome ends contain telomeric DNA. However, no direct evidence suggests that telomere uncapping could happen in humans, possibly because most of the shelterin components are essential for embryonic development.

Fig 1.4 A. Telomere attrition induced breakage-fusion-bridge cycle. B. Proposed model for spontaneous telomere loss in cancer cells.

1.5 The G2/M DNA damage checkpoint response in budding yeast

The G2/M checkpoint is the primary checkpoint response to DSBs as well as uncapped telomeres. In response to a DNA lesion components of the G2/M checkpoint will induce cell cycle arrest at the G2/M stage of the cell cycle and activate factors involved in the repair of DNA. All checkpoint pathways follow the central dogma of: DNA damage signal – sensor kinases – transducer kinases – effector kinases (A. John Callegari, 2007). In the G2/M checkpoint the DNA damage signal is Rpa bound single stranded DNA. In the event of a DSB (repaired by homologous recombination) or uncapped telomere exonucleases are recruited to the site of damage where they degrade one strand of DNA in the 5'-3' direction (several exonucleases are involved in this process including Exo1 and the MRX complex) (Bernstein & Rothstein, 2009) . ssDNA serves as the substrate for the binding of Rpa which binds along the whole length of the newly generated ssDNA to act as the damage signal. This damage signal is detected by two proteins, which belong to a group of proteins with similarity to phosphatidylinositol 3-kinases (PIKKs), which are Mec1 (ATR in mammals) and Tel1 (ATM in mammals) – although Mec1 is the primary sensor kinase in response to DSBs (Harrison & Haber, 2006b). Mec1 forms part of a heterodimer along with its binding partner Ddc2, Mec1 itself does not bind DNA but is instead recruited to the site of damage by Ddc2 which does bind DNA. In addition to the PIKKs, there is also a third sensor kinase referred to as the 9-1-1 complex. The 9-1-1 complex is a heterotrimeric ring structure composed of Ddc1-Mec3-Rad17 (mammalian homologues: Rad9-Hus1-Rad1) which is loaded by Rad24-Rfc onto the junction between double stranded and single stranded DNA generated by exonucleolytic degradation of the 3'-5' strand (Kondo et al, 2001). In the case of DSBs loading occurs on the 3' dsDNA/ssDNA junction, this specificity is dependent on Rpa. The co-localisation of both Mec1 and the 9-1-1 complex is essential for a fully functional G2/M checkpoint response (Majka et al, 2006). Once recruited to damaged DNA, the 9-1-1 complex is believed to

activate the kinase activity of Mec1, and once activated Mec1 is able to phosphorylate downstream targets of the signal transduction pathway which in turn induce cell cycle arrest (Majka et al, 2006). The immediate target of activated Mec1 is the transducer kinase Rad9, which is recruited to the site of damage via specific histone modifications (e.g. γ -H2AX and H3K79me) mediated by Mec1. Subsequently, Mec1 phosphorylates Rad9 which in turn recruits the effector kinase Rad53 for phosphorylation by Mec1 (Lisby et al, 2004). Phosphorylated Rad53 then dissociates from the DNA damage foci and multimerizes allowing auto-phosphorylation of Rad53. Rad53 is then able to interact with a number of downstream targets which affect the cell cycle machinery as well as up-regulating genes involved in the repair of DNA damage (Harrison & Haber, 2006a).

Fig 1.5 G2/M DNA damage checkpoint in *S.cerevisiae*.

1.6 Telomere uncapping model systems

1.6.1 The *cdc13-1* model system

The first model system for studying telomere uncapping was *cdc13-1* (Garvik et al, 1995). In this system a point mutation (P371S) in the 3' telomere overhang binding protein Cdc13 leads to a temperature sensitive phenotype. This point mutation only affects the telomere capping function of Cdc13 and does not influence telomerase recruitment (Nugent et al, 1996). Furthermore *cdc13-1* cells have intact DNA binding ability and associate with Ten1 and Stn1 (Grandin et al, 2001; Hughes et al, 2000).

Temperatures that allow *cdc13-1* growth are called permissive and temperatures at which the strain fails to grow are termed non-permissive or restrictive. The permissive temperature for *cdc13-1* is below 26°C when the cells have a wild type phenotype. At restrictive temperatures above 26.5°C the cells increase in size and arrest in G2/M phase in a characteristic dumbbell shape. This happens because at non-permissive temperatures the mutant *cdc13-1* fails to cap the telomere, which leads to extensive resection of the 5' strand spanning up to 30kb into the chromosome (Booth et al, 2001; Garvik et al, 1995). The main exonuclease responsible for single stranded DNA damage in *cdc13-1* is Exo1 (Booth et al, 2001; Zubko et al, 2004). However ssDNA is still present in *cdc13-1 exo1Δ* double mutants suggesting that Exo1 is not the only exonuclease acting at uncapped telomeres. These have not yet been identified, however Mre11, Sae2, Sgs1 and Dna2 contribute together with Exo1 in DSB processing (Mimitou & Symington, 2008; Raynard et al, 2008; Zhu et al, 2008). None of those candidates have been confirmed at uncapped telomeres. Mre11 has been found to participate in telomere capping rather than resection in *cdc13-1* (Foster et al, 2006).

Interestingly, some checkpoint proteins have been found to regulate ssDNA production. Rad24 drives resection, while Rad9 participates in ssDNA inhibition (Zubko et al, 2004).

After the telomere has been processed checkpoint sensors are responsible for DNA damage recognition. In *cdc13-1* these are the PCNA-like clamp Ddc1-Mec3-Rad17, loaded onto DNA by the clamp loader Rad24-Rfc and Ddc2-Mec1, which is recruited through Ddc2's interaction with Rpa coated single stranded DNA. The signal is transduced downstream to Rad9.

Two paralleled DNA damage checkpoint pathways downstream of Rad9 regulate the arrest in *cdc13-1*. These are Rad53-Dun1 and Chk1-Pds1 (Gardner et al, 1999). Rad53-Dun1 regulates the mitotic exit network (MEN) and Chk1-Pds1 modulates the Cdc fourteen early anaphase release (FEAR) (Liang & Wang, 2007). This way the DNA damage checkpoint prevents exit from mitosis. During normal cell cycle progression Pds1 is stabilized by phosphorylation from the cyclin-dependent kinase Cdk1 (Enserink & Kolodner, 2010). In damaged *cdc13-1* cells Chk1 phosphorylates and prevents Pds1 degradation leading to arrest (Wang et al, 2001). Phosphorylated Pds1 binds the separin Esp1 preventing chromosome segregation. Only when Pds1 is dephosphorylated by the phosphatase Cdc14 can it be degraded and release Esp1.

In addition to the DNA damage checkpoints, the Bub2 branch of the spindle damage checkpoint also contributes to *cdc13-1* arrest; this is achieved through regulation of the MAN pathway (Grandin & Charbonneau, 2008; Maringele & Lydall, 2002).

Fig 1.6.1 Schematic representation of checkpoint pathways in *cdc13-1* cells leading to G2/M arrest.

1.6.2 The *yku70Δ* model system

Yku70Δ cells represent another model system to study telomere uncapping in budding yeast. Similar to *cdc13-1*, deletion of *YKU70* or *YKU80* also triggers telomere uncapping, which activates the G2/M checkpoint at non-permissive temperatures (37°C for *yku70Δ*). Exo1 is responsible for the degradation of the C strand whereas Mre11 is protective for ssDNA generation in *yku70Δ*.

Despite these similarities, there are several different aspects between these two model systems. For example, the resection rate in *yku70Δ* is much slower than that in *cdc13-1*. In *yku70Δ* cells after prolonged incubation at 37°C, ssDNA only reaches the subtelomeres but not internal loci (Maringele & Lydall, 2002). Consistent with smaller amounts of ssDNA generation, *yku70Δ* cells grown at non-permissive temperatures activate a different set of checkpoint proteins in the DNA damage response: Chk1, Mec1, and Rad9 are all required for efficient cell cycle arrest of *yku70Δ* cells at 37°C. However, the 9-1-1 complex and dun1 play insignificant roles (Maringele & Lydall, 2002).

The molecular basis of the temperature sensitivity of *yku70Δ* mutant still remains an enigma. It is known that in addition to the telomere capping defect, *yku70Δ* mutants also display other abnormalities e.g. telomere shortening and over-elongated G tails (Gravel et al, 1998). However these abnormalities do not activate the checkpoint response at permissive temperatures. It was recently found that *yku70Δ* cells progressively lose telomere repeats at non-permissive temperatures (Gravel & Wellinger, 2002), therefore it was suggested that this loss accounts for the temperature sensitivity of these cells. An alternative theory for the temperature sensitivity of *yku70Δ* cells is that very short

telomeres in *yku70Δ* cells along with its long G tail triggers a reorganisation of the telomere structure, and this structure is temperature sensitive.

1.7 Checkpoint adaptation

After a prolonged cell cycle arrest, budding yeast cells can re-enter the cell cycle by either successfully repairing the DNA damage (checkpoint recovery), or by inactivating checkpoint pathways despite still harbouring the unrepaired damage (checkpoint adaptation). Checkpoint adaptation was first demonstrated in budding yeast (Sandell & Zakian, 1993). In this experiment, an irreparable DSB was induced near a telomere in wild type cells, causing the loss of a telomere. These cells were initially arrested at G2/M phase of the cell cycle, however, after 8-10hrs most of cells resumed cell cycle, despite still harbouring the broken chromosome. Strikingly, the broken chromosome can be normally replicated and segregated in yeast cells for as many as 10 cell divisions without triggering subsequent cell cycle arrest. This experiment demonstrates that yeast cells can adapt to a broken chromosome. Using this system, it is possible to screen for adaptation mutants, because compared to WT cells that can form microcolonies after the cell cycle arrest, adaptation defective mutants remain permanently arrested as large-budded cells (Toczyski et al, 1997). *Cdc5-ad* was the first characterised adaptation mutant; it contains a single mutation in the *CDC5* gene, which encodes an essential polo-like kinase. Cdc5 can phosphorylate many downstream targets and is required for the completion of anaphase. Other genes required

for checkpoint adaptation include *CKB1* and *CKB2*, which encodes the non-essential regulatory subunit of casein kinase II (Toczyski et al, 1997).

Similarly, yeast cells were also found to be able to adapt to an internal, irreparable DSB. Interestingly, wild type cells can only adapt to a single DSB but not to two or more DSBs. *Cdc5* and *Yku70* were found to be required for this adaptation process (Lee et al, 1998). However, these two proteins act through distinct pathways, because *yku70Δ* mutant has a much increased rate of 5'-3' resection compared to wild type, whereas *cdc5-ad* did not affect resection (Lee et al, 1998; Pellicoli et al, 2001). In addition, the helicases *Sae2* and *Srs2* have been found to be required for adaptation (Clerici et al, 2006). Overexpression of *SAE2* completely rescued the adaptation defect caused by *cdc5-ad*. Deletion of *Sae2* did not affect resection, and it was suggested that *Sae2* functions by modulating the association of the MRX complex at damaged DNA ends. Furthermore, histone modification also plays a role in adaptation (Clemenson & Marsolier-Kergoat, 2009).

Interestingly, yeast cells can also adapt to persistent telomere damage triggered by *cdc13-1* mutation. In an experiment by Toczyski et al, after 24hrs at the non-permissive temperature of 32°C, the majority of the *cdc13-1* cells formed small microcolonies, whereas *cdc5-ad* and *ckb2Δ* mutation remained arrested at G2/M phase (Toczyski et al, 1997). It therefore seems that *yku70Δ* cells can also adapt to telomere uncapping as they form microcolonies at 37°C (Maringele & Lydall, 2002).

Despite the progress in characterising adaptation defective mutants, the molecular mechanism of checkpoint adaptation is only beginning to emerge. The prevailing view is that central to checkpoint adaptation, checkpoint effectors like *Rad53* and *Chk1* must be inactivated. Four lines of evidence support this idea. (1) Loss of *Rad53* phosphorylation and kinase activity always accompanies the adaptation process in time. Also, *Chk1* is

dephosphorylated during adaptation (Pellicoli et al, 2001). (2) Rad53 phosphorylation remains high in *yku70*, *cdc5-ad*, *sae2Δ* cells which are defective in adaptation (Clerici et al, 2006; Pellicoli et al, 2001). (3) Removing the PP2C-like phosphatases Ptc2 or Ptc3, which directly interact with Rad53, leads to an adaptation defect (Leroy et al, 2003). (4) Cdc5 seems to operate in the same pathway as Rad53, either as a substrate of Rad53, or is involved in a feedback loop to switch off Rad53 (Pellicoli et al, 2001; Sanchez et al, 1999). Since Ptc2 is a phosphorylation substrate of Ckb1 and 2 (Leroy et al, 2003) while Rad53 is a potential target of Ptc2 and Ptc3, it was proposed that Cdc5, casein kinase II and PP2C-like phosphatases may act in a common pathway to inactivate Rad53, therefore allowing checkpoint adaptation (Syljuasen, 2007) (See Fig 1.7)

A second hypothesis for the molecular mechanism of adaptation is that the initial DNA structure that triggers the checkpoint response becomes processed into a non-signalling structure over time (Clemenson & Marsolier-Kergoat, 2009). It is a less explored hypothesis because at this time, the precise pathological DNA structure that triggers checkpoint response is still under debate. The fact that many adaptation mutants such as *yku70Δ*, *Sae2Δ*, *Srs2Δ* have DNA end processing activity supports this idea.

Why would cells adapt to irreparable damage? It is suggested that adaptation would allow yeast cells to repair the damage in the subsequent cell cycle therefore increasing the chances of survival for individual cells (Galgoczy & Toczyski, 2001). Thus, for unicellular organisms like yeast, adaptation could confer an evolutionary advantage. Intriguingly, however, adaptation has recently been discovered in *Xenopus laevis* in response to the replication inhibitor aphicolin (Yoo et al, 2004) and in human cancer cells in response to γ -irradiation (Andreassen et al, 2001; Syljuåsen et al, 2006). It has been suggested that adaptation in higher eukaryotes may be required for triggering apoptosis, a safer choice for multi-cellular organisms (Lupardus & Cimprich, 2004).

Fig 1.7 A possible adaptation controlling pathway in budding yeast

1.8 Non-Homologous End Joining and Homologous Recombination

DSBs present a severe threat to genomic stability because a lack of repair may result in loss of the damaged chromosome during mitosis. Furthermore, a broken chromosome could easily fuse to other chromosomes and lead to chromosome translocations and neoplastic transformation (Burma et al, 2006). Therefore cells have evolved two complex mechanisms to efficiently repair DSBs: the Non-Homologous End Joining (NHEJ) and the Homologous Recombination (HR) pathways. In mammalian cells NHEJ is also important for repair of DSBs produced during V(D)J recombination.

HR uses homologous sequence as a template to repair the DSB, and is the primary repair pathway in the G2 phase of the cell cycle when the homologous sister chromatid is available as the donor. Since a template is used, DSB is repaired with high fidelity. In contrast, NHEJ is a simple end-to-end ligation method for joining in the DSB, hence does not need any homologous sequence. As a consequence, NHEJ can be error-prone. In yeast and humans, NHEJ is predominant in G1 phase of the cell cycle. The choice between NHEJ and HJ repair pathway is dictated in part by the extent of 5'-3' resection of the DNA ends. This resection has recently been shown to be controlled by the master cell cycle kinase Cdk1 (Ira et al, 2004) .

The core vertebrate NHEJ machinery includes the Ku70/80 heterodimer, DNA-dependent protein kinase (DNA-PK_{CS}) and DNA ligase complex. These factors are sufficient to join compatible DNA ends that have a free 5' phosphate and a free 3' hydroxyl group. A similar subset of NHEJ proteins is found in yeast comprising of γ Ku70/ γ Ku80 and the yeast DNA ligase complex Dnl4/Lif1 (Krogh & Symington, 2004). Budding yeast also contains the MRX complex comprising Mre11, Rad50 and Xrs2, and this complex is the homolog of the

vertebrate MRN complex (Mre11-Rad50-Nbs1). To date no known DNA-PKcs have been identified in budding yeast.

Upon a DSB, the yKu70/yKu80 complex recognises the broken DNA ends and binds them together with the MRX complex (see Fig 1.8). The yKu complex forms a basket structure that can cap a double stranded DNA end and bring the ends together (Aylon & Kupiec, 2004). Mammalian studies show that Ku sliding onto the DNA requires no ATP (de Vries et al, 1989; Ristic et al, 2003). After yKu assembles onto the broken chromosome it recruits the yeast DNA ligase complex Dnl4/Lif1, which is analogous to the mammalian Ligase VI/XRCC4. Interestingly, most DSBs need to be processed before NHEJ can occur by either small deletions or extra nucleotide additions at the DNA end, leading to an error-prone repair. The MRX complex has been found to be important for this processing (Chen et al, 2001a). When NHEJ fails to repair a DSB, the HR mechanism ensures repair. There is evidence showing that the NHEJ machinery assembles at each DSB but if no repair occurs, the broken ends are resected allowing repair through HR (Aylon & Kupiec, 2004). Resection is carried out by different exonucleases. Mre11/Sae2 complex initiates this process but Exo1 and Sgs1/DNA2 lead to further 5' to 3' resection (Mimitou & Symington, 2008; Zhu et al, 2008). Immediately after resection, the naked ssDNA is coated by Rpa. Afterwards Rad51 displaces Rpa and binds the newly formed 3' overhang and this process requires Rad52 and is also mediated by Rad54, Rad55 and Rad57 (Sugawara et al, 2003). This way Rad51 can form filaments at the DSB that facilitate the search for a suitable region of homology that can be either double stranded or single stranded DNA. Rad55 and Rad57 are also required for stabilization of the Rad51 filaments. Consequently the HR machinery facilitates strand invasion and alignment with the homologous region, which is then used as a template for an error-free repair.

Fig 1.8 A comparison between NHEJ and HR.

1.9 Cellular senescence and crisis

Cellular senescence is defined as the gradual decline in the proliferation capacity of cells, leading to permanent, irreversible growth arrest. This process usually occurs in multicellular organisms after a defined number of cell divisions and is also termed as the Hayflick limit. A number of factors govern the onset of senescence, including the down-regulation of telomerase in adult mammalian cells, DNA damage responses that triggers cell cycle arrest, and ectopic expression or suppression of certain genes (Rodier & Campisi, 2011). Due to the diversity of cells in the human body it is difficult to name any senescence specific markers, however senescent cells display a number of features, e.g. more than twofold increase in size, expression of the senescence-associated β -galactosidase and p16INK4a, persisted DDR foci, and the secretion of certain factors and cytokines (Rodier & Campisi, 2011).

When telomeres shorten and the cells become senescent they enter Mortality Stage 1 (M1). However upon inactivation of the tumour suppressor p53 or retinoblastoma (Rb) protein, human cells can bypass senescence and continue to proliferate. At this point the cells have extremely short telomeres and enter Mortality Stage 2 (M2) or crisis. These cells experience high levels of chromosomal instability and apoptosis. (Bassi & Sacco, 2009; Hara et al, 1991; Shay & Wright, 1989). Only about one in a million cells become immortalised, usually through telomerase re-activation.

Since yeast cells continuously express telomerase, cellular senescence is not observed in culture. However a senescence phenotype can be observed upon deletion of telomerase components. The most commonly used model of senescence in yeast is the *t/c1Δ* mutant, where the RNA component of telomerase has been removed. These cells are characterised by an increase in size and progressive telomere shortening which triggers a checkpoint response and permanent cell cycle arrest (Singer & Gottschling, 1994). Interestingly, the

only difference in the checkpoint response between a critically short telomere and a DSB appears to be the lack of Mrc1 requirement for signal transduction in DSBs (Grandin et al, 2005; Kondo et al, 2001).

1.10 Type I and Type II survivors

Similar to mammalian cells, *tlc1Δ* cells can escape senescence but in this case the mechanism is different because re-activation of telomerase is impossible. Instead, yeast cells use HR to amplify telomere and subtelomere regions and maintain telomeres (Lundblad & Blackburn, 1993). The appearance of these survivors depends entirely on the HR gene *RAD52*. In the majority of the survivors, the Y' element are copied several times and the cells continue to proliferate slowly and remain immortal. These survivors are called type I survivors (Chen et al, 2001b; Teng & Zakian, 1999). Apart from *RAD52*, the emergence of type I survivors also is dependent on several other genes including *RAD51*, *RAD54*, *RAD55*, *RAD57*. In about 10% of the survivors, the TG repeats will be copied, leading to very long and heterogeneous telomeres and these survivors are known as type II survivors. Type II survivors grow as fast as telomerase-proficient cells and require the MRX complex together with *RAD52*, *RAD59*, *SRS2*, *SGS1* and *TID1* for survival but is *RAD51* independent (Chen et al, 2001b; Teng & Zakian, 1999). Furthermore, formation of type II survivors can be inhibited by both Rif1 and especially Rif2 (Teng et al, 2000). About 10% of human cancer cells that do not re-activate telomerase use a similar mechanism to amplify their telomeres. This mechanism is termed ALT for alternative lengthening of telomeres (Henson et al, 2002). ALT cells have telomere associated foci that contain DDR proteins such as Rad52 and RPA (Henson et al, 2002). These foci are called ALT-associated PML bodies or APBs. Rif1 has been found to co-localise to APBs in some ALT cells (Silverman et al, 2004).

1.11 PAL survivors

It was previously thought that telomerase and recombination were the only two ways of maintaining linear chromosomes in budding yeast. However, it was later discovered that yeast survivors (PAL survivors) can use a third mechanism to maintain viability: by forming large palindromes near chromosome ends (Maringele & Lydall, 2004). When *tlc1Δ rad52Δ exo1Δ* strains were generated, they lacked telomerase activity and homologous recombination, however, about half of the tested strains still escaped senescence after a period of propagation on plates (Maringele & Lydall, 2004). Early survivors grew slowly but their growth rate increased significantly at a later stage. The established survivors could grow as well as WT cells and seem to be immortalised, as they kept growing after 300-400 days in the culture. After 100 days, most survivors had lost telomeric sequences but still maintained linear chromosomes with abnormal size. DNA microarray analysis revealed a large numbers of gene duplications and deletions at chromosome ends in PAL survivors; and in some cases, the duplications were extremely large and spanned the entire chromosome arm. These duplications were found to be inverted repeats i.e. palindromes. Little is known about how palindromes form in PAL survivors; however it was found that palindrome junctions contained wild type inverted repeats. Therefore it was proposed that short inverted repeats naturally present in the genome can catalyse palindrome formation in PAL survivors (Maringele & Lydall, 2004). Once formed, palindromes may contribute to cell viability by amplifying essential genes close to chromosome ends, which would otherwise be lost during constant degradation (Maringele & Lydall, 2004).

A central question on the emergence of all types of survivors including PAL survivors (and perhaps also human pre-cancerous cells), is that how do they overcome the checkpoint barrier to continue cell cycle progression? The current hypothesis for PAL survivor generation requires three major steps: 1) adaptation to telomere defects, 2) early post-

senescent stage and 3) activation of strategies for long term chromosome maintenance (see Fig 1.11.1 for details). The first step is known as checkpoint adaptation, a process where cells override the cell cycle arrest with unrepaired damage (Toczyski et al, 1997). To date, it is still not known what factors are required for adaptation to extremely short telomeres.

PAL survivors exhibit some unusual characteristics that resemble cancer cells. For example, both PAL and cancer cells can activate alternative mechanisms for long term maintenance of chromosome ends; while PAL survivors rely on palindromes, ~5% of cancer cells activate the ALT pathway (Reddel & Bryan, 2003). Additionally, PAL survivors display chromosome instability (i.e. deletions, duplications and palindromes), the hallmark of cancer cells; hence identifying factors that are required for survival of PAL survivors may be relevant for understanding the initiation and maintenance of CIN.

In our lab, a screen was performed to identify proteins that are essential for the survival of *tlc1Δ rad52Δ exo1Δ* cells (Laura Maringele, unpublished data). Proteins that have been tested include the non-essential telomeric proteins Est2, Tel1, Mre11, Yku70, Rif1 and Sir3. As shown in Figure 1.11.2, about half of the tested *tlc1Δ rad52Δ exo1Δ* strains escaped senescence and generated PAL survivors. While deletion of *EST2*, *TEL1*, or *SIR3* did not affect survival rates, deletion of *MRE11* alone or with *YKU70* dramatically increased survival rate. However, by contrast, none of the strains with *RIF1* deletion escaped senescence. Therefore, among all the tested telomeres-associating proteins, Rif1 is the only one that is essential for the survival of PAL survivors.

Fig 1.11.1 A proposed model for PAL survivor generation (Maringele & Lydall, 2004).

Fig 1.11.2 Survival of *tlc1Δ rad52Δ exo1Δ* strains carrying deletions in non-essential telomere interacting genes.

1.12 Aim

The aim of my PhD project is to further investigate the essential role of Rif1 in the survival of *tlc1Δ rad52Δ exo1Δ* cells, and to elucidate the molecular mechanisms of how Rif1 confers protection in PAL survivors. Additionally, I will investigate whether Rif1 also contributes to cell survival in response to different types of telomeric and non-telomeric DNA damage. For this purpose I will use two telomeric uncapping model systems, the *cdc13-1* and *yku70Δ* cells, and an inducible DSB system. Since each system contains different types of DNA damage, using different systems would allow me to perform a detailed and comprehensive study of Rif1 function under different conditions. Furthermore, I would like to investigate potential protein modifications of Rif1 and to identify whether Rif1 modification can regulate its function. Specially, I would like to address these following questions:

- Is Rif1 required for checkpoint adaptation to telomere damage in *tlc1Δ rad52Δ exo1Δ* cells?
- Is Rif1 required for checkpoint adaptation to uncapped telomeres and DSBs?
- Does Rif1 contribute to the survival of telomere uncapped cells including *cdc13-1* and *yku70Δ* cells?
- Can Rif1 be recruited to non-telomeric chromosome ends such as those in PAL survivors and DSBs?
- Does Rif1 contain specific functional domains?
- Is Rif1 protein modified during DNA damage and how does it affect its function?
- Is Rif1 involved in DNA damage repair at DSBs and at uncapped telomeres?

Chapter II: Materials & Methods

2.1. Yeast strains

All yeast strains used were in the W303 background, containing the following mutations: *ade2-1 trp1-1 can1-100 leu2-3, 112 his3-11,15 ura3 GAL+ psi+ ss1l-d2 RAD5*. Yeast Strains are listed in Table 2.1.1

2.2 Recipes for yeast media

1) YEPD

For 1 L medium: 10 g yeast extract (Difco), 20 g Bacto peptone (Difco) were mixed in 945 ml 18.2mQ water. For solid medium: 20 g Bacto agar was also added to the mixture, then the mixture was autoclaved and cooled to 60°C before 50 ml sterile 40% (w/v) dextrose and 5 ml sterile 1% adenine were added.

2) YEP-Raffinose and YEP-galactose

20% (w/v) raffinose (Formedium) or galactose (Sigma) stock was prepared by dissolving the sugar in dH₂O and filter sterilisation. Medium was prepared the same as for YEPD media expect that raffinose or galactose was added to a 2% final concentration.

3) Complete minimum medium

For 1 L solid medium: 1.7 g of yeast nitrogen base (Difco), 5 g of ammonium sulphate (Sigma), 20 g of Bacto agar, and 1.3 g of amino acid powder missing the appropriate amino acid (e.g. –ura means all amino acids without uracil), were mixed in a bottle and 945 ml

distilled water was added. The mixture was autoclaved and cooled to 60°C before 50 ml sterile 40% (w/v) dextrose and 5 ml sterile 1% (w/v) adenine was added.

4) Antibiotic selective medium

Final concentration of 400 µg/ml of G418 (Formedium) or 100 µg/ml of Natamycin/Nourseothricin-dihydrogen sulphate (Werner BioAgents, 5001000) were added to cooled YEPD medium to make G418 or Natamycin plates.

Table 2.1.1 Yeast strains used in this study.

2.3 Cryogenic storage and growing of yeast strains

All yeast strains were stored in 15% sterile glycerol in Nunc CryoTube vials (377267; 479-6843) and frozen at -80°C. Strains were taken out by a sterile toothpick from the stock and gently streaked on YEPD plates and incubated at the appropriate temperature before experiment.

2.4 Mating and sporulation

Haploid yeast cells with opposite mating types were mated on solid YEPD plates by mixing the cells together. After two-day incubation at 23°C, cells were transferred to selective plates for diploid screening. The diploid should contain markers from both parents. Diploid yeast cells were grown to saturation in 1.5 ml YEPD on a rotating wheel at 23°C. 0.5 ml of the saturated culture was washed twice in sterile H₂O and resuspended in 2 ml 1% potassium acetate (Sigma). Strains were supplemented with appropriate amino acids. Sporulation occurred at 23°C on a rotating wheel for 2-3 days. The presence of spores was examined by phase contrast microscopy. When 70% of cells have sporulated, the culture was washed twice in 5 ml sterile water at 1 500 rpm for 3 min. Cell pellets were resuspended in 0.5 ml of 1 mg/ml sterile zymolase solution (Seikagaku Corporation) with 10 µl of β-mercaptoethanol (Sigma) . Cells were incubated at 30°C overnight on a wheel to lyse the sac around tetrads. In the next days, spores were washed in sterile water and resuspended in 5 ml of detergent 1.5% Igepal (Sigma). After 15 min of incubation on ice,

spores were separated by sonication for 30 sec at 10 μ A, and then centrifuged at 4 500 g for 1 min. Then, spores were resuspended in 1 ml of 1.5% Igepal, and sonicated again as described. Finally, spores were spun down at 13 000 rpm for 20 sec, resuspended in 1 ml water and vortexed vigorously to get single spores. The number of spores was counted using a haemocytometer, and spores were seeded on each selective plate. Spores were then germinated at 30°C for 3-4 days. Geminated spores were streaked on a fresh YEPD plate. The YEPD plate was incubated overnight at 25°C, then replica plated onto selective plates to determine the genotype of spores.

2.5 Passage of telomerase negative strains on YEPD plates

After selection, *tlc1 Δ* spores were streaked on a fresh YEPD plate (day 0). Additional gene deletions (e.g. *rif1 Δ*) was verified by PCR, and those with the correct gene deletions were passaged on fresh YEPD plates. From this point, about equal amounts of yeast cells (~10 million cells) were passaged every 5 days on solid YEPD plates. Images were captured using the Fujifilm Luminescent Image Analyser (LAS-3000).

2.6 Spot test

Yeast cells were grown on fresh YEPD plates overnight at 23°C. In the morning, a small amount of cells were transferred by a toothpick from plates to a 1.5 ml eppendorf containing 500 μ l YEPD. The number of cells was determined on a haemocytometer and samples were diluted to 2×10^7 cells/ml in 200 μ l of YEPD liquid. Then, samples were serially diluted in a sterile 96 well plate by a multi-channel pipette, with 5 fold dilution between each column. The plate was covered up to avoid contamination. Meanwhile, a frog ponder was sterilised by dipping in 100% ethanol and flaming twice so that no ethanol remained on

the metal probes. Then the frog ponder was cooled on the bench for several minutes before transferring diluted samples on YEPD plates. This was done by gently lowering the frog ponder on to the plate, and touching the plate for 1 sec and lifting up very quickly. Plates were dried and incubated at the appropriate temperatures for several days and photos were captured by the Fujifilm Luminescent Image Analyser (LAS-3000).

2.7 Scoring of G2/M arrested cells

1 ml of yeast culture was harvested in 1.5 ml eppendorf and spun down in a benchtop centrifuge, at top speed for 5 seconds and the supernatant was removed by aspiration. The cells were resuspended in 70% ethanol. To stain the cells, samples were washed with dH₂O once at 13 000 rpm for a few seconds, and resuspended in 200-300 µl of DAPI solution (2 µg/ml, Sigma). Samples were separated by sonication at 5 µA for 5 sec, and examined under a fluorescent microscope. There are four cell types representing four stages from the cell cycle. Single cells with one nucleus were regarded as cells in G1; budded cells with a bud 50% smaller than the mother cell and with one nucleus represented cells in S phase; budded cells with a bud greater than 50% of the mother cell with the nucleus in one cell or a nucleus positioned between the mother cell and the bud were considered as in G2/M phase; and cells with two nuclei separated between the mother and daughter cells were scored as late M phase. 300 cells were scored for every sample.

2.8 Gene disruption using Longtine plasmids

2.8.1 One-step gene deletion and tagging

Gene deletion and tagging was performed by one-step *in vivo* substitution of the wild type gene with a PCR fragment amplified from a plasmid (Longtine plasmids or their derivatives) (Longtine et al, 1998; Van Driessche et al, 2005). This reaction relies on homologous recombination using at least 40bp homologous sequence flanking the target gene. The PCR fragment contained varied selective markers, such as Kanamycin and Natamycin, therefore allowing the selection of transformed cells.

For example, the plasmid pFA6a-kanMX6 was used as a template to create a PCR fragment that contains the gene for G418 resistance. The forward primer was designed to anneal to the first 20 bp of the *KanMX6* gene, and also contained 40bp homologous sequence to the upstream sequence of the gene of interest. The reverse primer annealed to the last 20bp of *kanMX6* and had homology to downstream sequence of the gene of interest. After homologous recombination, this PCR product will be integrated in the place of the target gene, resulting in gene deletion.

The same principle applies for gene tagging. For example, to tag *RIF1* with *MYC::kanMX6*, the forward primer was designed to anneal just upstream of the stop codon of *RIF1*, and the reverse primers was designed to anneal just downstream of the stop codon of *RIF1*. This way the *MYC::kanMX6* cassette will be integrated and following translation the Myc tagged Rif1 protein will be produced. The plasmids used for the gene tagging were pFA6a-13myc-kanMX6 and pFA6a-3HA-natMX6.

To amplify the cassettes containing selective markers, PCR reactions were set up as follows:

Master Mix for each reaction:

39 μ l ddH₂O

5 μ l 10 x Ex Taq Buffer - Takara Bio Inc.

5 μ l dNTPs (2.5 mM) – Takara Bio Inc.

2 μ l pFA6a-kanMX6 plasmid (1.5 ng/ μ l stock)

0.5 μ l Primer Mix (4 μ l dH₂O + 1 μ l forward primer (200 μ M stock) + 1 μ l reverse primer (200 μ M stock))

0.5 μ l Ex-Taq Polymerase (250 Units) – Takara Bio Inc.

The PCR conditions were as follows: step 1 - 94°C 4 min, step 2- 35 cycles of 95°C 30 sec, 55°C 1 min, 72°C (1 min per 1kb PCR product). Afterwards, the 1 μ l PCR product was checked on a 1% agarose gel for the correct size, and the rest of the PCR product was used for transformation.

2.8.2 High efficiency Lithium Acetate (LiAc) yeast transformation

Yeast cells were inoculated in 5 ml YEPD medium and grown on a roller overnight at 23°C. Afterwards, the overnight culture was counted, and the appropriate amount of cells was inoculated into 50 ml of YEPD medium to a cell density of 5×10^6 cells/ml. The culture was then incubated at 28°C in a shaking water bath at 220 rpm for 3-4 hours, until the cell density reached 2×10^7 cells/ml, and most of the cells were in a vegetative growth state. Cells were harvested in a sterile 50 ml tube at 3 000 g for 3 min, and resuspended in 25 ml sterile water and centrifuged again as before. Then, cells were resuspended in 1 ml 1 X LiAc (freshly diluted in TE), and transferred into a 1.5 ml eppendorf. Cells were then pelleted at 13 000 rpm for 15 sec and LiAc was removed by aspiration. Pellets were resuspended to a final volume of 500 μ l in about 400 μ l of 1 X LiAc and kept on ice. For each transformation,

50 μ l of cell suspension was spun down (14 000rpm, 15 sec) and LiAc was removed by aspiration. The transformation mix ingredients were added in the following order:

- 1) 240 μ l 50% (w/v) PEG (polyethylene glycol)
- 2) 36 μ l 10 X LiAc
- 3) 50 μ l 2 mg/ ml salmon sperm DNA (boiled for 5 min and cooled on ice for 2 min to generate single-stranded carrier DNA)
- 4) 50 μ l purified PCR product (diluted 1:3 in dH₂O)

The mixture was vortexed vigorously before incubating at 30°C for 30 min. Cells were heat shocked in a 42°C water bath for 20-30 min. Then, cells were pelleted at 6 000 rpm for 15 sec, washed with 300 μ l sterile H₂O spun again at 6 000 rpm for 15 sec, and resuspended in 300 μ l YEPD. Cells were gently plated on YEPD plates and incubated overnight at 25°C. The next day, yeast cells were replica plated on G418 plates (300 μ g/ml) using sterile velvet and incubated for a further 2 days at 25°C. On average, 2-20 big colonies appeared on each plate. These colonies were streaked on fresh G418 plates and verified for gene deletion using a hot-start PCR method described later.

2.8.3 Hot-Start PCR test for gene deletion

To detect the presence of the wild type gene or gene deletion in the cells, a hot-start PCR was performed on freshly grown yeast cells. Specifically, a forward primer (P1) was designed to anneal to 75bp upstream of the target gene, and reverse primer (P2) was designed to bind ~500bp inside the target genes, therefore P1 and P2 produce a ~575bp PCR fragment corresponding to the WT gene. A second reverse primer (P3) was designed to bind inside the gene deletion cassette (e.g. KanMX6), and together with P1, these primers produce a

~790bp PCR product corresponding to the gene deletion. This way the presence of the WT gene or gene deletion could be easily distinguished.

Hot Start PCR was set up as follows:

Master Mix for each reaction:

15 µl dH₂O

2.5 µl Hot Start Taq Buffer - Qiagen

2.5 µl dNTPs (2.5mM) – Takara Bio Inc.

0.25 µl MgCl₂ (25mM stock) - Qiagen

0.5 µl Primer Mix (4µl dH₂O + 2 µl P1 primer (200µM stock) + 1 µl P2 primer (200 µM stock) + 1µl P3 primer (200µM stock))

0.25 µl Hot Start Taq Polymerase - Qiagen

1 µl fresh yeast cells diluted in dH₂O

The PCR conditions were as follows: step 1 - 94°C, 15 min, step 2- 35 cycles of 94°C 30 sec, 56°C 20 sec, 72°C 30 sec. Consequently, 6 µl of PCR product was checked on a 1% agarose gel.

2.8.4 Marker swapping

In order to disrupt a gene using *kanMX6* construct in a diploid yeast strain (LMY3) that already contains *kanMX6* marker; the *kanMX6* marker was swapped for a *URA3* marker. The 'marker swapping' plasmid used was *kanMX::URA3* (Voth et al, 2003), which harbours a *URA3* gene flanked by *KanMX* sequences. 10 µl of miniprep *kanMX::URA3* plasmid was digested with the restriction enzyme NOT1 in a final volume of 50 µl, 15 µl of the resulting restriction mixture was transformed directly into LMY3 cells using the LiAc method as

described before. Cells were spread on YEPD plates and allowed to recover at 23°C overnight and replica plated on -URA plates. After 2 days, cells were replica plated again on G418 plates and incubated at 25°C overnight. Colonies that only grew on -URA plates but not on G418 plates were selected and their genotype verified by hot-start PCR. Three primers were used to determine the presence of the swapped marker. A forward primer (P1) was designed to anneal upstream of the target gene, and a second reverse primer (P2) was designed to bind internally of the target gene. Together P1 and P2 give a ~575bp PCR fragment corresponding to the WT gene, which is expected to be present in the diploid strain. A third reverse primer (P3) was designed to bind internally of the *KanMX6* marker and gives a ~790bp PCR fragment with P1, indicating the presence of the *KanMX6* marker. However if the marker is successfully swapped to the *URA3* marker, this ~790bp PCR fragment will not be produced in the PCR reaction.

2.8.5 *RIF1* overexpression and C-terminal deletion

To overexpress *RIF1* gene, the 500bp sequence in front of the *RIF1* starting codon was substituted with either *GAL1* promoter, *GAL1* promoter with GFP tag (at the N terminus) or the *ADH1* promoter with HA tag (also at the N terminus). The forward primer was designed to anneal at 500bp upstream of *RIF1* and the reverse primers bound the first 40bp in the *RIF1* sequence. The plasmids used for the substitution were pFA6a-kanMX6-PGAL1, pFA6a-kanMX6-PGAL1-GFP and pFA6a-natMX6-PADH1-3HA (Longtine et al, 1998; Van Driessche et al, 2005). The same principles as for one-step PCR deletions were applied. For testing whether the construct was inserted at the targeted sequences three primers were designed: Two alternative forward primers recognised either the sequence upstream of *RIF1* or the *GAL1* promoter. The reverse primer was designed to bind inside the *RIF1* coding sequence.

The three primers generate different sized PCR products, therefore the wild type *RIF1* sequence could be distinguished from overexpressed *RIF1*.

RIF1 C-terminal deletion was generated by substituting the DNA sequence encoding 1351-1916 amino acids with *MYC::kanMX6*. The forward primer bound 40bp before the coding sequence of amino acid 1351 and the reverse primer bound 40bp after the *RIF1* stop codon. The pFA6a-13Myc-kanMX6 plasmid was used for this substitution (Longtine et al, 1998). *RIF1* C-terminal deletion was verified by DNA sequencing (MWG Operon).

2.9 QAOS assay

2.9.1 The principle of QAOS

Quantitative amplification of single-stranded DNA (QAOS) is a qPCR method for measuring ssDNA generated *in vivo*. The principle of QAOS assay was described previously by Booth *et al* (Booth *et al*, 2001). As shown in Fig 2.9.1, a tagging primer was designed to share homology with a locus of interest but also contains a non-yeast sequence known as the tag. In the pre-cycling phase of the PCR, the tagging primer can only anneal to DNA molecules that bare a single-stranded region at the locus of interest. During this phase the temperature rises slowly from 40°C to 72° C, which allows the tagging primer to anneal and extend. In the second stage of the PCR the newly created strand that contains the tagging primer sequence will be amplified by a reverse primer that is complimentary to the tag sequence and a forward primer that binds upstream of its sequence. A probe is designed to bind a short sequence between the forward and reverse primer. The probe is a normal primer with an additional tagging at both ends. The 5' end carries a fluorescent molecule (either FAM or VIC) and the 3' end has a TAMRA quencher. When the probe is intact the quencher prevents light remittance from the fluorescent molecules. When ExTaq polymerase amplifies the tagged sequence it will degrade the probe and release the fluorescent molecule from its quencher, leading to release of light that indicates amplification. By this method single-stranded gaps in the DNA can be measured confidently. If no ssDNA is present, the tagging primer will not be able to anneal in the pre-cycling stage and no amplification will occur.

Fig 2.9.1 The principle of QAOS assay

2.9.2 ssDNA preparation

cdc13-1 cells were grown overnight to a final concentration of 2×10^7 cells/ml in liquid YEPD media at 21°C. The temperature was shifted to either 27°C or 36°C to induce ssDNA accumulation. At specific time points, 40ml of cells were collected (including time 0 prior to the temperature shift) in a 50 ml falcon tube with 300 µl NaN₃ and 4 ml 0.5 M EDTA (pH8.5) previously added. Ice water was added to the falcon tube to a final volume of 50 ml and the cells were centrifuged at 3 000 rpm for 2 minutes at 4°C, and the supernatant was discarded. The cells were resuspended in 1ml of ice water and transferred to a 1.5 ml eppendorf tube, and spun briefly at 13 000 rpm at 4°C. The supernatant was aspirated and the cells stored at -80°C ready for ssDNA extraction.

After cells were removed from -80°C and thawed on ice, they were resuspended in 1ml nuclear isolation buffer (NIB) and transferred to a 2 ml Sarstedt tube. The 2 ml tubes were quickly spun (~7s) at 13 000 rpm to harvest the cells, the supernatant was discarded and the cell pellets resuspended in 600 µl of nuclear isolation buffer by vortexing and transferred to a 2 ml Sarstedt tube. 0.5 mm diameter acid-washed glass beads (Sigma) were added to the 1.5 ml mark of the Sarstedt tube and the cells were lysed using a ribolyser (Precellys24 lysis and homogenisation ribolyser, Bertin Technologies) with the following parameters: 6 X 5 500 for 5 seconds, with the tubes placed on ice for 1 minute between each cycle. A hole was punctured in the bottom of the Sarstedt tube using a 36G needle, and the tubes placed in 1.5 ml eppendorf tubes which have had their caps removed and bottom cut off. The two tubes were then placed in a 15 ml falcon tube and centrifuged at 2000 rpm for 2 minutes at 4°C. The glass beads were then washed twice with 1ml NIB buffer (2000 rpm, 2 minutes, 4°C) to ensure all the lysed cells are collected in the falcon tube. The falcon tube was vortexed and then centrifuged at 6 500 rpm for 20 minutes at 4°C, the supernatant was then discarded and the cell pellets resuspended in 2 ml G2 buffer containing 200 µg/ml RNase A

and incubated at 37°C for 30 minutes. 60 µl of proteinase K (20 mg/ml) was added and the samples were incubated at 37°C for 1 hour with periodic mixing of the tubes. The caps were removed from the falcon tubes and then centrifuged at 6 500 g for 10 minutes at 4°C, in the meantime 1 ml QBT buffer was added to a 20g Qiagen column and 2 ml QBT buffer added to fresh 15 ml falcon tubes. The supernatant was poured into the fresh 15 ml falcon tubes containing 2 ml QBT buffer and the samples were gently vortexed, the DNA mix was then added to the equilibrated 20g Qiagen columns and allowed to flow through. After the DNA mix had flowed through, the 20g Qiagen tubes were washed three times with 1 ml QC. The DNA was eluted from the Qiagen columns with 2 X 1 ml QF (the QF was pre-warmed to 50°C), the DNA was eluted into 15 ml falcon tubes. To precipitate the DNA, 0.7 volume of isopropanol (1.4 ml) was added to the eluted DNA mix, vortexed, and then spun at 7 700 g for 20 minutes at 4°C. The supernatant was removed and the pellets were washed in 70% ethanol at 7 700 g for 20 minutes at 4°C. The supernatant was discarded and the pellets were air dried. The pellets were then resuspended in 600 µl TE and incubated at 25°C in a rotating wheel for 48 hours.

2.9.4 Buffers

G2, QTB, QC and QF buffers for genomic DNA extraction were prepared according to the manufactures' (Qiagen) instruction. To make the NIB buffer, 170 ml Glycerol, 10.46 g MOPS, 14.72 g Potassium Acetate, 2 ml 1M MgCl₂, 0.55 ml 0.9M Spermidine and 52 mg powder Spermine were dissolved in 700 ml dH₂O. The pH was adjusted to 7.2 and the volume was topped up to 1 litre. All buffers were filter sterilized and stored at 4°C.

2.9.5 Equilibration of total genomic DNA

Because the extracted DNA varies in quantity between different samples, it is necessary to equalise them before measuring ssDNA, in order to minimize error. The amount of DNA for each sample was determined using qPCR to measure the amount of the *PAC2* locus, which lies close to the centromere and therefore does not become single-stranded in *cdc13-1* mutants at non-permissive temperatures. qPCR master mixes were set up in multiples of 12 PCR reactions in the following amounts.

Master Mix for 12 reactions:

32 μ l 10X ExTaq PCR buffer– Takara Bio Inc

24 μ l dNTPs (2.5mM stock) – Takara Bio Inc

3.2 μ l forward primer (300 nM final concentration)

3.2 μ l reverse primer (300 nM final concentration)

3.2 μ l Taqman probe (200 nM final concentration)

1.5 μ l ExTaq polymerase (0.025 U/ μ l)

124 μ l dH₂O.

For each individual PCR reaction, 15 μ l of the master mix were added to 10 μ l of DNA to make a 25 μ l reaction mix for PCR. The qPCR parameters to determine *PAC2* concentration were as follows: Step 1 - 95°C 5 minutes, step 2 – 40 cycles; 95°C 15 seconds, 63°C 1 minute. Afterwards, all samples were diluted to 20 ng/ μ l and run again in the same PCR conditions. A dilution coefficient was generated as 20 ng/ μ l divided by DNA quantity.

2.9.6 Prepare ssDNA standards

To create the ssDNA standards, the first step is to prepare a ssDNA stock of 20 ng/ μ l. This is achieved by boiling the double-stranded DNA stock (at 20 ng/ μ l) in PCR tubes for 7 min at 98°C. The samples were vortexed vigorously and chilled on ice immediately. Then samples were vortexed again after 2 min to ensure DNA become single-stranded. Thereafter ssDNA standards were prepared as below and put on ice.

0.8% ssDNA: 198.4 μ l ds DNA+1.6 μ l Boiled DNA

3.2% ssDNA: 193.6 μ l ds DNA+6.4 μ l Boiled DNA

12.8% ssDNA: 174.4 μ l ds DNA+25.6 μ l Boiled DNA

51.2% ssDNA: 97.6 μ l dsDNA+ 102.4 μ l Boiled DNA

2.9.7 ssDNA measurement using Taqman probes

To measure the amount of ssDNA a PCR master mix was made that comprised for 12 reactions (with final concentration indicated in the brackets).

32 μ l ExTaq buffer (1X)

24 μ l dNTP (200 μ M)

3.2 μ l tagging primer (33nM)

3.2 μ l Tag (330nM)

3.2 μ l reverse primer (330nM)

3.2 μ l Taqman probe (200nM)

1.5 μ l ExTaq polymerase

124 μ l dH₂O.

The PCR cycling conditions for measuring ssDNA were as follows: step 1; 40°C for 5 minutes, ramp to 72°C at 2°C/minute. Step 2; 72°C for 10 minutes followed by 95°C for 5 minutes. Step 3; 40 cycles of 95°C for 15 seconds, 67°C for 1 minute. Standards containing 51.2, 3.2 and 0.8% ssDNA were used to construct a standard curve of ssDNA quantity. To obtain an equilibrated ssDNA value, the measured ssDNA quantity was multiplied by the dilution coefficient obtain by qPCR of the *PAC2* locus.

2.9.8 Development of a SYBR Green based QAOS assay

To measure ssDNA accumulation at a double strand break, the QAOS assay was tailored to work with SYBR Green rather than the Taqman probes. Three sets of tagging, tag and reverse primers have been designed to recognise ssDNA gaps at 1.6kb, 10kb or 20kb upstream of the HO cutting site, allowing the dynamics of ssDNA accumulation to be monitored (Fig 6.4). SYBR Green is a dye that binds dsDNA, thus newly synthesised DNA molecules during qPCR will be labelled and emit light.

The SYBR Green mixture contains an antibody that inhibits the activity of Taq polymerase to avoid any reaction that may occur at the room temperature. Usually this antibody is inactivated in the DNA denaturing step of PCR for a 'Hot-Start' PCR. However in QAOS assay, the first step of the PCR is performed at 40°C for ssDNA annealing and no boiling of the sample is allowed at this step. To ensure the activity of Taq polymerase in the SYBR Green mixture, the antibody was inactivated by boiling the SYBR Green mix for 15 min at 95°C followed by 2 min incubation on ice. The reactions were set up as follows: 10 µl Platinum™ SYBR™ Green qPCR SuperMix UDG (Invitrogen, Cat. 11733-046), 8 µl DNA sample, 0.6 µl primer mix (1:10 dilution of tagging, tag and forward primer form 200 µM stock), and 1.4 µl H₂O. The same PCR conditions as for Taqman QAOS were used afterwards.

2.10 Western Blot

2.10.1 TCA protein extraction

Yeast cells were inoculated in 50 ml of YEPD liquid media and grown in water bath at appropriate temperatures. Cells were counted, and 2×10^8 cells were harvested by spinning at 2 000 rpm for 3 min at 4°C. Cells were washed with ice cold 10% trichloroacetic acid (TCA) to prevent proteolysis (2 000 rpm, 3 min). Cell pellets were resuspended in 500 μ l 10% TCA, transferred in to Sarstedt screw cap tubes and centrifuged at 13 000 rpm for 10 sec. Afterwards the supernatant was removed and cell pellets were resuspended in 200 μ l of 10% TCA. ~200 μ l of glass beads (Sigma) were added to the tube just below the liquid surface. Cells were then lysed using in a ribolyser (Precellys24 lysis and homogenisation ribolyser, Bertin Technologies) at 6 500 rpm for 10 sec. This cycle was repeated for a total of 3 times and samples were incubated on ice for 5 min between each cycle. Then, A hole was punctured in the bottom of the Sarstedt tube with a needle, and the tubes were placed in 1.5 ml eppendorfs which have had their caps removed and bottom cut off. The two tubes were then placed in a 15 ml falcon tube and centrifuged at 2 000 rpm for 2 minutes at 4°C. The glass beads were then washed once with 200 μ l TCA to ensure all the lysed cells were collected. Samples were subsequently centrifuged at 13 000 rpm for 10 min. Pellets containing crude protein extracts were resuspended in 100 μ l 2 X Laemmili buffer (Sigma) and neutralized by adding of 1 M Tris base until the colour of the sample turns blue. Sample were then boiled at 95°C for 5 min, and chilled on ice for 2 min. Finally, samples were centrifuged again at 3 000 rpm for 10 min and supernatants containing protein extracts were collected, aliquoted into fresh tubes and frozen at -20°C for long term storage.

2.10.2 SDS-PAGE, blotting and detection

Protein lysate was separated using a polyacrylamide gel, made with 4% stacking gel and an appropriate percentage of resolving gel for the size of the proteins being detected (e.g. 7.5 – 12% resolving gel for proteins <200 KDa, 5-6.5% resolving gel for proteins >200 KDa). Gels were run at 95V for 30 minutes until the protein band of interest entered the resolving gel, and then 120V until the required degree of protein separation had been achieved (usually 1-2 hours). Transfer of the gel to a nitrocellulose membrane (Amersham Hybond ECL™) was performed at 250 mA for 1 hour; the membrane was subsequently stained for 5 minutes with Ponsaeu (Sigma) with gentle shaking. After de-staining with ddH₂O to reveal protein bands, the membrane was blocked with 5% milk dissolved in 1 X TBST with gentle shaking at room temperature for 1 hour. The membrane was then incubated overnight with the primary antibody diluted to the recommended concentration in 2.5% milk dissolved in 15ml 1 X TBST. Incubation was performed at 4°C with gentle shaking. The following morning, the membrane was washed 3 times in 1 X TBST for 10 minutes with gentle shaking at room temperature. The membrane was then subsequently incubated for 45 minutes with the appropriate secondary antibody (diluted to the recommended concentration in 2.5% milk dissolved 1 X TBST). Incubation with the secondary antibody was carried out at room temperature with gentle shaking. The membrane was washed a further 3 times with 1 X TBST for 10 minutes, before the membrane was prepared for detection by incubation with ECL™ Western Blotting Detection Reagents (GE healthcare) for 5 minutes. ECL (enhanced chemiluminescence) detection is based on the oxidation of luminol by horseradish peroxidase (conjugated on the secondary antibody) in the presence of hydrogen peroxide, and this process emits light that is proportional to the protein amount. The membrane was imaged on the Fujifilm LAS-3000 imaging system.

2.10.3 Buffers

10 X TBST stock was made by dissolving 12.11 g Tris base, 29.22 g NaCl and 10 ml Tween 20 in 700 ml of dH₂O. The pH was adjusted to 7.5 and the total volume adjusted to 1 litre. This stock solution was diluted to 1 X before use. Buffer for running and transferring the SDS-PAGE were bought from Biorad and diluted to 1 X working concentration before use. 200 ml methanol was supplemented to the 1 X transfer buffer. For transferring proteins larger than 200 KDa, 0.1% SDS (final concentration) was supplemented to the transfer buffer.

2.11 Southern Blotting

Southern blotting was performed using a Digoxigenin (DIG)-based system from Roche to label and detect target nucleic acid sequences. The DIG system involves the incorporation of Digoxigenin-dUTP into a nucleic acid probe by PCR. Subsequently, the hybridised DIG-labelled probe can be detected using an anti-DIG antibody and the chemiluminescence based detection.

2.11.1 Yale Quick DNA extraction from yeast

Before extraction, a spheroplasting solution containing 0.1M EDTA pH7.5, 1 mg/ml Zymolase and 1:1000 β -mercaptoethanol was made fresh. The solution was mixed by vortexing and was kept on ice. $\sim 5 \times 10^6$ yeast cells grown on YEPD plates were scraped off then transferred to a 1.5 ml eppendorf and resuspended in 1 ml dH₂O and spun down at 13 000 rpm for 30sec. The supernatant was removed by aspiration and 250 μ l of the spheroplasting solution was added to each sample. Samples were vortexed vigorously until cells were homogenously resuspended before being incubated at 37°C in a water bath for 1hr. 50 μ l of miniprep mix (0.25M EDTA pH8.5, 0.5M Tris Base and 2.5% SDS) was made fresh and added to each sample. Samples were mixed by inversion and incubated at 65C for 30 min. Then, 63 μ l of 5M KAc was added to each sample and the samples were then mixed by inverting 5 times and subsequently incubated on ice for 30 min. This step precipitates dodecyl sulfate bound protein from DNA. Afterwards, samples were spun down at 13 000 rpm for 10 minutes. The supernatant was then transferred to a new tube containing 720 μ l 100% ethanol. After mixing the samples by inverting 5 times, a DNA precipitate became visible. The DNA was pelleted for 5 minutes at 13 000 rpm, the ethanol was then poured out and any residue was removed by aspiration. The DNA pellets were resuspended by pipetting in 130 μ l of TE containing 1 mg/ml RNase A and incubated at 37°C in a water bath for 35

minutes. After the first 10 minutes when the pellets began to soften, gentle pipetting was performed to re-suspend the pellet in the solution. DNA was precipitated again by adding 130 μ l of isopropanol and mixed by inversion and spun down at 13 000 rpm for 5 minutes. The pellet was washed once with 70% ethanol and spun for 5 minutes at 13 000 rpm. Ethanol was poured off and any residue was removed by aspiration. The pellet was then air-dried in a PCR hood for 10-20 minutes, and resuspended in 50 μ l TE followed by incubated at 37°C in a water bath for 30 min. DNA samples were then stored at -20°C.

2.11.2 Digoxigenin (DIG) labelling of nucleic acid probe

A nucleic acid probe against the telomeric TG sequences was synthesised using the PCR DIG probe synthesis kit (Roche). PCR reactions were set up as follows: 28 μ l H₂O, 5 μ l PCR buffer, 5 μ l PCR DIG mix, 10 μ l primer mix (contains forward and reverse primer M933 and M934 at 10 μ M concentrations), 0.75 μ l enzyme mix, DNA template (plasmid pDL912 diluted 1:200 in TE). The PCR conditions were as follows: step 1 - 95°C 3 minutes; Step 2- 33 cycles of - 95°C 30 seconds, 60°C 30 seconds, 72°C 1 minute. The DIG labelled probe was then boiled for 5 minutes and then incubated on ice before use.

2.11.3 Procedure and buffers

DNA samples prepared from the Yale quick method were equalised on a 0.8% agarose gel. DNA was diluted in TE and 5 μ l of each DNA sample was added in a solution containing 2 μ l 5 X buffers, 2.5 μ l ddH₂O and 0.5 μ l of XhoI (New England Biolabs). Enzyme digestion was performed in a PCR machine at 37°C for 3.5 hrs. Then, DNA samples were loaded on to a 0.8% agarose gel made with 0.5 x TBE buffer. 6 μ l DIG molecular weight marker (Roche) was added in the first lane. The gel was run at 25V overnight in a clean tank filled with 0.5 X TBE buffer. In the morning, the gel was checked under UV light to ensure digestion is complete

before proceeding. Then, the gel was cut with a clean razor blade to remove excess agarose just above the well and at the bottom of the gel. Acid treatment was performed by soaking the gel twice for 10 minutes in freshly made 0.25M HCl with gentle shaking in a clean sandwich box. This step depurinates the DNA and breaks large DNA fragments which facilitates subsequent transfer. When finished, the acid solution was poured off and the gel was rinsed quickly with ddH₂O. Then the gel was washed twice for 20 minutes in freshly made alkali solution (1.5M NaCl 0.5M NaOH) with gentle shaking. This alkaline treatment denatures the DNA and permits hybridization to the ssDNA probe. Finally, the gel was neutralised by soaking twice for 20 minutes in fresh 1M NH₄OAc with gentle agitation then proceed to transfer. The gel was then transferred to a positively charged nylon membrane (Amersham HybondTM- N+) for 48 hours. Afterwards the nylon membrane was transferred to a clean sandwich box and washed in 2 x SSC buffer (300 mM NaCl, 30 mM trisodium citrate, pH 7.0) for 2 minutes. The DNA was then cross-linked to the membrane by exposing the membrane to UV light at a dose of 0.125 J/cm² using the Stratalinker UV crosslinker. After UV exposure, the membrane was transferred to a clean and dry hybridisation tube to which 20 ml of DIG easy hybridisation fluid (Roche) pre-warmed to 37°C and the hybridisation tube was then placed in a rolling oven for 40 minutes at 37°C. Following the incubation, the appropriate DIG labelled DNA probe was added to the buffer (not directly to the membrane) and the membrane was left to hybridise overnight in a rolling oven at 37°C with gentle rotation. The following morning the membrane was removed from the hybridisation tube and transferred to a clean and dry sandwich box and was washed twice for 5 minutes in 50 ml HOT buffer (0.5x SSC, 0.1% SDS) pre-warmed to 65°C. After the initial washes, the membrane was washed a further two times for 10 minutes with 200 ml HOT buffer. Washing steps were carried out at room temperature; however the HOT buffer was maintained at 65°C. Subsequently, the membrane was rinsed briefly in 20 ml 1 X DIG washing buffer (Roche) diluted 1:10 in 18.2 mQ H₂O, the membrane was then transferred to a fresh sandwich box and blocked for 30 minutes in 100 ml 1 x DIG blocking solution (Roche)

with gentle shaking. After the blocking step, the blocking solution was removed and 1.5 μ l of anti-DIG-alkaline phosphatase conjugate (Roche) (this is the antibody that detects Digoxigenin) was added to 30 ml 1 X blocking solution and incubated with the membrane for 30 minutes. The membrane was then washed twice for 15 minutes in 100 ml 1 X DIG washing buffer, and subsequently equilibrated in 20 ml 1 X DIG detection buffer. The membrane was then prepared for alkaline phosphatase-based chemiluminescent detection, by incubating for 5 minutes with 1 ml CDP-star reagent (New England Biolabs). Finally, the membrane was imaged on the Fujifilm LAS-3000 imaging system.

2.12 Chromatin immunoprecipitation

2.12.1 Procedures

Yeast cells were grown overnight in YEPD liquid media to a final concentration of 2×10^7 /ml. 40ml of cells were then collected at specified time points to which 1.1 ml of 37% formaldehyde (1% final concentration) was added to cross link the proteins to DNA. Samples were incubated at room temperature for 15 minutes with gentle shaking. To stop the cross linking reaction, 6 ml of 2.5M glycine was added and the cells was incubated for 5 minutes at room temperature. The cells were then harvested by spinning for 2 minutes at 3 500 rpm at 4°C, followed by washing twice with ice cold TBS for 2 minutes at 3 500 rpm at 4°C. The supernatant is discarded after each wash. A final wash was performed with 10 ml ice cold FA lysis buffer (50mM HEPES pH7.5, 150mM NaCl, 1mM EDTA, 1% (v/v) Triton X-100, 0.1% (w/v) sodium deoxycholate, 0.1% (w/v) SDS) for 2 minutes at 3 500 rpm at 4°C. The supernatant was aspirated and cell pellets were stored at -80°C ready for extraction.

To extract chromatin, cells were defrosted on ice and resuspended in 600 µl ice cold FA lysis buffer with 2 mM PMSF freshly added to the buffer. The sample was then transferred to a 2 ml Sarstedt tube and 0.5mm diameter acid-washed glass beads (Sigma) were added till the liquid reached the 750 µl level. The cells were then lysed using a ribolyser (Precellys24 lysis and homogenisation ribolyser, Bertin Technologies) using the following parameters: 9 x 6 500 at 4°C with the samples being placed on ice between each cycle. A hole was punctured in the bottom of the Sarstedt tube using a 36G needle, the Sarstedt tube was then placed in a 1.5 ml eppendorf tube with the cap removed. The two tubes were subsequently placed in a 15 ml falcon tube and spun at 2 000 rpm for 2 minutes at 4°C. The 1.5 ml eppendorf containing the lysed cells was further spun at 13 000 rpm for 15 minutes at 4°C, the supernatant was discarded and the cell pellets resuspended in 1 ml ice cold FA lysis buffer.

The samples were sonicated using a sonicator (Sanyo MSE Soniprep 150 sonicator) with the following parameters: 5 x 15 sec at 7 μ A, with 1 min incubation on ice between each cycle. This process produces fragmented chromatin with an average size of 500bp. The sonicated chromatin samples were centrifuged at 13 000 rpm for 30 minutes at 4°C, and the supernatant was transferred to a fresh 15 ml falcon tube. The chromatin samples were further diluted by adding 4 ml of ice cold FA lysis buffer, aliquoted and stored at -80°C. For immunoprecipitation, 800 μ l of sonicated chromatin samples (IP samples) was defrosted on ice, and incubated with 3 μ g of primary antibody or the same amount of anti-goat secondary antibody, which served as a negative control (and its binding is referred to as the background). The amount of antibody used was optimised by a titration experiment using antibodies ranging from 1 μ g-10 μ g. After the antibody was added, samples were incubated at 4°C in an end-over-end rotator. Meanwhile, 50 μ l of Dynabeads Protein G (Invitrogen, 100-09D) was equilibrated by washing with 250 μ l ice cold FA lysis buffer for three times at 4°C in an end-over-end rotator. After the three wash steps, the chromatin/antibody mix was combined with the equilibrated dynabeads and incubated overnight at 4°C in an end-over-end rotator. The next morning a magnet (Invitrogen) was used to keep the Dynabeads to one side as the supernatant was removed. The beads were then washed 5 times in 700 μ l of ice cold FA lysis buffer with the help of the magnet. Following the final wash and subsequent removal of FA lysis buffer, the beads were resuspended in 100 μ l of the ChIP elution buffer (50 mM Tris-Cl pH 7.5, 10 mM EDTA, 1% (w/v) SDS) and incubated at 65°C for 10 minutes to elute the bound chromatin. After incubation the supernatant was transferred to fresh eppendorf tubes and the following ingredients were added: 80 μ l TE and 20 μ l proteinase K (20 mg/ml). In the meantime, 80 μ l of the previously sonicated chromatin samples (Input samples) is thawed on ice and to which the following ingredients were added: 100 μ l ChIP elution buffer, 100 μ l TE and 20 μ l proteinase K (20 mg/ml). Both the IP and Input samples were then incubated at 37°C for 2 hours to degrade unwanted proteins, and subsequently incubated at 62°C overnight to reverse the cross-links. The following

morning the samples were purified using the Qiagen PCR purification kit. IP samples and Input were then quantified by Taqman or SYBR Green based qPCR. The ChIP enrichment was determined by the following formula: $\text{ChIP (\%)} = (\text{IP}/\text{Input-Background}) \times 100\%$.

2.12.2 qPCR measurement of ChIP samples using Taqman probes

qPCR master mixes were set up in multiples of 12 PCR reactions in the following amounts: 12 PCR reactions (final concentrations in brackets) – 32 μl ExTaq PCR buffer (1X), 24 μl dNTP's (200 μM), 3.2 μl forward primer (300nM), 3.2 μl reverse primer (300nM), 3.2 μl Taqman probe (200nM), 1.5 μl ExTaq polymerase (0.025 U/ μl), 124 μL water. For each individual PCR reaction, 15 μl of the master mix was added to 10 μl of DNA to the reaction well to make a 25 μl reaction mix for PCR. PCR conditions were as follows: Step 1 - 95°C 5 minutes, step 2 – 40 cycles; 95°C 15 seconds, 63°C 1 minute. The quantity of DNA was determined by running DNA standards of 20 ng, 2 ng and 0.2 ng to generate a standard curve of DNA quantity, which was used to determine the amount of DNA of the unknown samples. All samples were run in triplicates.

2.12.2 SYBR green qPCR measurement of ChIP samples

2 X SYBR green master mix (Invitrogen) was used for SYBR green based PCR. Master mixes for PCR were set up for multiples of 12 reactions; the following concentrations of reagents were set up for a 12 reaction master mix: 60 μl 2 X SYBR green master mix (Invitrogen), 2.4 μl primer mix (forward primer at 20 μM + reverse primer at 20 μM), 9.6 μl dH₂O. To each reaction well 6 μl of the PCR master mix was added, along with 4 μl of the DNA samples to make a 10 μl reaction mix for PCR. PCR conditions were as follows: step 1 - 50°C 2 minutes, step 2 - 95°C 2 minutes, step 3 - 40 cycles of 95°C 15 seconds, 60°C 30 seconds. Similar to the Taqman based qPCR, the quantity of DNA of target samples was determined by running

quantity standards of 20 ng, 10 ng and 0.2 ng to generate a standard curve of DNA quantity. All samples were run in triplicates.

2.12.3 qPCR primers for the inducible DSB system

Primers used for the amplification of the sites proximal to the DSBs were previously designed (Wang & Haber, 2004) and ordered from MWG.

2.13 Gene expression and RT-PCR

2.13.1 RNA extraction

RNA was extracted using the RNeasy mini kit (Qiagen) following the manufacturer's instructions. The yeast cell wall was digested by enzymatic cell lysis. Cells were grown overnight to a final concentration of 1×10^7 cells/ml, a total of 2×10^7 cells was harvested by centrifuging at 1 000 g for 5 minutes at 4°C. The cells were then washed with sterile H₂O, and again centrifuged at 1 000 g for 5 minutes at 4°C. The cells were then resuspended in 100 µl of Y1 buffer with freshly added Zymolase (Qiagen); the resuspended cells were then incubated at 30°C for 30 minutes in a shaking waterbath. This step leads to the generation of yeast spheroplasts. After the 30 minute incubation, 350 µl of buffer RLT (containing freshly added β-mercaptoethanol) was added to the spheroplasts followed by vigorous vortexing, leading to lysis of the spheroplasts. 250 µl of 100% ethanol was added to the homogenised lysate and mixed well by pipetting; the samples were then ready for RNA extraction. Samples were transferred to an RNeasy spin column and centrifuged for 15 seconds at 10 000 rpm at room temperature, the flow-through was discarded. To remove DNA contamination an on-column DNase digestion was performed. 350 µl Buffer RW1 was added to the spin column and the samples were centrifuge for 15 sec at 10 000 rpm at room temperature to wash the spin column membrane. The flow-through was discarded. 10 µl DNase I stock solution was added to 70 µl buffer RDD and samples were mixed by gently inverting the tubes. Afterwards the mixture (80 µl) was added directly to RNeasey spin column membrane, and incubated on benchtop (20-30°C) for 15 min. 350 µl buffer RW1 was added to the RNeasy spin column and samples were centrifuge for 15 sec at 10 000 rpm. The flow-through was discarded. 500 µl of buffer RPE was then added to the spin column and was centrifuged for 15 seconds at 10 000 rpm at room temperature, and this

step was repeated. The spin column was then transferred to a new 1.5 ml collection tube, 50 μ l of RNase-free H₂O was added directly to the spin column membrane and then centrifuged for 1 minute at 10 000 rpm at room temperature to elute the RNA.

2.13.2 Reverse transcription

cDNA was synthesised from ~1 μ g of the extracted RNA using the SuperScript III cDNA synthesis kit (Invitrogen). 1 μ g of RNA was added to 1 μ l of random hexamer primers (Invitrogen) and 4 μ l of 2.5 mM dNTPs. Water was added to a final volume of 13 μ l. The 13 μ l reaction mix was incubated at 65°C for 5 minutes and then placed immediately on ice for 1 minute. 4 μ l of 5 X first strand buffer and 1 μ l each of 0.1M DTT, RNase out (Invitrogen) and SuperScript III reverse transcriptase (Invitrogen) were added to the 13 μ l reaction mixture. cDNA synthesis conditions were as follows: 5 minutes at 25°C, 60 minutes at 50°C and 15 minutes at 70°C. The cDNA was then diluted 1:10 by adding 180 μ l of dH₂O to the 20 μ l sample.

2.13.3 qPCR

All qPCR reactions were performed in a volume of 10 μ l using SYBR green. The PCR reaction mix was composed of 4 μ l cDNA, 5 μ l of SYBR Green mix (Invitrogen), 0.2 μ l of 200 μ M primers and 0.8 μ l of dH₂O. PCR conditions were as follows: step 1 - 50°C 2 minutes, step 2 - 95°C 2 minutes, step 3 - 40 cycles of 95°C 15 seconds, 60°C 30 seconds. The relative quantification method ($\Delta\Delta$ Ct) (Livak & Schmittgen, 2001) was used to quantify the gene expression levels of selected genes relative to the expression levels of the reference gene *ALG9*. *ALG9* is one of the best housekeeping genes for RT-PCR for *S. cerevisiae* because its expression is stable regardless of growth conditions and strain background (Teste et al,

2009). The following formulas were used for calculating the relative gene expression levels: $\Delta\text{Ct} = \text{Ct target gene} - \text{Ct reference gene}$; $\Delta\Delta\text{Ct} = \Delta\text{Ct test sample} - \Delta\text{Ct control sample}$ (e.g. WT); Fold difference in expression = $2^{-\Delta\Delta\text{Ct}}$. The amplification efficiencies of the target gene (*RIF1*) and reference gene (*ALG9*) are checked to ensure that they are approximately equal, before applying the $\Delta\Delta\text{Ct}$ calculation.

2.14 Statistics

To compare the difference between the numbers of survivors, one way ANOVA test followed by Newman-Keuls Multiple comparison test has been performed on the Prism software. P value of <0.05 is considered significant.

2.15 Antibody used in the study

Antibodies used for ChIP and WB experiments are listed in Table 2.14.

Table 2.14

Primary Antibody	Origin	cat. No.	company
monoclonal anti-Myc	mouse	sc-40	Santa Cruz
monoclonal anti-GFP	mouse	11814460001	Roche
monoclonal anti-HA	rat	11867423001	Roche
polyclonal anti-Rad53	goat	sc-6749	Santa Cruz
polyclonal anti-Sgss1	goat	sc-11993	Santa Cruz
polyclonal anti-Rap1	goat	sc-6663	Santa Cruz
polyclonal anti-Rad9	goat	sc-50442	Santa Cruz

Secondary antibody	Origin	cat. No.	company
anti-mouse	rabbit	ab6728	Abcam
anti-goat	donkey	sc-2020	Santa Cruz
anti-rat	rabbit	ab6734	Abcam

Chapter III: The role of Rif1 in PAL survivors

3.1 Rif1 is essential for the survival of *tlc1Δ rad52Δ exo1Δ* cells.

Preliminary data from our lab suggests that Rif1 is required for the proliferation of cells lacking telomeres. To verify this finding I repeated the experiment by generating a new diploid strain heterozygous for *TLC1*, *RAD52*, *EXO1* and *RIF1*. Following sporulation, 12 independent *RIF1+* or *rif1Δ* haploid strains (also containing *tlc1Δ rad52Δ exo1Δ*) were obtained on selective plates, and *RIF1* deletion was verified by PCR as described in the methods. Afterwards, ~10 million cells from each strain were propagated every 5 days on to a fresh YEPD plate for 35 days.

As shown in Fig 3.1, both *RIF1+* and *rif1Δ tlc1Δ rad52Δ exo1Δ* strains became senescent after a few days of passage. However, while 8 of the 12 *RIF1+* strains escaped senescence and generated survivors, none of the *rif1Δ tlc1Δ rad52Δ exo1Δ* strains was able to generate survivors. This experiment confirmed that *RIF1* is essential for the survival of *tlc1Δ rad52Δ exo1Δ* strains.

Fig 3.1 Effect of RIF1 on escaping senescence.

3.2 Effect of Rif2, Ckb2, Lig4 and checkpoint proteins on escaping senescence

Since Rif1 physically and functionally interacts with Rif2, I further investigated whether Rif2 can affect the survival of *tlc1Δ rad52Δ exo1Δ* cells. As shown in Fig 3.2, most of the *rif2Δ* strains (~70%) escaped senescence after a period of passage, indicating that Rif2 does not play a significant role in the survival of *tlc1Δ rad52Δ exo1Δ* strains.

The next protein tested was Ckb2, the regulatory subunit of casein kinase II. Ckb2 is known to be required for adaptation of yeast cells to a persistent DSB and to unprotected telomeres (Toczyski et al 1997), therefore I reasoned that Ckb2 might be required for adaptation in PAL survivors. However, *ckb2Δ tlc1Δ rad52Δ exo1Δ* cells produced survivors at similar frequency to *CKB2+* cells, suggesting that *CKB2* is not required for the survival of *tlc1Δ rad52Δ exo1Δ* cells.

To date it is still not known how palindromes form at chromosome ends in early *tlc1Δ rad52Δ exo1Δ* survivors. One hypothesis is that palindromes form by chromosome end-to-end ligation through the NEHJ pathway followed by DNA replication and chromosome breakage (Maringele & Lydall, 2004). *LIG4* encodes a DNA ligase essential for NHEJ, therefore according to this hypothesis *LIG4* should be indispensable for the formation of PAL survivors. Surprisingly, *lig4Δ tlc1Δ rad52Δ exo1Δ* cells were able to generate survivors at high frequency (~70%), suggesting that *LIG4* is not required for the survival of *tlc1Δ rad52Δ exo1Δ* cells, and other mechanisms are likely to be responsible for palindrome formation in these cells.

Rad9, Rad24, and Chk1 are checkpoint proteins which regulate the G2/M arrest in response to DSBs and uncapped telomeres. Therefore it is possible that these checkpoint proteins could also affect the rate that *tlc1Δ rad52Δ exo1Δ* cells escape from senescence. ~75% of

the *chk1Δ*, *rad9Δ*, and *rad24Δ* cells (also *tlc1Δ rad52Δ exo1Δ*) escaped senescence, compared to ~56% checkpoint in proficient cells (*RAD+*). This data suggest that deletion of checkpoint genes slightly improves the survival of *tlc1Δ rad52Δ exo1Δ* cells.

In addition, I tested if Mrc1 has a role in the survival of *tlc1Δ rad52Δ exo1Δ* cells. Mrc1 is a multifunctional protein in yeast; being a S phase checkpoint protein as well as a core component of the replication fork (Lou et al, 2008). My result shows that *mrc1Δ* strains (also *tlc1Δ rad52Δ exo1Δ*) generated survivors at a much lower frequency (~10%) compared to *MRC1+* cells (~56%), suggesting that unlike other checkpoints, Mrc1 facilitates the escape from senescence.

Fig 3.2 Survival of *tlc1Δ rad52Δ exo1Δ* strains carrying different gene deletions.

3.3 Deletion of RAD9 and RAD24 bypass the requirement of RIF1 in generating PAL survivors

If Rif1 allows *tlc1Δ rad52Δ exo1Δ* cells escape senescence through a checkpoint inhibitory mechanism, then deletion of the major checkpoint genes should bypass the requirement of Rif1 for survival. Rad9, Rad24 and Chk1 are major checkpoint proteins required for the cell cycle arrest in response to uncapped telomeres (induced by the *cdc13-1* mutation). Therefore I investigated if deletion of any of these checkpoints would allow *rif1Δ tlc1Δ rad52Δ exo1Δ* cells to survive. Interestingly, deletion of *CHK1* in *rif1Δ tlc1Δ rad52Δ exo1Δ* cells did not have any effect on survival. In contrast, deletion of *RAD9* or *RAD24* dramatically increased survival frequency. This data suggest that deletion of *RAD9* and *RAD24* can bypass the requirement of *RIF1* in generating PAL survivors.

Fig 3.3 Effect of checkpoints on the survival of *tlc1Δ rad52Δ exo1Δ rif1Δ* cells

3.4 Discussion

In this chapter, I confirmed the essential role of Rif1 in the survival of telomerase, recombination and Exo1 defective cells. Interestingly, the Rif1 interacting partner, Rif2, appears to have no effect. In addition, none of the five previously tested telomere-associated proteins (Est2, Tel2, Sir3, Mre11, and Yku70) were essential for the survival of *tlc1Δ rad52Δ exo1Δ* cells. Together, these data indicate that Rif1's function is unique and is not shared with other telomere associated proteins.

3.4.1 The role of Rif1 in adaptation

To generate PAL survivors, cells need to escape senescence despite the presence of extremely short telomeres. This process of cells overriding cell cycle arrest with damage is known as checkpoint adaptation (Toczyski et al, 1997). My data show that deletion of *RIF1* abolished survival of *tlc1Δ rad52Δ exo1Δ* cells, suggesting that Rif1 may be required for the checkpoint adaptation process. Interestingly, adaptation in *tlc1Δ rad52Δ exo1Δ* cells is not dependent on regulatory subunit of casein kinase II (which is required for the adaptation to a DSB), as deletion of *CKB2* did not affect survival frequency.

If Rif1 allows cells with extremely short telomeres to escape senescence through a checkpoint adaptation (i.e. checkpoint inhibitory) pathway, it is to be expected that inactivating major checkpoints should bypass the need of Rif1. Indeed, deletion of the checkpoint genes *RAD9* and *RAD24* fully rescues *rif1Δ tlc1Δ rad52Δ exo1Δ* cells. However, deletion of *CHK1* has no effect. This is probably because Rad9 and Rad24 act as the major checkpoints responsible for the arrest of *tlc1Δ rad52Δ exo1Δ* cells, whereas Chk1 does not. In support of this view, a study reported that the G2/M arrest in telomerase negative cells is dependent on Mec3 (a component of the 9-1-1 complex) and Rad9, but does not require

Chk1 (Grandin et al, 2005). Although the importance of Rad24 in *tlc1Δ*-induced arrest has not been established, it is very likely that Rad24 is also required for arrest, because Rad24 participates in the loading Mec3 and other 9-1-1 components on to DNA damage. Together my results suggest that Rif1 opposes the cell cycle arrest in *tlc1Δ rad52Δ exo1Δ* cells.

Based on current experimental approaches, the difference between checkpoint suppression and checkpoint adaptation during *tlc1Δ*- induced senescence is difficult to distinguish. Rif1 could act on either pathway to promote the survival of PAL survivors. Firstly, it is possible that Rif1 may facilitate cells to bypass senescence by directly associating with chromosome damage. Once bound to damage, Rif1 may physically block the access of checkpoint proteins to DNA substrates (such as ssDNA), thus hampering the signal amplification process which would otherwise lead to cell cycle arrest. Alternatively, Rif1 may inhibit the checkpoint response indirectly, by modulating the overall chromatin structure to a 'closed' conformation, which is undetectable by the DNA damage surveillance machinery. On the other hand, Rif1 may be required for cells to re-enter cell cycle by reversing an already initiated G2/M arrest. This could be achieved by recruiting adaptation-promoting proteins such as phosphatases to the damage. Indeed it was found that Rif1 physically interacts with several phosphatases including Glc7, cdc14, Ptp1 and Psr2 (Breitkreutz et al, 2010). A different hypothesis is that Rif1 may stimulate a limited level of repair at the chromosome terminus, which keeps the overall damage below the threshold of maintaining a persistent cell cycle arrest.

These possibilities are not mutually exclusive; however they require Rif1 to be associated with damaged chromosome ends. Unfortunately, I was not able to establish whether Rif1 bind to chromosome ends in PAL survivors. This is because it is extremely difficult to identify the 'real' ends of chromosomes in PAL survivors due to the large amount of palindromes that form randomly in the genome. However, in the following chapters I further investigated

the recruitment of Rif1 to chromosome ends using the *cdc13-1* and inducible DSB model systems.

3.4.2 Rif1 is not essential for long-term maintenance of PAL survivors

It is still a mystery how PAL survivors maintain their chromosome ends. Interestingly, terminal inverted repeats have been found in certain types of adenovirus and bacteriophage, which carry linear plasmids (Meinhardt et al, 1997; Sakaguchi, 1990). In addition, the mitochondrial genome of the yeast *Candida subhashii* also contains linear plasmids terminating with inverted repeats (Fricova et al, 2010). In these organisms, a protein is covalently bound to the 5' end of the linear DNA and interacts with DNA polymerase to initiate a 'protein-priming' mechanism for DNA synthesis (Salas, 1991). It is therefore possible that PAL survivors may employ similar mechanisms for end replication and protection, and Rif1 might be one of the specialised proteins required for these functions.

However, my data show that although Rif1 is important for *tlc1Δ rad52Δ exo1Δ* cells to escape senescence, it is not essential for maintaining the long term survival of these cells, because in the absence of Rif1, *tlc1Δ rad52Δ exo1Δ* cells still generated survivors when *RAD9* or *RAD24* is deleted. These survivors can grow for more than 100 days in the culture and seem to be immortalised (data not shown). Therefore, other proteins or mechanism may play redundant roles in end protection and replication in established survivors.

Interestingly, compared to other checkpoint proteins (*Rad9*, *Rad24* and *Chk1*), *Mrc1* seems to play a positive role in the survival of *tlc1Δ rad52Δ exo1Δ* cells, as deletion of *MRC1* decreases the survival frequency from ~56% to ~10%. Clearly, this effect is not due to the

checkpoint function of Mrc1, but may be due to its role in DNA replication. It is known that, although Mrc1 is not essential, it is required for normal DNA replication. Mrc1 was shown to interact with and stabilise Pol2 (the catalytic subunit of DNA pol ϵ) at replication forks (Lou et al, 2008). In its absence, all replication forks move at only half of the normal speed, and cells experience extensive replication fork damage even in the absence of exogenous damaging agents (Szyjka et al, 2005). It is possible that the unusual end structure in PAL survivors poses a great challenge for DNA replication, and in the absence of Mrc1, some cells cannot cope with the replication stress and eventually die.

In summary, my results suggest that Rif1 is required for the initial checkpoint adaptation stage essential for generating early post-senescent survivors. However, Rif1 is not essential for long term survival of *tlc1 Δ rad52 Δ exo1 Δ* cells once the palindrome based mechanism is established.

Chapter IV: The role of Rif1 in *cdc13-1* mutants

4.1 Deletion of Rif1 lowers the maximum permissive temperature of *cdc13-1* cells

To understand the function of Rif1 at damaged telomeres, Rif1 was deleted in a *cdc13-1* strain. *cdc13-1* is one of the best studied model systems for telomere uncapping. *cdc13-1* is a temperature sensitive allele of the Cdc13 protein, which is essential for telomere capping. At the restrictive temperature of 27°C, *cdc13-1* is unable to protect the telomeres; this triggers a robust G2/M checkpoint response which in turn arrests the cell cycle.

Consistent with previous studies, *cdc13-1* grew normally at 25°C but could not grow at 27.5°C (Fig 4.1.1). Whereas a *cdc13-1 rif1Δ* strain was unable to grow at 25°C. In contrast, a *cdc13-1* strain carrying a *RIF2* deletion grew slightly better than *cdc13-1* cells at 27.5°C. The *cdc13-1 rif1Δ rif2Δ* triple mutant displayed very similar temperature sensitivity as the *cdc13-1 rif1Δ* double mutant, suggesting that Rif1 plays a vital role in the growth of *cdc13-1 rif2Δ* cells.

The reason that *cdc13-1 rif1Δ* cells failed to grow at 25°C could be either due to cell cycle arrest or cell death. To differentiate between these possibilities, *cdc13-1 rif1Δ* cells were stained with DAPI and the percentage of cells arrested in G2/M phase was scored as described in the methods. As shown in Fig 4.1.2A, as early as 80min at 25°C, about 60% of *cdc13-1 rif1Δ* cells became arrested in G2/M phase, and the cells were completely arrested after 160 min. In contrast, *cdc13-1* and *cdc13-1 rif2Δ* cells arrested extremely slowly, with less than 50% cells arresting during the 400 min experiment. This data suggests that *cdc13-1 rif1Δ* cells could not grow at 25°C due to cell cycle arrest.

Consistent with this finding, western blot analysis showed that the checkpoint proteins Ddc2 and Rad53 were differentially phosphorylated in *cdc13-1* and *cdc13-1 rif1Δ* cells at 25°C (Fig 4.1.2B). As mentioned in the introduction, Ddc2 is a damage sensor which acts in conjugation with Mec1; and phosphorylation of Ddc2 stimulates its activity. Rad53 is an important downstream checkpoint signalling protein. The phosphorylation of Ddc2 and Rad53 was much stronger in *cdc13-1 rif1Δ* cells compared to *cdc13-1* cells, suggesting that the checkpoint response was elevated in *cdc13-1 rif1Δ* cells. This elevated checkpoint response is not restricted to 25°C, but was also detectable at 27°C. DAPI staining revealed that *cdc13-1 rif1Δ* cells arrested earlier than *cdc13-1* cells and *cdc13-1 rif2Δ* cells at 27°C (Fig 4.1.3A). Western blot analysis confirmed this result (Fig 4.1.3B): the phosphorylated forms of Ddc2, Rad9 and Rad53 accumulated earlier and reached higher levels in *cdc13-1 rif1Δ* cells compared to *cdc13-1* cells.

Together these data demonstrate that in the absence of *RIF1*, *cdc13-1* cells arrested at lower temperatures due to an enhanced checkpoint response.

Fig 4.1.1 *RIF1* contributes to the viability of *cdc13-1* mutant at 25°C

Fig 4.1.2 Checkpoint activation in *cdc13-1* cells versus *cdc13-1 rif1Δ* cells at 25°C.

Fig 4.1.3 checkpoint activation in *cdc13-1* cells and *cdc13-1 rif1Δ* cells at 27°C.

4.2 The DNA damage checkpoint pathway arrests *cdc13-1 rif1Δ* cells at 25°C

As previously described in the introduction, two parallel DNA checkpoint pathways are responsible for the arrest in *cdc13-1* cells at non permissive temperatures. In addition, the spindle checkpoint protein Bub2 is also involved in this arrest. To identify which pathway is responsible for the arrest of *cdc13-1 rif1Δ* cells, I combined *cdc13-1 rif1Δ* mutation with several checkpoint deletions and assessed cell growth at different temperatures in liquid or on solid media.

On solid YEPD, *cdc13-1* cells could not grow at 27°C, but its growth was restored when the checkpoint proteins *RAD9* or *RAD24* were deleted (Fig 4.2.1A). Curiously, in the absence of *RIF1*, *cdc13-1 rad9Δ* and *cdc13-1 rad24Δ* cells grow worse than either of the double mutant. Deletion of *RAD24* or *EXO1* partially rescued *cdc13-1 rif1Δ* cells at 25°C, whereas deletion of *RAD9* or *MEC1* had little effect. Since Rad24 and Exo1 are known to be responsible for generating ssDNA damage in *cdc13-1* cells, whereas Rad9 and Mec1 negatively regulate ssDNA levels, the survival of these strains was likely to be an outcome of the amount of ssDNA accumulated in the cells. Deletion of the spindle checkpoint Bub2 or Mad2 did not rescue the temperature sensitivity of *cdc13-1 rif1Δ* cells, indicating that these checkpoints are not involved in the arrest of *cdc13-1 rif1Δ* mutants.

Spot tests provide combined information on both cell survival and cell cycle escape. To differentiate these possibilities, I also performed a growth test in liquid YEPD (Fig 4.2.2A). At 25°C, *cdc13-1 rif1Δ* cells arrested rapidly at the G2/M phase of the cell cycle. Deletion of *RAD9*, *RAD24* or *MEC1* completely abolished this arrest. In contrast, deletion of the spindle checkpoints *BUB2* or *MAD2* resulted only in a mild delay in the arrest, with the majority of cells arrested from 240min onwards. This data suggested that the arrest in *cdc13-1 rif1Δ* cells is mostly depended on the Rad9, Rad24 and Mec1 mediated DNA damage checkpoint

pathway. All together these results above indicate that the damage in *cdc13-1 rif1Δ* cells activates a similar checkpoint cascade as in *cdc13-1* cells.

Fig 4.2.1

Fig 4.2.2

4.3 ssDNA accumulation in *cdc13-1* and *cdc13-1 rif1Δ* cells

The fact that *cdc13-1 rif1Δ* cells display an enhanced checkpoint response in comparison to *cdc13-1* cells raises a key question whether *cdc13-1 rif1Δ* cells accumulate more DNA damage than *cdc13-1* cells. For this I used a QAOS assay (described in the methods) to measure the amount of ssDNA accumulated at different loci on the right arm of chromosome V (Fig 4.3)

In unsynchronised cultures at 25°C, *cdc13-1 rif1Δ* cells accumulated 4.8% ssDNA at 0.6kb away from the telomeres and 7% ssDNA at the YER188W locus, 8kb away from the telomeres. In contrast, neither *cdc13-1* nor *cdc13-1 rif2Δ* cells accumulated more than 2% ssDNA at these loci. There was no detectable ssDNA on the AC strand, meaning that ssDNA damage was specific to the TG strand. This result demonstrates that at 25°C, *cdc13-1 rif1Δ* accumulated more ssDNA at subtelomeric regions than *cdc13-1* cells, which contributes to its arrest.

Previous experiments (Fig 4.1.3) show that at 27°C *cdc13-1 rif2Δ* and *cdc13-1* cells arrest at a similar rate, with *cdc13-1 rif1Δ* cells arresting slightly earlier. Consistent with this, ssDNA levels were found to be similar in these cells at subtelomeric region (0.6kb locus). At the 8kb locus, more ssDNA was detected in *cdc13-1 rif1Δ* cells compared to *cdc13-1* cells at later time points, however these differences were not significant (due to overlapping error bars). Two additional experiments have been performed by my colleague Michael Rushton and the data obtained by him also show that the ssDNA levels were not significantly different between *cdc13-1* and *cdc13-1 rif1Δ* cells at the 8kb locus at 27°C.

Fig. 4.3

4.4 Overexpression of *RIF1* rescues *cdc13-1* mutants at non-permissive temperatures

Since *cdc13-1* strains lacking Rif1 are more temperature sensitive, it is possible that excess amount of Rif1 can rescue *cdc13-1* cells at non-permissive temperatures. To test this hypothesis, I overexpressed *RIF1* by replacing its endogenous promoter (500bp upstream of *RIF1* start codon) with the *GAL1* promoter via homologous recombination (Fig 4.4.1A, for details see method section). As a result, *RIF1* expression could be controlled by different carbon sources in the media. When cells were grown in dextrose (a suppressing sugar) or raffinose (a neutral sugar) media, *RIF1* expression was suppressed. The addition of galactose to cells which have been maintained in raffinose would induce rapid expression of *RIF1*.

To monitor the level of *RIF1* expression, I also constructed a strain with a GFP tag at the N-terminus of *RIF1*, under the control of the *GAL1* promoter. Western blot analysis revealed that the expression of *GFP-RIF1* was absent in cells grown in raffinose media (Time 0), but was induced strongly after the addition of galactose (Fig 4.4.1B).

For untagged strains the expression of *RIF1* gene was monitored by RT-PCR as described in the methods. Upon induction, *GAL1-RIF1* cells shown a 20-40 fold increase in *RIF1* expression compared to the basal expression of *RIF1* (Fig 4.4.1 C).

Fig 4.4.1 overexpression Rif1

Once the overexpression system had been established and validated, *cdc13-1 GAL1-RIF1* cells were tested for temperature sensitivity on a spot test (Fig 4.4.2A.) As expected, *cdc13-1 GAL1-RIF1* cells did not grow on dextrose plate at 25°C, suggesting that *RIF1* was suppressed, and the strain behaved similar to a *cdc13-1 rif1Δ* strain. On galactose plates however, *cdc13-1 GAL1-RIF1* cells grew well at 25°C, and could even grow at 29°C, at the temperature that *cdc13-1* was unable to grow. Overexpressing *RIF1* displayed a similar phenotype as deleting *RAD24* or components of the 9-1-1 complex. This data suggested that overexpression of *RIF1* can rescue the temperature sensitivity of *cdc13-1* cells, to a similar level as checkpoint deletions. Consistent with this finding, Western blotting analysis revealed that a *cdc13-1* strain overexpressing the GFP-tagged *RIF1* was unable to activate Rad53 at 27°C (Fig.2.4.2B). Together these data suggest that excess amount of Rif1 is protective against telomere damage triggered by the *cdc13-1* mutation.

Fig. 4.4.2

4.5 Overexpression of *RIF1* overrides G2/M checkpoint in *cdc13-1* cells

How does Rif1 protein protect telomeres in *cdc13-1* cells at high temperatures? One possibility is that Rif1 may have a capping function at chromosome ends, similar to Cdc13 protein. At non permissive temperatures, increased amount of Rif1 protein may prevent ssDNA accumulation at subtelomeric regions therefore prevent triggering a checkpoint response. Therefore I tested if Rif1 overexpression would allow *cdc13-1* cells that have already arrested with damage to escape G2/M arrest.

In this experiment, *cdc13-1 GAL1-RIF1* cells were grown overnight in raffinose media at 20°C before the temperature was shifted to 27°C to induce telomere uncapping (Fig 4.5.1). After 160min at 27°C, the majority of the cells (~86%) were arrested in G2/M phase as revealed by DAPI staining (Fig 4.5.1A). The culture was then split in two, and either dextrose or galactose was added to the media. As previously mentioned, dextrose suppresses the expression of Rif1 from the GAL promoter whereas galactose induces it. Samples were collected every 80min for DAPI and Western blot analysis.

DAPI staining shows that cells treated with dextrose became fully arrested, whereas cells treated with galactose escaped G2/M arrest. Further analysis revealed that at 400min, about 18% of cells treated with galactose had entered mitosis.

In agreement with this, Rad53 was fully activated in cells treated with dextrose, as evident by a complete shift of the electrophoretic band on Western blotting (Fig 4.5.1B). In contrast, the phosphorylated form of Rad53 gradually decreased in cells treated with galactose. However, it should be noted that a proportion of Rad53 still remained phosphorylated, when compared to the time 0 sample loaded on the right hand side. This is consistent with the fact that not all cells escaped from G2/M arrest.

Fig 4.5.1

Fig 4.5.2

To understand why *cdc13-1* cells overexpressing *RIF1* escaped cell cycle arrest, I measured ssDNA levels by a QAOS assay (Fig 4.5.2). By 160min at 27°C, cells growing in raffinose media accumulated 3.3% ssDNA at the 0.6kb locus. ssDNA rose steadily in cells treated with dextrose, but decreased immediately in cells treated with galactose. Curiously, at the 8kb locus, ssDNA continued to rise from 160min to 320min, before decreased at 400min and onwards. This data, together with the DAPI results suggest that excess amount of Rif1 protein protects the telomeres in *cdc13-1* cells by modulating ssDNA levels in these cells.

4.6 Rif1 is recruited to telomere damage

My data implies that Rif1 plays a protective role at telomeres, but how Rif1 exerts this protective function at the molecular level is still unknown. One possibility is that Rif1 might be directly recruited to the damage and ‘hides’ it from further damage or promotes its repair. To test this hypothesis, I used a chromatin immunoprecipitation (ChIP) assay to measure if Rif1 protein is associated with subtelomeric regions in *cdc13-1* cells grown at non-permissive temperatures.

For ChIP experiments, I created a *cdc13-1* strain carrying a Myc tagged *RIF1*, because no commercial antibody is available for the *S. cerevisiae* Rif1. In general, the Myc tagging has little effect on the function of Rif1, because 1) Myc tagging did not affect the temperature sensitivity of *cdc13-1* cells, and 2) the *RIF1-Myc* strain does not dramatically affect telomere homeostasis (Fig 4.6.1 A and C).

Fig 4.6.1

Having shown that the Myc tagged *RIF1* is functional, I performed ChIP experiments in *cdc13-1 RIF1-MYC* cells grown at 36°C. As shown in the ChIP analysis (Fig 4.6.2A), Rif1 was naturally tethered to telomeres and a ~2.4% enrichment was detected very close to the telomere end (at the 0.6kb locus, time 0). As telomeres became uncapped, Rif1 binding steadily increased at the 0.6kb locus over 3.5 and 7hrs. The increase in Rif1 binding correlates well with the extensive ssDNA generation at these loci (Fig 4.6.2 B). Interestingly, increasing amounts of Rif1 protein was also detected at 8kb and 14kb away from telomeres, where ssDNA was less extensive. The binding of Rif1 appeared to be damage specific, because no binding was detectable at internal regions when telomere was capped (time 0), and little Rif1 binding was found at the control locus (*PAC2*, located close to the centromere). To monitor the specificity of the Myc antibody, I also included an untagged *cdc13-1* control strain probed with a Myc antibody. No non-specific binding of the Myc antibody was detected at either 0.6kb or 8kb locus. Together these data demonstrate that Rif1 is recruited to internal damaged loci.

Since Rif1 is known to interact with Rap1 (Hardy et al, 1992), I further investigated if Rif1 is recruited by Rap1 to the DNA damage by measuring Rap1 binding in the same samples. Surprisingly, unlike Rif1, Rap1 binding consistently decreased at subtelomeres, and only a tiny amount (less than 1%) of Rap1 was detected at the 8kb and 14kb loci. The distinct patterns of Rif1 and Rap1 binding suggested that Rif1 can be recruited to DNA damage independently of Rap1.

Fig 4.6.2

Fig 4.6.2 Rif1 and Rap1 binding in *cdc13-1* cells at 36°C (continued)

A. ChIP analysis of Rif1 and Rap1 binding at different loci on ChrVR. The numbers on the top of the graphs indicate the distance of each locus to the chromosome end. *PAC2* gene is located 410kb away from telomeres and no DNA damage should reach this region. *cdc13-1 RIF1-MYC* cells (LMY78) were grown at 21°C overnight (Time 0) and the temperature was shifted to 36°C and samples were collected for ChIP analysis at 3.5 and 7hrs. ChIP was performed using a c-Myc antibody against the Rif1-Myc protein and a Rap1 antibody. An untagged strain (LMY420) was also probed by the Myc antibody to measure unspecific binding of the Myc antibody. ChIP values were calculated as described in the method section. Error bars represent the standard deviation between three independent qPCR measurements of each sample. At least three independent experiments were performed and a representative experiment is shown. **B.** ssDNA accumulation in *cdc13-1* cells cultured in the same conditions as in the ChIP experiment. The same loci were used for ssDNA measurement and for ChIP. ssDNA data is kindly provided by Michael Rushton.

Having established that Rif1 moves internally with ssDNA accumulation upon telomere uncapping, I next investigated the binding of other telomere associated proteins including Rif2, Sir2 and Sir4. As mentioned in the introduction, Rif2 forms a complex with Rif1 and Rap1 and acts synergistically with Rif1 to regulate telomere length. Sir2 and Sir4 are essential for telomere silencing. All of the three proteins have been shown to bind telomeres and spreading several kilobases internally from chromosomal ends (Smith et al, 2003a), but no studies have been carried out to investigate whether they bind the damage induced by uncapped telomeres. As shown in the ChIP assay, Rif2, Sir2 and Sir4 appear to bind damaged chromatin internally at the 8kb and 14kb loci, similar to Rif1.

Fig. 4.6.3

4.7 Effect of Rif1 on the recruitment of checkpoint proteins and helicase to DNA damage

My previous data suggested that Rif1 may behave like a telomere capping protein and is recruited to damaged chromosome regions. One possibility is that Rif1 physically occupies the space on the chromatin at these damaged loci, and thus inhibits the recruitment of other proteins, such as checkpoint and helicase proteins.

To test this hypothesis, ChIP analysis was performed to detect the binding of Ddc2, Rad9 and Sgs1 in *cdc13-1* cells with or without *RIF1* gene at non-permissive temperatures. As mentioned before, Ddc2 and Mec1 form a complex and are recruited to ssDNA regions coated with Rpa proteins. Sgs1 is an important helicase that unwinds DNA during resection. As revealed by ChIP, Ddc2 was recruited to the subtelomere (0.6kb) and internal chromosome regions (8kb) after telomere uncapping. *cdc13-1* cell without *RIF1* accumulated consistently more (4-7 fold) Ddc2 than *cdc13-1* cells at both loci, indicating that Ddc2 is preferably recruited to the damage in the absence of Rif1. Similar results were found for Rad9 binding, except that the difference in binding was only detected at 7hrs. No major difference in Sgs1 binding was detected in *cdc13-1 rif1Δ* cells compared to *cdc13-1* cells at 36°C, suggesting that Sgs1 recruitment is independent of Rif1 under this condition. This is consistent with the fact that at high temperatures (27°C and above), *cdc13-1 rif1Δ* cells accumulated very similar amount of ssDNA at 0.6kb and 8kb compared to *cdc13-1* cells (Fig 4.3 B)

Fig 4.7

4.8 C-terminal deleted Rif1 is recruited to telomere damage in *cdc13-1* cells

My previous results (Fig 4.6.2) imply that Rif1 might be able to bind DNA damage independent of Rap1. To further explore this possibility, I deleted a large region in the C terminus of Rif1 protein from 1351 to 1916 amino acids, encompassing almost one third of the full length protein. This region contains the sequence known to interact with Rap1 (Hardy et al, 1992). The C-terminal deleted Rif1 was also tagged with Myc to allow ChIP and Western blot analysis. Deleting the C terminus of Rif1 did not affect the temperature sensitivity of *cdc13-1* cells, suggesting that the N terminus of Rif1 is sufficient for Rif1 function (Fig 4.6.1 B) In addition, general telomere maintenance appeared to be normal in *RIF1cΔ* cells, although their telomere length was slightly longer than wild type cells (Fig 4.6.1 C).

ChIP analysis revealed that *RIF1cΔ* has a remarkably similar binding dynamics to damaged chromatin compared to the full length Rif1. Notably, the time 0 binding of *RIF1cΔ* at 0.6kb was much lower than the full length Rif1 protein (0.7% vs 2.4%). This suggests that deletion of the C terminus of Rif1 disrupted its binding to telomere/sublomere region, possibly due to a loss of interaction with Rap1. However this deletion did not affect Rif1 binding when telomere was uncapped, suggesting that the N terminus of Rif1 remains effective in binding damaged chromatin.

Fig 4.8

4.9 Overexpression of C-terminal deleted Rif1 rescues *cdc13-1* at 32°C

It seems that the N terminus of Rif1 is sufficient for the binding of DNA damage and protecting telomeres in *cdc13-1* cells. This raises the possibility that over-expressing this part of the Rif1 would rescue *cdc13-1* cells as well as over-expressing the full length of Rif1.

To test this hypothesis, I created a *cdc13-1* strain overexpressing the N terminus of Rif1 from the *GAL1* promoter as described in the method. On a spot test, the *cdc13-1 GAL1-RIF1cΔ* strain grew well at 29°C, whereas *cdc13-1* cells completely failed to grow. Surprisingly, *cdc13-1* cells overexpressing C-terminal deleted Rif1 can even grow at 32°C, better than cells overexpressing the full length Rif1 (Fig 4.9). This data suggests that the C-terminal deleted Rif1 can better protect the damage resulting from telomere uncapping.

Fig 4.9

4.10 scRif1 contains potential N-terminal HEAT-repeats but lacks the C-terminal DNA binding domain

To better understand the function of the budding yeast Rif1, I analysed the amino acid sequence of Rif1 in hope to find any functional domains that could explain the capping property of Rif1. However, a search in the conserved domain database in the NCBI website yielded no known domains for the budding yeast Rif1. This is probably because many domains rely on their secondary structure for function, and are poorly conserved at the primary sequence level; therefore it can be very difficult to predict protein structures using traditional methods. HHpred is a recently developed protein structural predication tool, which uses prolife comparisons to solve protein structure, therefore is more powerful than sequence-sequence comparison tools such as BLAST (Kippert & Gerloff, 2009).

After submitting Rif1 sequence to the HHpred server, over 10 sequences that are structurally related to scRif1 were detected. Among them, 5 belonged to the importin and exportin proteins from human, mouse and yeast. Three belonged to microtubule binding proteins. The protein motifs that share similarity to Rif1 all contained multiple HEAT repeats (Huntingtin, elongation factor 3 (EF3), protein phosphatase 2A (PP2A), and the yeast PI3-kinase IOR1). Usually HEAT repeats consist of two anti-parallel α helices, which form a hairpin structure comprises ~ 30 amino acids. When the adjacent helices pack together in parallel via hydrophobic interactions, an elegant superhelix is formed (Andrade et al, 2001). I further analyzed Rif1 using I-TASSER (Roy et al, 2010), an excellent protein structure prediction tool, to generate a 3D structure of Rif1 N-terminus. It is very clear from the 3D structure that a large portion of Rif1 protein is folded into multiple anti-parallel α -helices, characteristic of HEAT repeats. Together, these data strongly suggest that the N terminus of budding yeast Rif1 contains HEAT repeats.

Fig4.10.1

Since human Rif1 has a C-terminal DNA binding domain, it is possible that budding yeast Rif1 also contains this sequence, which may be responsible for its recruitment to the DNA damage. However, alignment of the human and budding yeast Rif1 sequence revealed that the C-terminal domain is absent in budding yeast (Fig 4.10.2). Together, these data suggest that the relatively conserved N-terminus region of budding yeast Rif1 contains large HEAT repeats, like Rif1 in humans. However, scRif1 lacked the C terminal domain required for DNA binding.

Fig. 4.10.2

4.11 Discussion

While the PAL survivors provided limited clues of Rif1's function, the *cdc13-1* system yielded clearer insights in to how Rif1 confers end protection at damaged telomeres. In this chapter, I found that deletion of Rif1 increases the temperature sensitivity of *cdc13-1* mutants, by inducing a cell cycle arrest via the DNA-damage checkpoint pathway dependent on Rad9, Rad24 and Mec1. In contrast, overexpression of *RIF1* allowed *cdc13-1* cells to proliferate at previously non-permissive temperatures. In addition, the overexpression of *RIF1* allows cells to adapt to telomere damage (discussed below). These data strongly suggest that Rif1 contributes to telomere capping in the *cdc13-1* mutant.

The results from my genetic study have been recently confirmed by an independent research group (Anbalagan et al, 2011). However, in their study no molecular mechanism was discovered as to how Rif1 confer this end capping effect. Here, I provide evidence that Rif1's effect could be due to its direct association with chromatin damage, where it inhibits checkpoint proteins. ChIP experiments reveals that upon telomere uncapping, Rif1 and other Rap1-bound proteins (Rif2, Sir2 and Sir4) are increasingly associated with damaged chromatin at subtelomeres, as well as with internal loci up to 14kb away from telomeres. This telomere-independent association could mean that Rif1 is actively recruited to DNA damage and subsequently may recruit other proteins. Alternatively, a conformation change of the chromatin could be induced by telomere resection, which in turn sequesters multiple proteins to the damaged loci. However, the telomere-protective function is only observed in Rif1, but not in Rif2 (since *rif2Δ* improved the growth of *cdc13-1* cells) or Sirs (Sir2 and Sir4 did not affect the growth of *cdc13-1* cells; data not shown), suggesting that Rif1 may possess unique structural and functional domains.

4.11.1 Checkpoint inhibitory role of Rif1

At damaged loci, the binding of checkpoint proteins Ddc2 and Rad9 in *rif1Δ cdc13-1* cells is several fold higher than *RIF1+ cdc13-1* cells. Since ssDNA is very similar at these loci, this result suggests that Rif1 may inhibit the checkpoint protein binding to the localised damage, possibly by competing with them for the same DNA substrate. Similar inhibitory effects were observed with the checkpoint protein Ddc1, Rpa (Xue et al, PLOS Genetics, data from Michael Rushton) and Tel1 (Hirano et al, 2009). Since Rpa functions upstream of the Ddc2/Mec1 sensor kinase, the inhibitory effect of Rif1 on Ddc2 binding could be explained by its inhibition on Rpa binding. The fact that Rif1 could inhibit both ssDNA and dsDNA binding proteins implies that Rif1 may occupy a variety of DNA damage induced structures. Interestingly, high levels of Rif1 were detected at internal loci (8kb and 14kb) which contained limited amount ssDNA damage. This suggests Rif1 may preferably bind sites of resection activity, at the ss-dsDNA 5' junction.

4.11.2 Nuclease inhibitory role of Rif1

In addition to its role in inhibiting checkpoints, Rif1 may also inhibit nuclease activity when bound to double-stranded telomere repeats. The intriguing finding that telomere resection in *RIF+* cells and *rif1Δ* cells proceed at almost the same pace, despite the fact that *rif1Δ* cells contain longer telomeres (300-400bp more TG repeats) , suggests that the terminal TG sequences are more rapidly degraded in the absence of Rif1. In support of this idea, deletion of *EXO1* partially rescued *cdc13-1 rif1Δ* cells at 25°C. A recent study also reported that the lack of Rif1 in *cdc13-1* cells causes the generation of extensive telomeric ssDNA even at the permissive temperature of 20°C (Anbalagan et al, 2011). This ssDNA was diminished when *EXO1* is deleted, suggesting that nuclease-dependent degradation occurs at the telomeres in

cdc13-1 rif1Δ cells. Since it was found that *rif1Δ* alone does not cause ssDNA accumulation at the telomeres (Anbalagan et al, 2011), the nucleases inhibitory effect of Rif1 seems to be partially Cdc13 dependent. All together, my data and others suggest that Rif1, in cooperation with Cdc13, protects the terminal telomere repeats from nuclease degradation. A possible model could be that budding yeast Rap1, possesses architectural abilities that can bend DNA in to a 'closed' conformation, while Rif1 provides the protein-protein interaction platform to hold this structure together (for reasons discussed below) (See figure 4.11 A). This model is inspired by the research from Blackburn's lab (Levy & Blackburn 2004). In their experiment, C-terminal deleted Rap1 is fused with a protein domain (PDZ domain) from mammalian cells. PDZ domain are known to homomultimerize and held telomere together in a 'sticky ball' formation. Interestingly it was found that this fusion protein is sufficient to confer telomere length regulation even in the absence of Rif1 and Rif2. It is hence possible that Rif1 could provide similar function as the PDZ domain. In my proposed model the 5' end of the telomere is tucked in, therefore this structure can prevent nuclease attack to the 5' end. Such structure could represent a unique end structure in budding yeast, since it is known that the budding yeast telomeres do not contain nucleosomes, instead, they are packed in larger particles called telosomes via unknown protein-protein interactions (Wright et al, 1992). It is therefore possible that Rif1 is involved in telosome formation in budding yeast. In addition, this structure could also provide an explanation as to how Rif1 and Rif2 proteins inhibit telomerase action.

4.11.3 Rap1 independent role of Rif1

For many years it was thought that the budding yeast Rif1 solely depends on Rap1 for its function. However, my results suggest that this is not the case. ChIP analysis revealed that Rif1 is recruited to damaged subtelomeres, while Rap1 is displaced from the same regions,

raising the possibility that Rif1 could act independently of Rap1. Using a Rif1 mutant in which the Rif1-Rap interacting sequence was deleted, it was found that the N terminus of Rif1 is completely functional in capping, and is largely normal in telomere length regulation. In addition, ChIP analysis revealed that the N terminus of Rif1 is recruited to telomere damage as efficiently as the full length Rif1. All these data strongly support the hypothesis that Rif1 has a distinct function that is independent of Rap1, and upon telomere damage, Rif1 may dissociate from Rap1 to perform end capping.

Further support came from the structural analysis of scRif1 protein. Using advanced structural prediction tools, the N-terminal region of budding yeast Rif1 was revealed to contain large HEAT-like repeats. Recent evidence suggest that HEAT repeats are a conserved feature of Rif1 protein from a diverse range of organisms, including human, fruit fly, and fission yeast (Xu et al, 2010). This structure have been found in proteins with diverse functions, including the DNA damage response proteins ATM, ATR and DNA-PKcs (Perry & Kleckner, 2003), and proteins involved in intracellular transport, such as exportin and importin. This explains why in the structure analysis, exportin and importins turned out as proteins with the closes structural similarities to scRif1. It is therefore possible that the N terminal HEAT repeats represents a functional domain of scRif1, and this domain is involved in chromosome end capping independently of Rap1. Unexpectedly, several microtubule binding proteins (such as Stu2) were also found to be structurally related to scRif1. It seems possible that the N terminus of Rif1 might bind microtubules, because hRif1 has been localised to microtubules in early anaphase (Xu & Blackburn, 2004). It therefore will be interesting to investigate in the future whether Rif1 plays a role in regulating microtubule functions, or *vice versa*.

4.11.4 The role of Rif1 in repair and adaptation

Overexpression of Rif1 allows *cdc13-1* cells to proliferate at 29°C, a temperature at which *cdc13-1* is almost completely non-functional. This suggests that when Cdc13 function is compromised, Rif1 provides additional capping at chromosome ends. Interestingly, overexpression of Rif1 also can rescue *cdc13-1* cells that are arrested due to accumulation of subtelomeric ssDNA (Fig 4.5.1 and 4.5.2). In this case, the majority of cells were arrested at 160min at 27°C, and upon Rif1 overexpression, ~10% cells escaped G2/M phase and entered mitosis. Almost simultaneously, ssDNA at subtelomeres (the 0.6kb locus) decreased. Intriguingly, ssDNA at internal 8kb locus continue to accumulate from 240min to 320min and only started to decrease after 320min. This suggests that 1) a repair process might have taken place to fill in the long ssDNA gap when additional telomere capping is provided by Rif1. And 2), this repair is likely to proceed from terminal region to internal loci. In support of this hypothesis, a recent study showed that Rif1 functionally interacts with the polymerase α -primase complex, a protein complex that is vital for lagging strand synthesis at telomeres (Anbalagan et al, 2011). Therefore it is possible that Rif1 could stimulate the activity of the primase complex to initiate the repair on the C strand. Alternatively, it is known that the CST complex also stimulates the primase complex: Cdc13 and Stn1 physically interact with the catalytic and the regulatory subunits of the Pol α -primase complex, respectively (Grossi et al, 2004; Qi & Zakian, 2000). So it is possible that Rif1 indirectly facilitates repair by stimulating the interactions between CST and Pol α .

In addition to the possible role of Rif1 in telomere repair, the above experiment also demonstrates a potential role of Rif1 in checkpoint adaptation to ssDNA damage. To show that adaptation has occurred, three criteria have to be met (proposed by Toczyski et al, 1997): 1) cells arrest in response to a signal (i.e.DNA damage); 2) cells eventually override this arrest; 3) cells still contain the signal at the time it resumes division. In this experiment,

ssDNA at subtelomeres and internal loci signalled the arrest of *cdc13-1* cells. When Rif1 was overexpressed, a population of cells override this arrest after about an hour (240min time point). At the precise time when cells escaped (240-320min) unrepaired ssDNA still remained at the 8kb locus. Therefore, this data suggests that checkpoint adaptation may have occurred in *cdc13-1* cells overexpressing *RIF1*.

To date, the molecular mechanism for checkpoint adaptation is still unknown. One hypothesis is that the initial DNA structure that triggers the checkpoint response may become processed into a non-signalling structure over time (Lupardus & Cimprich, 2004). The fact that many adaptation mutants such as *yku70Δ*, *sae2Δ*, *srs2Δ* have DNA end processing activity supports this idea. My data suggest that to adapt to ssDNA damage, a limited amount of repair may be required for converting long stretches of ssDNA to shorter gaps of ssDNA, and this may be sufficient for cells to override the checkpoint. In addition, ssDNA resection at uncapped telomeres is tightly regulated by the cell cycle, and once cells enter G1 phase they do not accumulate ssDNA (Vodenicharov & Wellinger, 2006). Therefore, checkpoint adaptation can also provide a selective advantage for the cells, allowing more chance to repair in the subsequent cell cycle.

In light of these observations, I propose a model explaining how Rif1 protects telomeres in *cdc13-1* cells (Fig 4.11) However, many questions still remain to be answered. E.g. Does the end capping role of Rif1 apply to other telomere uncapping systems, or to double strand breaks? What DNA structure or proteins are responsible for the recruitment of Rif1? Some of these questions will be addressed in the following chapters.

Fig 4.11

Fig 4.11 A proposed model of how Rif1 protects telomeres in *cdc13-1* cells

A. Rif1 and Cdc13 co-operate to protect the 5' end of telomeres from nuclease degradation in WT cells. At telomeres, Rap1-bound Rif1 may interact with each other or/and other telomere-binding proteins to form a 'closed' structure (such as a hairpin like structure). The HEAT-repeat domain of Rif1 may be critical for these protein-protein interactions. This structure conceals the 5' end from nucleases such as Exo1, and might represent the 'telosome' structure in budding yeast. In the absence of Rif1, *cdc13* is sufficient for the protection against the majority of end degradation. However, when *cdc13* function is compromised, Rif1 poses an additional layer of protection against nuclease attacks.

B. Rif1 protects against checkpoint recruitment at damage in *cdc13-1* cells. At 27°C, *cdc13-1* is non-functional, and nuclease activity overcomes the barrier of Rif1 and generates extensive ssDNA at the subtelomere region. As telomere repeats become single-stranded, Rap1 dissociates from DNA whereas Rif1 remain bound to single-stranded and double-stranded DNA damage. On ssDNA, Rif1 competes with the binding of Rpa, while on dsDNA, Rif1 blocks the loading of the 9/1/1 ring and competes with Tel1 and Rad9 for their binding to chromatin. However, due to continuous degradation, many checkpoint proteins are able to bind DNA damage and subsequently arrest the cell cycle.

C. Enhanced checkpoint response in *cdc13-1* cells in the absence of Rif1. The deletion of *RIF1* causes a 300-400bp increase in telomere length, however, without the structural protection, nuclease rapidly degrade the telomere region. In the absence of Rif1, all checkpoint proteins bind freely to damage, hence triggering a stronger checkpoint response.

D. *RIF1* overexpression allows *cdc13-1* cells to adapt to telomere damage. Excess amount of Rif1 is recruited to sites of damage, where it inhibits checkpoint signalling and nuclease

activity. Rif1 may also provide additional capping at telomeres and facilitate repair on the C rich strand, resulting in a decrease in ssDNA. This may be achieved by directly or indirectly stimulating the activity of polymerase α -primase complex. Lower amount of ssDNA at subtelomere regions allows a population of cells undergo checkpoint adaptation and to escape G2/M arrest.

Chapter V: The role of Rif1 in *yku70Δ* system

5.1 The effect of *RIF1* and *RIF2* deletion in *yku70Δ* cells

To further investigate the telomere protective role of Rif1, I extended my study to the *yku70Δ* model system. Deletion of YKU70 in budding yeast results in a similar but distinct telomere uncapping effect compared to the *cdc13-1* mutation, as described in the introduction. The *yku70Δ* strain exhibits temperature sensitivity at 37°C. If Rif1 is involved in telomere capping in *yku70Δ* cells, one would expect that deletion of *RIF1* in *yku70Δ* mutants will exacerbate this temperature sensitivity at 37°C. To test this, I explored two methods of obtaining *yku70Δ rif1Δ* and *yku70Δ rif2Δ* mutants. The first method was by a classic genetic technique: A diploid strain (LMY583) was generated by the mating of a *yku70Δ rif1Δ* and a *rif2Δ* strain; after sporulation, strains were assayed for temperature sensitivity by a spot test. In contrast to the results obtained in *cdc13-1* cells, *yku70Δ rif1Δ* and *yku70Δ rif2Δ* double mutants grow much better than *yku70Δ* cells at high temperatures (Fig 5.1). In addition, a synergetic effect of Rif1 and Rif2 was observed, as the *yku70Δ rif1Δ rif2Δ* triple mutant grew better than both double mutants. To confirm this result, *yku70Δ rif1Δ* and *yku70Δ rif2Δ* strains were generated by a second method involves one-step PCR based gene knock-out. Intriguingly, in this case, *yku70Δ rif1Δ* cells grow only slightly better than *yku70Δ* cells, and *RIF2* deletion did not affect the temperature sensitivity of *yku70Δ* cells. These results suggest that Rif1 does not have the same telomere protective role in *yku70Δ* cells compared to in *cdc13-1* cells.

Fig 5.1

5.2 The relationship between temperature sensitivity and telomere length

How can cells with the same genotype exhibit different phenotypes? One hypothesis is that an epigenetic (e.g. telomere length regulated) effect exists and it can influence temperature sensitivity. To test this hypothesis, *yku70Δ rif1Δ* strains obtained from either sporulation or gene disruption were passaged every 2-3 days on YEPD plates, and strains were analysed by a spot test (Figure 5.2.1). Interestingly, increased temperature sensitivity was observed for *yku70Δ rif1Δ* strains obtained from sporulation as they were passaged on YEPD plates, whereas *yku70Δ rif1Δ* cells obtained from genetic knockout showed no change for temperature sensitivity at 37°C during further passages. Telomere blots were performed to visualise the changes in telomere length in the same strains used for the spot test. The *YKU70/yku70Δ RIF1/rif1Δ RIF2/rif2Δ* diploid resulted from the mating had longer telomeres than both parents, indicating that telomere length is inherited. Immediately after sporulation, the telomere in *yku70Δ rif1Δ* strains dramatically shortened, and the telomere shortening continued with further passages. This suggests that deletion of *RIF1* did not cause telomere elongation as in normally observed in WT cells. Interestingly, the decrease in telomere length in sporulated *yku70Δ rif1Δ* cells correlated well with increased temperature sensitivity of these cells. In contrast, the *yku70Δ rif1Δ* knockout strains showed little changes in telomere length, which correlated with no change in temperature sensitivity. This seems to suggest that longer telomeres may have a protective role in *yku70Δ rif1Δ* strains.

When *yku70Δ rif2Δ* and *yku70Δ rif1Δ rif2Δ* cells were examined, very similar results were found (Fig 5.2.2 and 5.2.3) i.e. strains generated from sporulation had increased temperature sensitivity and shorter telomere length with further passages. In contrast, the telomere length in yeast strains generated from genetic knockout was largely stable.

Interestingly, the *yku70Δ rif2Δ* strain obtained from genetic knockout showed a slight decrease in temperature sensitivity (Fig 5.2.2).

Fig 5.2.1

Fig 5.2.2

Fig 5.2.3

5.3 *RAD51* and *RAD52* are essential for the survival of *yku70Δ rif1Δ* and *yku70Δ rif1Δ rif2Δ* cells at high temperatures

It was previously shown that inactivation of the helicase Pif1 (Pif1-m2) can also rescue the temperature sensitivity of *yku70Δ* cells at 37°C, and interestingly, this phenotype is dependent on homologous recombination (Smith et al, 2008). Deletion of *RIF1* and *RIF2* has a similar telomere elongation effect as the Pif1-m2 mutation. So, is it possible that HR is also required for the survival of *yku70Δ rif1Δ* and *yku70Δ rif1Δ rif2Δ* cells at non-permissive temperatures? I sought to address this question by deleting *RAD51* in *yku70Δ rif1Δ* background. This *yku70Δ rif1Δ* strain (LMY368) has inherited longer telomeres (Fig 5.2.1B) and grew moderately well at 37°C (Fig 5.3 A). Interestingly, the deletion of *RAD51* in all of the five *yku70Δ rif1Δ rad52Δ* triple mutants restored the temperature sensitivity at 37°C. Similar results were observed when a *rad52Δ* mutation was combined with a *yku70Δ rif1Δ rif2Δ* strain (Fig 5.3 B). Together these data suggest that HR proteins Rad51 and Rad52 are essential for the survival of *yku70Δ rif1Δ* and *yku70Δ rif1Δ rif2Δ* cells at high temperatures.

Fig 5.3

5.4 Recruitment of Rif1 protein in *yku70Δ* cells

Unlike in *cdc13-1* cells, my data suggest that Rif1 is not involved in telomere capping in *yku70Δ* cells. One possibility is that Rif1 is not recruited to the damage induced by *YKU70* deletion. To test this hypothesis, I measured Rif1 binding in a *yku70Δ RIF1-Myc* strain on both ChrV and ChrVI at 37.5°C (Fig 4.4A). Since it was previously shown that *yku70Δ* cells accumulate a very limited amount of ssDNA in the subtelomeric region on ChrVR at 37°C (Maringele & Lydall, 2002), measuring Rif1 enrichment on ChrVR may not be ideal due to insufficient damage. Unlike ChrVR, ChrVIR does not contain a Y' element, therefore the accumulation of ssDNA should be more efficient. The extent of the damage was monitored by Rfa1 and Sgs1 binding.

At 0.5kb and 1kb away from telomere on ChrVIR, Rfa1 binding increased steadily over time at 37.5°C, indicating ssDNA accumulated at this region (Fig 5.4B). But very limited binding of Rfa1 at 5kb was observed (especially after subtracting the ChIP value from the *PAC2* control locus, Fig 5.4C), suggesting that ssDNA did not reach this region. There was no binding of Sgs1 at the subtelomere on either ChrV or ChrVI, suggesting that unlike in *cdc13-1* cells and at DSB, Sgs1 is not required in unwinding the DNA for resection. Together, these data demonstrate that a limited amount of ssDNA accumulates at subtelomeric regions at 37.5°C in *yku70Δ* cells. Under these conditions, Rif1 binding was detected at the 0.5kb and 1kb loci on ChrVIR and the 0.6kb locus on ChrVR, but no increase of binding was observed after telomere uncapping (Fig 5.4 B and C). The same result was found for Rap1. These results suggest that unlike in *cdc13-1* cells, Rif1 is not actively recruited to the damage in *yku70Δ* cells.

Fig 5.4

5.5 Recruitment of Rif1 in *cdc13-1 yku70Δ* cells

Why is Rif1 not recruited to the damage in *yku70Δ* cells? One possibility is that *yku70* itself is required for the recruitment of Rif1. To test this hypothesis, *yku70Δ RIF1-Myc* strain was combined with the *cdc13-1* mutation and ChIP analysis was performed along with a *cdc13-1 RIF1-Myc* control strain. As shown in Fig 5.5, Rif1 binding was detected at the 0.6kb and 8kb loci on ChrVR, and no obvious difference was observed between the *cdc13-1 yku70Δ* strain and the *cdc13-1 RIF1-Myc* control strain. This result suggests that Yku70 is unlikely to be responsible for the recruitment of Rif1.

Fig. 5.5

5.6 Discussion

In this chapter I investigated if Rif1 has a similar 'capping' role in an alternative telomere uncapping model, *yku70Δ* cells. The *yku70Δ* model system has many subtle differences compared to the *cdc13-1* system. For example, the arrest of *yku70Δ* cells at 37°C depends only on Chk1, Mec1, and Rad9 checkpoint proteins but does not require the 9-1-1 complex, Rad17, and Dun1 (Maringele & Lydall, 2002), whereas *cdc13-1* cells require all of these factors for efficient arrest. In addition, the resection rate at telomeres is much faster in *cdc13-1* cells, reaching several thousand bases internally (Zubko et al, 2004).

Surprisingly, Rif1 appears to play an opposite role in *yku70Δ* cells compared to *cdc13-1* cells, because deletion of *RIF1* (by both gene deletion and sporulation) improved the growth of *yku70Δ* cells at 36°C. The same effect was also observed by an independent group (Gravel & Wellinger, 2002); however the molecular basis underpinning this improved growth of *yku70Δ rif1Δ* cells is still unclear. My results suggest that there is an intriguing correlation between temperature sensitivity and telomere length. For instance, the *yku70Δ rif1Δ* cells obtained from gene knockout contained short, but stable telomeres and grow poorly at 37°C. In contrast, telomeres are much longer in *yku70Δ rif1Δ* cells obtained from sporulation, and these cells were able to grow very well at 37°C immediately after sporulation. With further passage, telomeres progressively shortened in *yku70Δ rif1Δ* cells. This telomere shortening is accompanied by an increase in temperature sensitivity in these cells. Furthermore, deletion of *RIF2* in *yku70Δ rif1Δ* cells further increased telomere length, and improved cell growth at 37°C. Together, these results suggest that longer telomeres may have a protective role in *yku70Δ* mutants. Consistent with my data, a recent study showed that inactivating the helicase Pif1 (using a *pif1-m2* mutant) causes telomere elongation in *yku70Δ* cells, and rescues *yku70Δ* cells at high temperatures (Smith et al,

2008). This data further supports the correlation between telomere length and telomere stability in *yku70Δ* cells.

To date, there is no direct evidence suggesting that long telomeres *per se* confer end protection; it is likely that other telomere-interacting proteins are required for telomere stability. Interestingly, the HR protein Rad52 and Rad51 were found to be required for the temperature-resistant phenotype of *yku70Δ rif1Δ* cells and *yku70Δ rif1Δ rif2Δ* cells. Similarly, Rad51 and Rad52 were also essential for the growth of *pif1-m2 yku70Δ* cells at high temperatures (Smith et al, 2008). How can the homologous recombination pathway improve the survival of *yku70Δ* cells containing long telomeres? It appears that HR is used by some temperature-resistant *yku70Δ* survivors to amplify the subtelomere Y' elements, providing an alternative way to stabilize the uncapped telomeres (Fellerhoff et al, 2000). However, this amplification was only found in rare survivors but not in normal *yku70Δ* cells; therefore this mechanism is unlikely to be responsible for the improved survival in *yku70Δ rif1Δ* cells. A different suggestion was that HR could be essential for stabilising telomere structures in *yku70Δ* cells (Smith et al, 2008). According to this model, long single-stranded G overhangs in *yku70Δ* cells could form a stable terminal structure involving the generation of a G-strand loop, which is similar to the t-loop observed in mammals (Griffith et al, 1999). This structure could potentially block checkpoint activation, but requires the assistance of HR to maintain its stability. However, I was unable to find any supporting evidence in the literature that HR can stabilise telomere loops, and on the opposite, HR is known to excise t-loops which results in sudden telomere shortening (known as T-loop HR) (Wang et al, 2004). Rapid telomere deletion also occurs in budding yeast. It was reported that when the C-terminus of Rap1 is deleted, yeast telomeres undergo dramatic elongation and become highly unstable, subject to sudden deletion of the telomeric tracts. Interestingly this deletion is independent of Rad52 (Kyrion et al, 1992).

Why does Rif1 behave differently in *yku70Δ* cells compared to *cdc13-1* cells? The simplest explanation is that Rif1 is not recruited to the *yku70Δ*-induced damage, and the direct association of Rif1 to damaged sites may be required for its capping effect. Since CHIP experiments showed that Yku70 itself is not responsible for the recruitment of Rif1, other mechanisms must be required for Rif1 recruitment. It is possible that the recruitment of Rif1 needs special DNA substrates (such as extensive ssDNA) that are lacking in the *yku70Δ* mutant. Indeed, it was reported that telomere resection is very limited in *yku70Δ* cells, and does not reach internal loci (Maringele & Lydall, 2002). So perhaps this limited amount of ssDNA is not sufficient to recruit Rif1. Alternatively, specific DNA topology (e.g supercoiled DNA) may be required, and the 3D structure resulting from telomere uncapping in *cdc13-1* and *yku70Δ* cells might be vastly different.

In conclusion, Rif1 does not appear to perform telomere capping in *yku70Δ* mutants. Instead, deletion of *RIF1* leads to telomere elongation, which confers end protection. This end protection effect in *yku70Δ rif1Δ* cells is dependent on the HR pathway. Since Yku70 itself is not responsible for the recruitment of Rif1, the quest for the Rif1 recruiting factor goes on.

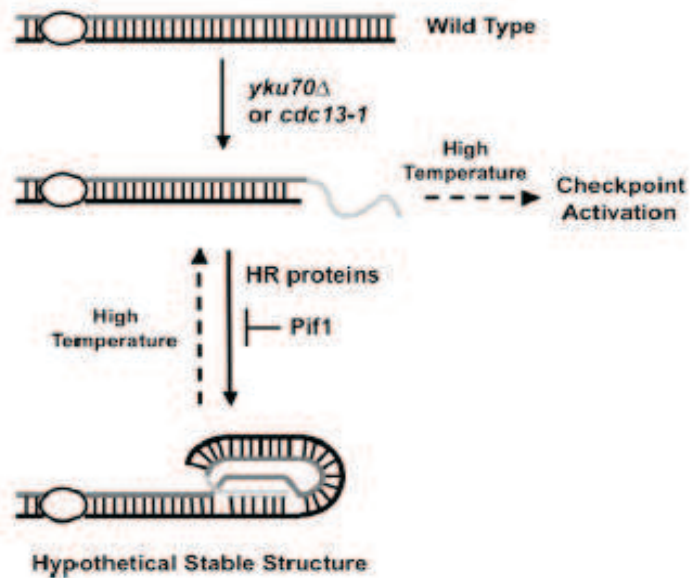


Fig 5.6 A model proposed by Smith et al (2008) explaining how HR pathway stabilises telomeres in *yku70Δ* cells. The ssDNA overhang in *yku70Δ* cells invades the double-stranded telomere repeats and base pairs with the C rich strand; this generates a G strand loop which is stabilised by the HR proteins.

Chapter VI: The role of Rif1 at double strand breaks

6.1 The HO-inducible DSB system

My previous results showed that upon telomere uncapping in *cdc13-1* cells, Rif1 is recruited to sites of damage and protects these regions against further damage. This raises an interesting question as to whether Rif1 can also bind a natural DSB, which share many similarities to an uncapped telomere. I therefore investigated whether Rif1 is recruited to a DSB, and whether Rif1 plays a protective role at DSB, e.g. inhibit checkpoint activation and promoting DNA repair.

To address these questions, I used a well characterized galactose inducible HO endonuclease DSB system (Fig 6.1A) (Sugawara et al, 2003; Wang & Haber, 2004). This system explores the mating type switching phenomenon in wild type yeast. During mating type switching, yeast expresses an HO endonuclease which cleaves a specific sequence located in the *MATa* or *MAT α* gene. The resulting DSB is immediately repaired by HR using the homologous sequences at the *HMR* or *HML* loci, which encodes for alternative mating type. In the experimental strain JMK139, HO was placed in a plasmid under the control of the *GAL10* promoter while the endogenous HO endonuclease gene was deleted. In the presence of galactose, HO is expressed continuously, causing cycles of cleavage and ligation at the cutting site, which leads to a robust G2/M arrest in cells. Since the *HML* and *HMR* loci were also deleted, DNA damage cannot be repaired by homologous recombination, hence the majority of cells die. However, a small number of cells (less than 1 in 1000) survive by mutating the HO cutting site, using an error-prone repair pathway mediated by NHEJ. NHEJ can introduce small insertions or deletions in the HO cutting site therefore abolishing the action of HO endonuclease.

To validate this system, the efficiency of DSB induction was monitored by qPCR using a set of primers spanning the cutting site of HO endonuclease (Fig 6.1B). The creation of the DSB is very rapid, since over 85% of *MATa* locus was cut within 30min after the addition of galactose, and virtually no *MATa* product was detectable after 2hrs. DAPI staining revealed that this single DSB created by HO cutting triggered a robust G2/M arrest in the cells (Fig 6.1C), with the majority (~75%) of cells arresting 3hr after the HO induction.

Fig 6.1.

6.2 Recruitment of Rif1 to a single DSB

Having validated the DSB system, I performed ChIP analysis in *RIF1-MYC* tagged JKM139 strains using 9 sets of primers located on either side of the break (Fig 6.2.1A). By this means, a detailed map of protein binding around the DSB could be achieved. As shown in Fig 6.2.1B, it appeared that Rif1 did not significantly associate with the DSB induced by HO endonuclease. Further analysis with the Myc antibody alone against an untagged strain further confirmed this finding (Fig 6.2.1C).

Why is Rif1 not recruited to a DSB? One possibility is that there is simply not enough amount of Rif1 to be mobilised to a DSB. Therefore I further investigated whether overexpressed Rif1 would be recruited to a DSB. For this purpose, the Rif1 is overexpressed from the *ADH1* promoter and tagged with HA (for details see methods). As shown by the ChIP analysis (Fig 6.2.2A), overexpressed Rif1 was recruited to a large region spanning 10kb on either side of the break. The enrichment of Rif1 around the DSB can be detected 2hrs after the break was induced and Rif1 continued to accumulate at 4hrs. Intriguingly, maximum enrichment of Rif1 was observed 2-5kb away from the break site, but not immediately adjacent the break (+0.2kb). Rif1 protein showed a relative symmetrical distribution around the break, suggesting that both ends are processed similarly. Importantly, no non-specific binding of the HA antibody was detected around a DSB (Fig 6.2.2B), suggesting that the binding of overexpressed Rif1 was genuine. Rif1 appeared to bind to a vast region on damaged chromatin as the enrichment of Rif1 was detected up to 30kb away from the break (data not shown). The biphasic association of Rif1 to the DSB is reminiscent to that of γ -H2AX, which is found to associate preferably at 2-5kb on either side of the DSB but not directly adjacent to the break site (Shroff et al, 2004). Similar to Rif1, γ -H2AX also showed a broad range of association (up to 50kb surrounding the DSB) to the damaged chromatin. In addition, the biphasic binding pattern was also detected in Rad9

(data not shown), and this protein is recruited by H3K79me. In contrast, several DNA binding proteins including Rad51 (Sugawara et al, 2003), Rpa1 (Wang & Haber, 2004) and Mre11 (Shroff et al, 2004) display an opposite binding pattern, with maximum enrichment close to the break site and their association drops sharply away from the DSB. Together these data suggest that the biphasic Rif1 association is genuine, and it is likely that Rif1 might be recruited by damaged chromatin rather than by direct DNA binding.

Fig 6.2.1

Fig 6.2.2

6.3 Recruitment of Rap1 to a DSB

Due to the interaction between Rif1 and Rap1, I further investigated if Rap1 can also be recruited to a DSB. For this purpose the *MAT α* JKM139 strain was utilized, because this strain does not contain any endogenous Rap1 binding sites. As expected, no Rap1 binding was detected around the HO site before the break was induced (time 0, Fig3.3 A). After DSB induction, however, Rap1 increasingly accumulated around the DSB region. Interestingly, the maximum enrichment was observed closely adjacent the break (+0.2kb), a site that is distinct from the maximum enrichment sites of Rif1. The binding of Rap1 was lower on either side of the break and decreases even further at remote loci. This data suggests that Rap1 can be recruited to a DSB independent of its binding sequence.

It was previously proposed that telomeres serve as a reservoir for factors involved in DSB processing, and upon a DSB, these factors leave telomere regions and move to the internal damage sites to participate in repair (Martin et al, 1999). I therefore tested this idea by measuring Rap1 binding at the subtelomeric region in the same experiment. Interestingly, at 0.6kb away from telomeres, Rap1 binding consistently decreased overtime upon DSB induction. This data suggest that Rap1 may indeed be displaced from telomeres/subtelomeres upon a DSB and relocate to the damage.

Fig 6.3

6.4 Strand resection is independent of Rif1 and Rif2

Since Rif1 protects telomeres from degradation in *cdc13-1* cells, I next investigated if Rif1 has an effect on strand resection at a DSB, as strand resection is crucial for the recognition and repair of a DSB. To study strand resection, a SYBR Green based QAOS assay was developed to measure ssDNA at -1.6kb, 10kb and 20kb upstream of the HO cutting site (Fig 6.4A, for details see methods). This way DNA resection could be monitored and compared between wild type, *rif1Δ* and *rif2Δ* cells. As shown by QAOS assay, in WT cells ssDNA accumulated very rapidly at 1.6kb away from the DSB, reaching ~50% within 4hrs. After 4hrs, ssDNA decreased; this decrease was partly due to a loss of total DNA at this locus (Fig 6.4 B). The accumulation of ssDNA at -10kb locus was much slower than that of -1.6kb locus, and the accumulation of ssDNA was even slower at -20kb with only ~5% ssDNA detectable during the 8hr experiment. In any of the loci measured, however, no significant differences in ssDNA levels were observed between wild type, *rif1Δ*, and *rif2Δ* JKM139 strains, indicating that Rif1 and Rif2 do not affect strand resection at a DSB.

Fig 6.4

6.5 Checkpoint activation at DSB is independent of Rif1

Since Rif1 overexpression in *cdc13-1* cells inhibits checkpoint activation at non-permissive temperatures, I next investigated if Rif1 can delay checkpoint responses triggered by a single DSB. For this purpose, the number of G2/M arrested cells upon DSB induction were scored and compared between WT and *rif1Δ* JKM139 cells (Fig 6.5.1A). As shown by DAPI staining, no significant differences were found, indicating that Rif1 does not affect checkpoint activation.

Since overexpressed Rif1 was shown to bind DSB, I further tested if Rif1 overexpression has an effect on DSB induced arrest. As shown in Fig 6.5.1B, two independent strains overexpressing Rif1 from the *ADH1* promoter arrested at a similar pace compared to the WT cells. Western blot analysis revealed that Rad53 phosphorylation also occurred in a similar rate in Rif1 overexpressed cells compared to the WT.

In agreement with these results, ChIP analysis showed no significant differences in the recruitment of checkpoint proteins Ddc2, Rpa or Rad9 to the DSB between WT and *rif1Δ* cells (Fig 6.5.2). Together these data suggest that Rif1 does not affect checkpoint activation triggered by a DSB.

Fig 6.5.1

Fig 6.5.2

6.6 Overexpression of *RIF1* promotes checkpoint adaptation to a single DSB

Although a single, persistent DSB triggers an extremely strong checkpoint signal, most WT cells can override the cell cycle arrest despite of the unrepaired DSB; this process is known as checkpoint adaptation (as described in the introduction). I next investigated if Rif1 affects checkpoint adaptation using an adaptation assay. In this assay, G1 cells were spread on galactose plates to induce a DSB, and the formation of microcolonies was monitored after 18hrs under a microscope. A microcolony containing two cells indicates that the mother cells have not escaped arrest, whereas a microcolony containing more than four cells indicates that the mother cell has undergone more than two cell divisions. Overexpression of *SAE2* was known to promote checkpoint adaptation (Clerici et al, 2006); therefore these cells were used as a positive control. Consistent with previous observations (Clerici et al, 2006), around 50% of the WT cells formed microcolonies containing more than four buds/cells after 18hrs, with the rest of the microcolonies distributed evenly between the 2 cells to 4 cells stage (Fig 6.6). *rif1* Δ cells showed a very similar adaptation pattern to the WT cells. In contrast, cells overexpressing *RIF1* or *SAE2* produced higher percentages (70% and 82% respectively) of large microcolonies which contained more than four cells. These data suggest that excess amounts of Rif1 promote checkpoint adaptation to a DSB.

Fig 6.6

6.7 Overexpression of Rif1 facilitates NHEJ repair of a DSB

My previous results showed that overexpressed Rif1 is recruited to the DSB, but its function at the DSB is still unclear. One possibility is that Rif1 might participate in damage repair. As previously mentioned, the survival of cells continuously expressing HO relies on the repair of the DSB via the NEHJ pathway. To understand if Rif1 is involved in NHEJ repair, a survival assay was performed with 2×10^5 cells seeded on galactose plates, and the number of colonies was scored after 3 days. As shown in Fig 6.7, about 120 WT cells and ~140 *rif1Δ* cells formed colonies after 3 days. In contrast, a *yku70Δ* strain defective in NEHJ showed a dramatic decrease (over 100 fold) in survival, whereas strains overexpressing Rif1 or Sae2 significantly increased the survival frequency. This result suggests that excess amounts of Rif1 promote the error-prone NHEJ repair of a DSB.

Fig 6.7

6.8 Discussion

6.8.1 Recruitment of Rif1 to a DSB

In this chapter, my aim was to find if Rif1 has a protective role at a DSB, similar to its role observed at uncapped telomeres induced by the *cdc13-1* mutation. However, upon the creation of a DSB by the HO endonuclease, Rif1 was not recruited to the DSB lesion. In agreement with this finding, deletion of Rif1 does not affect either DNA resection or the checkpoint response. Why is Rif1 not recruited to a DSB? One possibility is that the specific DNA or protein substrates that are responsible for recruiting Rif1 to uncapped telomeres are not present at a DSB. Alternatively, since telomeric sequences are intact in the cells, the majority of Rif1 could be still tethered at telomeres. Hence, there could be simply not enough Rif1 to be mobilised to a DSB that is created far away from the telomeres. This hypothesis is supported by the fact that high levels of Rif1 were detectable at a DSB when Rif1 was overexpressed from the *ADH1* promoter.

The binding pattern of overexpressed Rif1 is distinct from that of its interacting partner Rap1, suggesting that Rif1 may be recruited independently of Rap1. This result is consistent with the observation in *cdc13-1* cells, where Rif1 is recruited to damage at subtelomeres while Rap1 is displaced from the same region. The maximum enrichment region of Rif1 was 2-4kb away from the break site, which seems to correlate with maximum resection activity.

6.8.2 Functions of Rif1 at a DSB

Intriguingly, although recruited to the damage, overexpression of Rif1 did not delay the checkpoint response to a DSB. This is mostly likely because a DSB is perceived by the cells as

a much severer damage than the uncapped telomere. For example, the resection at the 5'-3' strand of a DSB was extremely efficient and generated 40% ssDNA at the -1.6kb locus in 4hrs, whereas at uncapped telomeres, ssDNA typically reaches ~15% at the 0.6kb locus during the same period (at 27°C). Furthermore, the degradation at a DSB proceeds at a similar rate in a population of cells, whereas the degradation speed varies greatly at different telomeres due to their heterogeneous composition (e.g some telomeres contain both X and Y' elements while others contains only X elements). Therefore, it seems overexpression of Rif1 is unable to affect the checkpoint activation at such severe damage like a DSB.

Despite not having an effect on checkpoint activation, Rif1 overexpression improved the adaptation phenotype. The level of resection is intimately linked with adaption. For example, in the adaptation defective *yku70Δ* strains, ssDNA levels were twice as much as WT cells (Lee et al, 1998). Hence, it is possible that when associated with a DSB, overexpressed Rif1 may inhibit ssDNA generation by inhibiting nucleases. The second hypothesis is that Rif1 may recruit other adaptation-promoting proteins via its protein-protein interaction domain. For example, the phosphatases Ptc2 and Ptc3 are known to affect adaptation, possibly by dephosphorylating Rad53 (Leroy et al, 2003). In support of this idea, it was recently found that Rif1 physically interacts with several phosphatases including Glc7, Cdc14, Ptp1 and Psr2 (Breitkreutz et al, 2010)

My results suggest that both Rif1 and *yku70* are positive regulators of NHEJ, and *yku70* seems to have a predominant role in NHEJ. It is possible that Rif1 could interact with *yku70* to promote NHEJ at a DSB. A future experiment to explore this possibility could involve the generation of a yeast strain overexpressing Rif1 but lacking *YKU70* (*ADH1-HA-Rif1, yku70Δ*)

and compare its NHEJ efficiency to a *yku70Δ* strain. If both strains have the same NHEJ efficiency it would indicate that Rif1's function in NHEJ is dependent on *yku70*.

It is not clear why Rif1 overexpression improves illegitimate NHEJ repair at a DSB. It could be that cells overexpressing Rif1 have less ssDNA lesions in the first place, and therefore easier to repair. Or, Rif1 may stabilise the DSB via interacting with the surrounding chromatin, similar to the MRX complex, hence allowing the NHEJ machinery to repair the lesion with improved efficiency. Or perhaps overexpressed Rif1 could stimulate the activity of some polymerases to fill in the ssDNA gaps. Nonetheless, it is clear that this type repair did not correctly mend the HO cutting site; otherwise cells would have died from subsequent rounds of HO cleavage.

Overall, it appears that Rif1 only has a minor role at DSB, provided that it is abundant enough to be recruited to the lesion. The fact that Rif1 helps cells to adapt to unrepaired DSB, suggests that Rif1 could play a role in the initiation of chromosome instability in these cells. Furthermore, Rif1 has a role in promoting error-prone repair at a DSB which cannot be repaired by conventional means.

Chapter VII: Phosphorylation of Rif1

7.1 Introduction

Protein phosphorylation is a post-translational modification used by both prokaryotic and eukaryotic cells to regulate a wide range of cellular processes, such as cell cycle arrest, signal transduction and cytoskeletal rearrangement (Cohen, 2002; Tarrant & Cole, 2009). The addition of the phosphate group on the serine/threonine residues can cause a conformational change in the protein, which may lead to its activation or deactivation. Phosphorylation usually occurs on multiple distinct sites of a protein and it was estimated that between 10-50% of proteins are phosphorylated in a give cellular state. Therefore the phosphorylate state of a particular protein could provide insights in understanding its function.

Previously, four large scale mass spectrometry studies in the phosphoproteomics in budding yeast have yielded 9 different phosphorylation sites on scRif1 (Albuquerque et al, 2008; Chi et al, 2007; Li et al, 2007; Smolka et al, 2007). However, none of these phosphorylation sites have been further characterised and it is still a mystery of how phosphorylation could regulate Rif1 function. Since these studies focused on protein phosphorylation at baseline levels or in response to MMS treatment, it is not known if Rif1 could be phosphorylated upon telomere dysfunction. Hence, I analysed by western blot the modification of Rif1 in response to telomere shortening and uncapping.

7.2 Rif1 modification during senescence

To test if Rif1 undergoes post-translational modification during telomere shortening, I used a freshly germinated *tlc1Δ RIF1-MYC* strain continuously cultured in liquid YEPD, until the strain had escaped senescence. Samples were harvested everyday for Western blot analysis and the cell number was determined at the same time points for the generation of a growth curve. As showed in Fig 7.2 A, the growth rate of *tlc1Δ RIF1-MYC* cells consistently dropped from day 1 to day 7 in liquid culture, indicating that progressive telomere erosion has triggered senescence. At day 8 and further, cell proliferation rate increased dramatically, indicating that recombination dependent survivors had taken over the culture. Interestingly, slow migrating forms of Rif1 (diffused band) were observed only during senescence (day 2-7) but not after the cells have escaped. This data suggest that Rif1 in *tlc1Δ* cells is modified during senescence; however it is not clear if this modification is due to phosphorylation.

7.3 Rif1 is phosphorylated upon telomere uncapping

To test if Rif1 undergoes post-translational modification during telomere uncapping, Western blot analysis was performed with *cdc13-1 RIF1-MYC* cells grown at 21°C (time 0) or 36°C for 6hrs (Fig 7.3A). As revealed by WB, the Myc tagged Rif1 protein migrates as a distinct band around 250KDa in normal conditions (time 0). But when cell were incubated at the non-permissive temperature of 36°C, slow migrating forms of Rif1 were detected as soon as 2hr. At 4hr and 6hr, the electrophoretic band of Rif1 completely shifted.

Slow migration of proteins on a SDS-PAGE gel may represent several post-translational modifications such as phosphorylation, glycosylation or ubiquitination. I therefore

performed a phosphates assay to identify if this slow mobility of Rif1 protein is due to phosphorylation. Upon alkaline phosphatase treatment, the shift of the electrophoretic band of Rif1 was diminished, along with the slow migrating form of the phosphorylated Rad53 in the same sample. This indicates that the slow migrating Rif1 was indeed caused by phosphorylation.

Fig 7.2

Fig 7.3

7.4 Phosphorylation of Rif1 upon telomere uncapping depends on cell cycle arrest

Having established that Rif1 is phosphorylated in *cdc13-1* cells at non-permissive temperatures, I wondered if the checkpoint activation is required for Rif1 phosphorylation. For this I analysed Rif1 phosphorylation in *cdc13-1* cells carrying deletions of several checkpoint proteins including Rad9, Rad24, Mec1 and Tel1. Rad9, Mec1 and Tel1 are the major checkpoint kinases acting during *cdc13-1* dysfunction, and once activated, they can phosphorylate a cascade of substrates to arrest the cell cycle. Rad24 is a component of the 9-1-1 complex which acts as a damage sensor upstream of the signalling pathway. Deletion of *RAD9*, *RAD24*, *MEC1* are known to completely abolish the G2/M arrest in *cdc13-1* cells (Jia et al, 2004). In addition, a *cdc13-1 exo1Δ* strain was also examined because *EXO1* is the major nuclease responsible for telomere resection in *cdc13-1* cells, and deletion of *EXO1* results in a partial relieve of the cell cycle arrest (Maringele & Lydall, 2002). Interestingly, phosphorylation of Rif1 was abolished in *cdc13-1* cells grown at 36°C when the checkpoint proteins *RAD9*, *RAD24*, *MEC1* and *TEL1* were deleted (Fig 7.4). Curiously, in the absence of Exo1, Rif1 phosphorylation was attenuated but not fully inhibited, correlating with the partial G2/M arrest. These data suggest that the G2/M arrest by checkpoints is required for the phosphorylation of Rif1 during telomere uncapping. However, it remains to be determined if the kinase activity of Rad9, Mec1 or Tel1 is required for Rif1 phosphorylation.

Fig 7.4

7.5 C-terminal deleted Rif1 is phosphorylated upon telomere uncapping

Previous large scale mass spectrometry studies showed that Rif1 has multiple phosphorylation sites which are mainly located in the C terminus (Fig 7.5A). In order to identify which region of Rif1 is phosphorylated in *cdc13-1* cells, I created a C-terminal truncated Rif1 removing seven of the known phosphorylation sites; this results in a 173kDa MYC tagged protein (Rif1cΔ-MYC) compared to the original 234kDa Rif1-MYC tagged protein. The Rif1cΔ-MYC was then combined with the *cdc13-1* mutation and the phosphorylation of Rif1 was analysed by Western blot. As seen on the WB (Fig 7.5B), Rif1 lacking the C terminus was increasingly phosphorylated when *cdc13-1* cells were incubated at 36°C, indicating that the N terminus of Rif1 is phosphorylated upon telomere uncapping.

7.6 C-terminal deleted Rif1 is phosphorylated upon global DNA damage

The phosphorylation of Rif1 could be directly regulated by checkpoint kinases or by the cell cycle. To explore these possibilities, I studied the phosphorylation of Rif1cΔ in cells treated with different genotoxic agents. As previously mentioned, several genotoxic agents cause global damage to the cells leading to arrest at different phases of the cell cycle. E.g. Nocodazole activates the spindle checkpoint by inhibiting the polymerisation of the microtubules and arrest cells in early mitosis, while hydroxyurea (HU) activates the S phase checkpoint by causing stalled replication forks (Alvino et al, 2007). Methyl methanesulfonate (MMS) is thought to induce DSBs and stalled replication forks in yeast cells (Lundin et al, 2005). UV radiation induces cyclobutane–pyrimidine dimers (CPDs) and 6–4 photoproducts (Sinha & Hader, 2002). The phosphorylation of Rad53 is considered a good indicator for DNA damage, because Rad53 is a major transducer of the DNA

checkpoint signalling pathway, and its phosphorylation (ie. activation) directly correlates with the strength of the damage signal.

As seen on WB (Fig 7.6), nocodazole, HU and mild UV (30 J/m²) all induced phosphorylation of Rif1cΔ, although to a less extent as that of telomere uncapping. This phosphorylation correlated with the high percentage of cell arrested at S phase, G2 and early mitosis, but not with strong Rad53 phosphorylation. In contrast, cells treated with high doses of UV (100 J/m²) or MMS (0.1%) did not induce Rif1cΔ phosphorylation, despite having activated high levels of Rad53 phosphorylation. In this case, only a small amount of cells were at G2/M phase, while higher percentage of cells (32% and 50%) were detected in G1, indicating that these doses of UV or MMS preferably trigger the G1 checkpoint. Together, these data suggest that Rif1cΔ is not a downstream target of Rad53 kinase.

Curiously, the time 0 samples in WT cells contained residue phosphorylation in Rif1cΔ, possibly due to a population of cell in different cell cycle. To test this hypothesis, cells were synchronised in G1 by alpha-factor, the yeast mating pheromone. Upon alpha factor treatment, WB revealed that the residue phosphorylation has disappeared. This data suggested that G1 cells are unable to phosphorylate the C-terminal deleted Rif1.

Fig 7.5

Fig 7.6

7.7 Rif1 contains putative phosphorylation sites of Cdk1 and ATM/ATR

Since Rif1 is phosphorylated upon telomere dysfunction and global DNA damage, I wondered which kinases are responsible for its phosphorylation. In *S. cerevisiae*, a single cyclin-dependent kinase Cdk1 (Cdc28) coordinates the serial events required for the cell division. Cdk1 has 75 well-characterised phosphorylation targets and a further 300 potential targets in cells (Enserink & Kolodner, 2010). Cdk1 targets were found to control important cellular events, such as DNA replication, mitotic exit, checkpoint activation and telomere homeostasis (Enserink & Kolodner, 2010). Mec1 and Tel1 are the homologues of human ATM and ATR and the major checkpoint kinases in budding yeast. Hence I further analysed if Rif1 contains specific amino acid sequences that are likely to be targets of Cdk1 and Mec1/Tel1 *in vivo*.

It is known that the *in vivo* targets of ATM/ATR usually contain SQ/TQ motifs organised in clusters (Tseng et al, 2006). Sequence analysis identified 14 SQ/TQ motifs which were potential targets of the Mec1/Tel1 kinases in the scRif1 amino acid sequence (Fig 7.7.1). Among them, only S1351 has been identified by previous mass spectrometry. Interestingly, there seems to be several SQ/TQ motifs clustering between 1300-1600 amino acids, making this region a preferred substrate *in vivo*. In addition, 18 putative phosphorylation sites of CDK1 was identified in *RIF1* (Fig 7.7.2), including 3 full length Cdk1 consensus sites (ST*-P-x-K/R, where x is any amino acid) and 15 minimal consensus site (ST*/P). These data suggest that scRif1 is likely to be a target of both Cdk1 and Mec1/Tel1 *in vivo*.

MSKDFSDKKKHTIDRIDQHILRRSQHDNYSNGSSPVMKTNLPPSPQAHM	50
HIQSDLSPTPKRRKLASSSDCENKQFDLSAINKNLYPEDTGSRLMQSLPE	100
LSASNSDNVSPVTKSVAFSDRIESSPIYRIPGSSPKPSPSSKPGKSILRN	150
RLPSVRTVSDLSYNKLOYTOHKLHNGNIFTSPYKETRVNPRALEYWVSGE	200
IHGLVDNESVSEFKEIEGGLGILRQESEDYVARRFEVYATFNNIIPILT	250
TKNVNEVDQKFNILIVNIESIEICIPHLQIAQDTLLSSSEKKNPFVIRL	300
YVQIVRFFSAIMSNFKIVKWLTKRPDLVNKLKVIYRWTGALRNENSNI	350
IITAQVSFLRDEKFGTFFLSNEEIKPIISTFTEIMEINSHNLIYEKLLLI	400
RGFLSKYPKLMIEVTVSWLPGEVLPRIIGDEIYSMKILITSIVVLELL	450
KKCLDFVDEHERIYQCIMLSPVCETIPEKFLSKLPLNSYDSANLDKVTIG	500
HLLTQQIKNYIVVKNDNKIAMDLWLSMTGLLYDSGKRVDLTSESNKVWF	550
DLNNLCFINNHKPTRLMSIKVWRIITYCICTKISQKNQEGNKSLLSLLRT	600
PFQMTLPYVNDPSAREGIYHLLGVVYTAFTSNKNLSTDMFELFWDHLIT	650
PIYEDYVFKYDSIHLQNVLFTVLHLLIGGKNADVALERKYKHHHPMSVI	700
ASEGVKLDISSLPPQIIKREYDKIMKVVVFQTEVAISNVNLAHDLILTS	750
LKHLPEDRKDQTHLESFSSLILKVTQNNKDTPIFRDFFGAVTSSFVYTF	800
DLFLRKNDSSLVNFNIQISKVGISQGNMTLDDLKDVIRKARNETSEFLII	850
EKFLELDDKKTEVYAQNWVGSTLLPPNISFREFOQLANIVNKVPNENSIE	900
NFLDLCLKLSFPVNLFTLLHVMWSNNNFIYFIQSYVSKNENKLNVDLIT	950
LLKTSLPGNPELFSGLLPFLRRNKFMIDILEYCIHSNPNLLNSIPDLNSDL	1000
LLKLLPRSRASYFAANIKLFCSEQLTLVRWLLKGQOLEQLNQNFSIEIN	1050
VLQNASDSELEKSEIIRELLHLAMANPIEPLFSGLLNFCIKNNMADHLDE	1100
FCGNMTSEVLFKISPELLKLLTYKEKPNGKLLAAVIEKIENGDDDYILE	1150
LLEKIIIQKEIQILEKLKEPLLVFFLNPVSSNMQKHKKSTNMLRELVL	1200
LTKPLSRSAAKFFSMLISILPPNPNYQTIDMVNLLIDLKSHNRKFKDK	1250
RTYNATLKTIGKWIQESGVVHQGDSSKEIEAIPDTKSMYIPCEGSENKLS	1300
NLQRKVDSDIQVPAQGMKEPPSSIQISSQISAKDSDSISLKNTAIMNS	1350
SQ QESHANRSRSDIDETLEEVDNESIREIDQOMKSTOLDKNVANHSNICS	1400
TKSDEVDVTELHESIDTQSSSEVNAYQPIEVLTSSELKAVTNRSIKTNP	1450
VVNSDNPLKRPSPKETPTSENKRSKGHETMVDVLVSEEQAVSPSSDVICTN	1500
IKSIANEESLALRNSIKVETNCNENSLNVTLDLDLQQTITKEDGKGQVEH	1550
VQRQENQESMNKINSKSFQDNIAQYKSVKKARPNEGENDYACNVEQA	1600
SPVRNEVPGDGIQIPSGTILLNSSKQTEKSKVDDLRSDEDEHGTVAQEKH	1650
QVGAINSRKNNDRMDSTPIQGTSEESREVVMTTEEGINVRLEDSGTCELN	1700
KNLKGPLKGDKANINDDFVPVEENVRDEGFLKSMEHAVSKETGLEEQPE	1750
VADISVLPEIRIPIFNLSLMQGSKSQIKEKLLKRLQRNELMPPDSPRMT	1800
ENTNINAQNGLDTPVKTIGGKEKHHEIQLGQAHTADGEPLGGDGNEDA	1850
TSREATPSLVHFFSKKSRRLVARLRGFTPGDLNGISVEERRNLRIELLD	1900
FMMRLEYYSNRDNDMNX	1950

Fig 7.7.1 Predicted Mec1/Tel1 phosphorylation sites in *S. cerevisiae* Rif1

Sequence analysis identified 14 SQ/TQ motifs (highlighted in blue) which are potential targets of the MEC1/TEL1 kinases in vivo. Among them, only S1351 has been identified by previous mass spectrometry studies (shown in a box).

MSKDFSDKKKHTIDRIDQHILRRSQHDNYSNGS	SPWMKTNLPPP	SPQAHM	50	
HIQSDL	SPTPKRRK	CLASSSDCENKQFDLSAINKNLYPEDTGSRLMQSLPE	100	
LSASNSDNV	SPVTKSVAFSDRIES	SPYIRIPGSSPKP	SPSSKPGKSILRN	150
RLPSVRTVSDLSYNKLYTQHKLHNGNIFT	SPYK	ETRVNPRALEYWVSGE	200	
IHGLVDNESVSEFKEIEGGLGILRQESDYVARRFEVYATFNNIIPILT			250	
TKNVNEVDQKFNILIVNIESIEICIPHLQIAQDTLLSSSEKKNPFVIRL			300	
YVQIVRFFSAIMSNFKIVKWLTKRPDLVNKLKVIYRWTGALRNENSNI			350	
IITAQVSFLRDEKFGTFFLSNEEIKPIISTFTEIMEINSHNLIYEKLLLI			400	
RGFLSKYPKLMIEVTVSWLPGEVLPRIIGDEIYSMKILITSIVVLELL			450	
KKCLDFVDEHERIYQCIML	SPVCETIPEKFLSKLPLNSYDSANLDKVTIG		500	
HLLTQQIKNYIVVKNDNKIAMDLWLSMTGLLYDSGKRVDLTSESNKVWF			550	
DLNNLCFINNHKPTRLMSIKVWRIITYCICTKISQKNQEGNKSLLSLLRT			600	
PFQMTLPYVNDPSAREGIYHLLGVVYTAFTSNKNLSTDMFELFDHLIT			650	
PIYEDYVFKYDSIHLQNVLFTVLHLLIGGKNADVALERKYKKHIHPMSVI			700	
ASEGVKLDISSLPQIKREYDKIMKVVFQTVVAISNVNLAHDLILTS			750	
LKHLPEDRKDQTHLESFSSLILKVTQNNKD	TP	IFRDFGAVTSSFVYTF	800	
DLFLRKNDSSLVNFNIQISKVGISQGNMTLDLLKDVIRKARNETSEFLII			850	
EKFLELDDKKTEVYAQNWVGSTLLPPNISFREFQSLANIVNKVPNENSIE			900	
NFLDLCLKLSFPVNLFTLLHVSMMWSNNFIYFIQSYVSKNENKLNVDLIT			950	
LLKTSLPGNPELFSGLLPFLRRNKFMIDILEYCIHSPNLLNSIPDLNSDL			1000	
LLKLLPRSRASYFAANIKLFCSEQLTLVRWLLKGQOLEQLNQNFSIEIEN			1050	
VLQNASDSELEKSEIIRELLHLAMANPIEPLFSGLLNFCIKNNMADHLDE			1100	
FCGNMTSEVLFKI	SP	ELLKLLTYKEKPNGKLLAAVIEKIENGDDDYILE	1150	
LLEKIIIQKEIQILEKLKEPLLVFFLNPVSSNMQKHKKSTNMLRELVL			1200	
LTKPLSRSAAKKFFSMLISILPPNPYQIDMVNLLIDLKSHNRKFKDK			1250	
RTYNATLKTIGKWIQESGVVHQGDSSKEIEAIPDTKSMYIPCEGSENKLS			1300	
NLQRKVDSDIQVPATQGMKEPPSSIQISSQISAKSDSISLKNNTAIMNS			1350	
SQQESHANRSRISIDDETL EEVDNESIREIDQOMKSTQLDKNVANHSNICS			1400	
TKSDEVDVTELHESIDTQSSEVNAYQPIEVLTSSELKAVTNRSIKTNP			1450	
VDNNDNPLKRPSKE	TP	TSENKRSKGHETMVDVLVSEEQAV	SPSSDVICTN	1500
IKSIANEESLALRNSIKVETNCNENSLNVTLDLDQQTITKEDGKGQVEH			1550	
VQRQENQESMNKINSKSF	TQDNIAQYKSVKKARP	NEGENDYACNVEQA	1600	
SPVR	NEVPGDGIQIPSGTILLNSSKQTEKSKVDDLRSDEDEHGTVAQEKH		1650	
QVGAINSRNKNNDRMD	SP	IQGTEEESREVMTEEGINVRLEDSGTCELN	1700	
KNLKGPLKGDKANINDDFVPVEENVRDEGFLKSMEHAVSKETGLEEQPE			1750	
VADISVLPEIRIPIFNSLKMQGSKSQIKEKLLKRLQRNELMPPD	SPPR	MT	1800	
ENTNINAQNGLDVTPKTIGGKEKHHEIQLGQAHTADGEPLGGDGNE			1850	
TSREAT	TPSLKVHFFSKSRRLVARLRGF	TP	GDLNGISVEERRNLRIELLD	1900
FMMRLEYYSNRDNDMN			1950	

Fig 7.7.2 Predicted Cdk1 phosphorylation sites in *S. cerevisiae* Rif1

Sequence analysis identified 18 putative Cdk1 phosphorylation sites in scRif1 amino acid sequence. Three full length Cdk1 consensus sites (S/T*-P-x-K/R, are shown in boxes and 15

minimal consensus sites (ST*/P) are underlined and highlighted in red. S1795 has been identified in previous mass spectrometry studies.

7.8 Discussion

In this chapter, I provided evidence that Rif1 can be phosphorylated upon telomere uncapping and in response to the treatment of a variety of genotoxic agents including nocodazole, hydroxyurea and UV. Rif1 is likely to be phosphorylated during cellular senescence as well, since the slow migrating form of Rif1 detected in *tlc1Δ* cell was very similar to that in telomere uncapped cells. Although the known phosphorylation sites were mostly mapped at the C terminus of Rif1, my results suggest that there are likely to be new, unidentified phosphorylation sites at the N terminus of Rif1, because a C-terminal deleted Rif1 removing the majority of known phosphorylation sites is still highly phosphorylated upon telomere damage.

Which kinases are responsible for the phosphorylation Rif1? My data suggest that Rif1cΔ is not a downstream target of Rad53, because high doses of MMS and UV treatment resulted in a strong Rad53 phosphorylation, without but lack of Rif1 phosphorylation. On the other hand, the major cell-cycle dependent kinase Cdk1 turned out to be a good candidate, as sequence analysis revealed 18 putative Cdk1 phosphorylation sites in Rif1, and one of which (S1795) was identified in previous mass spectrometry studies. Another line of evidence is that when cells are arrested by nocodazole, HU, and alpha factor at different stages of the cell cycle, it was found that Rif1 phosphorylation was present in S phase, G2 phase and early mitosis, but absent in G1 arrested cells. Therefore it seems that the cell cycle controls at

least part of the phosphorylation in Rif1 protein. However, there is a possibility that checkpoint kinases may also be involved in this phosphorylation, since nocodazole and HU triggers spindle and DNA damage checkpoint, respectively, and the phosphorylation of Rif1 could be a result of the direct action of checkpoint kinases. In support of this hypothesis, sequence analyse revealed 14 SQ/TQ motifs in Rif1 that are potential substrates of Mec1/Tel1 kinases *in vivo*. Therefore, it seems that Rif1 could be a target of both Cdk1 and checkpoint kinases, and perhaps both cell cycle and checkpoint pathways need to coordinate in modulating Rif1 function.

How could phosphorylation regulate the function of Rif1? An attractive hypothesis is that the phosphorylation of Rif1 by Cdk1 could contribute to the cell cycle-mediated telomere elongation. As previously mentioned, telomerase preferably elongates short telomeres at the late S /G2 phase of the cell cycle, but how telomerase action is controlled by the cell cycle is still not fully understood. It was recently discovered that Cdk1-dependent phosphorylation of cdc13 on T308 is essential for efficient recruitment of telomerase complex to telomeres by favouring the interaction of Cdc13 with Est1 (Li et al 2009). Therefore it is possible that phosphorylation of Rif1 at S/G2 phase could also favour telomerase recruitment. Although no telomerase component was found to physically interact with Rif1 to date, this recruitment of telomerase could be indirect, e.g. through changing the overall telomere structure from a 'closed' to an 'open' state, which allows telomerase to access the 3' overhang. Furthermore, the phosphorylation of Rif1 by Mec1/Tel1 might be important for the capping function of Rif1 at damaged chromatin.

Overall, my study implies that Rif1 may be phosphorylated by several checkpoint kinases as well as Cdk1, and its phosphorylation could play a significant role in regulating telomere

metabolism. The potential phosphorylation sites of Rif1, mainly unidentified by mass spectrometry, need to be characterised in the future. In addition, Rif1 could also be subject to other modifications such as SUMOylation as its middle coiled-coil region serve an ideal substrate. SUMOylation is involved in various cellular processes, such as nuclear transport, transcriptional regulation, protein stability, and progression through the cell cycle. It therefore remains to be an exciting area of research, particularly in the understanding the functional significance of Rif1 modification.

Chapter VIII: Final discussion

8.1 Rif1 in budding yeast and humans

Budding yeast Rif1 and its human ortholog were considered to have very different functions for many years. Previous knowledge suggests that the role of Rif1 in budding yeast is restricted to telomeres (i.e. telomere length regulation and telomere silencing), whereas its functions in humans are mostly non-telomeric, most notably in DNA damage response and repair. However, results from my PhD research suggest that Rif1 functions are more conserved in yeast and humans than previously thought, for the following reasons:

Firstly, in humans, Rif1 was found to bind uncapped telomeres induced by a dominant negative allele of TRF2 (Silverman et al, 2004); my ChIP data revealed that budding yeast Rif1 is also recruited to uncapped telomeres triggered by the *cdc13-1* mutation. Secondly, it was thought that human Rif1 does not interact with hRap1, and is not associated with telomeres; whereas the budding yeast Rif1 is permanently tethered to telomeres by its interaction with the Rap1 C terminus. However, my ChIP data show that upon DNA damage, budding yeast Rif1 is increasingly recruited to internal damaged loci. This recruitment is independent of Rap1. Thirdly, Human Rif1 is recruited to DSBs induced by IR, MMS (Silverman et al, 2004; Xu & Blackburn, 2004) , whereas my results show that scRif1 is also recruited to an HO-induced DSB, providing that it is overexpressed in the cells. Therefore, it seems that human Rif1 represents a more 'free' or mobile version of the scRif1, allowing it to participate in many other cellular functions. In contrast, due to its interaction with Rap1 at telomeres, budding yeast Rif1 needs to fulfil its duty at telomeres, but still retains other functions similar to human Rif1. Finally, because of the low homology in the primary amino acid sequences shared between human and yeast Rif1, it was thought that the structure of

these proteins were vastly different. However, my study using recently developed software reveals that the N terminus of scRif1 contained Heat-like repeats. Heat repeats are conserved in a diverse range of organisms including human, mouse, chicken, zebra fish and fruit flies (Xu et al, 2010).

Due to the above similarities between human and budding yeast Rif1, studies using budding yeast are still relevant for understanding Rif1's function in humans, and may still provide new avenues of research. On the other hand, it would be expected that human Rif1 may have obtained novel functions during evolution, because the C-terminal DNA binding domain is a newly evolved motif and exists only in vertebrates. This domain is found to be associated with the helicase BLM complex and may be important for DNA replication (Xu et al, 2010). Interestingly, telomeric proteins seem to experience rapid evolution, in contrast to other proteins such as the DDR proteins. This rapid evolution may reflect that telomere structure and components need to be 'flexible' to adapt to the ever-changing environment.

8.2 Checkpoint adaptation and the initiation of CIN

From budding yeast to humans, the DNA damage checkpoint machinery is highly conserved and its primary function is to halt the cell cycle in response to DNA damage, giving enough time for repair. In the case of severe damage including telomere dysfunction, checkpoints can trigger a permanent cell cycle arrest (senescence) or in some higher eukaryotic cells, apoptosis (Fagagna et al, 2003). Both senescence and apoptosis ensure cells do not proliferate with damaged DNA. Therefore, the DNA damage checkpoint was proposed to be a potent anti-cancer barrier in early human carcinogenesis (Negrini et al, 2010). Clearly, pre-cancerous cells will need to escape cell cycle arrest to become malignant. Indeed, several

studies have demonstrated that checkpoint activation precedes early cancer development. E.g. Markers of activated DDR including ATM, Chk1, and phosphorylated histone H2AX and p53 are commonly expressed in different types of pre-malignant lesions (Bartkova et al, 2005; Gorgoulis et al, 2005).

Escaping the cell cycle arrest of pre-cancerous cells is thought to be caused by mutations in the major checkpoint genes (DePinho, 2000). It was estimated that ~50% of all human cancers contain allelic loss or mutations in the tumour suppressor p53, and the remainder contain alterations of regulators of p53 (Toledo & Wahl, 2006). Additionally, the ATM checkpoint kinase is among the most frequently mutated genes (5% incidence) in human cancers (Ding et al 2008). However, how these mutations arise in sporadic cancers is still a mystery. Interestingly, several studies showed that genomic instability is present before p53 mutation. For example, in an analysis of colorectal tumours, p53 mutation was rare in benign tumours carrying normal karyotype, but its frequency increased dramatically (up to 86%) in tumours that have lost one copy of the chromosome 17 (Baker et al, 1990). The mutation of p53 appeared to occur at the transition from benign to malignant growth. In another study using a heterozygous p53^{+/+}/p53^{-/-} mouse model, it was found that the loss of the wild-type p53 allele is preceded by loss of many gene loci on chromosome 3, indicating that CIN has occurred prior to p53 loss (Perez-Losada et al, 2005). Furthermore, recent research on human pre-cancerous lesions also showed that genomic instability is present before p53 mutation, and p53 mutation increases with increased genomic instability (Gorgoulis et al 2005, Bartkova et al 2005). This evidence suggests that checkpoint mutations could be a consequence of CIN. It is possible that a mechanism could exist to allow cells with severe damage to escape cell cycle arrest and proliferate with increased CIN. In the subsequent cell cycle, cells would have the opportunity to acquire new mutations in p53 or other checkpoint and tumour suppressor genes, sending them on the way of malignant transformation.

Checkpoint adaptation is defined as the process of cells overriding the cell cycle arrest despite the presence of unrepaired damage (Toczyski et al, 1997). It was initially observed in budding yeast in response to irreparable damage, e.g. a persistent DSB, telomeres loss, or uncapped telomeres (Sandell & Zakian, 1993). In principle, checkpoint adaptation could be a cause of genomic instability, because it promotes the segregation of broken or damaged chromosomes. Although the majority of cells die following adaptation, a small population of cells might survive and proliferate with unstable genomes (Syljuasen, 2007). Indeed, microarray analysis revealed that *tlc1Δ rad52Δ exo1Δ* survivors contain large deletion and duplications near chromosome ends. Further evidence came from the study of adaptation defective mutants (Galgoczy & Toczyski, 2001). In this study, adaptation was found to be an important strategy for yeast cells to achieve the maximal survival after exposure to X-ray radiation. However, survival was accompanied by increased genomic instability, such as chromosome loss and translocations.

Despite the link between checkpoint adaptation and initiation of CIN, the importance of adaptation for carcinogenesis in humans has not been established. This is mainly because for a long time checkpoint adaptation was considered non-existent in human cells (Lupardus & Cimprich, 2004), and it was generally thought that apoptosis is a safer choice for multicellular organisms. However, recent evidence suggests that adaptation also exists in human cells. In response to γ -irradiation, human colon carcinoma cells (HCT116 p53+/+) undergo adaptation to the G2 DNA damage checkpoint, and enter mitosis. This results in incomplete chromosome segregation and cause these cells to re-enter G1 with a tetraploid DNA content (Andreassen et al, 2001). Because this cell line contains functional p53, it was suggested that p53 was not sufficient to sustain stable G2 arrest in human colon carcinoma cells. A different study reported that in response to lethal doses of IR, human osteosarcoma cells (U2-OS, p53+/+) re-enter mitosis after a prolonged arrest, with r-H2AX foci, a common

marker for DSBs (Syljuåsen et al, 2006). The adaptation phenotype is dependent on the polo-like kinase PLK1, the human ortholog of the budding yeast Cdc5 (Golsteyn et al, 1994). These data suggest that checkpoint adaptation could be a mechanism for the initiation of CIN in humans.

Fig 8.2 The potential role of checkpoint adaptation in carcinogenesis.

8.4 Adaptation and cancer

Interestingly, several genes required for adaptation in budding yeast were also found to be involved in adaptation and recovery after DNA damage in human cells. Some of these genes also behave as oncogenes in humans. For example, the polo-like kinase Plk1 is the human homolog of the budding yeast Cdc5, and is also involved in adaptation to G2 arrest in human cells (van Vugt et al, 2004). Plk1 is overexpressed in a broad range of human tumours (Eckerdt et al, 2005). The constitutive expression of Plk1 causes the transformation of NIH 3T3 fibroblasts (Mundt et al, 1997). The mechanism by which Plk1 functions is possibly by inhibiting the pro-apoptotic function of p53 through direct phosphorylation (Ando et al, 2004). Another example is casein kinase II, the human homolog of yeast Ckb2. It was found that overexpression of CK2 induces neoplastic growth (Seldin & Leder, 1995; Tawfic et al, 2001). CK2 promotes proliferation by phosphorylation of p53 and its downstream targets (Meek et al, 1990). Furthermore, the PP2C phosphatase Wip1, the human homolog of Ptc2 and Ptc3, was recently found to inhibit the activity of Chk2 kinase, the mammalian homolog of Rad53 (Fujimoto et al, 2005; Oliva-Trastoy et al, 2006). Wip1 gene is amplified in 15% of human breast cancers, and its overexpression is associated with a poor prognosis (Hirasawa et al, 2003; Saito-Ohara et al, 2003).

From these examples, it seems that budding yeast still serve as a useful model organism to identify new genes and pathways involved in checkpoint adaptation in humans. Considering the potential role of checkpoint adaptation in carcinogenesis, continued research using the budding yeast model system may provide insights in the early oncogenesis. Genes involved in adaptation may serve as new targets of cancer treatments. Additionally, targeting adaptation may have the advantage of preventing cancer at an early stage. One of the most crucial determinants of cancer survival is an early diagnosis. Since adaptation, in principle, is

an initial step in carcinogenesis, adaptation markers may serve as early cancer markers to assist cancer diagnosis.

References

- A. John Callegari TJK (2007) Shedding Light on the DNA Damage Checkpoint. *Cell Cycle* **6**: 660-666
- Albuquerque CP, Smolka MB, Payne SH, Bafna V, Eng J, Zhou H (2008) A Multidimensional Chromatography Technology for In-depth Phosphoproteome Analysis. *Molecular & Cellular Proteomics* **7**: 1389-1396
- Alvino GM, Collingwood D, Murphy JM, Delrow J, Brewer BJ, Raghuraman MK (2007) Replication in hydroxyurea: it's a matter of time. *Mol Cell Biol* **27**: 6396-6406
- Anbalagan S, Bonetti D, Lucchini G, Longhese MP (2011) Rif1 supports the function of the CST complex in yeast telomere capping. *PLoS Genet* **7**: e1002024
- Ando K, Ozaki T, Yamamoto H, Furuya K, Hosoda M, Hayashi S, Fukuzawa M, Nakagawara A (2004) Polo-like Kinase 1 (Plk1) Inhibits p53 Function by Physical Interaction and Phosphorylation. *Journal of Biological Chemistry* **279**: 25549-25561
- Andrade MA, Petosa C, O'Donoghue SI, Müller CW, Bork P (2001) Comparison of ARM and HEAT protein repeats. *Journal of Molecular Biology* **309**: 1-18
- Andreassen PR, Lacroix FB, Lohez OD, Margolis RL (2001) Neither p21WAF1 Nor 14-3-3 σ Prevents G2 Progression to Mitotic Catastrophe in Human Colon Carcinoma Cells after DNA Damage, But p21WAF1 Induces Stable G1 Arrest in Resulting Tetraploid Cells. *Cancer Research* **61**: 7660-7668
- Arai K, Masutomi K, Khurts S, Kaneko S, Kobayashi K, Murakami S (2002) Two independent regions of human telomerase reverse transcriptase are important for its oligomerization and telomerase activity. *J Biol Chem* **277**: 8538-8544
- Aylon Y, Kupiec M (2004) DSB repair: the yeast paradigm. *DNA Repair (Amst)* **3**: 797-815
- Azzalin CM, Reichenbach P, Khoriantseva L, Giulotto E, Lingner J (2007) Telomeric repeat containing RNA and RNA surveillance factors at mammalian chromosome ends. *Science* **318**: 798-801

Bailey SM, Williams ES, Cornforth MN, Goodwin EH (2010) Chromosome Orientation fluorescence in situ hybridization or strand-specific FISH. *Methods Mol Biol* **659**: 173-183

Baker SJ, Preisinger AC, Jessup JM, Paraskeva C, Markowitz S, Willson JKV, Hamilton S, Vogelstein B (1990) p53 Gene Mutations Occur in Combination with 17p Allelic Deletions as Late Events in Colorectal Tumorigenesis. *Cancer Research* **50**: 7717-7722

Bartkova J, Horejsi Z, Koed K, Kramer A, Tort F, Zieger K, Guldborg P, Sehested M, Nesland JM, Lukas C, Orntoft T, Lukas J, Bartek J (2005) DNA damage response as a candidate anti-cancer barrier in early human tumorigenesis. *Nature* **434**: 864-870

Bassi P, Sacco E (2009) Cancer and aging: the molecular pathways. *Urol Oncol* **27**: 620-627

Baumann P, Price C (2010) Pot1 and telomere maintenance. *FEBS Lett* **584**: 3779-3784

Bernstein KA, Rothstein R (2009) At loose ends: Resecting a double-strand break. *Cell* **137**: 807-810

Bertuch AA, Lundblad V (2004) EXO1 contributes to telomere maintenance in both telomerase-proficient and telomerase-deficient *Saccharomyces cerevisiae*. *Genetics* **166**: 1651-1659

Bianchi A, Negrini S, Shore D (2004) Delivery of yeast telomerase to a DNA break depends on the recruitment functions of Cdc13 and Est1. *Mol Cell* **16**: 139-146

Bianchi A, Shore D (2007) Increased association of telomerase with short telomeres in yeast. *Genes Dev* **21**: 1726-1730

Booth C, Griffith E, Brady G, Lydall D (2001) Quantitative amplification of single-stranded DNA (QAOS) demonstrates that cdc13-1 mutants generate ssDNA in a telomere to centromere direction. *Nucleic Acids Res* **29**: 4414-4422

Boulton SJ, Jackson SP (1996) Identification of a *Saccharomyces cerevisiae* Ku80 homologue: roles in DNA double strand break rejoining and in telomeric maintenance. *Nucleic Acids Res* **24**: 4639-4648

Boulton SJ, Jackson SP (1998) Components of the Ku-dependent non-homologous end-joining pathway are involved in telomeric length maintenance and telomeric silencing. *EMBO J* **17**: 1819-1828

Braunstein M, Sobel RE (1996) Efficient transcriptional silencing in *Sacharomyces cerevisiae* requires a heterochromatic histone acetylation pattern. *Molecular and Cellular Biology* **16**: 4349-4356

Breitkreutz A, Choi H, Sharom JR, Boucher L, Neduva V, Larsen B, Lin ZY, Breitkreutz BJ, Stark C, Liu G, Ahn J, Dewar-Darch D, Reguly T, Tang X, Almeida R, Qin ZS, Pawson T, Gingras AC, Nesvizhskii AI, Tyers M (2010) A global protein kinase and phosphatase interaction network in yeast. *Science* **328**: 1043-1046

Burma S, Chen BP, Chen DJ (2006) Role of non-homologous end joining (NHEJ) in maintaining genomic integrity. *DNA Repair (Amst)* **5**: 1042-1048

Chakhparonian M, Wellinger RJ (2003) Telomere maintenance and DNA replication: how closely are these two connected? *Trends Genet* **19**: 439-446

Chen L, Trujillo K, Ramos W, Sung P, Tomkinson AE (2001a) Promotion of Dnl4-catalyzed DNA end-joining by the Rad50/Mre11/Xrs2 and Hdf1/Hdf2 complexes. *Mol Cell* **8**: 1105-1115

Chen Q, Ijpmma A, Greider CW (2001b) Two survivor pathways that allow growth in the absence of telomerase are generated by distinct telomere recombination events. *Mol Cell Biol* **21**: 1819-1827

Chi A, Huttenhower C, Geer LY, Coon JJ, Syka JEP, Bai DL, Shabanowitz J, Burke DJ, Troyanskaya OG, Hunt DF (2007) Analysis of phosphorylation sites on proteins from *Saccharomyces cerevisiae* by electron transfer dissociation (ETD) mass spectrometry. *Proceedings of the National Academy of Sciences* **104**: 2193-2198

Choi J, Southworth LK, Sarin KY, Venteicher AS, Ma W, Chang W, Cheung P, Jun S, Artandi MK, Shah N, Kim SK, Artandi SE (2008) TERT promotes epithelial proliferation through transcriptional control of a Myc- and Wnt-related developmental program. *PLoS Genet* **4**: e10

Chong L, van Steensel B, Broccoli D, Erdjument-Bromage H, Hanish J, Tempst P, de Lange T (1995) A human telomeric protein. *SCIENCE* **270**: 1663-1667

Cimino-Reale G, Pascale E, Alvino E, Starace G, D'Ambrosio E (2003) Long telomeric C-rich 5'-tails in human replicating cells. *J Biol Chem* **278**: 2136-2140

Clemenson C, Marsolier-Kergoat MC (2009) DNA damage checkpoint inactivation: adaptation and recovery. *DNA Repair (Amst)* **8**: 1101-1109

Clerici M, Mantiero D, Lucchini G, Longhese MP (2006) The *Saccharomyces cerevisiae* Sae2 protein negatively regulates DNA damage checkpoint signalling. *EMBO Rep* **7**: 212-218

Cohen P (2002) The origins of protein phosphorylation. *Nat Cell Biol* **4**: E127-E130

de Lange T (2005) Shelterin: the protein complex that shapes and safeguards human telomeres. *Genes Dev* **19**: 2100-2110

de Vries E, van Driel W, Bergsma WG, Arnberg AC, van der Vliet PC (1989) HeLa nuclear protein recognizing DNA termini and translocating on DNA forming a regular DNA-multimeric protein complex. *J Mol Biol* **208**: 65-78

DePinho RA (2000) The age of cancer. *Nature* **408**: 248-254

Eckerdt F, Yuan J, Strebhardt K (2005) Polo-like kinases and oncogenesis. *Oncogene* **24**: 267-276

Enserink JM, Kolodner RD (2010) An overview of Cdk1-controlled targets and processes. *Cell Div* **5**: 11

Faure V, Coulon S, Hardy J, Geli V (2010) Cdc13 and telomerase bind through different mechanisms at the lagging- and leading-strand telomeres. *Mol Cell* **38**: 842-852

Fellerhoff B, Eckardt-Schupp F, Friedl AA (2000) Subtelomeric repeat amplification is associated with growth at elevated temperature in *yku70* mutants of *Saccharomyces cerevisiae*. *Genetics* **154**: 1039-1051

Ferreira MG, Miller KM, Cooper JP (2004) Indecent exposure: when telomeres become uncapped. *Mol Cell* **13**: 7-18

Fisher TS, Zakian VA (2005) Ku: a multifunctional protein involved in telomere maintenance. *DNA Repair (Amst)* **4**: 1215-1226

Foster SS, Zubko MK, Guillard S, Lydall D (2006) MRX protects telomeric DNA at uncapped telomeres of budding yeast *cdc13-1* mutants. *DNA Repair (Amst)* **5**: 840-851

Fricova D, Valach M, Farkas Z, Pfeiffer I, Kucsera J, Tomaska L, Nosek J (2010) The mitochondrial genome of the pathogenic yeast *Candida subhashii*: GC-rich linear DNA with a protein covalently attached to the 5' termini. *Microbiology* **156**: 2153-2163

Fujimoto H, Onishi N, Kato N, Takekawa M, Xu XZ, Kosugi A, Kondo T, Imamura M, Oishi I, Yoda A, Minami Y (2005) Regulation of the antioncogenic Chk2 kinase by the oncogenic Wip1 phosphatase. *Cell Death Differ* **13**: 1170-1180

Galgoczy DJ, Toczyski DP (2001) Checkpoint adaptation precedes spontaneous and damage-induced genomic instability in yeast. *Mol Cell Biol* **21**: 1710-1718

Gao H, Cervantes RB, Mandell EK, Otero JH, Lundblad V (2007) RPA-like proteins mediate yeast telomere function. *Nat Struct Mol Biol* **14**: 208-214

Gao H, Toro TB, Paschini M, Braunstein-Ballew B, Cervantes RB, Lundblad V (2010) Telomerase recruitment in *Saccharomyces cerevisiae* is not dependent on Tel1-mediated phosphorylation of Cdc13. *Genetics* **186**: 1147-1159

Gardner R, Putnam CW, Weinert T (1999) RAD53, DUN1 and PDS1 define two parallel G2/M checkpoint pathways in budding yeast. *EMBO J* **18**: 3173-3185

Gartenberg MR (2000) The Sir proteins of *Saccharomyces cerevisiae*: mediators of transcriptional silencing and much more. *Current Opinion in Microbiology* **3**: 132-137

Garvik B, Carson M, Hartwell L (1995) Single-stranded DNA arising at telomeres in *cdc13* mutants may constitute a specific signal for the RAD9 checkpoint. *Mol Cell Biol* **15**: 6128-6138

Geserick C, Blasco MA (2006) Novel roles for telomerase in aging. *Mech Ageing Dev* **127**: 579-583

Giraud-Panis MJ, Pisano S, Poulet A, Le Du MH, Gilson E (2010) Structural identity of telomeric complexes. *FEBS Lett* **584**: 3785-3799

Golsteyn RM, Schultz SJ, Bartek J, Ziemiecki A, Ried T, Nigg EA (1994) Cell cycle analysis and chromosomal localization of human Plk1, a putative homologue of the mitotic kinases *Drosophila* polo and *Saccharomyces cerevisiae* Cdc5. *Journal of Cell Science* **107**: 1509-1517

Gorgoulis VG, Vassiliou LV, Karakaidos P, Zacharatos P, Kotsinas A, Liloglou T, Venere M, Ditullio RA, Jr., Kastriakis NG, Levy B, Kletsas D, Yoneta A, Herlyn M, Kittas C, Halazonetis TD

(2005) Activation of the DNA damage checkpoint and genomic instability in human precancerous lesions. *Nature* **434**: 907-913

Graham IR, Haw RA, Spink KG, Halden KA, Chambers A (1999) In vivo analysis of functional regions within yeast Rap1p. *Mol Cell Biol* **19**: 7481-7490

Grandin N, Bailly A, Charbonneau M (2005) Activation of Mrc1, a mediator of the replication checkpoint, by telomere erosion. *Biol Cell* **97**: 799-814

Grandin N, Charbonneau M (2008) Budding yeast 14-3-3 proteins contribute to the robustness of the DNA damage and spindle checkpoints. *Cell Cycle* **7**: 2749-2761

Grandin N, Damon C, Charbonneau M (2001) Ten1 functions in telomere end protection and length regulation in association with Stn1 and Cdc13. *EMBO J* **20**: 1173-1183

Grandin N, Reed SI, Charbonneau M (1997) Stn1, a new *Saccharomyces cerevisiae* protein, is implicated in telomere size regulation in association with Cdc13. *Genes Dev* **11**: 512-527

Gravel S, Larrivee M, Labrecque P, Wellinger RJ (1998) Yeast Ku as a regulator of chromosomal DNA end structure. *Science* **280**: 741-744

Gravel S, Wellinger RJ (2002) Maintenance of double-stranded telomeric repeats as the critical determinant for cell viability in yeast cells lacking Ku. *Mol Cell Biol* **22**: 2182-2193

Griffith JD, Comeau L, Rosenfield S, Stansel RM, Bianchi A, Moss H, de Lange T (1999) Mammalian telomeres end in a large duplex loop. *Cell* **97**: 503-514

Grossi S, Puglisi A, Dmitriev PV, Lopes M, Shore D (2004) Pol12, the B subunit of DNA polymerase alpha, functions in both telomere capping and length regulation. *Genes Dev* **18**: 992-1006

Hara E, Tsurui H, Shinozaki A, Nakada S, Oda K (1991) Cooperative effect of antisense-Rb and antisense-p53 oligomers on the extension of life span in human diploid fibroblasts, TIG-1. *Biochem Biophys Res Commun* **179**: 528-534

Hardy CF, Sussel L, Shore D (1992) A RAP1-interacting protein involved in transcriptional silencing and telomere length regulation. *Genes Dev* **6**: 801-814

Harrison JC, Haber JE (2006a) Surviving the breakup: the DNA damage checkpoint. *Annu Rev Genet* **40**: 209-235

Harrison JC, Haber JE (2006b) Surviving the breakup: The DNA damage checkpoint. *Annual Reviews in Genetics* **40**: 209-235

Henson JD, Neumann AA, Yeager TR, Reddel RR (2002) Alternative lengthening of telomeres in mammalian cells. *Oncogene* **21**: 598-610

Hirano Y, Fukunaga K, Sugimoto K (2009) Rif1 and Rif2 Inhibit Localization of Tel1 to DNA Ends. *Molecular Cell* **33**: 312-322

Hirasawa A, Saito-Ohara F, Inoue J, Aoki D, Susumu N, Yokoyama T, Nozawa S, Inazawa J, Imoto I (2003) Association of 17q21-q24 Gain in Ovarian Clear Cell Adenocarcinomas with Poor Prognosis and Identification of PPM1D and APPBP2 as Likely Amplification Targets. *Clinical Cancer Research* **9**: 1995-2004

Hockemeyer D, Sfeir AJ, Shay JW, Wright WE, de Lange T (2005) POT1 protects telomeres from a transient DNA damage response and determines how human chromosomes end. *EMBO J* **24**: 2667-2678

Howarth KD, Blood KA, Ng BL, Beavis JC, Chua Y, Cooke SL, Raby S, Ichimura K, Collins VP, Carter NP, Edwards PA (2008) Array painting reveals a high frequency of balanced translocations in breast cancer cell lines that break in cancer-relevant genes. *Oncogene* **27**: 3345-3359

Hughes TR, Weilbaecher RG, Walterscheid M, Lundblad V (2000) Identification of the single-strand telomeric DNA binding domain of the *Saccharomyces cerevisiae* Cdc13 protein. *Proc Natl Acad Sci USA* **97**: 6457-6462

Idrissi FZ, Garcia-Reyero N, Fernandez-Larrea JB, Pina B (2001) Alternative mechanisms of transcriptional activation by Rap1p. *J Biol Chem* **276**: 26090-26098

Idrissi FZ, Pina B (1999) Functional divergence between the half-sites of the DNA-binding sequence for the yeast transcriptional regulator Rap1p. *Biochem J* **341 (Pt 3)**: 477-482

Ira G, Pelliccioli A, Balijja A, Wang X, Fiorani S, Carotenuto W, Liberi G, Bressan D, Wan L, Hollingsworth NM, Haber JE, Foiani M (2004) DNA end resection, homologous recombination and DNA damage checkpoint activation require CDK1. *Nature* **431**: 1011-1017

Jia X, Weinert T, Lydall D (2004) Mec1 and Rad53 inhibit formation of single-stranded DNA at telomeres of *Saccharomyces cerevisiae* cdc13-1 mutants. *Genetics* **166**: 753-764

Kanoh J, Ishikawa F (2001) spRap1 and spRif1, recruited to telomeres by Taz1, are essential for telomere function in fission yeast. *Current Biology* **11**: 1624-1630

Karlseder J, Broccoli D, Dai Y, Hardy S, de Lange T (1999) p53- and ATM-dependent apoptosis induced by telomeres lacking TRF2. *Science* **283**: 1321-1325

Kippert F, Gerloff DL (2009) Highly Sensitive Detection of Individual HEAT and ARM Repeats with HHpred and COACH. *PLoS One* **4**: e7148

Kondo T, Wakayama T, Naiki T, Matsumoto K, Sugimoto K (2001) Recruitment of Mec1 and Ddc1 checkpoint proteins to double-strand breaks through distinct mechanisms. *Science* **294**: 867-870

Krogh BO, Symington LS (2004) Recombination proteins in yeast. *Annu Rev Genet* **38**: 233-271

Kyrion G, Boakye KA, Lustig AJ (1992) C-terminal truncation of RAP1 results in the deregulation of telomere size, stability, and function in *Saccharomyces cerevisiae*. *Mol Cell Biol* **12**: 5159-5173

Landry J, Sutton A, Tafrov ST, Heller RC, Stebbins J, Pillus L, Sternglanz R (2000) The silencing protein SIR2 and its homologs are NAD-dependent protein deacetylases *PNAS* **97**: 5807-5811

Lee SE, Moore JK, Holmes A, Umezaki K, Kolodner RD, Haber JE (1998) *Saccharomyces* Ku70, mre11/rad50 and RPA proteins regulate adaptation to G2/M arrest after DNA damage. *Cell* **94**: 399-409

Lendvay TS, Morris DK, Sah J, Balasubramanian B, Lundblad V (1996) Senescence mutants of *Saccharomyces cerevisiae* with a defect in telomere replication identify three additional EST genes. *Genetics* **144**: 1399-1412

Lengauer C, Kinzler KW, Vogelstein B (1997) Genetic instability in colorectal cancers. *Nature* **386**: 623-627

Leroy C, Lee SE, Vaze MB, Ochsenbien F, Guerois R, Haber JE, Marsolier-Kergoat MC (2003) PP2C phosphatases Ptc2 and Ptc3 are required for DNA checkpoint inactivation after a double-strand break. *Mol Cell* **11**: 827-835

- Levy DL, Blackburn EH (2004) Counting of Rif1p and Rif2p on *Saccharomyces cerevisiae* telomeres regulates telomere length. *Molecular and cellular biology* **24**: 10857-10867
- Li B, Oestreich S, de Lange T (2000) Identification of human Rap1: implications for telomere evolution. *Cell* **101**: 471-483
- Li X, Gerber SA, Rudner AD, Beausoleil SA, Haas W, Villén J, Elias JE, Gygi SP (2007) Large-Scale Phosphorylation Analysis of α -Factor-Arrested *Saccharomyces cerevisiae*. *Journal of Proteome Research* **6**: 1190-1197
- Liang F, Wang Y (2007) DNA damage checkpoints inhibit mitotic exit by two different mechanisms. *Mol Cell Biol* **27**: 5067-5078
- Lipps HJ, Rhodes D (2009) G-quadruplex structures: in vivo evidence and function. *Trends in Cell Biology* **19**: 414-422
- Lisby M, Barlow JH, Burgess RC, Rothstein R (2004) Choreography of the DNA Damage Response: Spatiotemporal Relationships among Checkpoint and Repair Proteins. *Cell* **118**: 699-713
- Livak KJ, Schmittgen TD (2001) Analysis of Relative Gene Expression Data Using Real-Time Quantitative PCR and the $2^{-\Delta\Delta CT}$ Method. *Methods* **25**: 402-408
- Longtine MS, McKenzie A, 3rd, Demarini DJ, Shah NG, Wach A, Brachat A, Philippsen P, Pringle JR (1998) Additional modules for versatile and economical PCR-based gene deletion and modification in *Saccharomyces cerevisiae*. *Yeast* **14**: 953-961
- Lou H, Komata M, Katou Y, Guan Z, Reis CC, Budd M, Shirahige K, Campbell JL (2008) Mrc1 and DNA Polymerase ϵ Function Together in Linking DNA Replication and the S Phase Checkpoint. *Molecular Cell* **32**: 106-117
- Louis EJ, Vershinin AV (2005) Chromosome ends: different sequences may provide conserved functions. *Bioessays* **27**: 685-697
- Luke B, Panza A, Redon S, Iglesias N, Li Z, Lingner J (2008) The Rat1p 5' to 3' Exonuclease Degrades Telomeric Repeat-Containing RNA and Promotes Telomere Elongation in *Saccharomyces cerevisiae*. *Molecular Cell* **32**: 465-477

Lundblad V, Blackburn EH (1993) An alternative pathway for yeast telomere maintenance rescues est1- senescence. *Cell* **73**: 347-360

Lundblad V, Szostak JW (1989) A mutant with a defect in telomere elongation leads to senescence in yeast. *Cell* **57**: 633-643

Lundin C, North M, Erixon K, Walters K, Jenssen D, Goldman AS, Helleday T (2005) Methyl methanesulfonate (MMS) produces heat-labile DNA damage but no detectable in vivo DNA double-strand breaks. *Nucleic Acids Res* **33**: 3799-3811

Lupardus PJ, Cimprich KA (2004) Checkpoint adaptation; molecular mechanisms uncovered. *Cell* **117**: 555-556

Majka J, Niedziela-Majka A, Burgers PM (2006) The checkpoint clamp activates Mec1 kinase during initiation of the DNA damage checkpoint. *Mol Cell* **24**: 891-901

Marcand S, Gilson E, Shore D (1997) A Protein-Counting Mechanism for Telomere Length Regulation in Yeast. *Science* **275**: 986-990

Marcand S, Pardo B, Gratias A, Cahun S, Callebaut I (2008) Multiple pathways inhibit NHEJ at telomeres. *Genes Dev* **22**: 1153-1158

Maringele L, Lydall D (2002) EXO1-dependent single-stranded DNA at telomeres activates subsets of DNA damage and spindle checkpoint pathways in budding yeast yku70Delta mutants. *Genes Dev* **16**: 1919-1933

Maringele L, Lydall D (2004) Telomerase- and recombination-independent immortalization of budding yeast. *Genes Dev* **18**: 2663-2675

Martin S, Laroche T, Suka N, Grunstein M, Gasser S (1999) Relocalization of telomeric Ku and Sir proteins in response to DNA strand breaks in yeast. *Cell* **97**: 621-633

Martin V, Du LL, Rozenzhak S, Russell P (2007) Protection of telomeres by a conserved Stn1-Ten1 complex. *Proc Natl Acad Sci U S A* **104**: 14038-14043

Maser RS, DePinho RA (2002) Connecting chromosomes, crisis, and cancer. *Science* **297**: 565-569

- McClintock B (1941) The Stability of Broken Ends of Chromosomes in Zea Mays. *Genetics* **26**: 234-282
- McMurray MA, Gottschling DE (2003) An age-induced switch to a hyper-recombinational state. *Science* **301**: 1908-1911
- Meek DW, Simon S, Kikkawa U, Eckhart W (1990) The p53 tumour suppressor protein is phosphorylated at serine 389 by casein kinase II. *EMBO Journal* **9**: 3253-3260
- Meinhardt F, Schaffrath R, Larsen M (1997) Microbial linear plasmids. *Appl Microbiol Biotechnol* **47**: 329-336
- Mills KD, Sinclair DA, Guarente L (1999) MEC1-dependent redistribution of the Sir3 silencing protein from telomeres to DNA double-strand breaks. *Cell* **97**: 609-620
- Mimitou EP, Symington LS (2008) Sae2, Exo1 and Sgs1 collaborate in DNA double-strand break processing. *Nature* **455**: 770-774
- Mishra K, Shore D (1999) Yeast Ku protein plays a direct role in telomeric silencing and counteracts inhibition by rif proteins. *Curr Biol* **9**: 1123-1126
- Mitchell MT, Smith JS, Mason M, Harper S, Speicher DW, Johnson FB, Skordalakes E (2010) Cdc13 N-terminal dimerization, DNA binding and telomere length regulation. *Mol Cell Biol*: MCB.00515-00510
- Miyake Y, Nakamura M, Nabetani A, Shimamura S, Tamura M, Yonehara S, Saito M, Ishikawa F (2009) RPA-like mammalian Ctc1-Stn1-Ten1 complex binds to single-stranded DNA and protects telomeres independently of the Pot1 pathway. *Mol Cell* **36**: 193-206
- Mrózek K, Heerema NA, Bloomfield CD (2004) Cytogenetics in acute leukemia. *Blood Reviews* **18**: 115-136
- Mundt KE, Golsteyn RM, Lane HA, Nigg EA (1997) On the Regulation and Function of Human Polo-like Kinase 1 (PLK1): Effects of Overexpression on Cell Cycle Progression. *Biochemical and Biophysical Research Communications* **239**: 377-385
- Murnane JP (2010) Telomere loss as a mechanism for chromosome instability in human cancer. *Cancer Res* **70**: 4255-4259

Negrini S, Gorgoulis VG, Halazonetis TD (2010) Genomic instability--an evolving hallmark of cancer. *Nat Rev Mol Cell Biol* **11**: 220-228

Nowell PC (1976) The clonal evolution of tumor cell populations. *Science* **194**: 23-28

Nugent CI, Hughes TR, Lue NF, Lundblad V (1996) Cdc13p: a single-strand telomeric DNA-binding protein with a dual role in yeast telomere maintenance. *Science* **274**: 249-252

Oliva-Trastoy M, Berthonaud V, Chevalier A, Ducrot C, Marsolier-Kergoat MC, Mann C, Leteurtre F (2006) The Wip1 phosphatase (PPM1D) antagonizes activation of the Chk2 tumour suppressor kinase. *Oncogene* **26**: 1449-1458

Oulton R, Harrington L (2004) A human telomerase-associated nuclease. *Mol Biol Cell* **15**: 3244-3256

Palm W, de Lange T (2008) How shelterin protects mammalian telomeres. *Annu Rev Genet* **42**: 301-334

Parenteau J, Wellinger RJ (1999) Accumulation of single-stranded DNA and destabilization of telomeric repeats in yeast mutant strains carrying a deletion of RAD27. *Mol Cell Biol* **19**: 4143-4152

Park JI, Venteicher AS, Hong JY, Choi J, Jun S, Shkreli M, Chang W, Meng Z, Cheung P, Ji H, McLaughlin M, Veenstra TD, Nusse R, McCrea PD, Artandi SE (2009) Telomerase modulates Wnt signalling by association with target gene chromatin. *Nature* **460**: 66-72

Pellicioli A, Lee SE, Lucca C, Foiani M, Haber JE (2001) Regulation of *Saccharomyces* Rad53 checkpoint kinase during adaptation from DNA damage-induced G2/M arrest. *Mol Cell* **7**: 293-300

Pennock E, Buckley K, Lundblad V (2001) Cdc13 delivers separate complexes to the telomere for end protection and replication. *Cell* **104**: 387-396

Perez-Losada J, Mao J-H, Balmain A (2005) Control of Genomic Instability and Epithelial Tumor Development by the p53-Fbxw7/Cdc4 Pathway. *Cancer Research* **65**: 6488-6492

Perry J, Kleckner N (2003) The ATRs, ATMs, and TORs Are Giant HEAT Repeat Proteins. *Cell* **112**: 151-155

Persengiev SP, Zhu X, Dixit BL, Maston GA, Kittler EL, Green MR (2003) TRF3, a TATA-box-binding protein-related factor, is vertebrate-specific and widely expressed. *Proc Natl Acad Sci U S A* **100**: 14887-14891

Petreaca RC, Chiu HC, Nugent CI (2007) The role of Stn1p in *Saccharomyces cerevisiae* telomere capping can be separated from its interaction with Cdc13p. *Genetics* **177**: 1459-1474

Pina B, Fernandez-Larrea J, Garcia-Reyero N, Idrissi FZ (2003) The different (sur)faces of Rap1p. *Mol Genet Genomics* **268**: 791-798

Prescott J, Blackburn EH (1997) Functionally interacting telomerase RNAs in the yeast telomerase complex. *Genes Dev* **11**: 2790-2800

Qi H, Zakian VA (2000) The *Saccharomyces* telomere-binding protein Cdc13p interacts with both the catalytic subunit of DNA polymerase alpha and the telomerase-associated est1 protein. *Genes Dev* **14**: 1777-1788

Raices M, Verdun RE, Compton SA, Haggblom CI, Griffith JD, Dillin A, Karlseder J (2008) *C. elegans* telomeres contain G-strand and C-strand overhangs that are bound by distinct proteins. *Cell* **132**: 745-757

Raynard S, Niu H, Sung P (2008) DNA double-strand break processing: the beginning of the end. *Genes Dev* **22**: 2903-2907

Reddel RR, Bryan TM (2003) Alternative lengthening of telomeres: dangerous road less travelled. *Lancet* **361**: 1840-1841

Ristic D, Modesti M, Kanaar R, Wyman C (2003) Rad52 and Ku bind to different DNA structures produced early in double-strand break repair. *Nucleic Acids Res* **31**: 5229-5237

Rodier F, Campisi J (2011) Four faces of cellular senescence. *J Cell Biol* **192**: 547-556

Roy A, Kucukural A, Zhang Y (2010) I-TASSER: a unified platform for automated protein structure and function prediction. *Nat Protocols* **5**: 725-738

Saito-Ohara F, Imoto I, Inoue J, Hosoi H, Nakagawara A, Sugimoto T, Inazawa J (2003) PPM1D Is a Potential Target for 17q Gain in Neuroblastoma. *Cancer Research* **63**: 1876-1883

Sakaguchi K (1990) Invertrons, a class of structurally and functionally related genetic elements that includes linear DNA plasmids, transposable elements, and genomes of adeno-type viruses. *Microbiol Rev* **54**: 66-74

Salas M (1991) Protein-priming of DNA replication. *Annu Rev Biochem* **60**: 39-71

Sanchez Y, Bachant J, Wang H, Hu F, Liu D, Tetzlaff M, Elledge SJ (1999) Control of the DNA Damage Checkpoint by Chk1 and Rad53 Protein Kinases Through Distinct Mechanisms. *Science* **286**: 1166-1171

Sandell LL, Zakian VA (1993) Loss of a yeast telomere: arrest, recovery, and chromosome loss. *Cell* **75**: 729-739

Seldin DC, Leder P (1995) Casein kinase II alpha transgene-induced murine lymphoma: relation to theileriosis in cattle. *Science* **267**: 894-897

Sfeir A, Kosiyatrakul ST, Hockemeyer D, MacRae SL, Karlseder J, Schildkraut CL, de Lange T (2009) Mammalian telomeres resemble fragile sites and require TRF1 for efficient replication. *Cell* **138**: 90-103

Shay JW, Wright WE (1989) Quantitation of the frequency of immortalization of normal human diploid fibroblasts by SV40 large T-antigen. *Exp Cell Res* **184**: 109-118

Shroff R, Arbel-Eden A, Pilch D, Ira G, Bonner WM, Petrini JH, Haber JE, Lichten M (2004) Distribution and Dynamics of Chromatin Modification Induced by a Defined DNA Double-Strand Break. *Current Biology* **14**: 1703-1711

Shubernetskaya O, Logvina N, Sharanov Y, Zvereva M (2011) Yeast telomerase protein Est3 is a novel type of GTPase. *Biochimie* **93**: 202-206

Silverman J, Takai H, Buonomo SB, Eisenhaber F, de Lange T (2004) Human Rif1, ortholog of a yeast telomeric protein, is regulated by ATM and 53BP1 and functions in the S-phase checkpoint. *Genes Dev* **18**: 2108-2119

Singer MS, Gottschling DE (1994) TLC1: template RNA component of *Saccharomyces cerevisiae* telomerase. *Science* **266**: 404-409

Sinha RP, Hader DP (2002) UV-induced DNA damage and repair: a review. *Photochem Photobiol Sci* **1**: 225-236

Sjoblom T, Jones S, Wood LD, Parsons DW, Lin J, Barber TD, Mandelker D, Leary RJ, Ptak J, Silliman N, Szabo S, Buckhaults P, Farrell C, Meeh P, Markowitz SD, Willis J, Dawson D, Willson JK, Gazdar AF, Hartigan J, Wu L, Liu C, Parmigiani G, Park BH, Bachman KE, Papadopoulos N, Vogelstein B, Kinzler KW, Velculescu VE (2006) The consensus coding sequences of human breast and colorectal cancers. *Science* **314**: 268-274

Smith CD, Smith DL, DeRisi JL, Blackburn EH (2003a) Telomeric Protein Distributions and Remodeling Through the Cell Cycle in *Saccharomyces cerevisiae*. *Mol Biol Cell* **14**: 556-570

Smith LL, Collier HA, Roberts JM (2003b) Telomerase modulates expression of growth-controlling genes and enhances cell proliferation. *Nat Cell Biol* **5**: 474-479

Smith S, Banerjee S, Rilo R, Myung K (2008) Dynamic regulation of single-stranded telomeres in *Saccharomyces cerevisiae*. *Genetics* **178**: 693-701

Smogorzewska A, Karlseder J, Holtgreve-Grez H, Jauch A, de Lange T (2002) DNA ligase IV-dependent NHEJ of deprotected mammalian telomeres in G1 and G2. *Curr Biol* **12**: 1635-1644

Smolka MB, Albuquerque CP, Chen S-h, Zhou H (2007) Proteome-wide identification of in vivo targets of DNA damage checkpoint kinases. *Proceedings of the National Academy of Sciences* **104**: 10364-10369

Sugawara N, Wang X, Haber JE (2003) In Vivo Roles of Rad52, Rad54, and Rad55 Proteins in Rad51-Mediated Recombination. *Molecular Cell* **12**: 209-219

Surovtseva YV, Churikov D, Boltz KA, Song X, Lamb JC, Warrington R, Leehy K, Heacock M, Price CM, Shippen DE (2009) Conserved telomere maintenance component 1 interacts with STN1 and maintains chromosome ends in higher eukaryotes. *Mol Cell* **36**: 207-218

Syljuasen RG (2007) Checkpoint adaptation in human cells. *Oncogene* **26**: 5833-5839

Syljuåsen RG, Jensen S, Bartek J, Lukas J (2006) Adaptation to the Ionizing Radiation-Induced G2 Checkpoint Occurs in Human Cells and Depends on Checkpoint Kinase 1 and Polo-like Kinase 1 Kinases. *Cancer Research* **66**: 10253-10257

Szyjka SJ, Viggiani CJ, Aparicio OM (2005) Mrc1 Is Required for Normal Progression of Replication Forks throughout Chromatin in *S. cerevisiae*. *Molecular Cell* **19**: 691-697

Taggart AK, Teng SC, Zakian VA (2002) Est1p as a cell cycle-regulated activator of telomere-bound telomerase. *Science* **297**: 1023-1026

Tarrant MK, Cole PA (2009) The chemical biology of protein phosphorylation. *Annu Rev Biochem* **78**: 797-825

Tawfic S, Yu S, Wang H, Faust R, Davis A, Ahmed K (2001) Protein kinase CK2 signal in neoplasia. *Histol Histopathol* **16**: 573-582

Teixeira MT, Arneric M, Sperisen P, Lingner J (2004) Telomere Length Homeostasis Is Achieved via a Switch between Telomerase- Extendible and -Nonextendible States. *Cell* **117**: 323-335

Teng SC, Chang J, McCowan B, Zakian VA (2000) Telomerase-independent lengthening of yeast telomeres occurs by an abrupt Rad50p-dependent, Rif-inhibited recombinational process. *Mol Cell* **6**: 947-952

Teng SC, Zakian VA (1999) Telomere-telomere recombination is an efficient bypass pathway for telomere maintenance in *Saccharomyces cerevisiae*. *Mol Cell Biol* **19**: 8083-8093

Teste MA, Duquenne M, Francois JM, Parrou JL (2009) Validation of reference genes for quantitative expression analysis by real-time RT-PCR in *Saccharomyces cerevisiae*. *BMC molecular biology* **10**: 99

Theobald DL, Wuttke DS (2004) Prediction of multiple tandem OB-fold domains in telomere end-binding proteins Pot1 and Cdc13. *Structure* **12**: 1877-1879

Toczyski DP, Galgoczy DJ, Hartwell LH (1997) CDC5 and CKII control adaptation to the yeast DNA damage checkpoint. *Cell* **90**: 1097-1106

Toledo F, Wahl GM (2006) Regulating the p53 pathway: in vitro hypotheses, in vivo veritas. *Nat Rev Cancer* **6**: 909-923

Tomita K, Cooper JP (2007) The Telomere Bouquet Controls the Meiotic Spindle. *Cell* **130**: 113-126

Tsantoulis PK, Kotsinas A, Sfikakis PP, Evangelou K, Sideridou M, Levy B, Mo L, Kittas C, Wu XR, Papavassiliou AG, Gorgoulis VG (2008) Oncogene-induced replication stress preferentially targets common fragile sites in preneoplastic lesions. A genome-wide study. *Oncogene* **27**: 3256-3264

Tseng SF, Lin JJ, Teng SC (2006) The telomerase-recruitment domain of the telomere binding protein Cdc13 is regulated by Mec1p/Tel1p-dependent phosphorylation. *Nucleic Acids Res* **34**: 6327-6336

Tsukamoto Y, Kato J, Ikeda H (1997) Silencing factors participate in DNA repair and recombination in *Saccharomyces cerevisiae*. *Nature* **388**: 900-903

Tuteja R, Tuteja N (2000) Ku autoantigen: a multifunctional DNA-binding protein. *Crit Rev Biochem Mol Biol* **35**: 1-33

Van Driessche B, Tafforeau L, Hentges P, Carr AM, Vandenhoute J (2005) Additional vectors for PCR-based gene tagging in *Saccharomyces cerevisiae* and *Schizosaccharomyces pombe* using nourseothricin resistance. *Yeast* **22**: 1061-1068

van Steensel B, Smogorzewska A, de Lange T (1998) TRF2 Protects Human Telomeres from End-to-End Fusions. *Cell* **92**: 401-413

van Vugt MATM, Brás A, Medema RH (2004) Polo-like Kinase-1 Controls Recovery from a G2 DNA Damage-Induced Arrest in Mammalian Cells. *Molecular Cell* **15**: 799-811

Vignais ML, Woudt LP, Wassenaar GM, Mager WH, Sentenac A, Planta RJ (1987) Specific binding of TUF factor to upstream activation sites of yeast ribosomal protein genes. *EMBO J* **6**: 1451-1457

Vodenicharov MD, Wellinger RJ (2006) DNA degradation at unprotected telomeres in yeast is regulated by the CDK1 (Cdc28/Clb) cell-cycle kinase. *Mol Cell* **24**: 127-137

Walker JR, Corpina RA, Goldberg J (2001) Structure of the Ku heterodimer bound to DNA and its implications for double-strand break repair. *Nature* **412**: 607-614

Wan M, Qin J, Songyang Z, Liu D (2009) OB fold-containing protein 1 (OBFC1), a human homolog of yeast Stn1, associates with TPP1 and is implicated in telomere length regulation. *J Biol Chem* **284**: 26725-26731

Wang H, Blackburn EH (1997) De novo telomere addition by *Tetrahymena* telomerase in vitro. *EMBO J* **16**: 866-879

Wang H, Liu D, Wang Y, Qin J, Elledge SJ (2001) Pds1 phosphorylation in response to DNA damage is essential for its DNA damage checkpoint function. *Genes Dev* **15**: 1361-1372

Wang H, Zhao A, Chen L, Zhong X, Liao J, Gao M, Cai M, Lee DH, Li J, Chowdhury D, Yang YG, Pfeifer GP, Yen Y, Xu X (2009) Human RIF1 encodes an anti-apoptotic factor required for DNA repair. *Carcinogenesis* **30**: 1314-1319

Wang RC, Smogorzewska A, de Lange T (2004) Homologous recombination generates T-loop-sized deletions at human telomeres. *Cell* **119**: 355-368

Wang X, Haber JE (2004) Role of Saccharomyces single-stranded DNA-binding protein RPA in the strand invasion step of double-strand break repair. *PLoS Biol* **2**: E21

Wellinger RJ, Ethier K, Labrecque P, Zakian VA (1996) Evidence for a new step in telomere maintenance. *Cell* **85**: 423-433

Wotton D, Shore D (1997) A novel Rap1p-interacting factor, Rif2p, cooperates with Rif1p to regulate telomere length in Saccharomyces cerevisiae. *Genes Dev* **11**: 748-760

Wright JH, Gottschling DE, Zakian VA (1992) Saccharomyces telomeres assume a non-nucleosomal chromatin structure. *Genes Dev* **6**: 197-210

Xu D, Muniandy P, Leo E, Yin J, Thangavel S, Shen X, Ii M, Agama K, Guo R, Fox D, 3rd, Meetei AR, Wilson L, Nguyen H, Weng NP, Brill SJ, Li L, Vindigni A, Pommier Y, Seidman M, Wang W (2010) Rif1 provides a new DNA-binding interface for the Bloom syndrome complex to maintain normal replication. *EMBO J* **29**: 3140-3155

Xu L, Blackburn EH (2004) Human Rif1 protein binds aberrant telomeres and aligns along anaphase midzone microtubules. *J Cell Biol* **167**: 819-830

Yoo HY, Kumagai A, Shevchenko A, Shevchenko A, Dunphy WG (2004) Adaptation of a DNA Replication Checkpoint Response Depends upon Inactivation of Claspin by the Polo-like Kinase. *Cell* **117**: 575-588

Zhu Z, Chung WH, Shim EY, Lee SE, Ira G (2008) Sgs1 helicase and two nucleases Dna2 and Exo1 resect DNA double-strand break ends. *Cell* **134**: 981-994

Zubko MK, Guillard S, Lydall D (2004) Exo1 and Rad24 differentially regulate generation of ssDNA at telomeres of *Saccharomyces cerevisiae* cdc13-1 mutants. *Genetics* **168**: 103-115

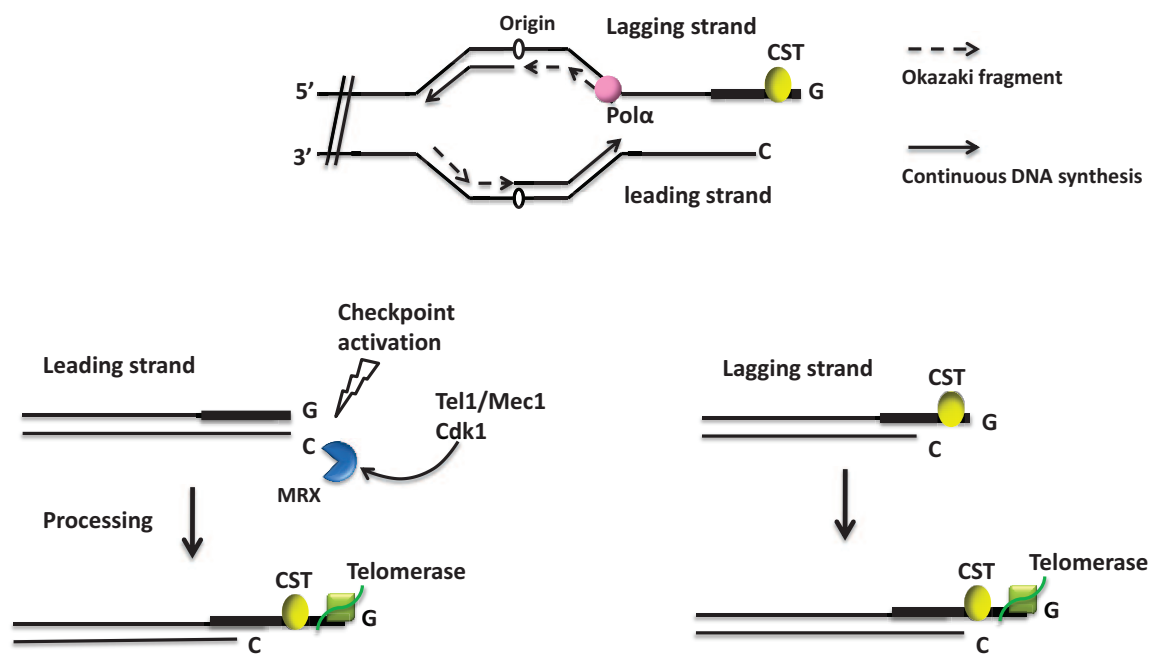


Fig 1.3.1 Telomere replication in *S. cerevisiae* (See text for detail)

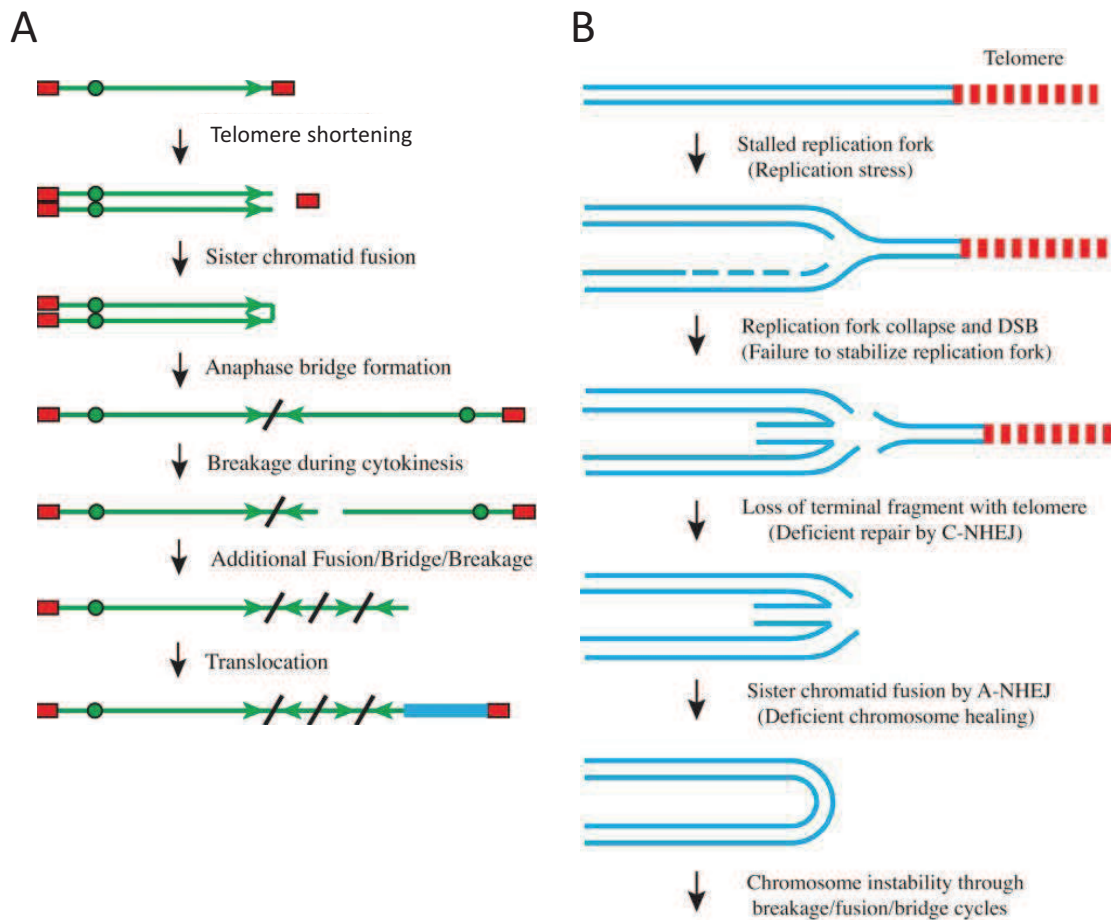


Fig 1.4 A. Telomere attrition induced breakage-fusion-bridge cycle (adapted from Murnane review Cancer Res. 2010). During crisis, telomeres erode to extremely short length, which induces inappropriate repair to create chromosome fusions. Fused sister chromatids break during anaphase, resulting in an inverted repeats on one of the chromosome end, and a terminal deletion on the other chromosome. Due to the absence of a telomere on the broken chromosomes, addition fusions, bridges and breaks occur in subsequent cell cycles, leading to more amplification and deletions. Eventually, a telomere is acquired from translocation from another chromosome to stabilize the chromosome. **B. Proposed model for spontaneous telomere loss in cancer cells** (Murnane review Cancer Res. 2010). See text for detail.

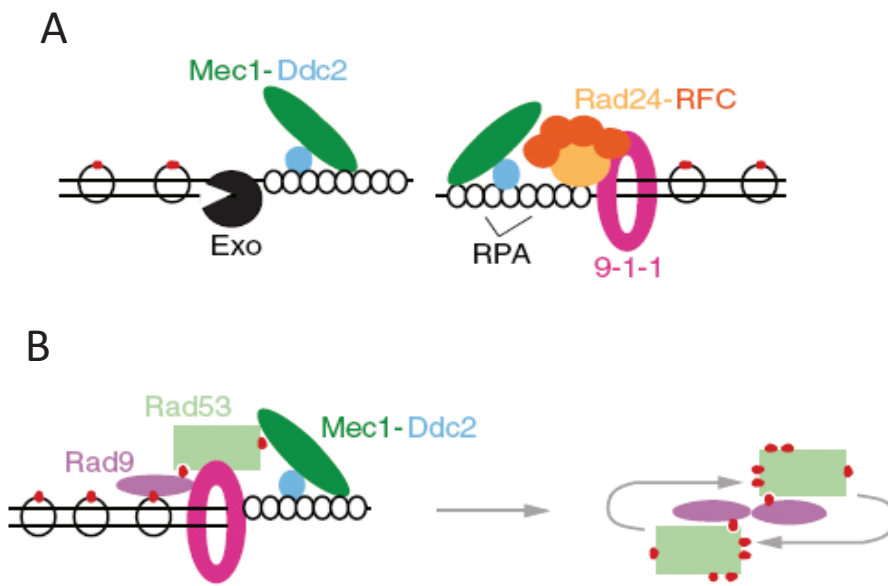


Fig 1.5 G2/M DNA damage checkpoint in *S.cerevisiae*. **A.** Exonuclease dependent resection at the site of damage creates long stretches of ssDNA which is bound by Rpa. Rpa bound ssDNA acts as a damage signal for the independent recruitment of the two damage sensor kinases Mec1 and the 9-1-1 complex. **B.** Once recruited to the site of damage, the 9-1-1 complex activates the kinase activity of Mec1. Mec1 then phosphorylates and activates the effector kinase Rad53, an interaction dependent on the transducer kinase Rad9. Rad53 is then able to undergo subsequent auto-phosphorylation and interact with a host of downstream targets inducing cell cycle arrest in G2/M and activation of DNA damage repair genes. Figures are from Harrison and Haber (2006).

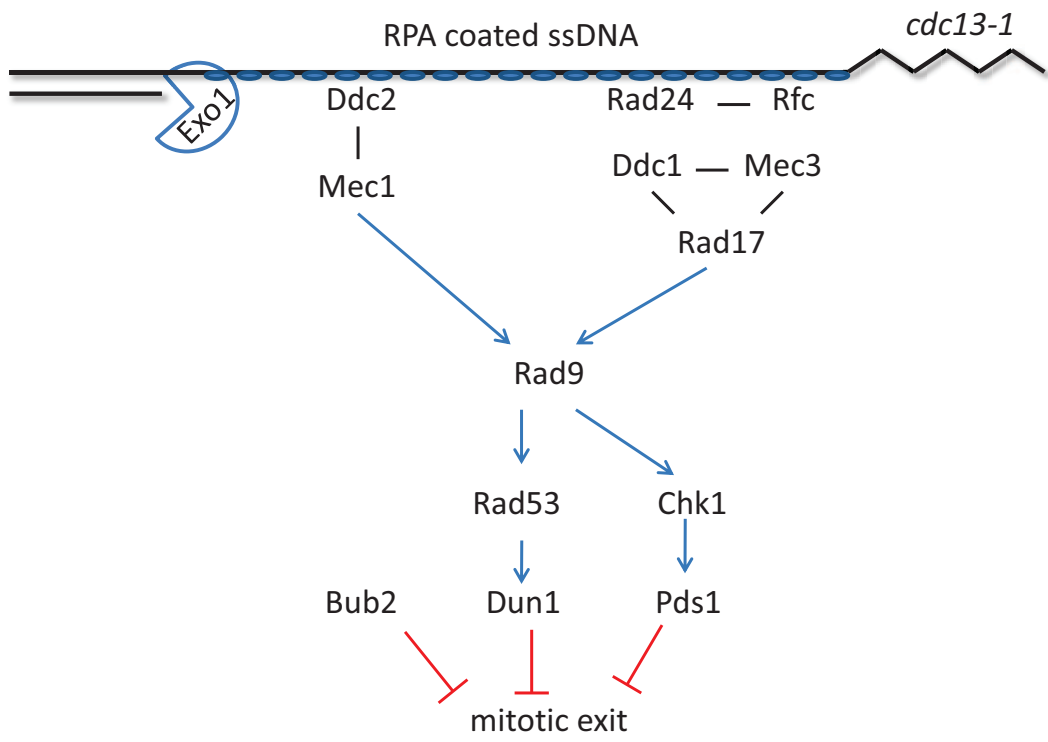


Fig 1.6.1 Schematic representation of checkpoint pathways in *cdc13-1* cells leading to G2/M arrest

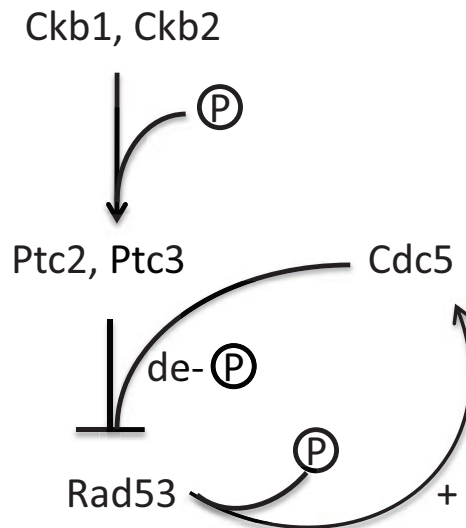


Fig 1.7 A possible adaptation controlling pathway in budding yeast (proposed by Syljuansen, 2007)

Cdc5, casein kinase II and PP2C-like phosphatase may act in a common pathway to inactivate Rad53. Ckb1 and Ckb2 may phosphorylate the phosphatases Ptc2 and Ptc3, which in turn dephosphorylated and therefore inactivate Rad53. The polo-like kinase Cdc5 may function upstream of Rad53 or as a part of the negative feedback loop to turn off Rad53.

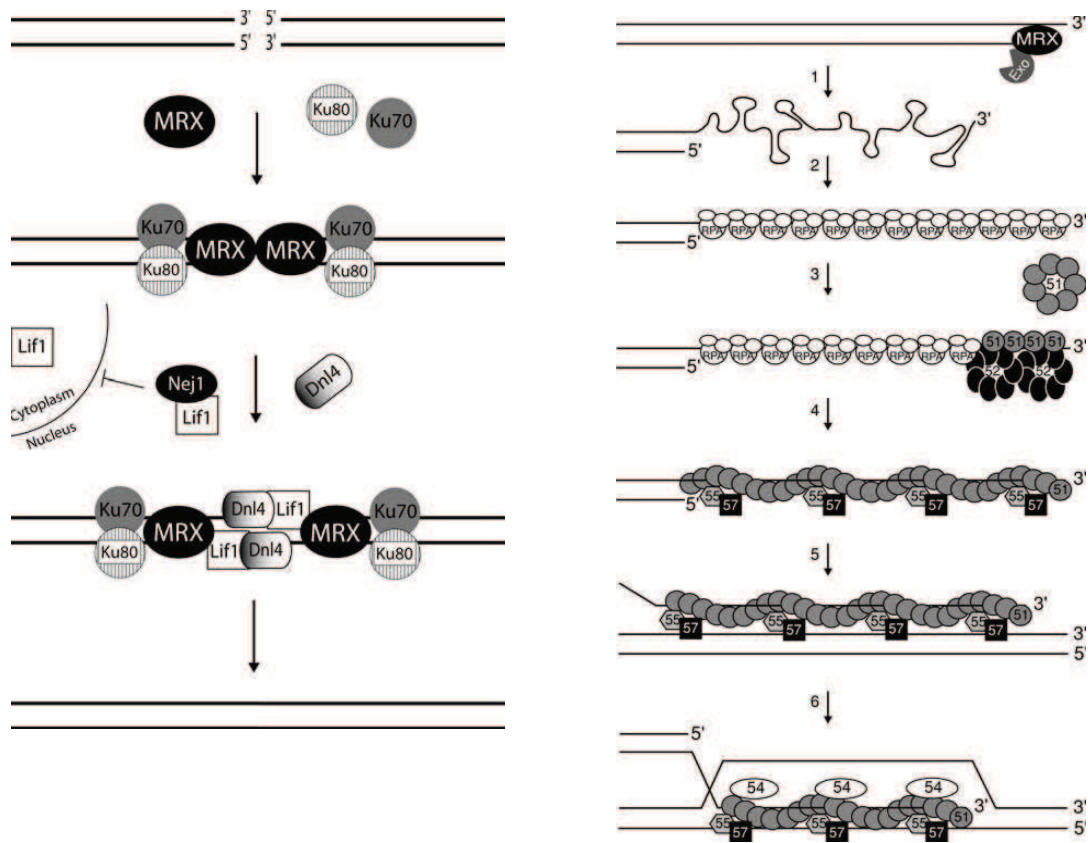


Fig 1.8 A comparison between NHEJ and HR (Krogh & Symington, 2004)

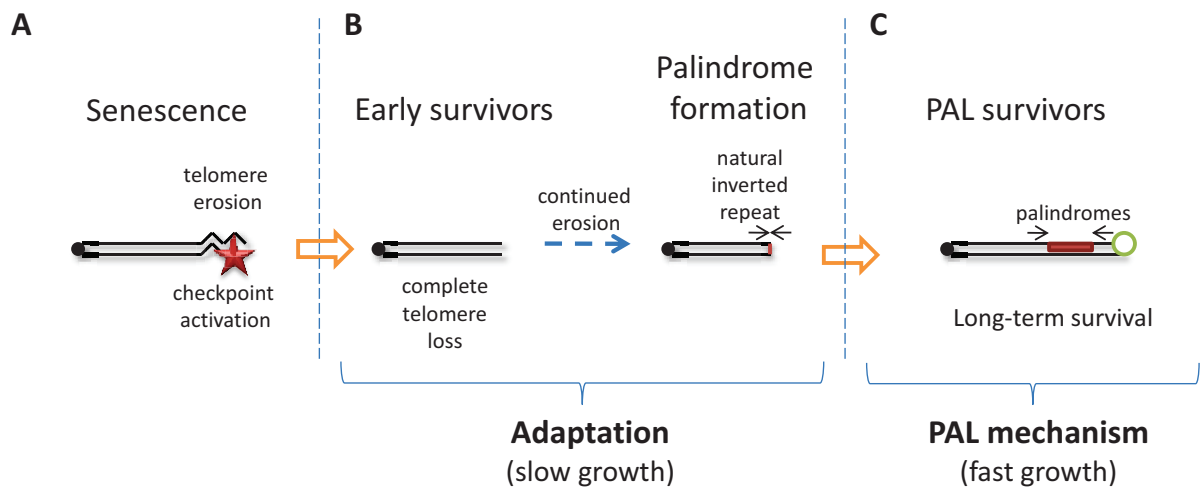


Fig 1.11.1 A proposed model for PAL survivor generation

A. Adaptation to telomere defects. Telomere loss (*tlc1Δ*) induced telomere erosion triggers cell cycle arrest mediated by the checkpoint proteins. While the majority of *tlc1Δ rad52Δ exo1Δ* cells remain arrested (senescent), a small population of cells was able to escape and continue proliferation. **B.** Early post-senescent stage. Continued proliferation leads to severe chromosome end degradation in early survivors, until the majority of telomeric repeats are lost in these cells. When degradation reaches a short inverted repeat naturally presents in the genome, palindrome formation initiates. **C.** Activation of strategies for long term survival. Large palindrome formation enable cells to activate a different mechanism for long term survival, possibly by recruiting proteins engaged in end capping and replication.

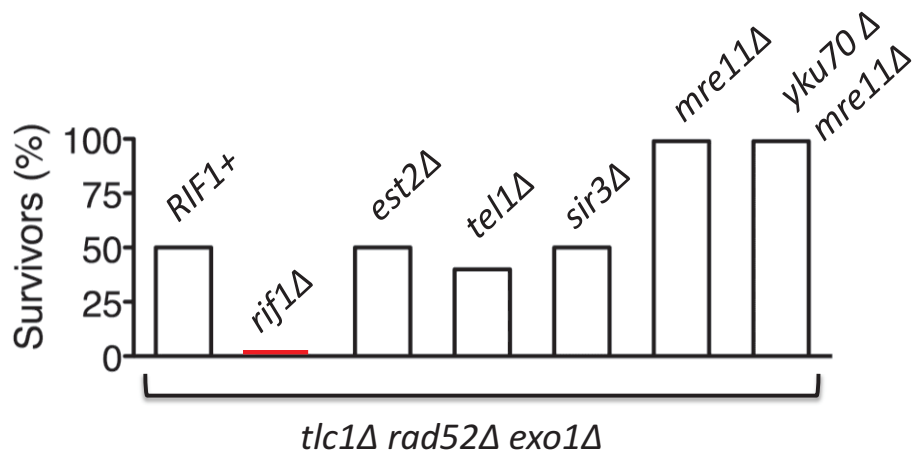


Fig 1.11.2 Survival of *tlc1Δrad52Δ exo1Δ* strains carrying deletions in non-essential telomere interacting genes.

Haploid strains of indicated genotypes were obtained from germination and were propagated every 5 days on YEPD plates. The number of survivors was scored after 20 days. 20 independent strains were tested for each genotype. Survival fractions were calculated as (the number of strains that generated survivors/ the number of strains tested) x 100%. Data was obtained by Dr. Laura Maringele.

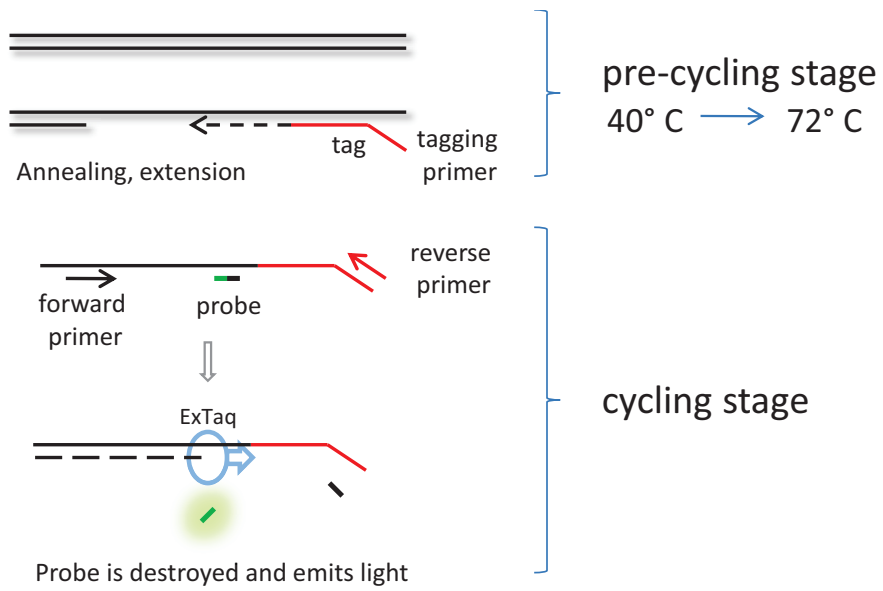


Fig 2.9.1 The principle of QAOS assay

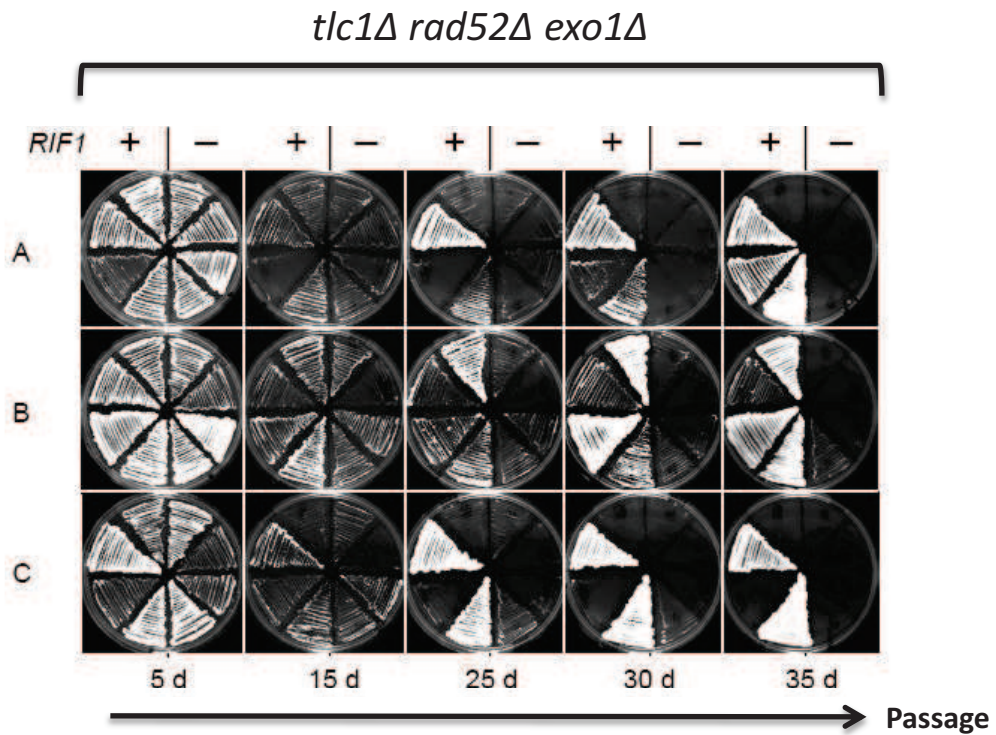


Fig 3.1 Effect of *RIF1* on escaping senescence

Lanes A-C shows the growth of independent *tlc1Δrad52Δexo1Δ* strains on YEPD plates. Strains on the right half of each plate also contained *rif1Δ*. ~10 million cells from each strain were propagated on a fresh plate every 5 days after germination. Plates were photographed at 5, 15, 25, 30 and 35 days.

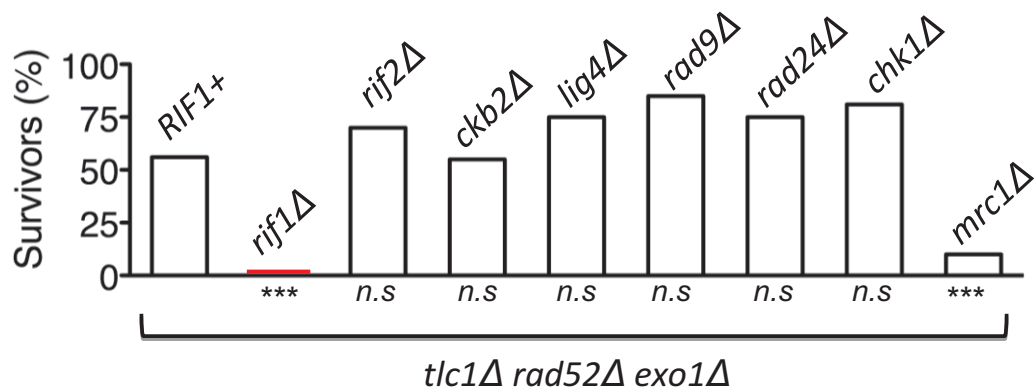


Fig 3.2 Survival of *tlc1Δ rad52Δ exo1Δ* strains carrying different gene deletions.

Haploid strains of indicated genotype were obtained from germination and were propagated every 5 days on YEPD plates. The number of survivors was scored after 35 days. Survival fractions were calculated as (the number of strains that generated survivors/ the number of strains tested) x 100%. 12-36 independent strains were tested for the each genotype. Chi-square statistical analysis was used to compare survival fractions between the *RIF1+* strain and strains with other genotypes. n.s. indicates non-significant. *** indicates $p < 0.001$.

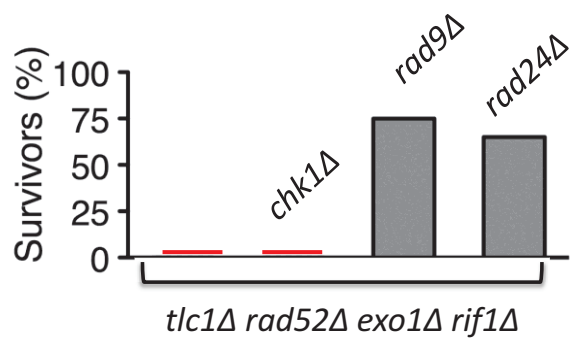


Fig 3.3 Effect of checkpoints on the survival of *tlc1Δrad52Δ exo1Δ rif1Δ* cells

tlc1Δ rad52Δ exo1Δ rif1Δ cells with indicated additional gene deletions were propagated every 5 days on YEPD plates since germination. Survival fraction was calculated as (the number of strains that generated survivors/ the number of strains tested) x 100%. Survival fractions were calculated at 45 days for *rad9Δ*, *rad24Δ* strains and at 35 days for *chk1Δ* strains. 16-20 independent strains were analysed for each genotype.

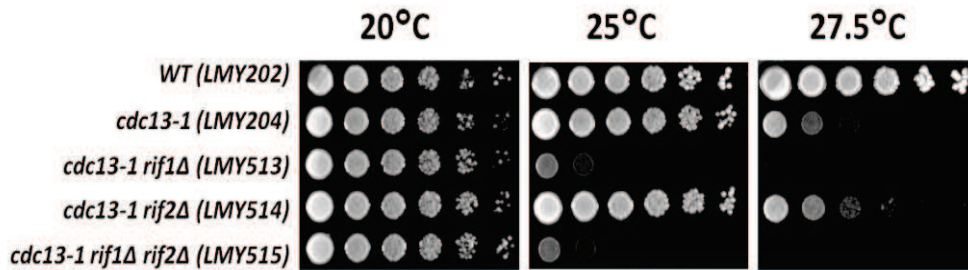


Fig 4.1.1 *RIF1* contributes to the viability of *cdc13-1* mutant at 25°C

5-fold serial dilution of yeast strains at indicated temperatures. Plates were incubated 2 days before being photographed. Strain numbers are indicated in brackets. Four independent spot tests were performed with the same strains and conditions and show the same result.

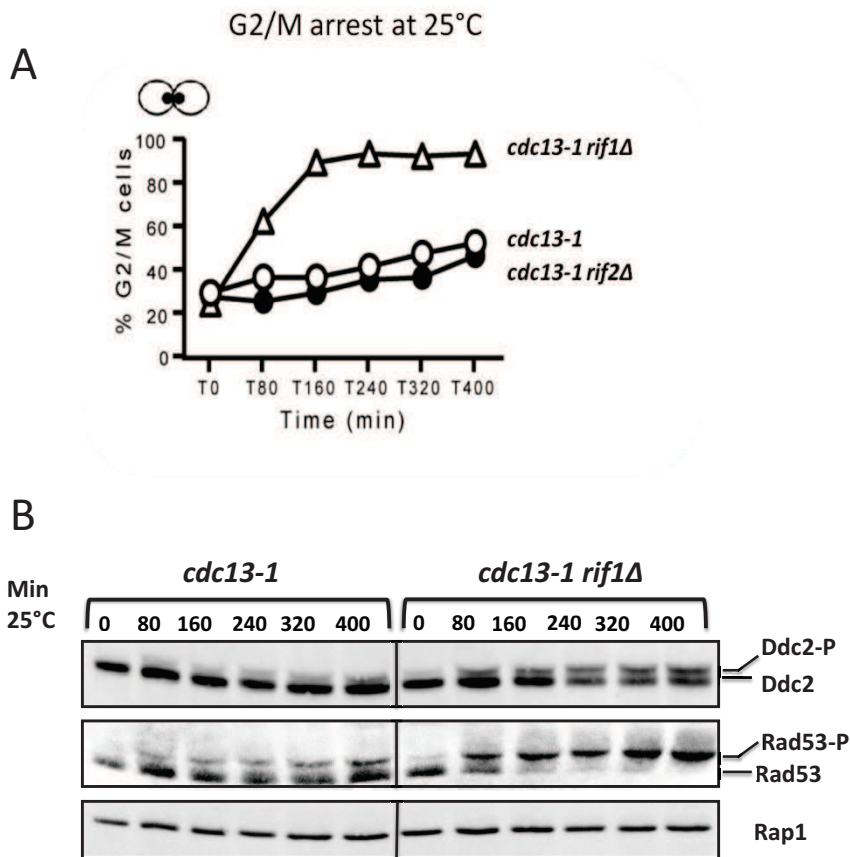


Fig 4.1.2 checkpoint activation in *cdc13-1* cells versus *cdc13-1 rif1Δ* cells at 25°C.

A. Percentage of G2/M arrested cells at 25°C. Cells were stained with DAPI and scored as described in the methods. For each time point, 300 cells were scored and the average value was plotted. Yeast strains are LMY420 (*cdc13-1 rif1Δ*), LMY204 (*cdc13-1*) and LMY514 (*cdc13-1 rif2Δ*). **B.** Western blot showing phosphorylation of the checkpoint proteins Ddc2 and Rad53 at 25°C. Rap1 serves as a loading control. Yeast strains *cdc13-1 DDC2-YFP* (LMY415) and *cdc13-1 DDC2-YFP rif1Δ* (LMY416) were used.

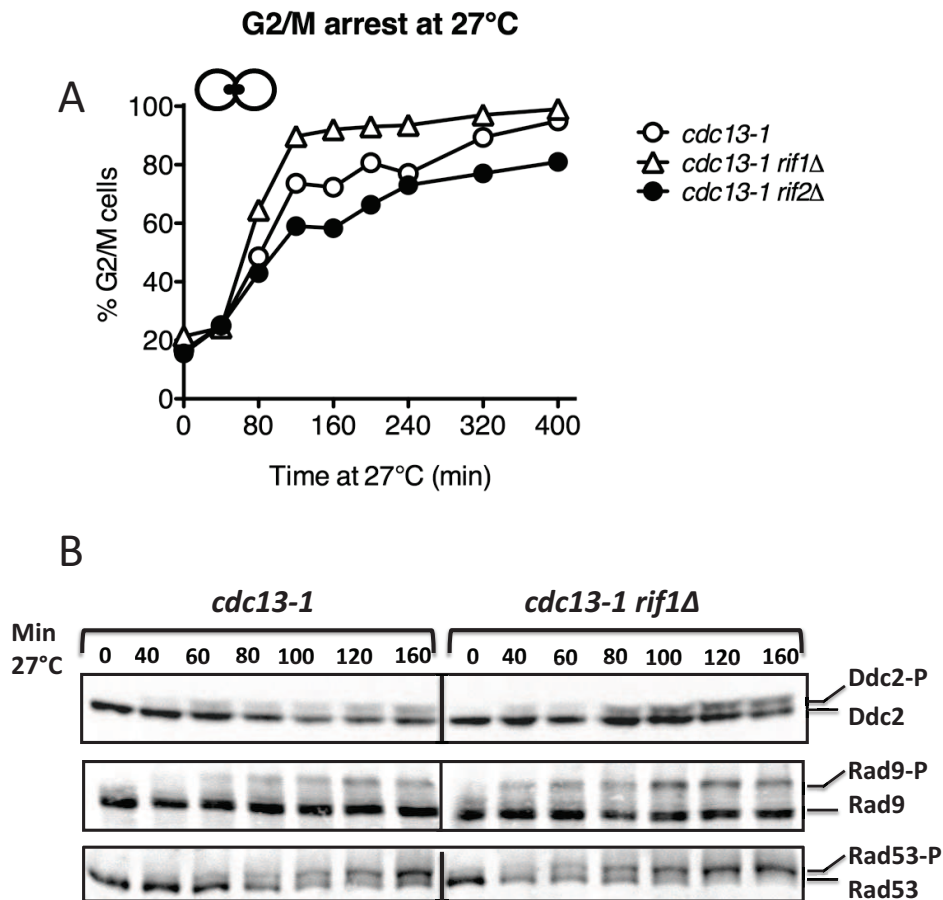


Fig 4.1.3 checkpoint activation in *cdc13-1* cells and *cdc13-1 rif1Δ* cells at 27°C.

A. Percentage of G2/M arrested cells at 27°C. Cells were stained with DAPI and scored as described in the methods. For each time point, 300 cells were scored and the average value was plotted. Yeast strains used are LMY420 (*cdc13-1 rif1Δ*), LMY204 (*cdc13-1*) and LMY514 (*cdc13-1 rif2Δ*). **B.** Western blot showing phosphorylation of checkpoint proteins Ddc2 and Rad53 at 27°C. Yeast strains *cdc13-1 DDC2-YFP* (LMY415) and *cdc13-1 DDC2-YFP rif1Δ* (LMY416) were used.

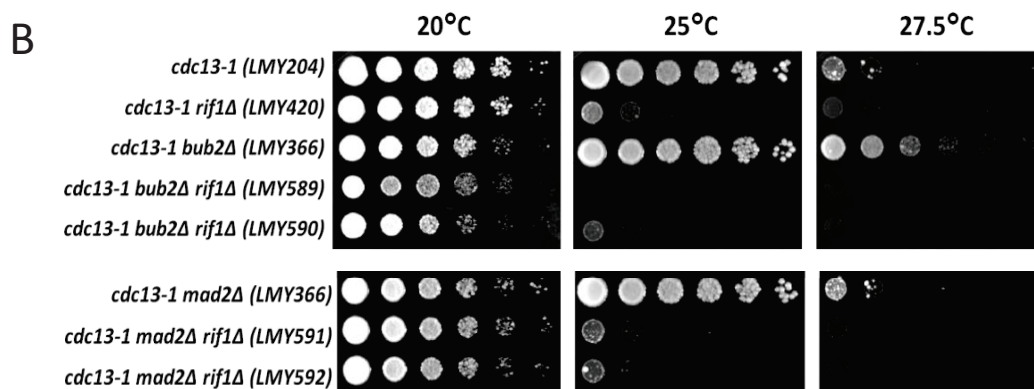
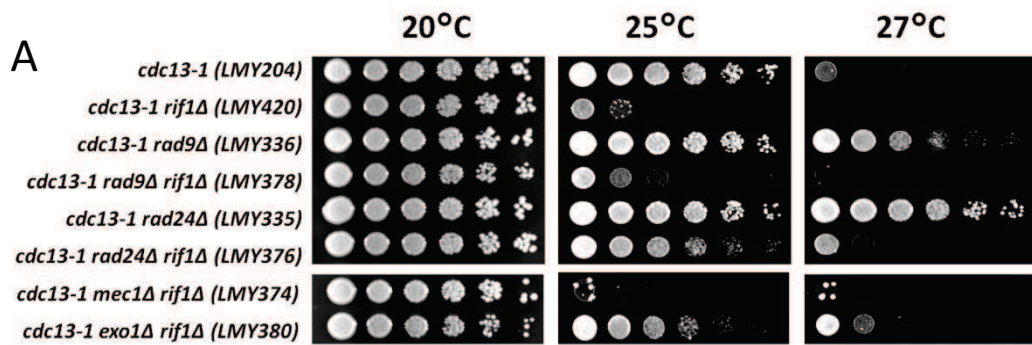


Fig 4.2.1 The role of DNA damage checkpoint and spindle checkpoint in the arrest of *cdc13-1 rif1Δ* cells. A and B. Serial dilution of yeast strains of different genotype on YEPD plates at indicated temperatures. Plates were incubated 2-3 days before being photographed.

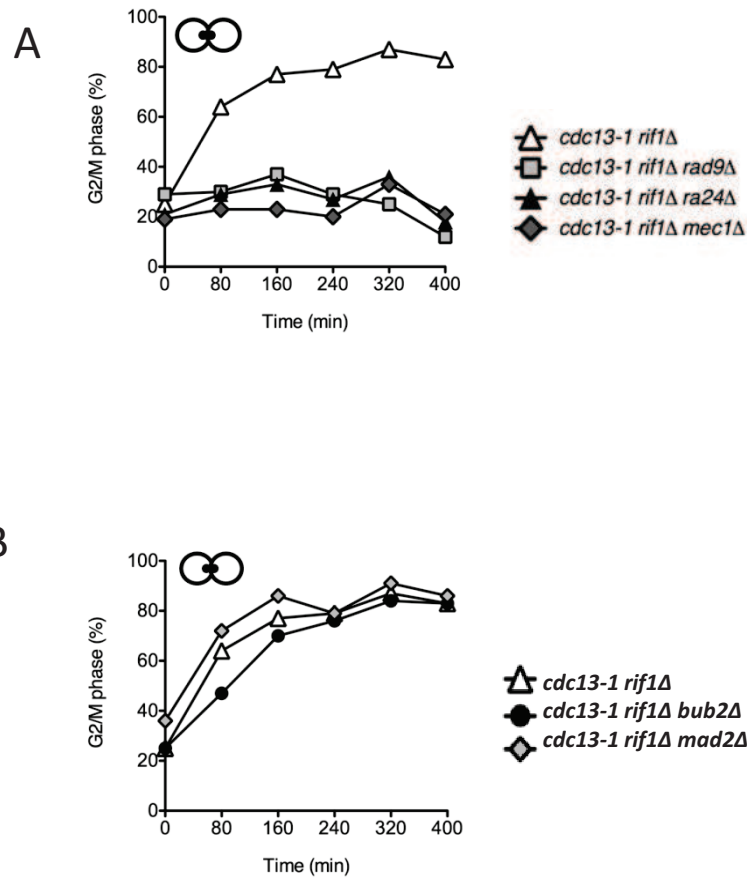


Fig 4.2.2 Percentage of G2/M arrested cells of indicated genotype at 25°C.

Cells were grown overnight in YEPD liquid at 21°C before the temperature was shifted to 25°C. Cells were stained with DAPI and scored as described in the methods. For each time point, 300 cells were scored and the average value was plotted. Strains used were LMY420, LMY378, LMY376, LMY374 (upper graph) and LM420, LMY589, LMY591 (lower graph).

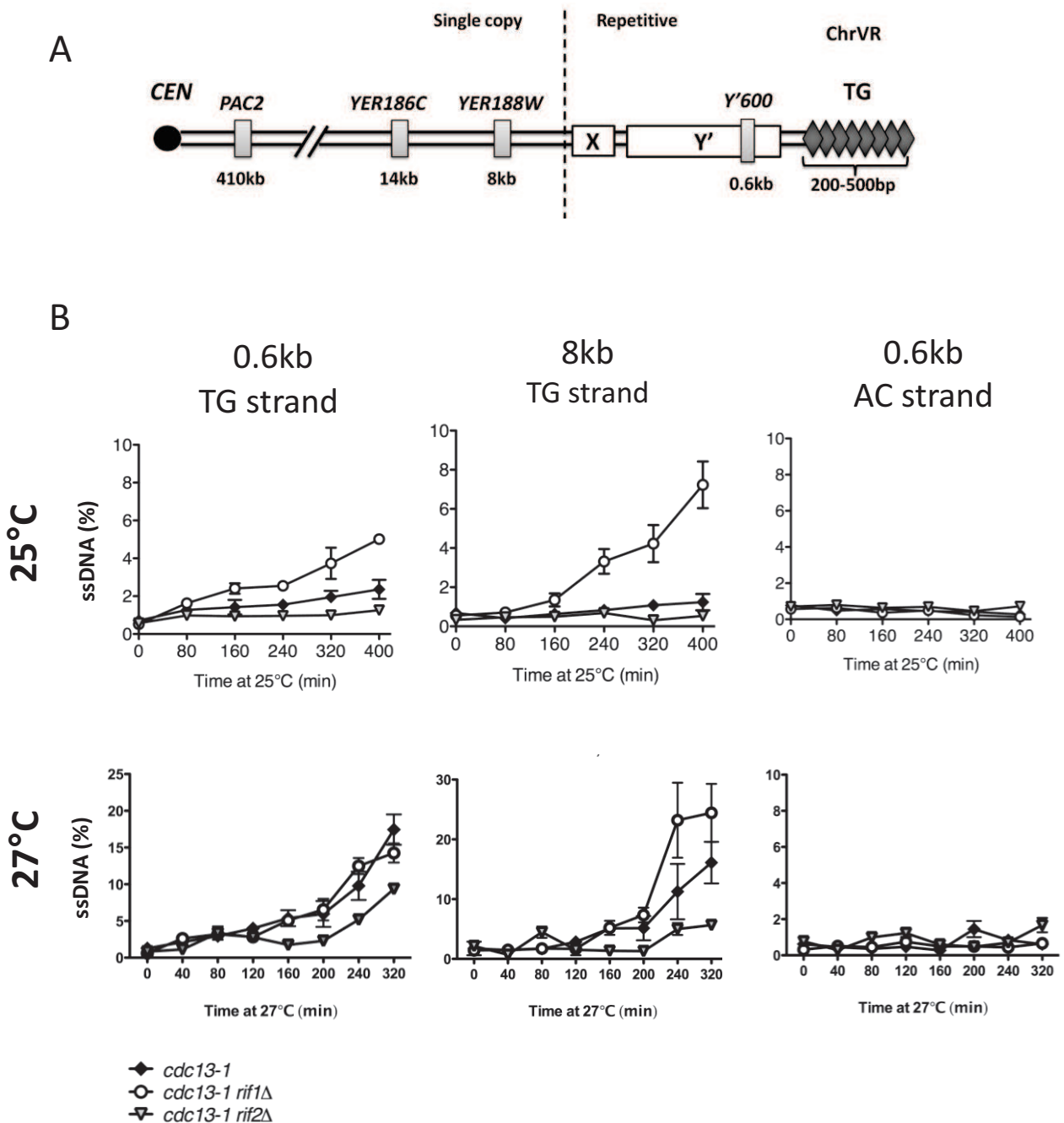


Fig 4.3 Single-stranded DNA accumulation in *cdc13-1*, *cdc13-1 rif1Δ* and *cdc13-1 rif2Δ* mutants

A. Schematic diagram representing the right arm of chromosome V. Genomic loci used for QAOS assay to measure single-stranded DNA are illustrated in grey bars, and their distance to telomeres are indicated at the bottom. **B.** ssDNA in *cdc13-1*, *cdc13-1 rif1Δ* and *cdc13-1 rif2Δ* mutants at indicated loci at 25°C and 27°C. Cells were grown in liquid YEPD at 21°C overnight before the temperature was shifted. The legend is shown at the bottom of the figures. Error bars represent the standard deviation between three qPCR measurements of each sample. Two independent experiments were performed. Yeast strains used are LMY204, LMY420 and LMY514.

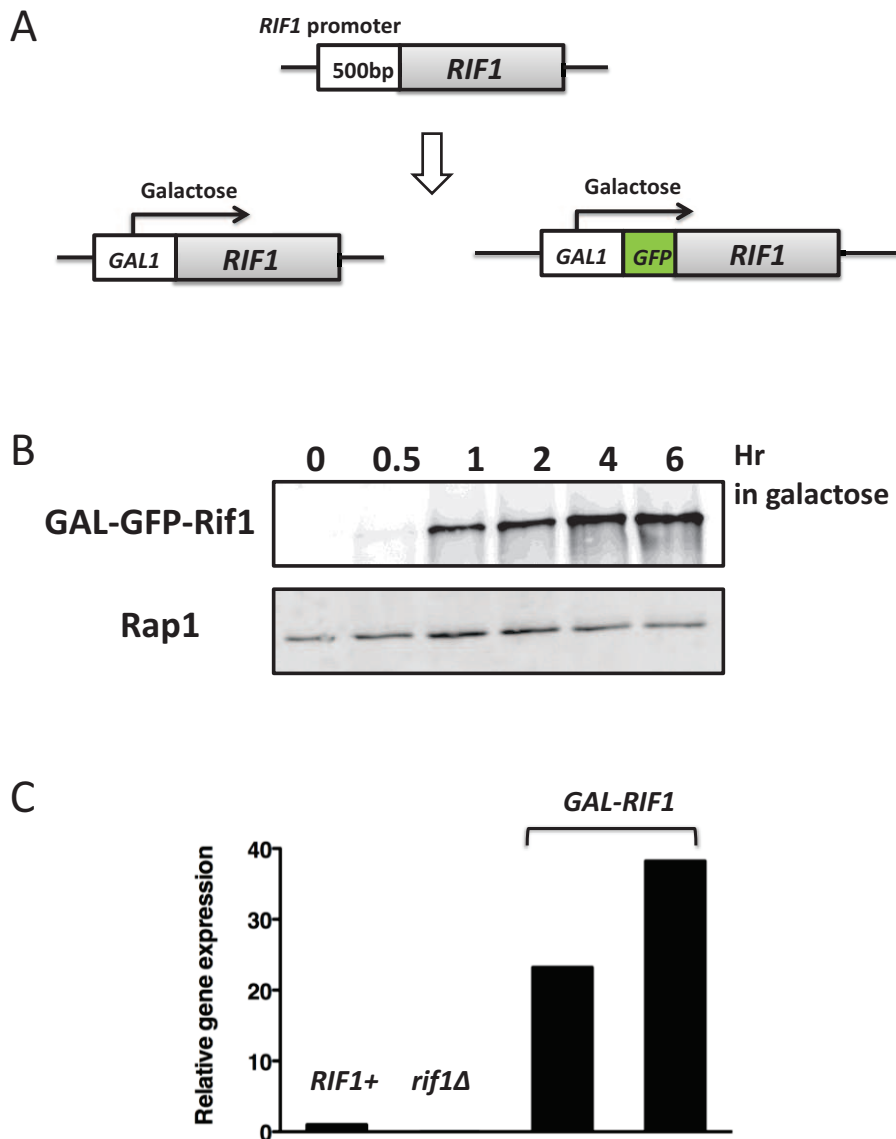


Fig 4.4.1. Overexpression of *RIF1*

A. Schematic representation of *in vivo* modification of *RIF1*. The endogenous promoter of *RIF1* (500bp upstream of the start codon) was replaced with the *GAL1* promoter, with or without GFP tagging. **B.** Western blot showing Rif1 expression in *GAL-GFP-RIF1* cells. Cells were grown in raffinose media overnight (0hr) and galactose was added to the media to a final concentration of 2% to induce expression. Rap1 serves as a loading control. **C.** Relative mRNA levels in strains containing wild type *RIF1*, *rif1*Δ, and two independent *GAL-RIF1* strains grown in 2% galactose medium for 2hrs. The value for *rif1*Δ cells is 0.025% therefore is too small to be visible on this scale. Yeast strains used are LMY565, LMY582, LMY635 and LMY637.

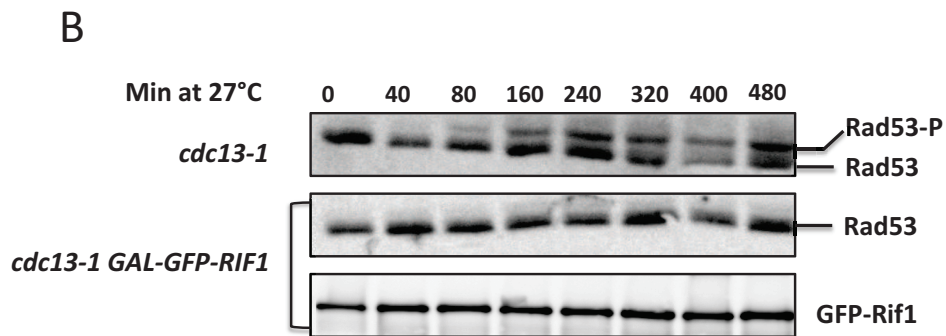
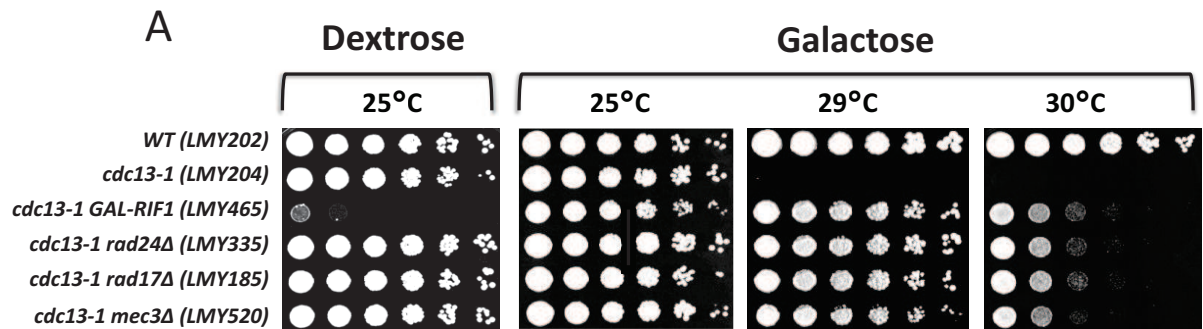


Fig 4.4.2 Overexpression of Rif1 rescues *cdc13-1* cells at non-permissive temperatures

A. Serial dilution of yeast strains grown on 2% dextrose or 2% galactose plates. Plates were incubated at indicated temperatures for 2 days before being photographed. **B.** Western blot showing Rad53 phosphorylation in *cdc13-1* and *cdc13-1 GAL-GFP-RIF1* cells at 27°C. Cells were grown in 2% galactose media at 21°C overnight (time 0) before the temperature was shifted to 27°C. A GFP antibody was used to detect GFP tagged Rif1.

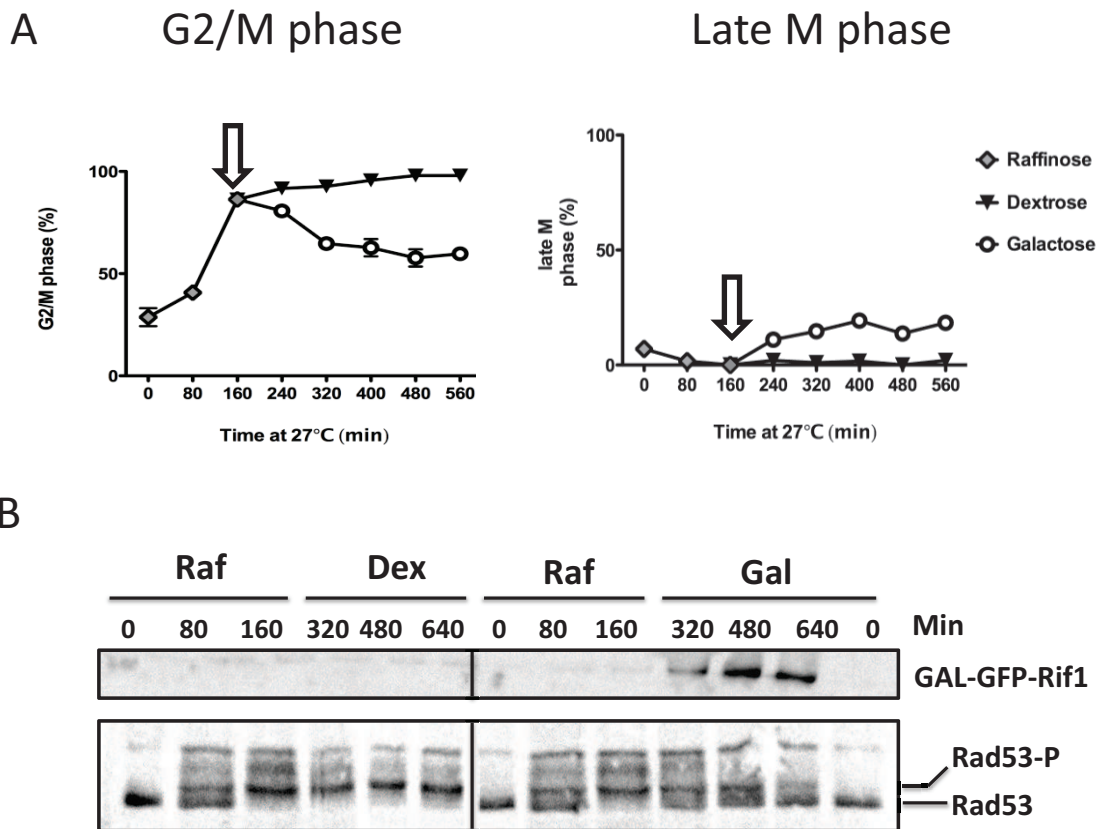
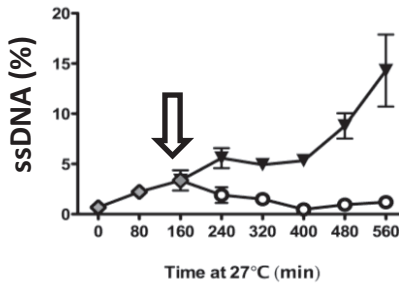


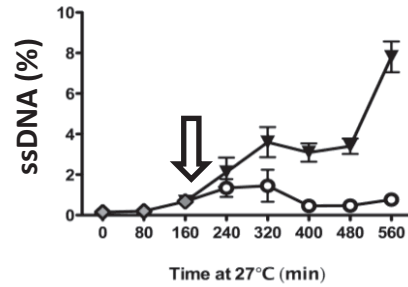
Fig 4.5.1 Overexpression of Rif1 rescues *cdc13-1* cells with damage

A. Percentage of *cdc13-1 GAL-GFP-RIF1* cells in G2/M phase (left) or late M phase (right) scored by DAPI staining. *cdc13-1 GAL-GFP-RIF1* cells were grown overnight in YEP-rafffinose at 20°C before the temperature was as shifted to 27°C. Cells were kept at 27°C for 160min until the majority of cells were arrested. The culture was then split, and either dextrose or galactose was added to the media at a final concentration of 2%. The arrow indicates the time when different sugar was added to the media. **B.** Western blot showing Rif1 expression in *cdc13-1 GAL-GFP-RIF1* cells and the phosphorylation of Rad53.

0.6kb, TG strand



8kb, TG strand



0.6kb, AC strand

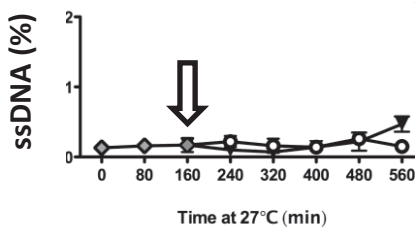


Fig 4.5.2 ssDNA accumulation in *cdc13-1 GAL-GFP* cells at 27°C

ssDNA was measured by QAOS assay at indicated loci as described before. Error bars represent the standard deviation between three independent qPCR measurements of each sample. Two independent experiments were performed and a representative experiment is shown. Shared legend is shown at the bottom right. This experiment is the same as in described in Fig 4.5.1. Arrows indicate the time when different sugar was added to the media.

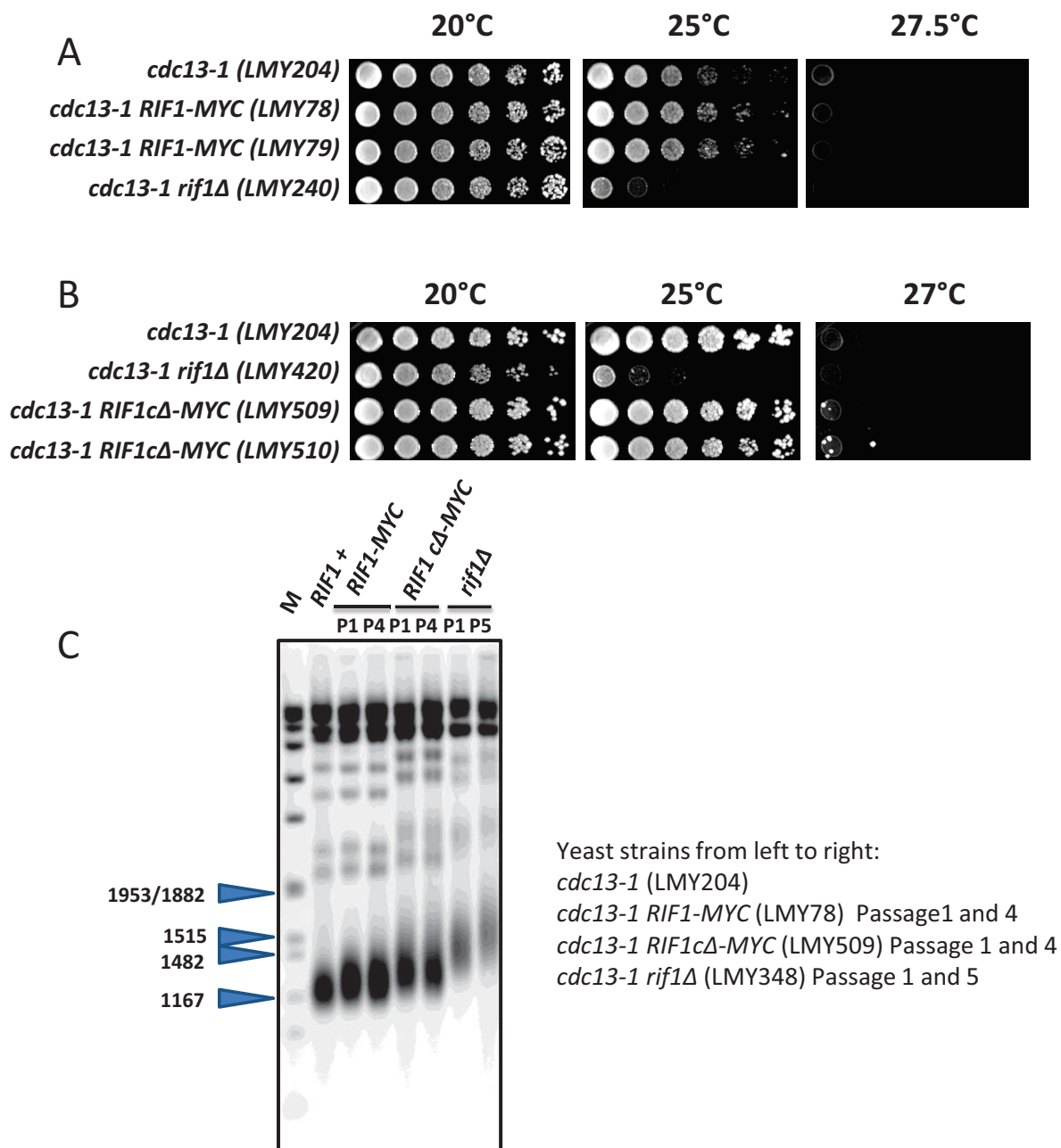


Fig 4.6.1 MYC tagging and C-terminal deletion of Rif1

A and **B**. Serial dilution of yeast strains grown on YEPD plates at indicated temperatures for 2-3 days. Rif1 was tagged with a MYC epitope tag by in vivo recombination as described in the methods. The C-terminus of Rif1 protein spanning 1351-1916 amino acids was deleted to create the *Rif1cΔ* protein; *Rif1cΔ* was also MYC tagged. **C**. Southern blot comparing telomere length in *RIF1+*, *RIF1-MYC*, *RIF1cΔ-MYC* and *rif1Δ* strains. All strains were in *cdc13-1* background and were grown at the permissive temperature of 20°C. Strain numbers and passages are indicated on the right of the southern blot.

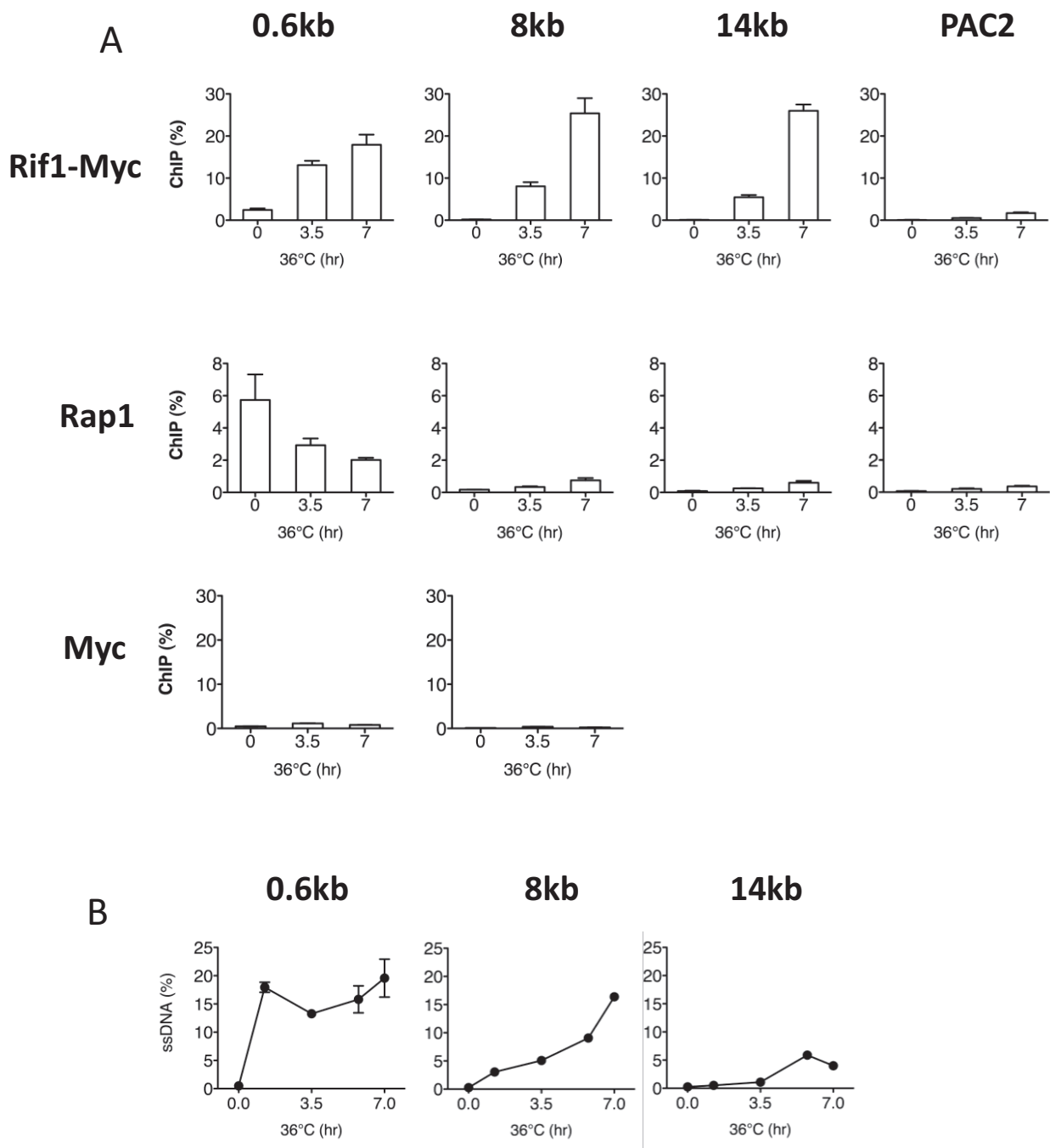


Fig 4.6.2 Rif1 and Rap1 binding in *cdc13-1* cells at 36°C (lengend on next page)

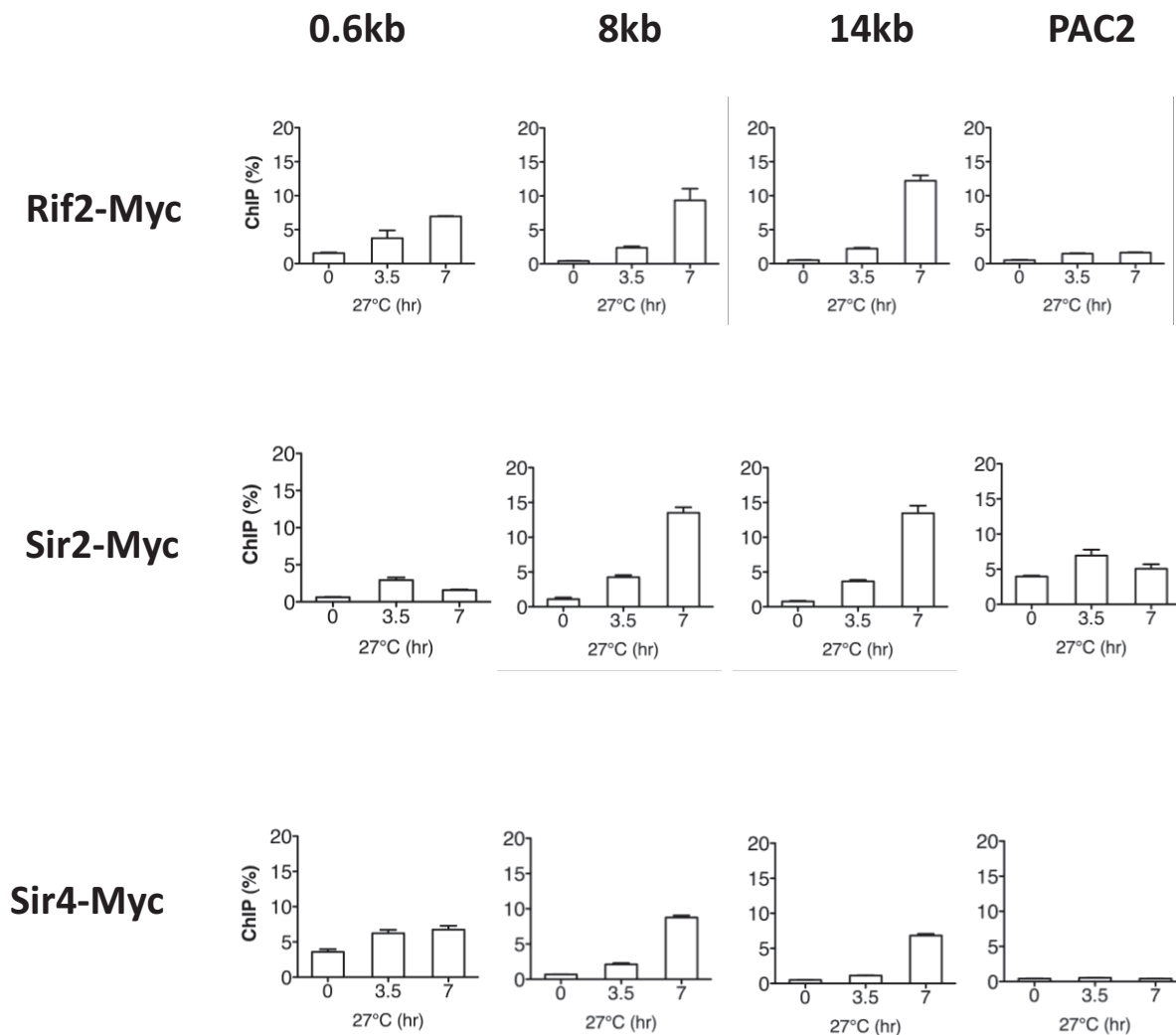


Fig 4.6.3 Rif2, Sir2 and Sir4 binding in *cdc13-1* cells at 27°C

ChIP analysis of Rif2, Sir2 and Sir4 binding at different loci on ChrVR. Numbers on the top of the graphs indicate the distance of each locus to chromosome end. *PAC2* gene is localised 410kb away from telomeres and no DNA damage should reach this region. Myc tagged *cdc13-1* cells (LMY680, LMY675 and LMY677) were grown at 21°C overnight (Time 0) and the temperature was shifted to 27°C and samples were collected for ChIP analysis at 3.5 and 7hrs. A c-Myc antibody was used to detect the Myc tagged Rif2, Sir2, and Sir4. ChIP values were calculated as described in the method section. Error bars represent the standard deviation between three independent qPCR measurements of each sample. Two independent experiments were performed and a representative experiment is shown.

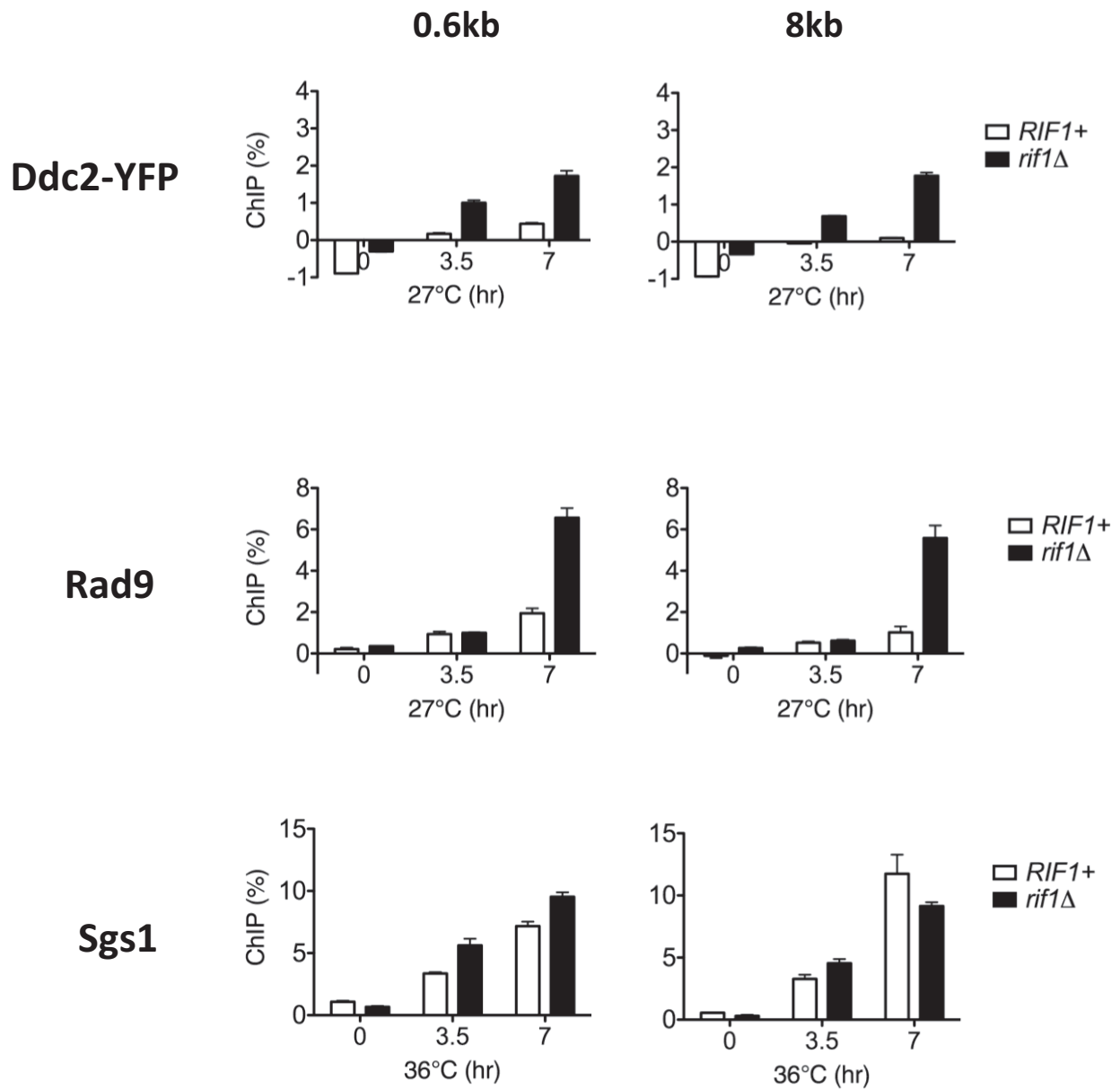


Fig 4.7 Effect of Rif1 on the recruitment of Ddc2, Rad9 and Sgs1 to damaged chromatin. *cdc13-1* cells carrying wild type *RIF1* or *rif1*Δ were grown overnight at 21°C (time 0) and the temperature was shifted to 27°C or 36°C to induce telomere uncapping. Samples were collected at 3.5 and 7hrs for ChIP analysis. ChIP was performed with an YFP antibody to detect the YFP tagged Ddc2, and a Rad9 and a Sgs1 antibody. ChIP values was calculated as described in the method. Error bars represent the standard deviation between three independent qPCR measurements of each sample. Two independent experiments were performed and a representative experiment is shown.

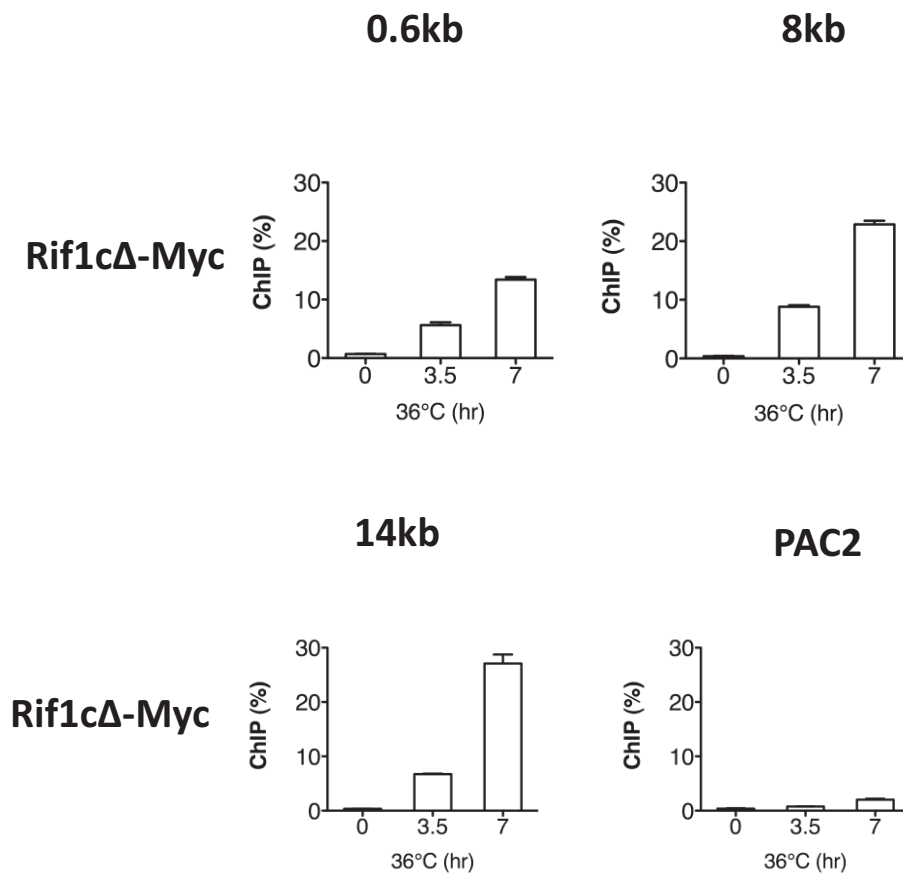


Fig 4.8 Binding of the C-terminal deleted Rif1 in *cdc13-1* cells at 36°C

ChIP analysis of Rif1cΔ-Myc binding at different loci on ChrVR. Numbers on the top of each graph indicate the distance of each locus to chromosome end. *PAC2* locus serves as a negative control. *cdc13-1 Rif1cΔ-MYC* cells (LMY509) were grown at 21°C overnight (Time 0) and the temperature was shifted to 36°C and samples were collected for ChIP analysis at 3.5 and 7hrs. A c-Myc antibody was used to detect the Myc tagged Rif1 protein containing the C terminal deletion. ChIP values was calculated as described in the method. Error bars represent the standard deviation between three independent qPCR measurements of each sample. Three independent experiments were performed and a representative experiment is shown.

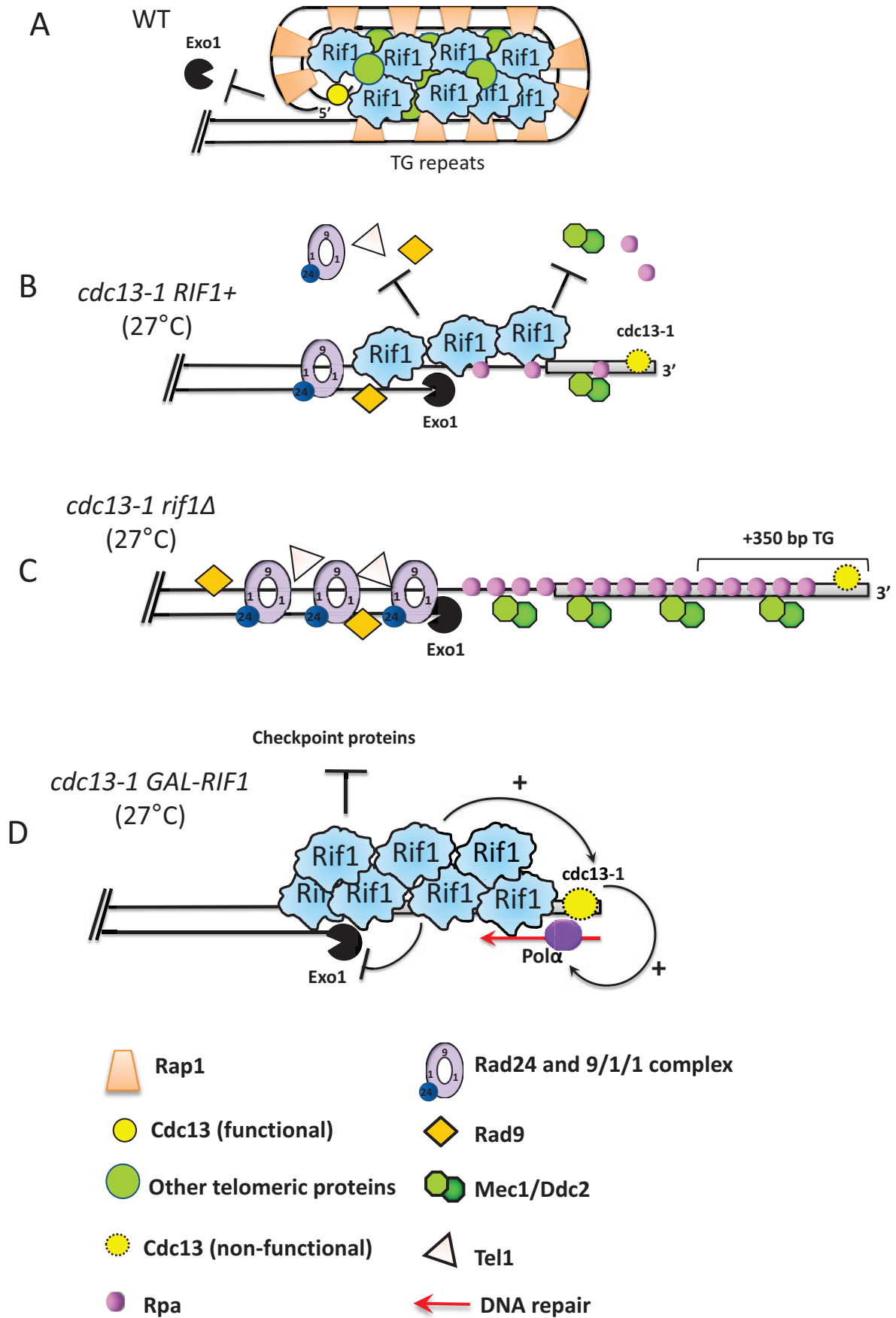


Fig 4.11 A proposed model showing how Rif1 protects telomeres in *cdc13-1* cells

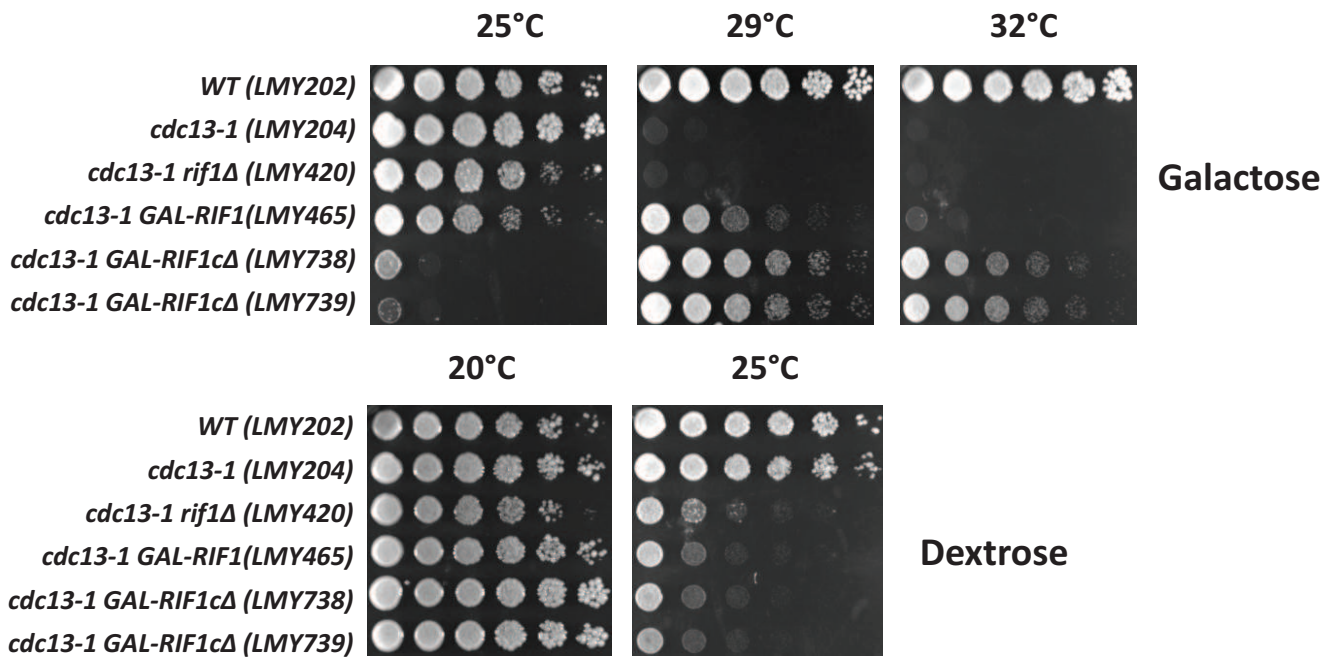
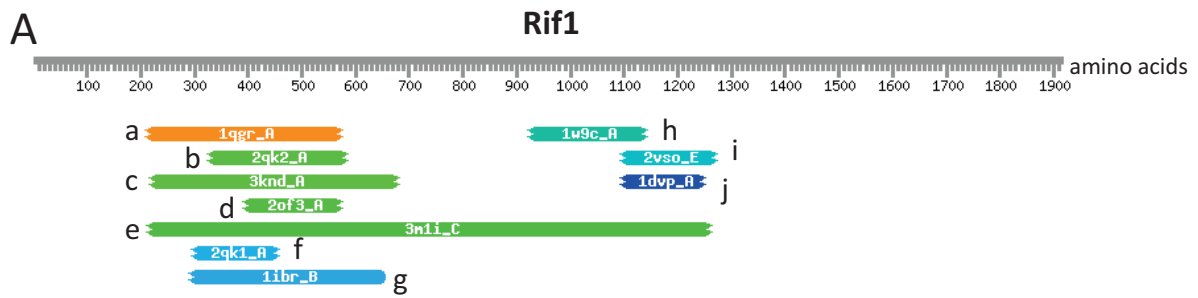


Fig 4.9 Overexpression of the C-terminal deleted Rif1 rescues *cdc13-1* cells at 32°C

Serial dilution of yeast strains grown on 2% dextrose or 2% galactose plates. Plates were incubated at indicated temperatures 2-3 days before being photographed. The full length Rif1 or the C-terminal deleted Rif1 were overexpressed from a *GAL1* promoter. Two independent *cdc13-1 GAL-RIF1cΔ* strains were tested.



B

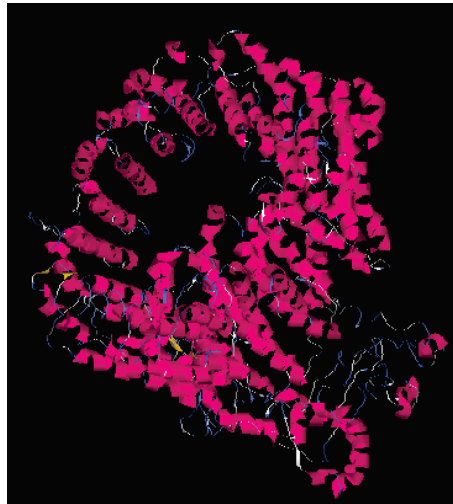


Fig 4.10.1 Structural analysis of *S.cerevisiae* Rif1

A. Structural homology in *S.cerevisiae* Rif1 predicated by the HHpred method. Full length scRif1 amino acid sequence was analysed with the HHpred server provided by the Max-Planck institute. Homologous or structural-related sequences are shown in coloured blocks at indicated position of the Rif1 protein. Individual HEAT-like motifs from proteins from a diverse organisms are labelled as a-j: a. importin β subunit (Human); b. microtubule plus end binding protein (*Drosophila*); c. importin α 2 subunit (Mouse); d. Microtubule associated protein (*C. elegans*); e. Exportin-1, human Crm1 homolog (*S. cerevisiae*); f. Stu2, a microtubule-associated protein (*S. cerevisiae*); g. importin β 1 subunit domain (Human); h. Crm1, nuclear exporter protein (human); i. eukaryotic initiation factor 4F subunit P150 (*S. cerevisiae*); j. hepatocyte growth factor-regulated tyrosine kinase substrate (*Drosophila*) **B.** Predicted 3D structure of the Rif1 N-terminus, spanning amino acids 1-1350. 3D structure was generated by the I-TASSER server provided by the University of Michigan (<http://zhanglab.ccmb.med.umich.edu/I-TASSER/about.html>).

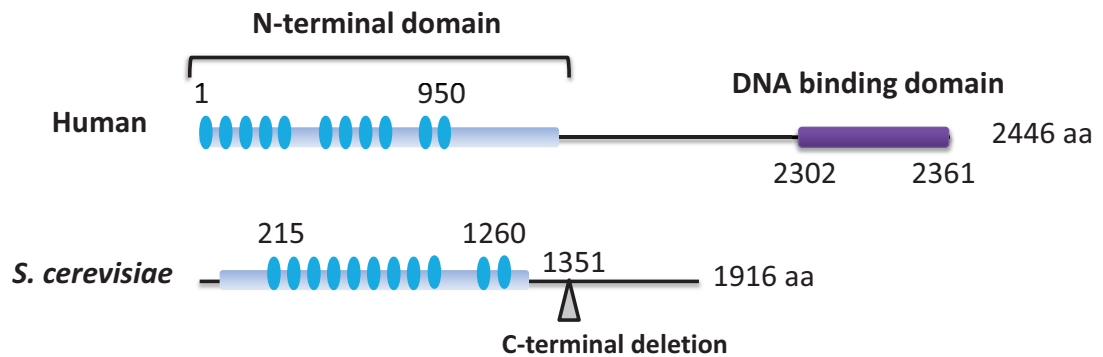


Fig 4.10.2 Comparison of Rif1 protein in human and budding yeast

Conserved N-terminal regions are labelled in light blue. Potential HEAT repeats are illustrated by blue ovals. The position of the C-terminal deletion of Rif1 is indicated by a grey triangle. Sequence of Rif1 orthologs were obtained from the NCBI database (human: AAV51403.1; *S.cerevisiae*: CAA85238.1). Sequence alignment was performed using Cobalt (Constraint-based Multiple Alignment Tool). HEAT-like repeats were predicted by the HHpred and the I-TASSER servers.

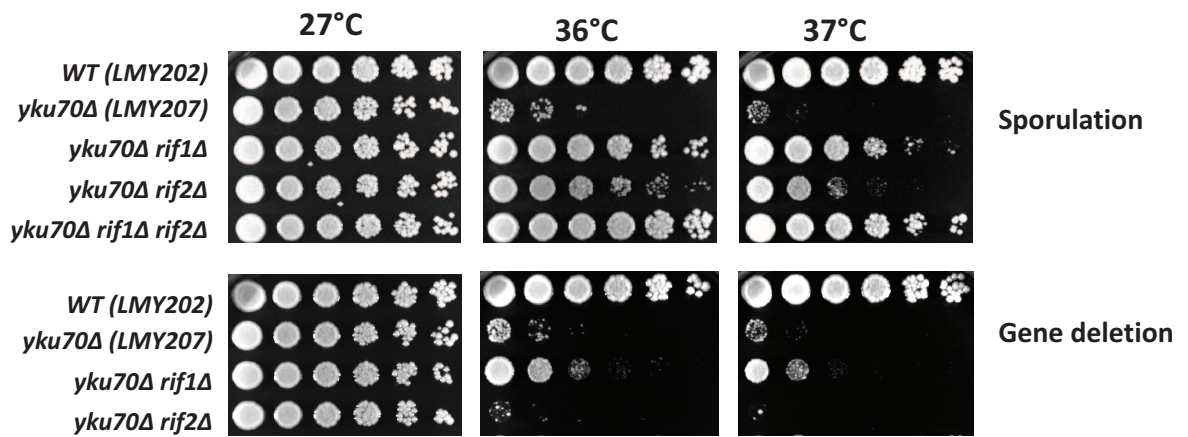


Fig 5.1 Effects of *RIF1* and *RIF2* deletion in *yku70Δ* mutant

Serial dilution of yeast strains generated by sporulation of a *YKU70/yku70 RIF1/rif1 RIF2/rif2* diploid strain (LMY538, upper panel) or generated by gene deletion from a haploid *yku70Δ* strain (LMY207, lower panel). Plates were incubated at indicated temperatures for 2 days before being photographed.

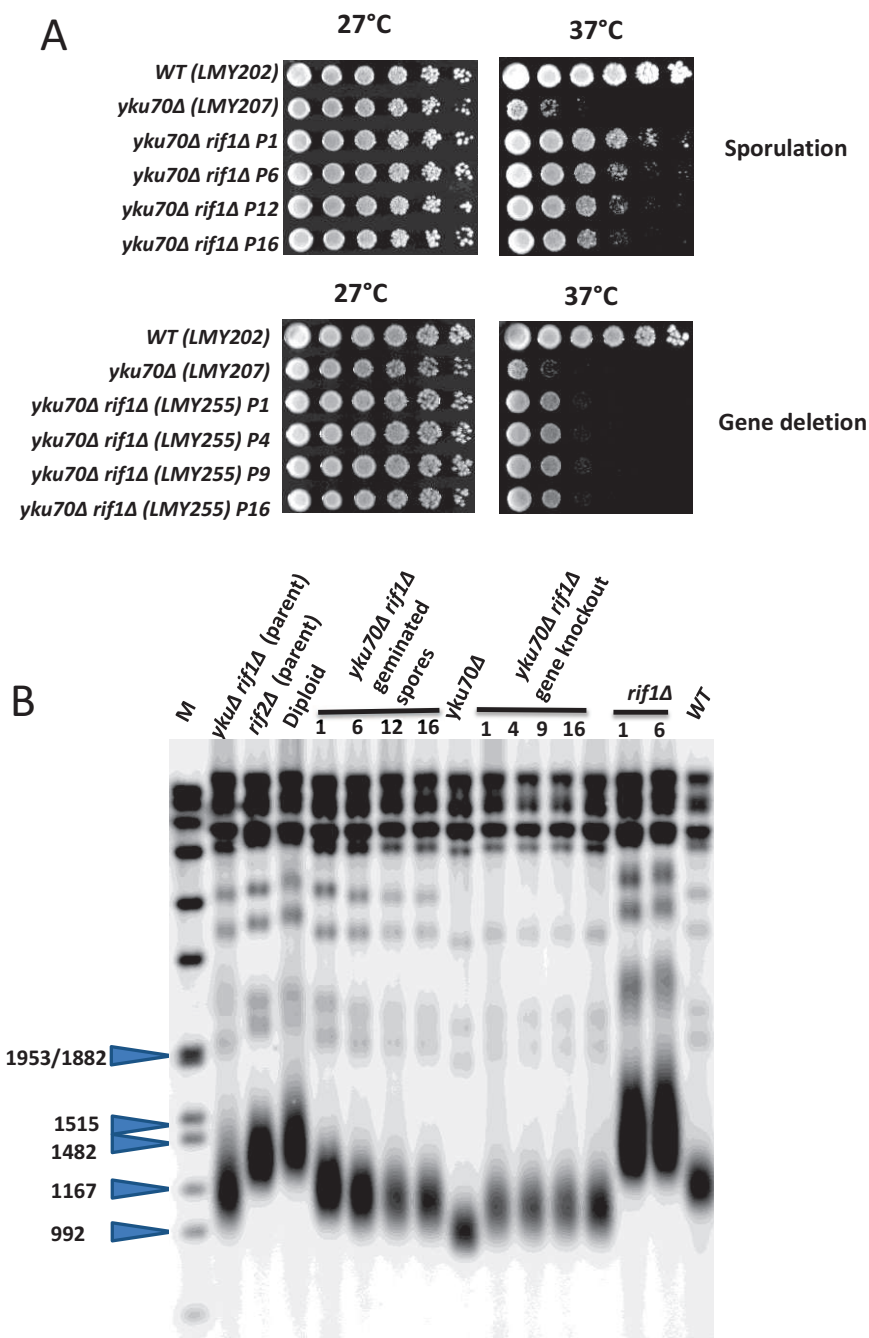


Fig 5.2.1 The relationship between temperature sensitivity and telomere length in *yku70Δ rif1Δ* cells **A.** Spot test comparing the growth of *yku70Δ rif1Δ* strains generated either from sporulation (upper panel) or gene deletion (lower panel). Cells were passaged on YEPD plates every 2-3 days and the indicated passages were used for spot test. At least two independent strains were tested. **B.** Southern blot comparing telomere length of indicated strains at different passages. Yeast strains from left to right are LMY368, LMY310, LMY538, *yku70Δ rif1Δ* germinated from LMY538, LMY207, LMY255, LMY307 and LMY202.

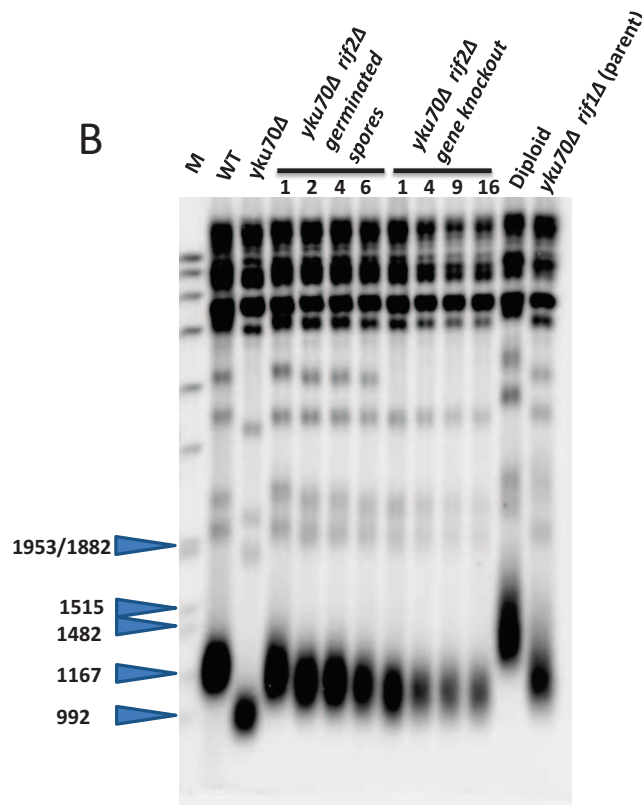
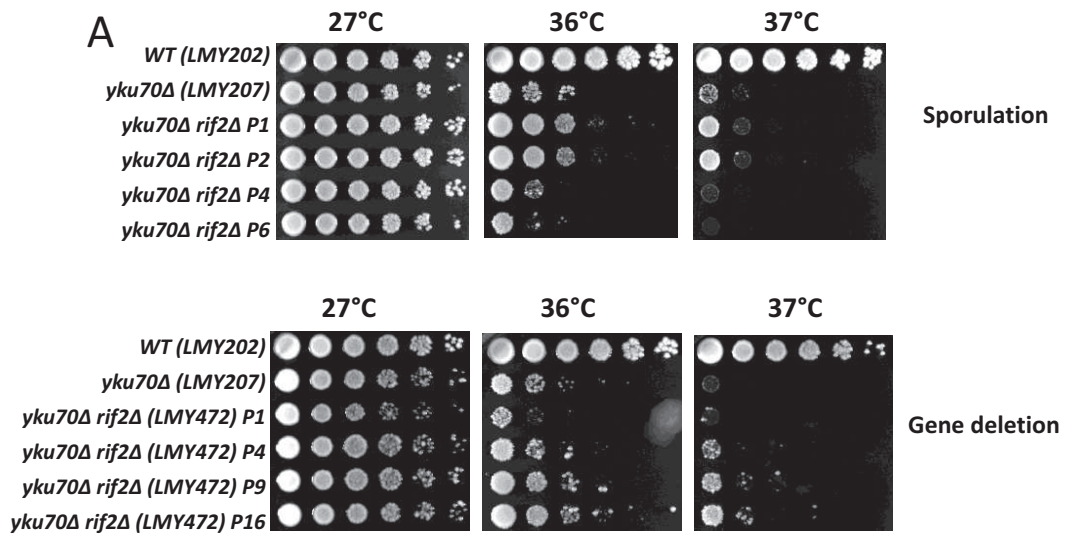


Fig 5.2.2 The relationship between temperature sensitivity and telomere length in *yku70Δ rif2Δ* cells. **A.** Spot test comparing the growth of *yku70Δ rif2Δ* strains generated either from sporulation (upper panel) or gene deletion (lower panel). Cells were passaged on YEPD plates every 2-3 days and the indicated passages were used for spot test. At least two independent strains were tested. **B.** Southern blot comparing telomere length of indicated strains at different passages. Yeast strains from left to right are LMY202, LMY207, *yku70Δ rif2Δ* strain germinated from LMY538, LMY472, LMY538 and LMY368.

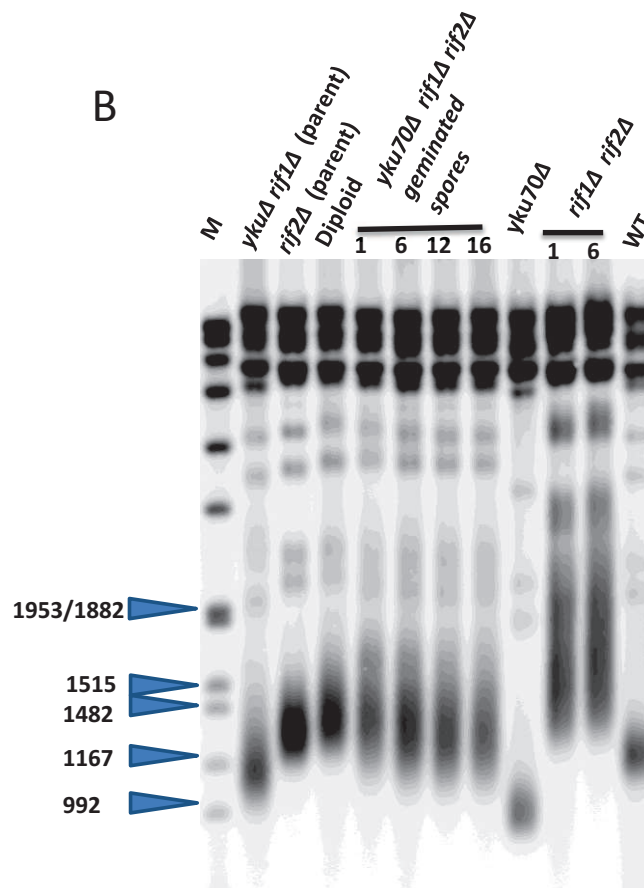
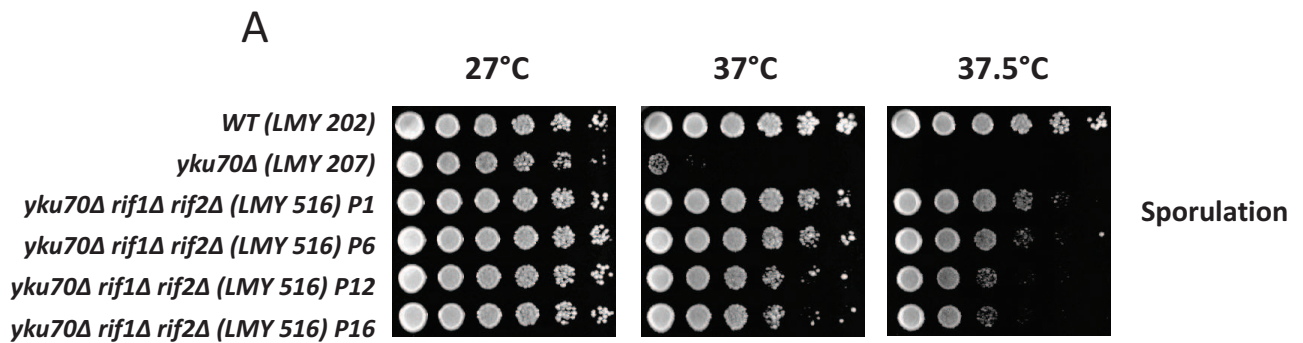


Fig 5.2.3 The relationship between temperature sensitivity and telomere length in *yku70Δ rif1Δ rif2Δ* cells. **A.** Spot test comparing the growth of *yku70Δ rif1Δ rif2Δ* strains generated from sporulation. Cells were passaged on YEPD plates every 2-3 days and the indicated passages were used for spot test. At least two independent strains were tested. **B.** Southern blot comparing telomere length of indicated strains at different passages. Yeast strains from left to right are LMY368, LMY310, LMY538, *yku70Δ rif1Δ rif2Δ* strain germinated from LMY538 (colony 2), LMY207, LMY593 and LMY202.

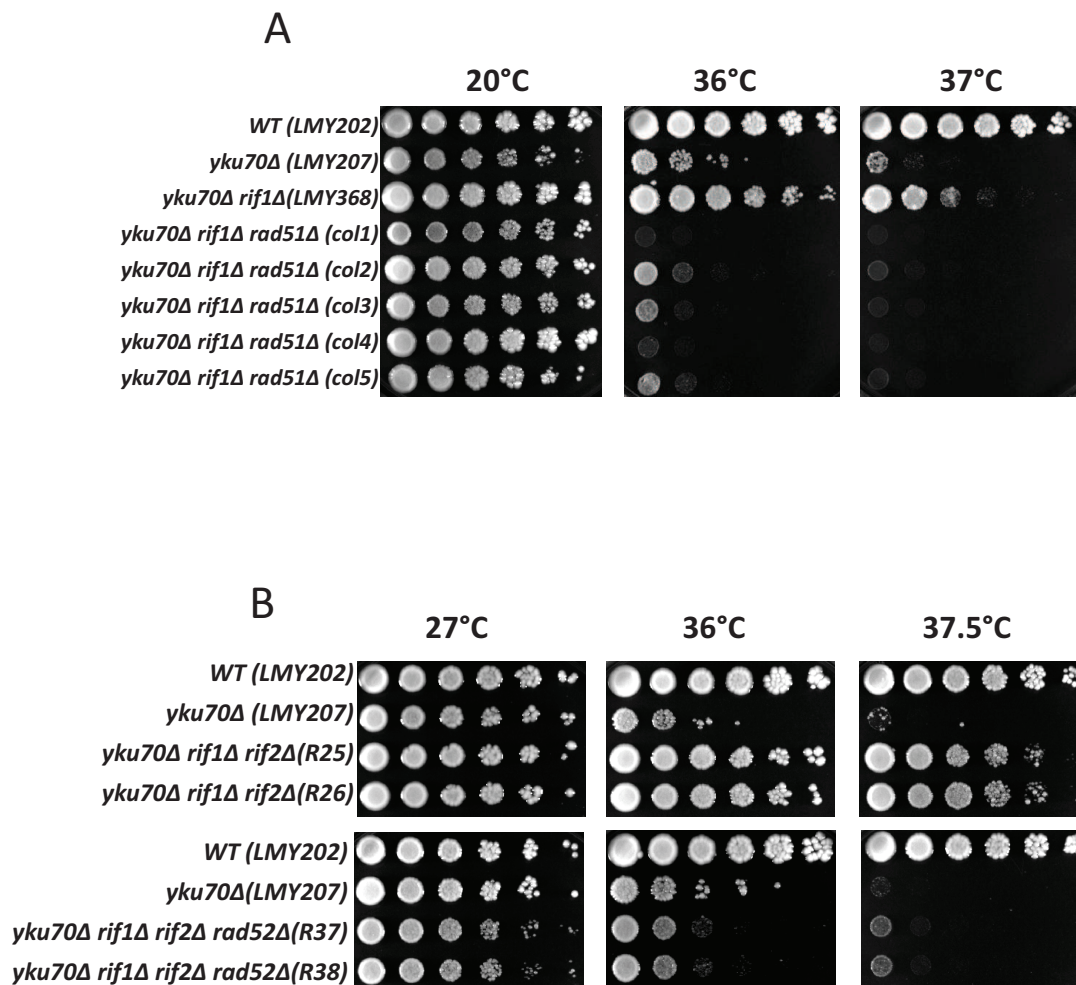


Fig 5.3 The role of *RAD51* and *RAD52* for the survival of *yku70Δ rif1Δ* and *yku70Δ rif1Δ rif2Δ* cells at high temperatures.

A. Serial dilution of yeast strains including five independent *yku70Δ rif1Δ rad51Δ* strains that were obtained by deleting *RAD51* from a *yku70Δ rif1Δ* strain (LMY368). Plates were incubated at indicated temperatures for 2-3 days before being photographed. **B.** Serial dilution of yeast strains generated by sporulation of a *YKU70/yku70Δ RIF1/rif1Δ RIF2/rif2Δ RAD52/rad52* diploid strain. Two independent *yku70Δ rif1Δ rif2Δ rad52Δ* strains were tested.

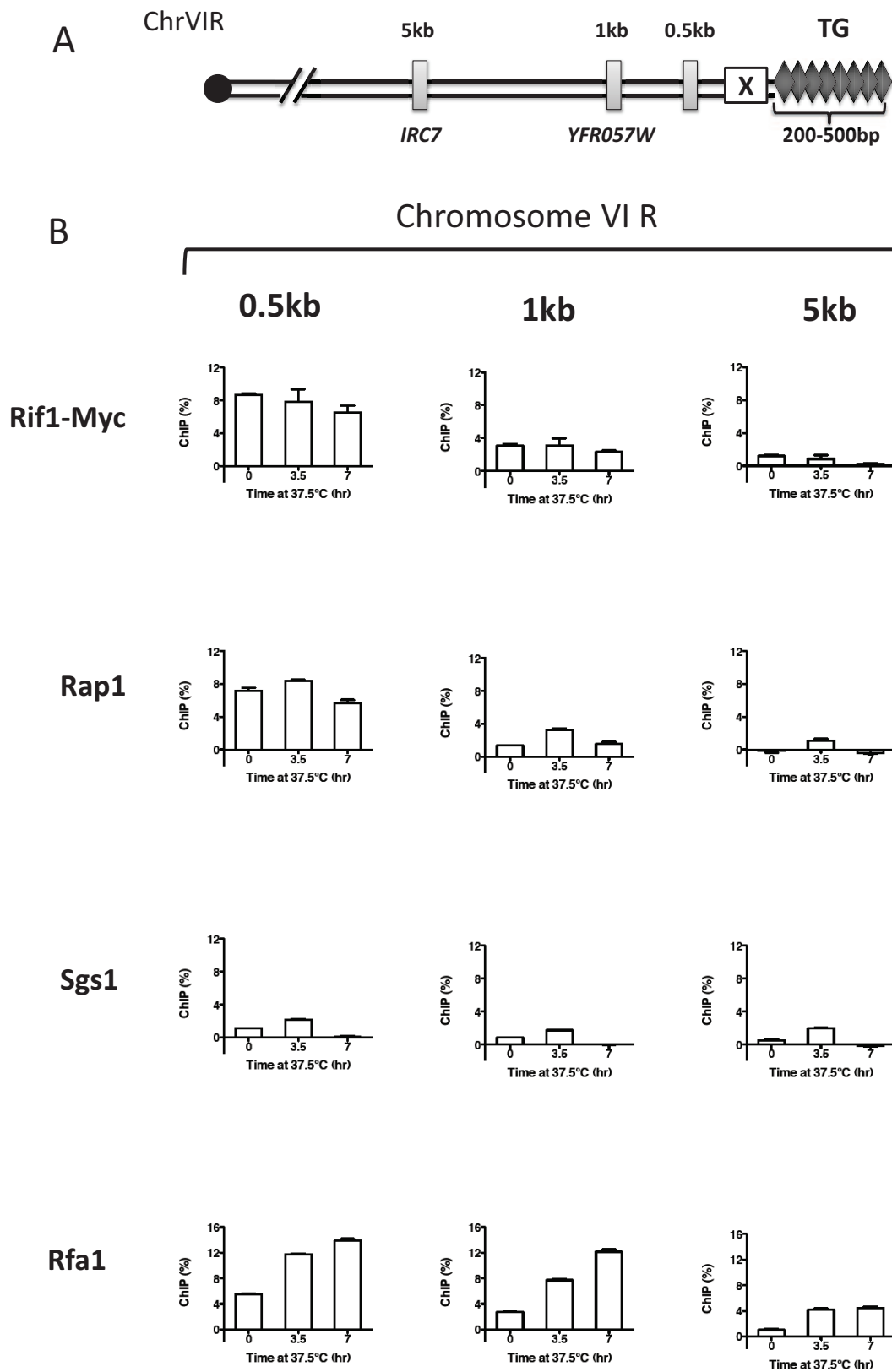


Fig 5.4 ChIP analysis of Rif1, Rap1, Sgs1 and Rfa1 binding in *yku70Δ* cells

A. Schematic diagram representing the right arm of chromosome VI. Primers designed and used for ChIP measurements are shown in grey bars, and their proximity to the TG sequence are indicated. The white box represents X element and TG sequences are shown as a series of diamonds.

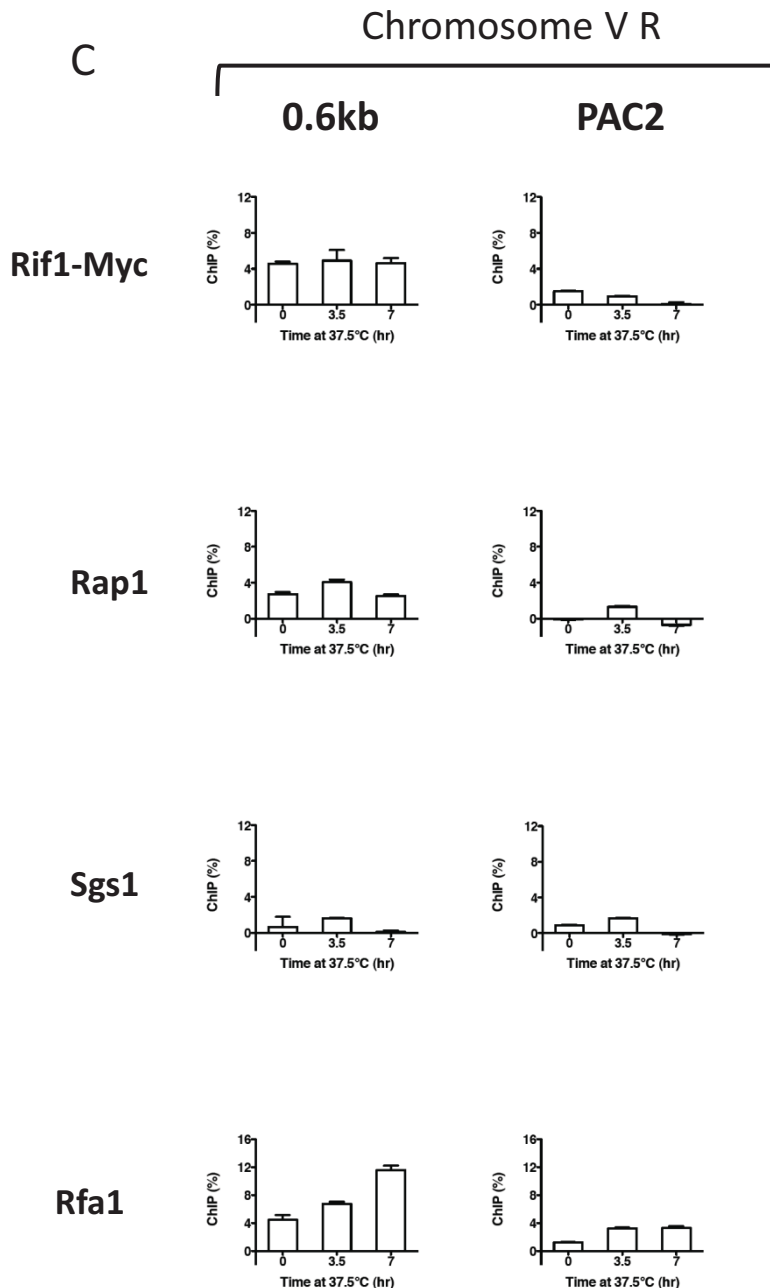


Fig 5.4 ChIP analysis of Rif1, Rap1, Sgs1 and Rfa1 binding in *yku70Δ* cells (continued)

B. ChIP analysis of Rif1-Myc, Rap1, Rfa1 and Sgs1 recruitment to indicated loci on Chromosome VI. *yku70Δ RIF1-Myc* cells (LMY150) were grown at 21°C overnight (Time 0) and the temperature was shifted to 37.5°C and samples were collected for ChIP analysis at 3.5 and 7hrs. Error bars represent standard deviation between three qPCR measurements of each sample. Three independent experiments were performed and one representative experiment is shown.

C. ChIP analysis of Rif1-Myc, Rap1, Rfa1 and Sgs1 recruitment to indicated loci on Chromosome V. The experiment was performed the same as in B. Error bars represent standard deviation between three qPCR measurements of each sample. Three independent experiments were performed and one representative experiment is shown. Yeast strain used was LMY150.

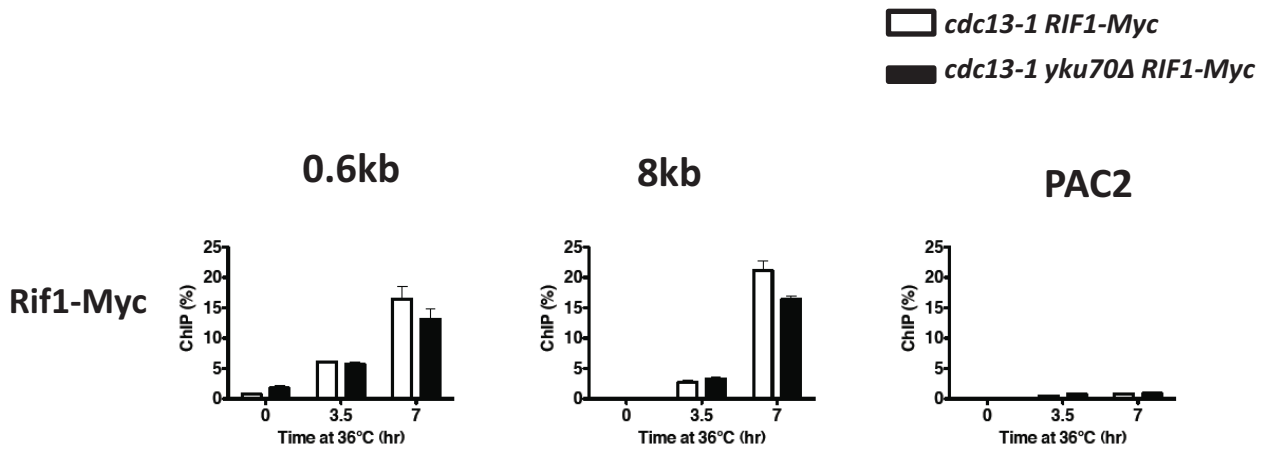


Fig 5.5 ChIP analysis of Rif1-Myc binding to indicated loci on Chromosome V.

cdc13-1 RIF1-Myc (LMY78) and *cdc13-1 yku70Δ RIF1-Myc* (LMY712) cells were grown at 21°C overnight (Time 0) and the temperature was shifted to 36°C and samples were collected for ChIP analysis at 3.5 and 7hrs. Error bars represent standard deviation between three qPCR measurements of each sample.

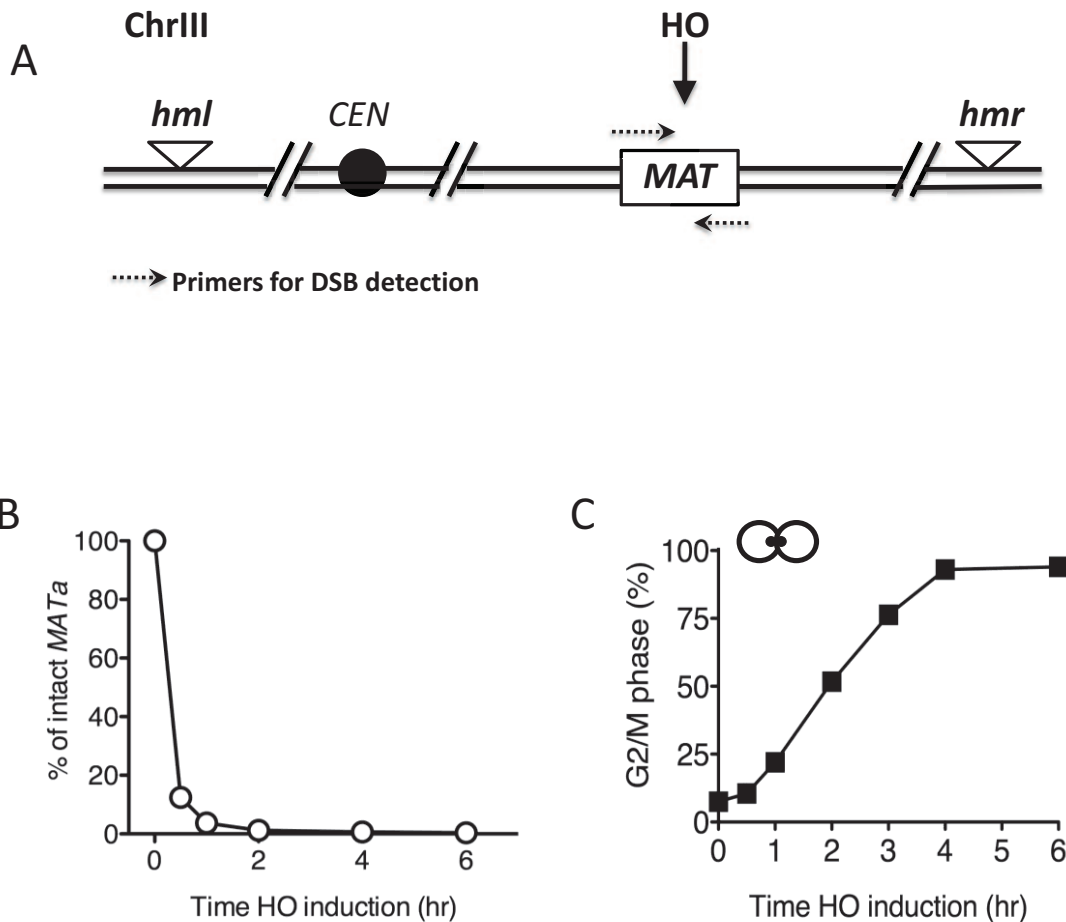


Fig 6.1 The HO-inducible DSB system

A. Schematic representation of ChrIII in the JKM139 strain which express a galactose-inducible HO endonuclease. HO endonuclease cuts within the *MATa* locus (indicated by the arrow) to create a DSB in the presence of galactose. The *HML* and *HMR* loci were also deleted to eliminate repair via homologous recombination. A set of primers spanning the *MATa* locus was used to monitor the efficiency of DSB induction. **B.** Efficiency of DSB induction in JKM139 strain. JKM139 cells were grown overnight in raffinose media (Time 0) and 2% galactose was added to the media to induce HO cutting. The amount of *MATa* DNA was measured by qPCR using primers spanning the HO cutting site and normalized to time 0. Error bars were plotted but are too small to be visible on this scale. Error bars represent the standard deviation between three independent qPCR measurements of the same sample. Two independent experiments were performed and an representative experiment is shown. **C.** The percentage of G2/M arrested cells after HO induction. JKM139 cells were treated in the same condition as in B and harvested for DAPI staining. 300 cells were scored for each sample and the average was plotted.

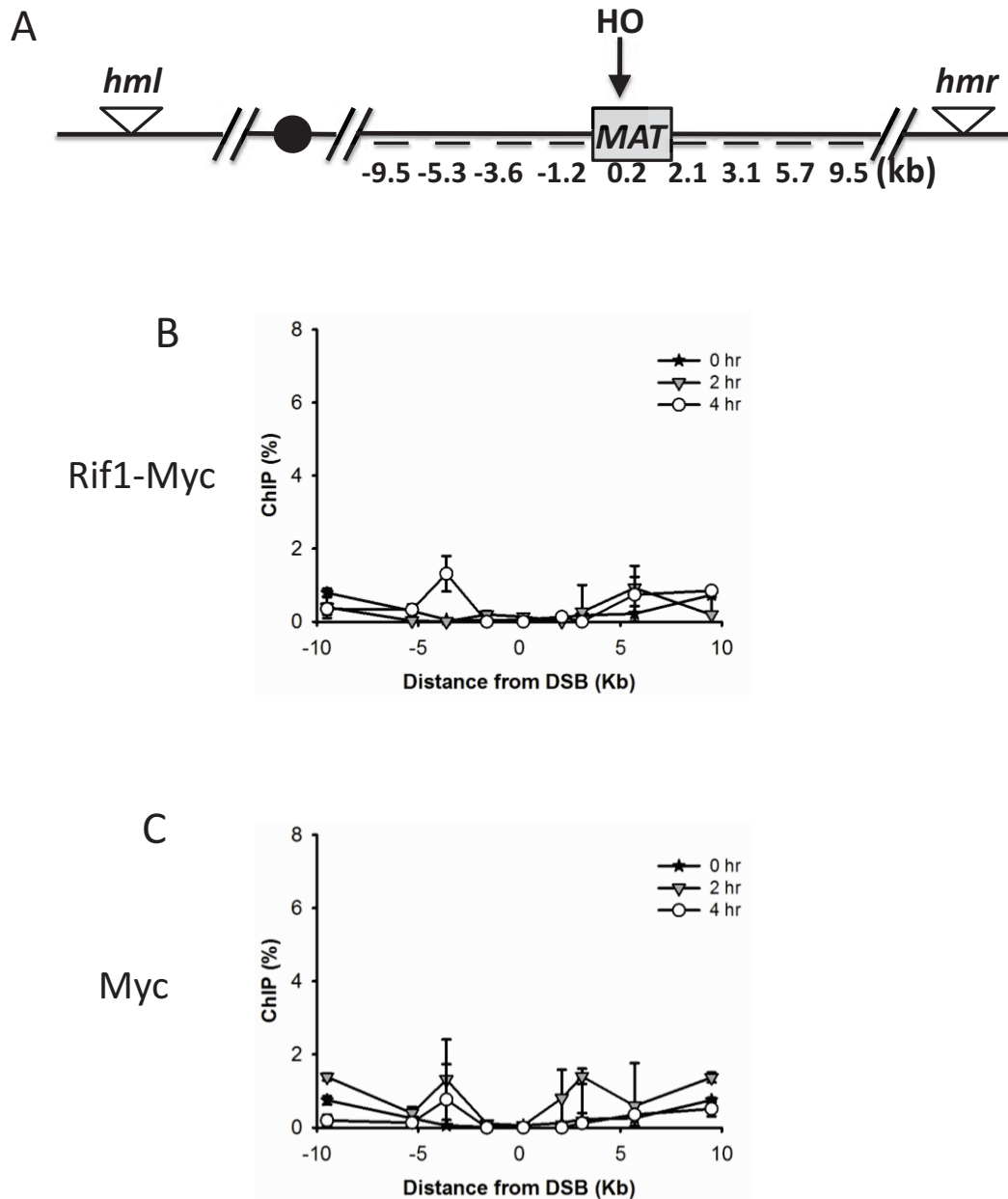


Fig 6.2.1 Recruitment of Rif1 to a DSB

A. Schematic diagram of ChrIII in JKM139 (*MAT α*) cells as presented in Fig 6.1A. Thin bars represent primers sets used for qPCR for ChIP experiments. Distance (kb) of these primers to the HO cutting site is indicated at the bottom. **B.** Rif1 binding to a DSB. A *RIF1-MYC* JKM139 isogenic strain (LMY565) was grown overnight in raffinose media (time 0) before 2% of galactose was added to the media to induce the DSB. ChIP was performed using a c-Myc antibody against the MYC tagged Rif1. **C.** An untagged strain (LMY581) was also probed by the c-Myc antibody to measure unspecific binding. ChIP values were calculated as before. Two independent experiments were performed and a representative experiment is shown. Results from B and C were kindly provided by Michael Rushton.

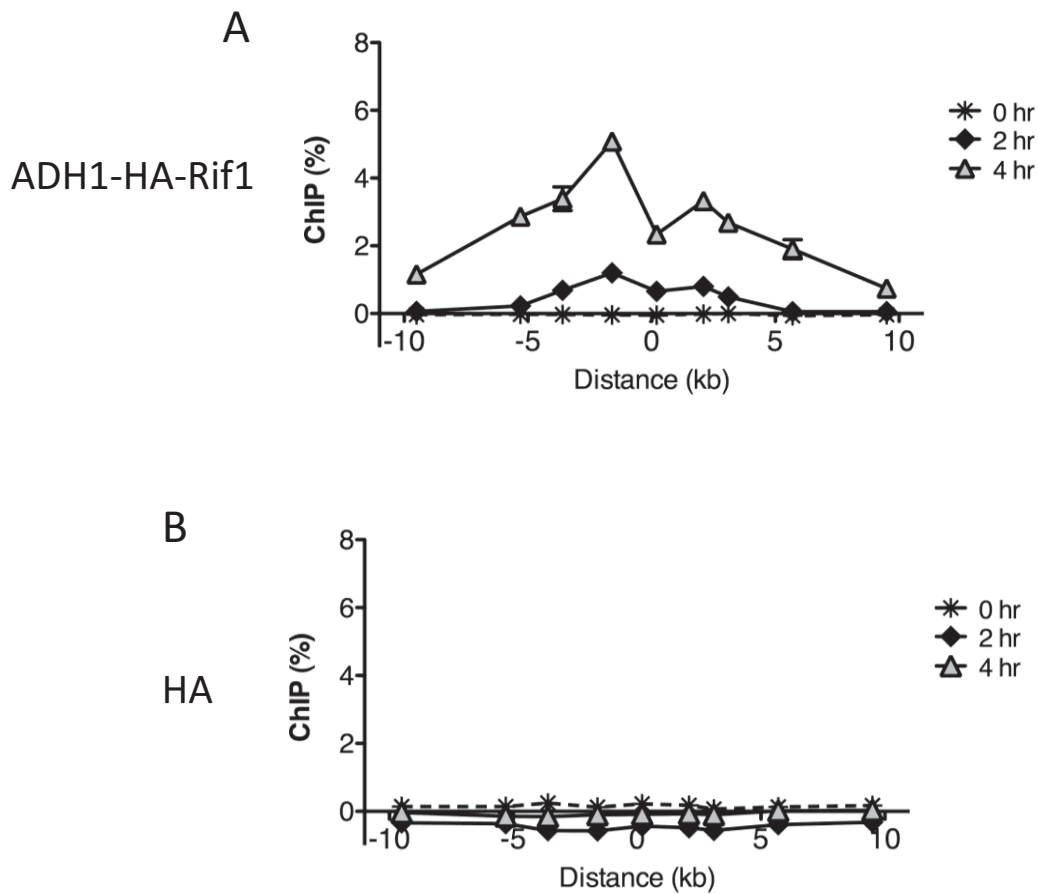


Fig 6.2.2 Recruitment of overexpressed Rif1 to a DSB

A. The binding of ADH1-HA-Rif1 to a DSB. An *ADH1-HA-RIF1* JKM139 isogenic strain (LMY735) was grown overnight in raffinose media (time 0) before 2% of galactose was added to the media to induce the DSB. ChIP was performed using a HA antibody against the HA tagged Rif1 and ChIP values was calculated as before. Error bars represents the standard deviation between three independent qPCR measurements of the same sample. Two independent experiments were performed and a representative experiment is shown. **B.** Binding of the HA antibody to a DSB. An untagged strain (LMY581) was used for ChIP and probed with a HA antibody to detect non-specific binding.

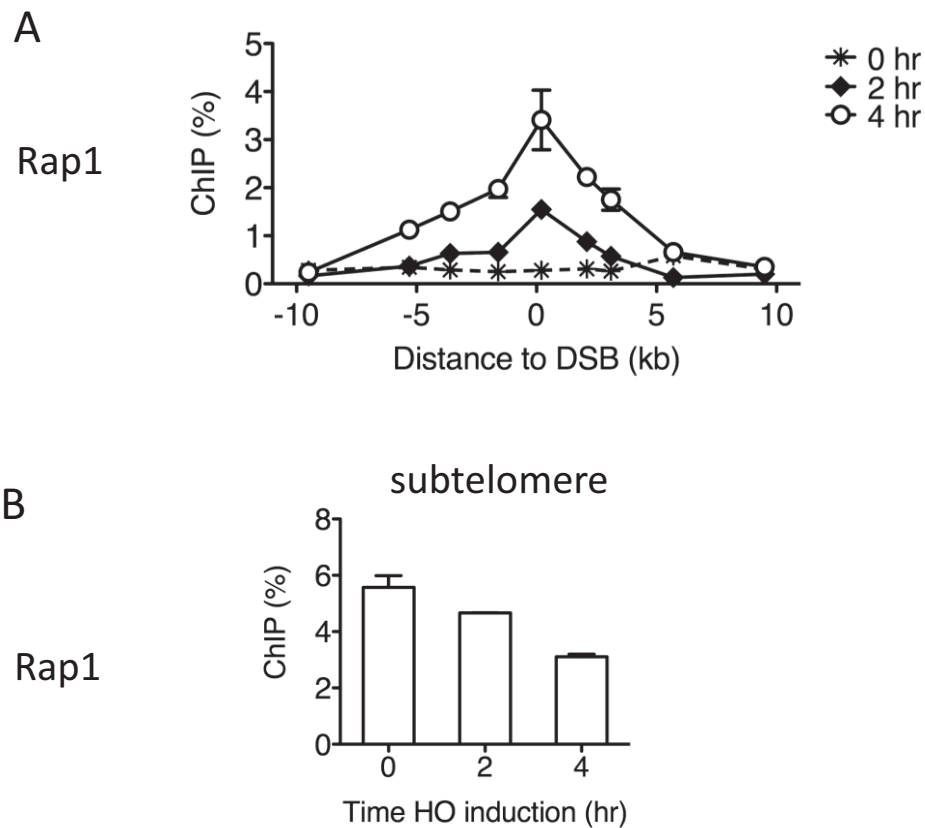


Fig 6.3 Recruitment of Rap1 to a DSB

A. Rap1 binding to a DSB in a *MATa* strain (JKM139). The JMK139 strain does not contain the Rap1 binding site at the *MATa* locus. ChIP experiments were performed as described in Fig 6.2.1 and samples were probed with a Rap1 antibody. ChIP values were calculated as before. Error bars represents the standard deviation between three independent qPCR measurements of the same sample. Two independent experiments were performed and an representative experiment is shown. **B.** Rap1 binding at the subtelomeric region (at the 0.6kb locus) after DSB induction. ChIP experiments were performed as in A. Error bars represents the standard deviation between three independent qPCR measurements of the same sample.

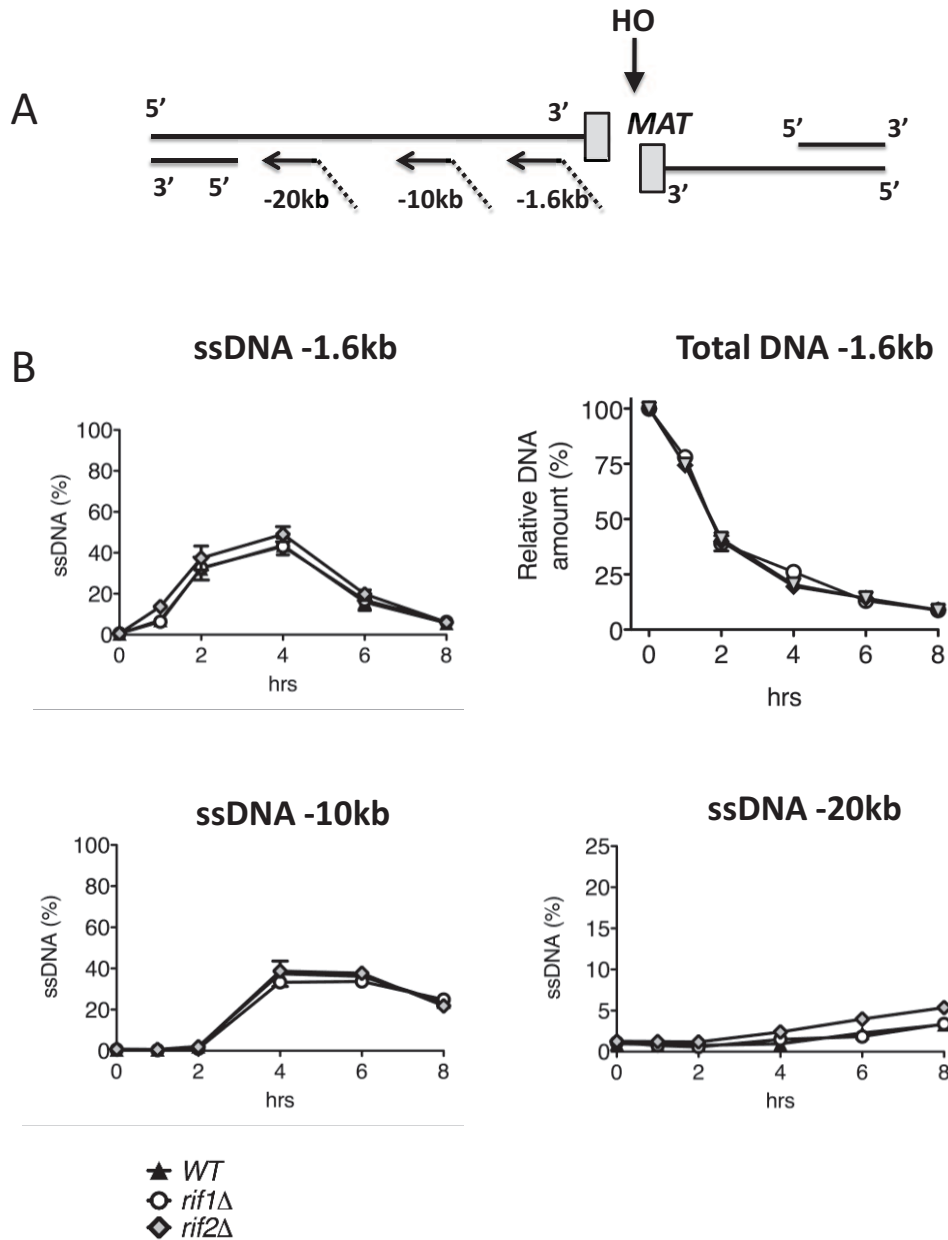


Fig 6.4 Effect of Rif1 and Rif2 on ssDNA generation

A. Schematic diagram representing DNA resection upon HO-induced DSB at the MATa locus. Primers were designed at three difference loci to measure ssDNA on the 5'-3' strand upstream of the HO cutting site. For simplicity, only the tagging primers are shown (arrow and dashed lines). **B.** ssDNA accumulation in wild type JKM139 cells and isogenic *rif1*Δ and *rif2*Δ cells at indicated loci. ssDNA was measured by SyBrGreen based QAOS assay as described in the methods (mean±SD). At least two independent experiments were performed and an representative experiment is shown.

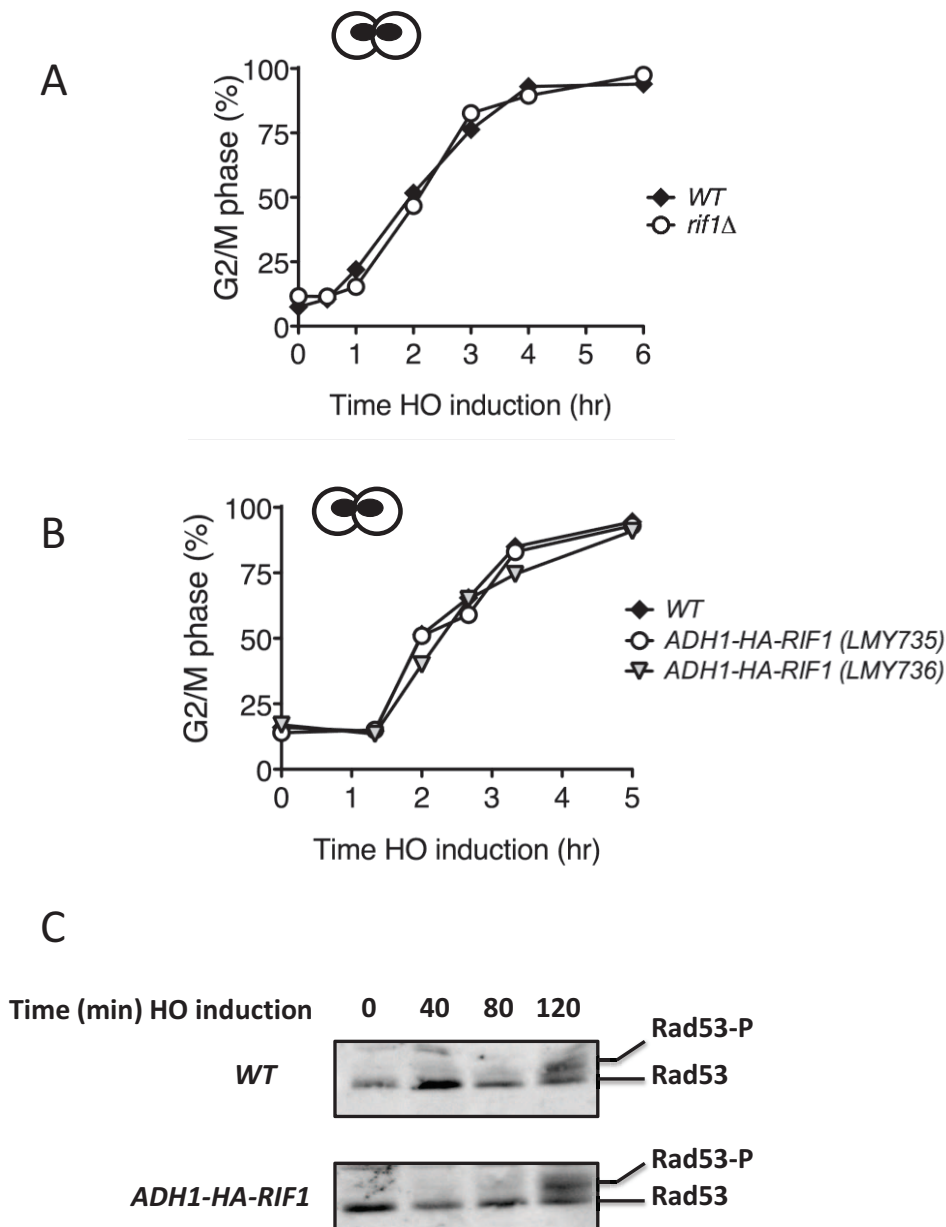


Fig 6.5.1 Effect of Rif1 on checkpoint activation upon a single DSB

A and **B**. Percentage of G2/M arrested cells of indicated genotype scored by DAPI staining. All cells were in JKM139 background. Cells were grown overnight in raffinose media (time 0) and 2% galactose was added to the media to induce HO cutting. 300 cells were scored for each sample and the average was plotted. **C**. Western blot showing Rad53 phosphorylation in wild type JKM139 and an isogenic *ADH1-HA-RIF1* strain (LMY735).

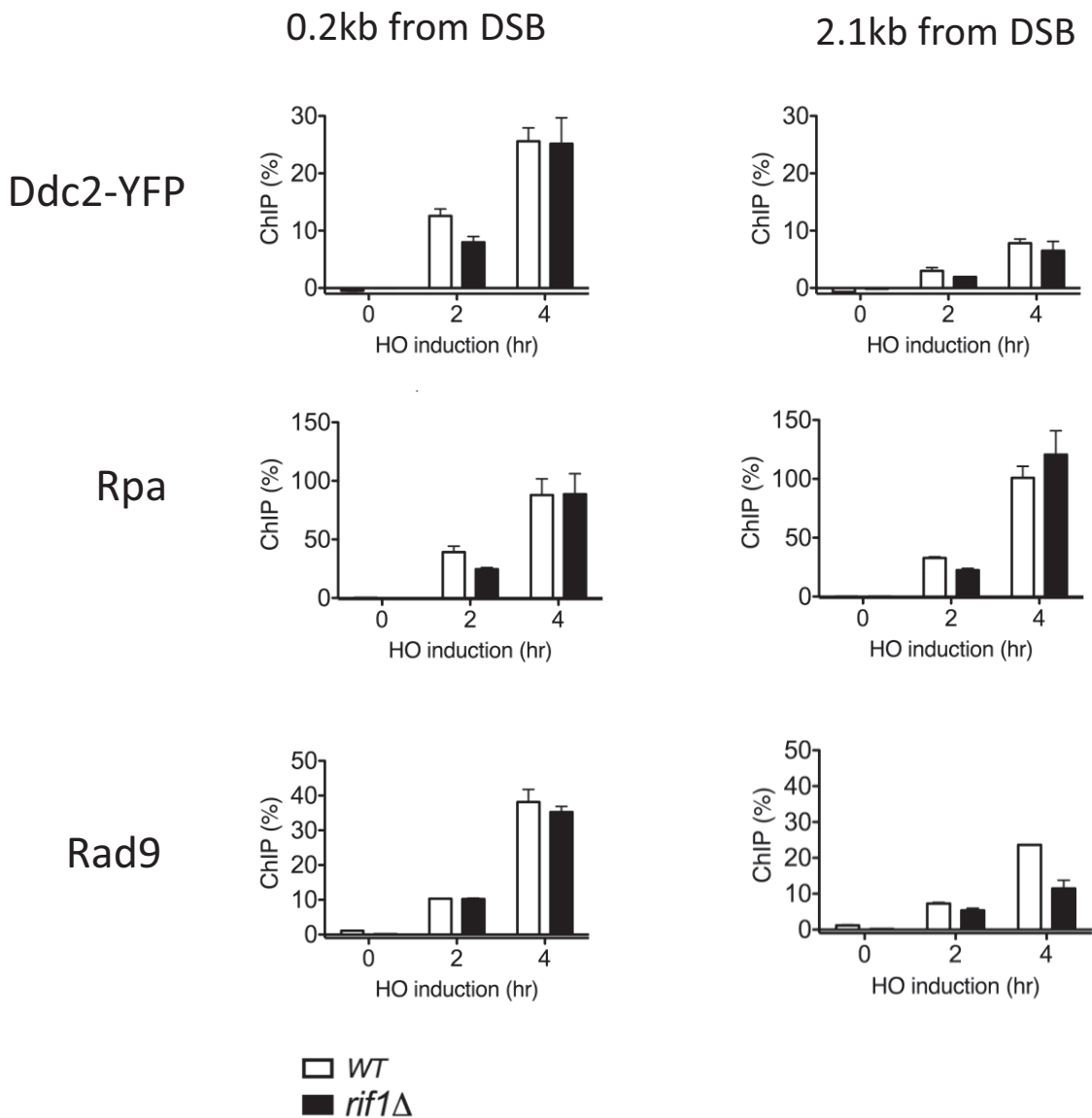


Fig 6.5.2 Effect of Rif1 on the recruitment of checkpoint proteins to DSB

JMK139 cells carrying wild type *RIF1* or *rif1*Δ were grown overnight in raffinose media (time 0) before 2% of galactose was added to the media to induce DSB. Samples were collected at 2 and 4hrs for ChIP analysis. The YFP tagged Ddc2 was detected by an YFP antibody, while Rad9 and Rpa were detected by their own antibodies. ChIP values was calculated as described in the method. Error bars represents the standard deviation between three qPCR measurements of the same sample. Two independent experiments were performed. Yeast strain used was LMY711.

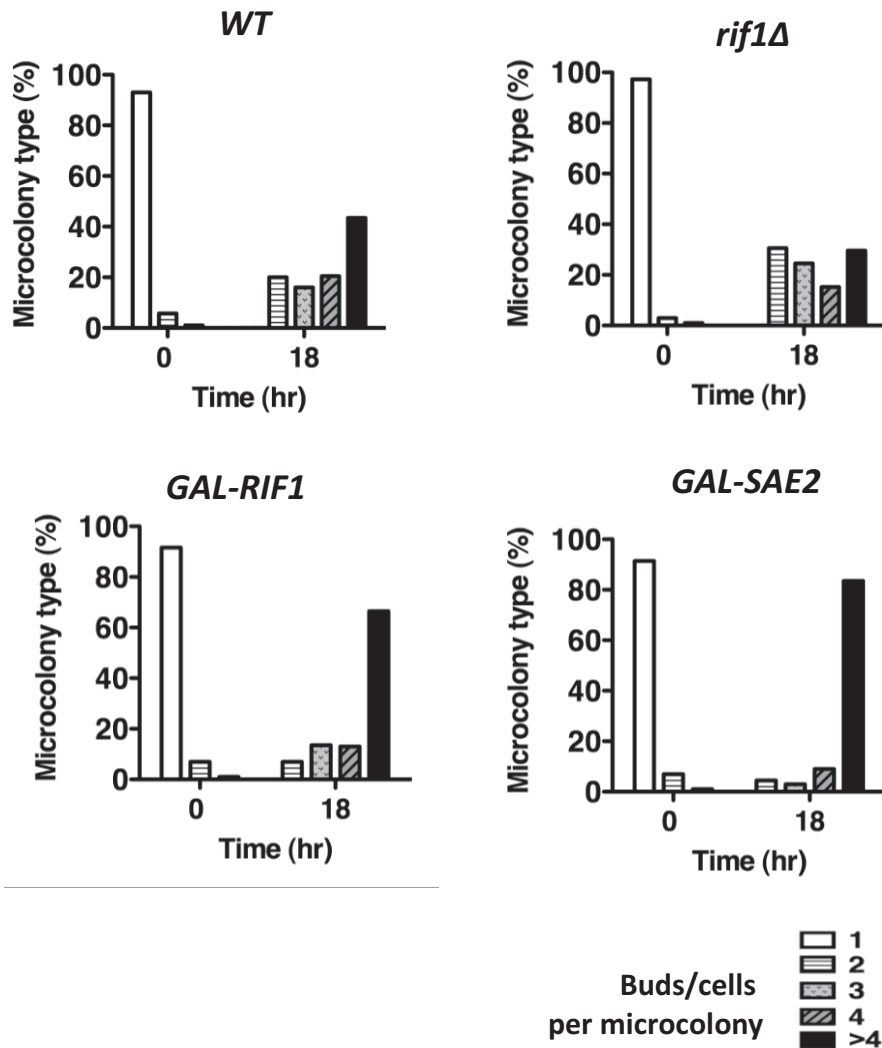


Fig 6.6 Effect of Rif1 on checkpoint adaptation to a single irreparable DSB

Wild type JKM139 and isogenic *rif1Δ*, *GAL-RIF1*, and *GAL-SAE2* strains were arrested in G1 by growing on raffinose plates until saturation. Cells were diluted in 2% galactose media and separated by sonication before spreading evenly on galactose plates. Plates were incubated at 30°C and the number of cells in each microcolony formed after 18hrs was scored under a microscope (buds were counted as cells). 300 microcolonies were analysed for each sample. Three independent experiments were performed and an representative experiment is shown.

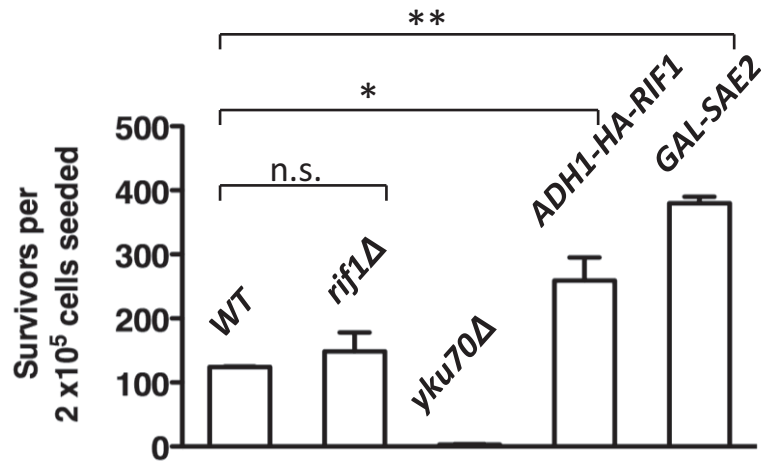
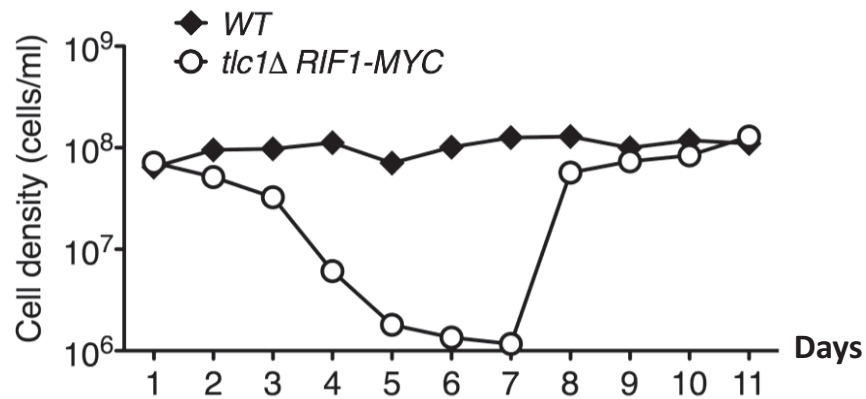


Fig 6.7 Effect of Rif1 on Non-Homologous End Joining repair of a DSB

Indicated JKM139 derivative strains were grown overnight in raffinose media and $\sim 2 \times 10^5$ cells were seeded on galactose plates. The number of colonies was scored after 3 days. Two independent experiments were performed. Error bars represent standard error of the mean. Yeast strains used were LMY581, LMY582, LMY735, LMY578 and LMY615. One-way ANOVA statistical analysis was performed followed by Tukey's multiple comparison test to compare the number of survivors. n.s. indicates non-significant. * indicates $p < 0.05$, and ** indicates $p < 0.001$.

A



B

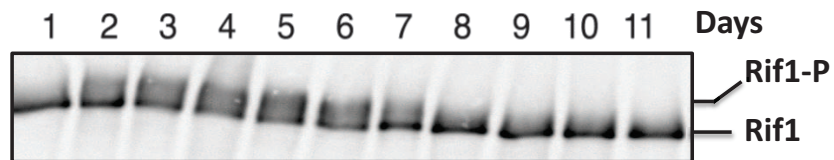


Fig 7.2 Rif1 modification in *tlc1Δ* cells

A. Growth curve of a wild type and a *tlc1Δ RIF1-MYC* strain in YEPD media. Strains with indicated genotypes were taken directly from germination plates and grown in liquid culture at 23°C. Every 24hrs, the number of cells was counted and samples were harvested for Western blot analysis. The rest of cells were diluted appropriately every day and cultured for a total of 11 days. Four independent *tlc1Δ RIF1-MYC* strains were examined and showed similar results. B. Corresponding Western blot analysis of Rif1 from *tlc1Δ RIF1-MYC* cells harvested each day, using a Myc antibody. Whole cell lysate was prepared by TCA extraction as described in the methods.

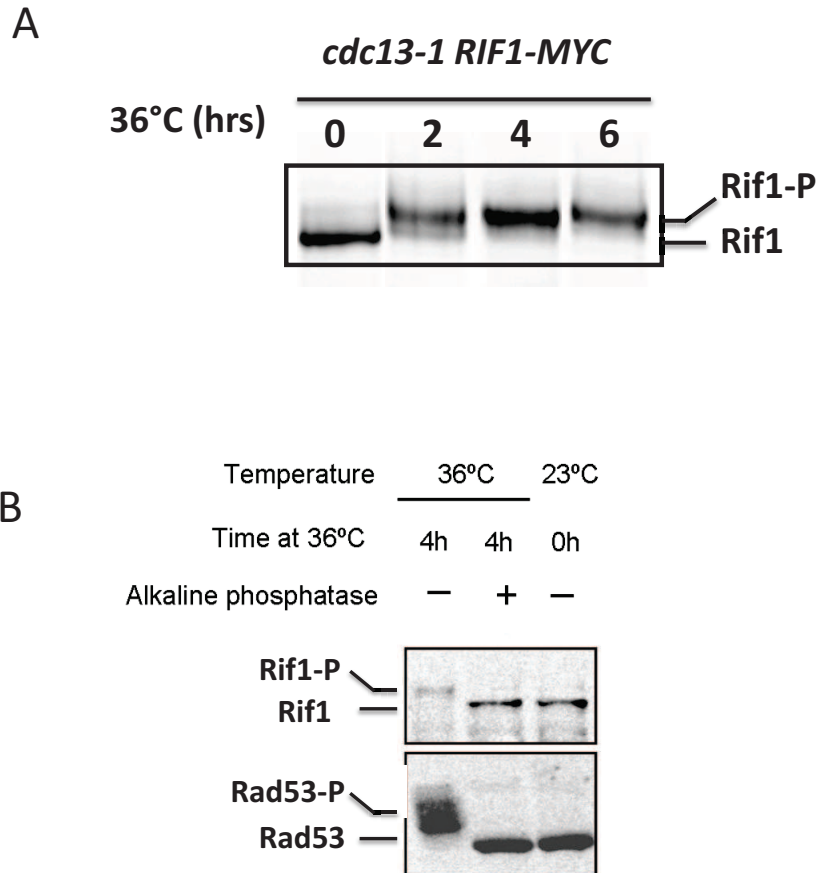


Fig 7.3 Rif1 phosphorylation upon telomere uncapping

A. Western blot showing Rif1 protein in *cdc13-1* cells. *cdc13-1 RIF1-MYC* cells (LMY78) were grown overnight at 23°C (time 0) before temperature was shifted to 36°C and samples were collected for protein extraction. Samples were separated on a 6% SDS-PAGE gel for 4 hrs followed by WB analysis using a c-Myc antibody. **B.** Phosphatase treatment of proteins in *cdc13-1* cells. Whole cell lysate was extracted from a *cdc13-1 RIF1-MYC* strain grown for 4hrs at 36°C. Protein lysate was split in two, and were either treated with alkaline phosphates (+) or mock treated (-). A protein sample extracted from *cdc13-1 RIF1-MYC* cells grown at the permissive temperature (23°C) was included as a negative control. WB was performed as described in A, and Rad53 phosphorylation was included as a control.

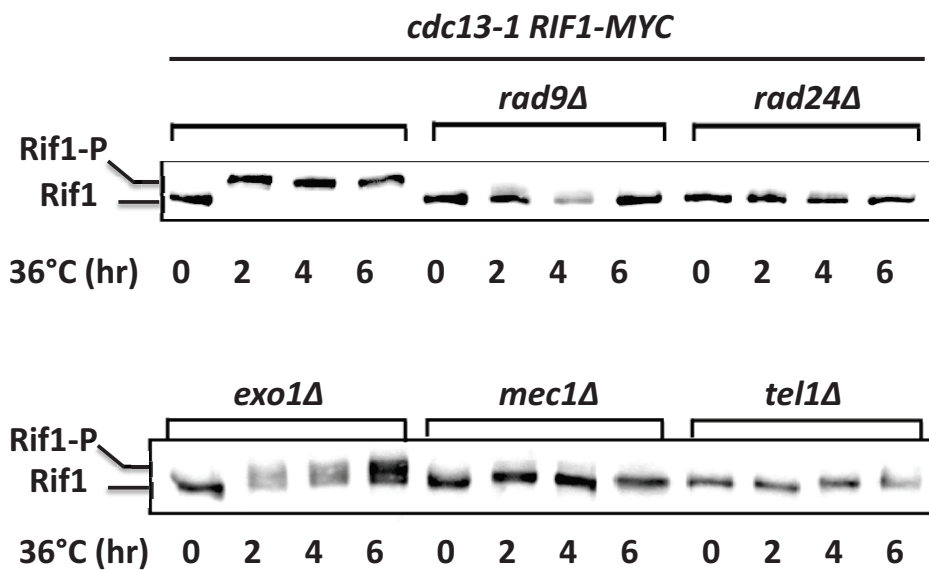


Fig 7.4 Phosphorylation of Rif1 in *cdc13-1* cells defective in checkpoint or nuclease

Western blot showing phosphorylation of the full length Rif1 in *cdc13-1 RIF1-MYC* strains with deletions in the checkpoint genes *RAD9*, *RAD24*, *MEC1*, *TEL1*, or with a deletion in *EXO1*. Cells were grown in liquid YEPD at 20°C overnight (time 0) and the temperature was shifted to 36°C for 6hrs and samples were collected every 2hrs for Western blot analysis. Protein lysate was prepared and analysed as previously described.

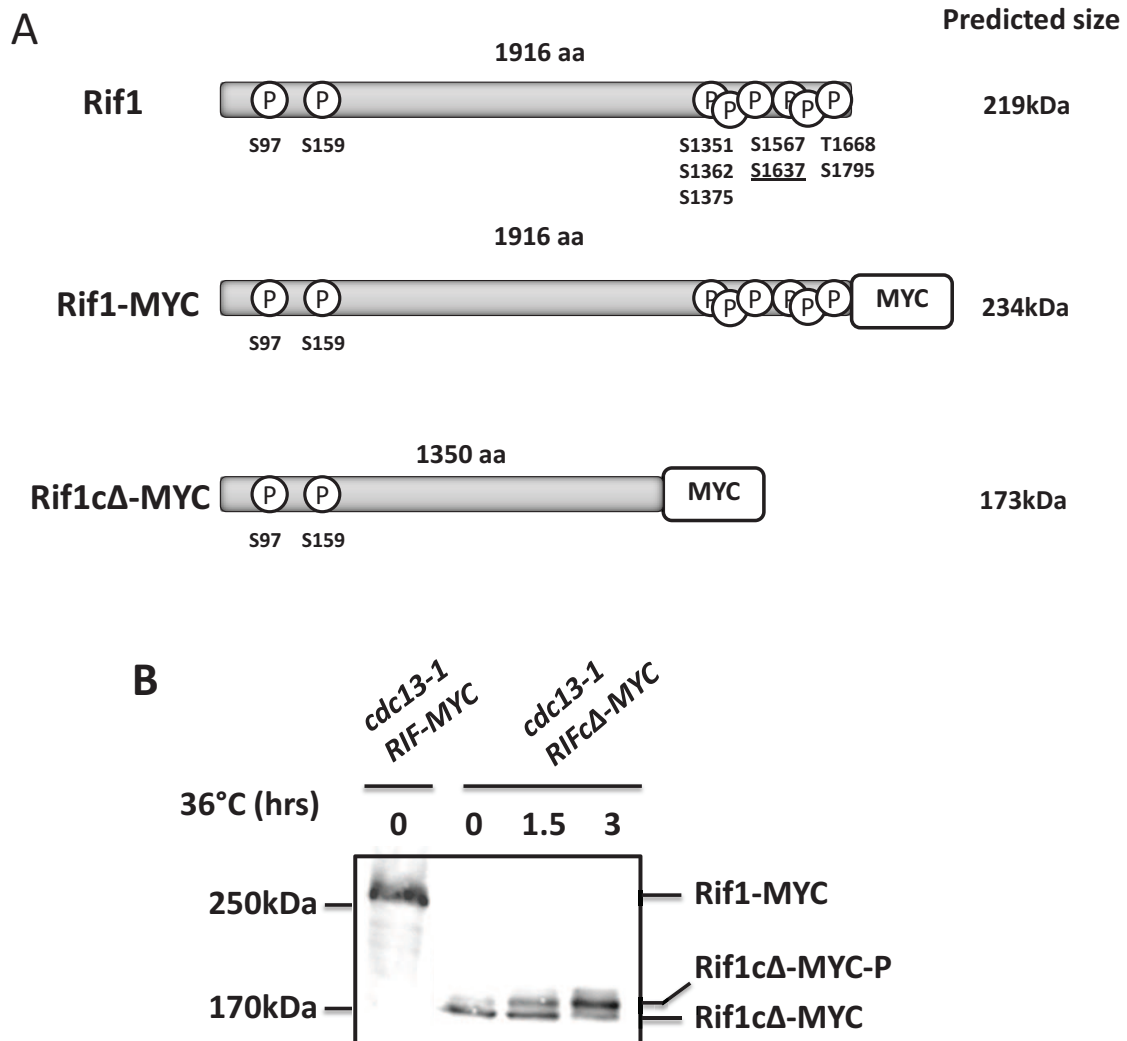


Fig 7.5 Tagging and C-terminal deletion of Rif1 protein

A. Schematic diagram showing the full length Rif1 protein, MYC tagged Rif1, and C-terminal deleted Rif1. The C terminal deletion spans amino acids 1351-1916. Previously identified serine/threonine phosphorylation sites are labelled as 'P'. The deletion of Rif1 was designed to eliminate the majority of phosphorylation sites localised in the C-terminus. Predicted size of each protein is indicated on the right of the graph. **B.** Western blot showing the phosphorylation of the C terminal deleted Rif1 protein. *cdc13-1 RIF1cΔ-MYC* cells (LMY510) were grown in liquid YEPD at 20° C overnight (time 0) and the temperature was shifted to 36° C and samples were collected at indicated time points for Western blot analysis. Protein lysate from a *cdc13-1 RIF1-MYC* strain was loaded as a control in the first lane.

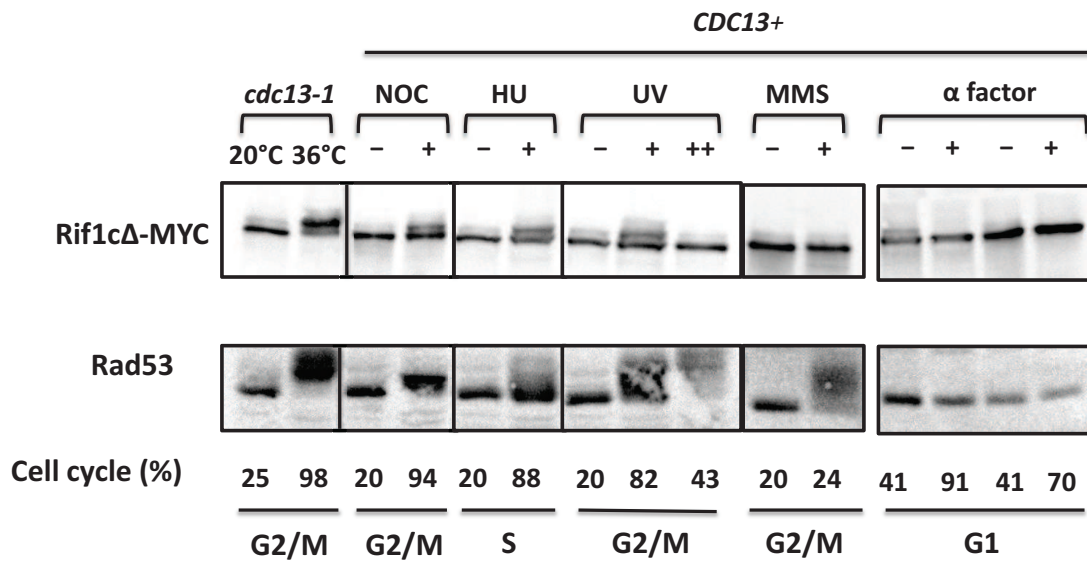


Fig 7.6 Phosphorylation of C-terminal deleted Rif1 protein in different conditions

cdc13-1 RIF1cΔ-MYC cells (LMY510) were grown at 20° C overnight before the temperature was shifted to 36° C for 3.5 hr and protein extracts were prepared and analysed on Western blot. A *RIF1cΔ-MYC* strain (LMY372) was treated with nocodazole (NOC, 20ug/ml, 2hr), hydroxyurea (HU, 100mM, 3hr), UV (UV+ equals 30 J/m², UV++ equals 100 J/m²), MMS (0.1%, 3.5hr) or mock treated, before proteins were extracted for WB analysis. Two independent *RIF1cΔ-MYC bar1Δ* strains were arrested in G1 by treating with 33 nM alpha factor for 3.5hrs before being harvested for WB. Samples were also collected for DAPI staining at indicated conditions and the percentage of cells at G1, S phase or G2/M are indicated at the bottom of each protein sample.

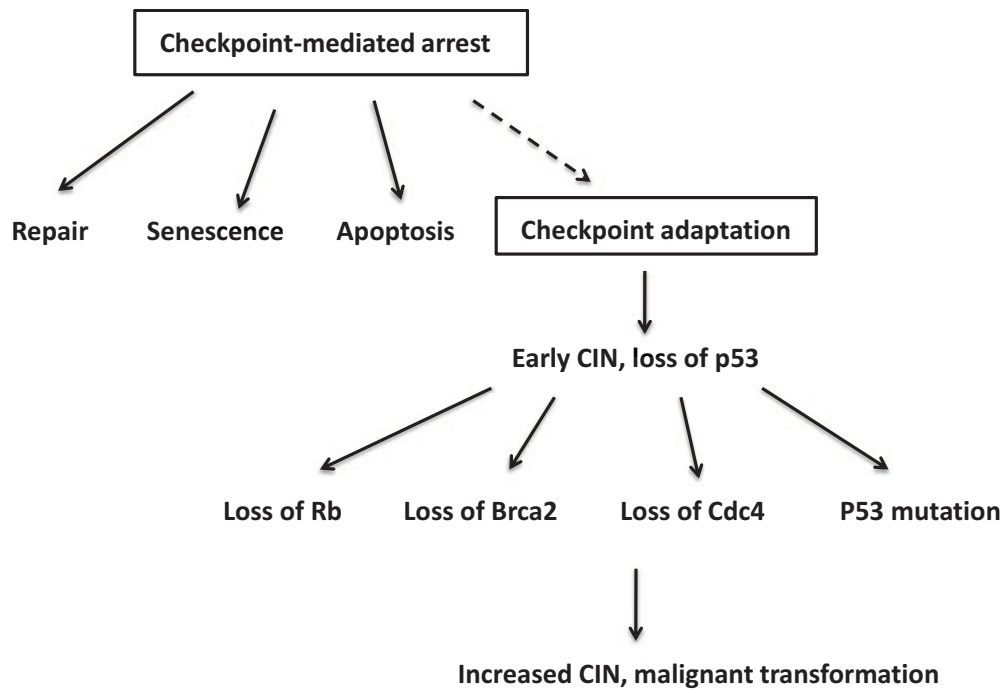


Fig 8.2 The potential role of checkpoint adaptation in carcinogenesis